Dissertation

Epigenetic reprogramming of macrophages in chronic diseases

Joschka Hey

2021

Dissertation

submitted to the
Combined Faculty of Natural Sciences and Mathematics
of the Ruperto Carola University Heidelberg, Germany

for the degree of
Doctor of Natural Sciences

Presented by

Joschka Hey,
M.Sc. in Molecular Biosciences

born in Weinheim, Germany

Oral examination: October 21st 2021

Epigenetic reprogramming of macrophages in chronic diseases

Referees:

Prof. Dr. Christoph Plass
PD Dr. Odilia Popanda

Contributions

Epigenetic reprogramming of airway macrophages drives polarization and inflammation in muco-obstructive lung disease

The project "Epigenetic reprogramming of airway macrophages drives polarization and inflammation in muco-obstructive lung disease" (**section 3.1**) was a collaboration between the research groups of **Prof. Dr. Christoph Plass** and **Prof. Dr. Marcus A. Mall**. The majority of the presented work has been performed by myself unless mentioned otherwise. **Dr. Michelle Paulsen**, **Prof. Dr. Marcus A. Mall**, **Prof. Dr. Christoph Plass**, and I conceived and designed the study. I prepared and analyzed immunofluorescence data, coordinated and performed library preparations, and the computational analysis of sequencing data, including processing and downstream analysis, assisted by **Dr. Reka Toth**, **Dr. Pavlo Lutsik**, and **Dr. Reinhard Liebers**. **Dr. Dieter Weichenhan** supervised and supported library preparations of whole-genome bisulfite sequencing. **Dr. Michelle Paulsen** coordinated and performed in vivo experimental details, animal work and processing of tissue samples, ex vivo cell cultures, data acquisition, and cell sorting, and analyzed the data. **Simone Butz** assisted specific experimental procedures and in vivo treatments. The **Flow Cytometry Core Facility** (EMBL, Germany) supported cell sorting and flow cytometry. The **Genomics and Proteomics Core Facility** (DKFZ, Germany) and **Gene Core Facility** (EMBL, Germany) supported and performed sequencing of next-generation sequencing libraries. The **Omics IT and Data Management Core Facility** (DKFZ, Germany) supported data storage of next-generation sequencing data.

The majority of the results in **section 3.1** are integrated into the manuscript "Epigenetic reprogramming of airway macrophages drives polarization and inflammation in muco-obstructive lung disease", which is currently under revision at Nature Communications. I am the first author of the article and contributed significantly to data generation, analysis, interpretation, figure design, and manuscript writing.

Cancer-specific DNA methylation landscape of tumor-associated macrophages and monocytes in breast cancer

The project "Cancer-specific DNA methylation landscape of tumor-associated macrophages and monocytes in breast cancer" (**section 3.2**) was a collaboration between the research groups of **Prof. Dr. Christoph Plass** and **Dr. Ruth Scherz-Shouval**. The majority of the presented work has been performed by myself unless mentioned otherwise. **Dr. Ruth Scherz-Shouval**, **Prof. Dr. Christoph Plass,** and I conceived and designed the study. I performed whole-genome bisulfite sequencing library preparations and the computational analysis of next-generation sequencing data, including processing and downstream analysis. **Coral Halperin** coordinated and performed in vivo experimental details, animal work, and processed tissue samples, in vitro cell culture, and cell sorting. Furthermore, she prepared RNAseq libraries and performed RNAseq. **Dr. Mark Hartmann** and **Maximilian Schönung** performed post-bisulfite adaptor tagging library preparations of whole-genome bisulfite sequencing. The **Genomics and Proteomics Core Facility** (DKFZ, Germany) and **Gene Core Facility** (EMBL, Germany) supported and performed sequencing of next-generation sequencing libraries. The **Omics IT and Data Management Core Facility** (DKFZ, Germany) and **Life Sciences Core Facility** (WIS, Israel) supported data storage and next-generation sequencing data processing.

Epigenetic reprogramming of macrophages in chronic diseases

Summary

Macrophages are innate immune cells and maintain a prominent role in host defense, tissue homeostasis, and immune response. Diverse macrophage populations reside in most tissues, and their immense plasticity, mediated through distinct gene-regulatory and epigenetic mechanisms, allows macrophages to react to an altered microenvironment quickly. The adaptation of macrophages occurs both in physiological and pathological conditions, making them a key determinant of many inflammatory and non-inflammatory diseases. The clear link between disease progression, epigenetic reprogramming, and functional adaptations is frequently unknown. This doctoral thesis aims to comprehensively characterize the epigenomes and coinciding transcriptional patterns of macrophages and monocytes in muco-obstructive lung disease and breast cancer, two chronic diseases with a significant health burden worldwide.

The first part of this doctoral thesis addresses the role of the mucostatic airway microenvironment on epigenetic reprogramming of airway macrophages (AMs). Mucus obstruction and chronic airway inflammation characterize many chronic lung diseases such as cystic fibrosis and chronic obstructive pulmonary disease. Utilizing the *Scnn1b*-transgenic mouse model of muco-obstruction, we determined epigenetically regulated and differentially activated pathways and transcription factors involved in inflammatory responses and macrophage polarization. Enhanced activation of AMs in muco-obstructive lungs was validated via single-cell surface marker expression. Ex vivo stimulation of AMs from healthy lungs with mucus per se induced gene expression changes, reminiscent of those observed in AMs from muco-obstructed lungs. Furthermore, *Scnn1b*-transgenic AMs showed functional impairment in efferocytosis and phagocytosis capacities. In addition, excessive inflammatory responses upon lipopolysaccharide stimulation, mediated through epigenetic priming by enhanced activity and expression of *Irf1*, were revealed.

Collectively, these results depict that mucostasis induces epigenetic reprogramming of AMs, leading to phenotypic and functional changes favoring tissue damage and disease progression. Targeting epigenetically altered AMs may support therapeutic approaches in patients with muco-obstructive lung disease.

The second part of this doctoral thesis examines the epigenetic reprogramming of tumor-associated macrophages (TAMs) by breast cancer. The development of breast cancer induces the accumulation of TAMs within the tumor microenvironment, which acquire a distinct phenotype and tumor-promoting functions. Yet, the epigenetic mechanism underlying the differentiation of TAMs from bone marrow-derived monocytes remains largely unknown.

Using the 4T1 orthotopic mouse model, we showed that the presence of breast cancer significantly altered the DNA methylation landscape of macrophages and monocytes. The cancer-specific methylome of TAMs was dissected in DNA methylation patterns originating from bone marrow-derived monocytes, as well as TAM-specific alterations. These modifications in the DNA methylation landscape coincided with a cancer-specific transcriptome enriched in aggressive breast cancer subtypes and associated with shorter cancer-specific survival. Utilizing a single-cell gene expression atlas of the tumor microenvironment, we linked disease-specific signals to the cancer-specific DNA methylation landscape of TAMs. Collectively, these analyses highlighted the role of TGF-β, IFN-γ, and CSF1 in the reprogramming of TAMs, mediated by the transcription factors FOSL2, RUNX3, and STAT1. Furthermore, using a reference-free deconvolution approach, we identified a TAM-specific DNA methylation signature associated with high tumor grade and immunosuppressive functions, such as the induction of *Cd274*, encoding for the immune inhibitory receptor-ligand PD-L1.

Together, these results provide evidence that the epigenetic landscape of macrophages and monocytes is perturbed by breast cancer, reflecting molecular mechanisms of TAM reprogramming and patient outcomes.

In summary, the epigenetic characterization of macrophages from different chronic diseases provides novel insights into the role of DNA methylation and chromatin accessibility in macrophage activation and reprogramming by an altered microenvironment. The results depict that the presence of a muco-obstructive airway or tumor microenvironment has a substantial impact on the epigenome of the respective tissue-resident macrophages and further affects their transcriptional landscapes as well as essential macrophage functions. Furthermore, the data allow the identification of prognostic and diagnostic markers and pave the development of macrophage-targeted therapies.

Epigenetische Umprogrammierung von Makrophagen in chronischen Erkrankungen

Zusammenfassung

Makrophagen sind angeborene Immunzellen und spielen eine zentrale Rolle bei der Gewebehomöostase, Wirtsabwehr und Immunantwort. Diverse Makrophagenpopulationen befinden sich in den unterschiedlichsten Geweben und ihre enorme Plastizität, die durch verschiedene genregulatorische und epigenetische Mechanismen ermöglicht werden, erlaubt es Makrophagen, schnell auf eine veränderte Mikroumgebung zu reagieren. Die Anpassung von Makrophagen erfolgt sowohl unter physiologischen sowie unter pathologischen Bedingungen, was sie zu einer wesentlichen Komponente vieler inflammatorischer und nicht-inflammatorischer Erkrankungen macht. Der direkte Zusammenhang zwischen Krankheitsprogression, epigenetischer Umprogrammierung und funktionellen Anpassungen ist häufig unbekannt. Ziel dieser Doktorarbeit ist es, die Epigenome und die damit einhergehenden Transkriptionsmuster von Makrophagen und Monozyten bei mukoobstruktiver Lungenerkrankung und Brustkrebs, zwei chronischen Erkrankungen mit einer signifikanten Gesundheitsbelastung weltweit, umfassend zu charakterisieren.

Der erste Teil dieser Doktorarbeit befasst sich mit dem Einfluss der mukostatischen Mikroumgebung der Atemwege auf die epigenetische Umprogrammierung von Atemwegsmakrophagen (AM). Mukusobstruktion und Atemwegsentzündung charakterisieren viele chronische Lungenerkrankungen wie Mukoviszidose und chronisch-obstruktive Lungenerkrankung (COPD). Unter Verwendung des *Scnn1b*-transgenen Mausmodells der Mukoobstruktion haben wir epigenetisch regulierte und differentiell aktivierte Signalwege und Transkriptionsfaktoren bestimmt, die an einer Entzündungsantwort und Makrophagenpolarisation beteiligt sind. Die verstärkte Aktivierung von AM in mukoobstruktiven Lungen wurde über die Expression von Einzelzell-Oberflächenmarkern validiert. Die Ex-vivo-Stimulation von AM aus gesunden Lungen mit nativem Mukus induzierte Genexpressionsveränderungen, die an jene erinnert, die in AM aus mukoobstruktiven Lungen beobachtet wurden. Darüber hinaus zeigten *Scnn1b*-transgene AM eine funktionelle Beeinträchtigung der Efferozytose- und Phagozytosekapazitäten. Außerdem wurden exzessive Entzündungsreaktionen nach Lipopolysaccharid-Stimulation festgestellt, die durch epigenetisches Priming in Form einer erhöhten Aktivität und Expression von *Irf1* vermittelt wurden.

Zusammengenommen zeigen diese Ergebnisse, das Mukostase eine epigenetische Umprogrammierung von AM induziert, die zu phänotypischen und funktionellen Veränderungen beiträgt und somit Gewebeschäden und Krankheitsprogression begünstigt. Die gezielte Behandlung epigenetisch veränderter AM könnte therapeutische Ansätze bei Patienten mit mukoobstruktiver Lungenerkrankung ermöglichen.

Der zweite Teil dieser Doktorarbeit untersucht die epigenetische Umprogrammierung von Tumor-assoziierten Makrophagen (TAM) durch Brustkrebs. Die Entwicklung des Mammakarzinoms induziert innerhalb der Tumormikroumgebung die Akkumulation von TAM, welche einen ausgeprägten Phänotyp und tumorfördernde Funktionen akquirieren. Der epigenetische Mechanismus, welcher der Differenzierung von TAMs aus Knochenmark stammenden Monozyten zugrunde liegt, ist jedoch noch weitgehend unbekannt.

Mit Hilfe des orthotopen 4T1-Brustkrebs-Mausmodells konnten wir zeigen, dass die Anwesenheit von Mammakarzinomen die DNA-Methylierungslandschaft von Makrophagen und Monozyten maßgeblich veränderte. Das krebsspezifische Methylom von TAM wurde in unterschiedliche DNA-Methylierungsmuster aufgeschlüsselt, die ihren monozytären Ursprung, sowie TAM-spezifischen Veränderungen reflektieren. Diese Modifikation der DNA-Methylierungslandschaft ging mit einem krebsspezifischen Transkriptom einher, das in aggressiven Brustkrebs-Subtypen angereichert und mit einem verkürzten Patientenüberleben assoziiert war. Unter Verwendung eines Einzelzell-Genexpressionsatlas der Tumormikroumgebung konnten wir krankheitsspezifische Signale mit der krebsspezifischen DNA-Methylierungslandschaft von TAMs in Verbindung bringen. Zusammengenommen verdeutlichten diese Analysen die Rolle von TGF-β, IFN-γ und CSF1 in der Umprogrammierung von TAMs, vermittelt durch die Transkriptionsfaktoren FOSL2, RUNX3 und STAT1. Darüber hinaus identifizierten wir mit Hilfe eines referenzfreien Dekonvolutionsansatzes eine TAM-spezifische DNA-Methylierungssignatur, die mit einem erhöhten Tumorgrad und mit immunsuppressiven Funktionen, wie der Induktion von *Cd274*, das für den immuninhibitorischen Rezeptor-Liganden PD-L1 kodiert, assoziiert war. Zusammengefasst liefern diese Ergebnisse den Beweis, dass die epigenetische Landschaft von Makrophagen und Monozyten durch Brustkrebs perturbiert wird, was wiederum die molekularen Mechanismen der TAM-Umprogrammierung und Patientenverläufe widerspiegelt.

Gemeinsam betrachtet liefert die epigenetische Charakterisierung von Makrophagen aus verschiedenen chronischen Erkrankungen neue Einblicke in die Rolle der DNA-Methylierung und Chromatinzugänglichkeit bei der Makrophagenaktivierung und -umprogrammierung durch eine veränderte Mikroumgebung. Die Ergebnisse zeigen, dass das Vorliegen einer muko-obstruktiven Atemwegs- oder Tumormikroumgebung einen wesentlichen Effekt auf das Epigenom der jeweiligen Makrophagen hat und darüber hinaus deren Transkriptionslandschaft sowie essentielle Funktionen beeinflusst. Zusätzlich ermöglichen die Daten die Identifizierung von prognostischen und diagnostischen Markern und ebnen den Weg für die Entwicklung von auf Makrophagen ausgerichteten Therapien.

Table of contents

1 Introduction

Macrophages are a heterogeneous population of innate immune cells residing in most tissues. They are involved in developmental processes, tissue homeostasis, host defenses, as well as the promotion or resolution of immune responses with potential consequences on tissue damage or repair[64]. Plasticity is a key hallmark of the monocyte to macrophage lineage and enables them to quickly adapt to a changing microenvironment. Responses to various signals are mediated through distinct gene-regulatory and epigenetic mechanisms, providing macrophage-specific phenotypes and functions[177,223,293]. Adaptation of macrophages occurs both in physiological and pathological conditions, making them a crucial determinant in the initiation and progression of both inflammatory and non-inflammatory diseases[177,223,293]. Yet, a clear link between disease progression, epigenetic reprogramming, and functional adaptations of macrophages has not been established for many pathologies.

The present thesis aimed to comprehensively characterize the epigenome and transcription dynamics of macrophages and monocytes, exemplified in two chronic

diseases with a worldwide health burden. We investigated how epigenetic mechanisms affect the phenotype and function of airway macrophages in muco-obstructive lung diseases as well as tumor-associated macrophages and bone marrow-derived monocytes in breast cancer. Accordingly, the introduction covers the topics epigenetics (**section 1.1**), ontogeny and functions of macrophages (**section 1.2**), muco-obstructive lung disease (**section 1.3**), and tumor-associated macrophages in breast cancer (**section 1.4**).

1.1 Epigenetics

1.1.1 Epigenetic layers

The term epigenotype has been perceived by Waddington in 1942, who described a molecular mechanism "by which the genes of the genotype bring about phenotypic effects"[316]. Thereby Waddington attempted to explain the developmental processes, linking the genotype to observable traits, known as the phenotype. In the 1970s and 1980s, the heritable aspect of epigenetics was introduced by Holiday based on various studies focusing on cellular memory[144]. The concept was further revised by Wu and Morris, who understood epigenetics as mitotically and meiotically heritable changes in gene function that do not involve alterations in the DNA sequence[327]. Nowadays, the term epigenetics can be defined as "the study of phenomena and mechanisms that cause chromosome-bound, heritable changes to gene expression that are not dependent on changes to DNA sequence"[69].

Epigenetic changes affect many cellular and physiological traits that may result from environmental factors or be part of normal developmental processes. Although the genome sequence is mostly static, the dynamic epigenome allows stem cells to differentiate into many distinct cell types with diverse phenotypes and functions[8]. Besides the development, additional factors, such as age, environment, and disease, can influence gene expression by various epigenetic mechanisms[227]. Specific processes with a prominent role of epigenetics include cellular differentiation, genomic imprinting, X chromosome inactivation, carcinogenesis, DNA repair, and drug resistance, among many other examples.

Based on the advent and rapid improvement of next-generation sequencing methods, various non-genetic factors contributing to cellular functions, traits, and phenotypes have been identified and characterized as the epigenome. Multiple layers constitute the epigenome, including DNA modifications, post-translational histone modifications, histone variants, nucleosome position and occupancy, RNA modifications, non-coding RNAs, and the three-dimensional chromatin conformation. These epigenetic layers can facilitate the interaction of transcription factors (TFs) at *cis*-regulatory elements and regulate gene expression (**Fig. 1.1**).

Modifications at the single nucleotide level include the covalent binding of a methyl

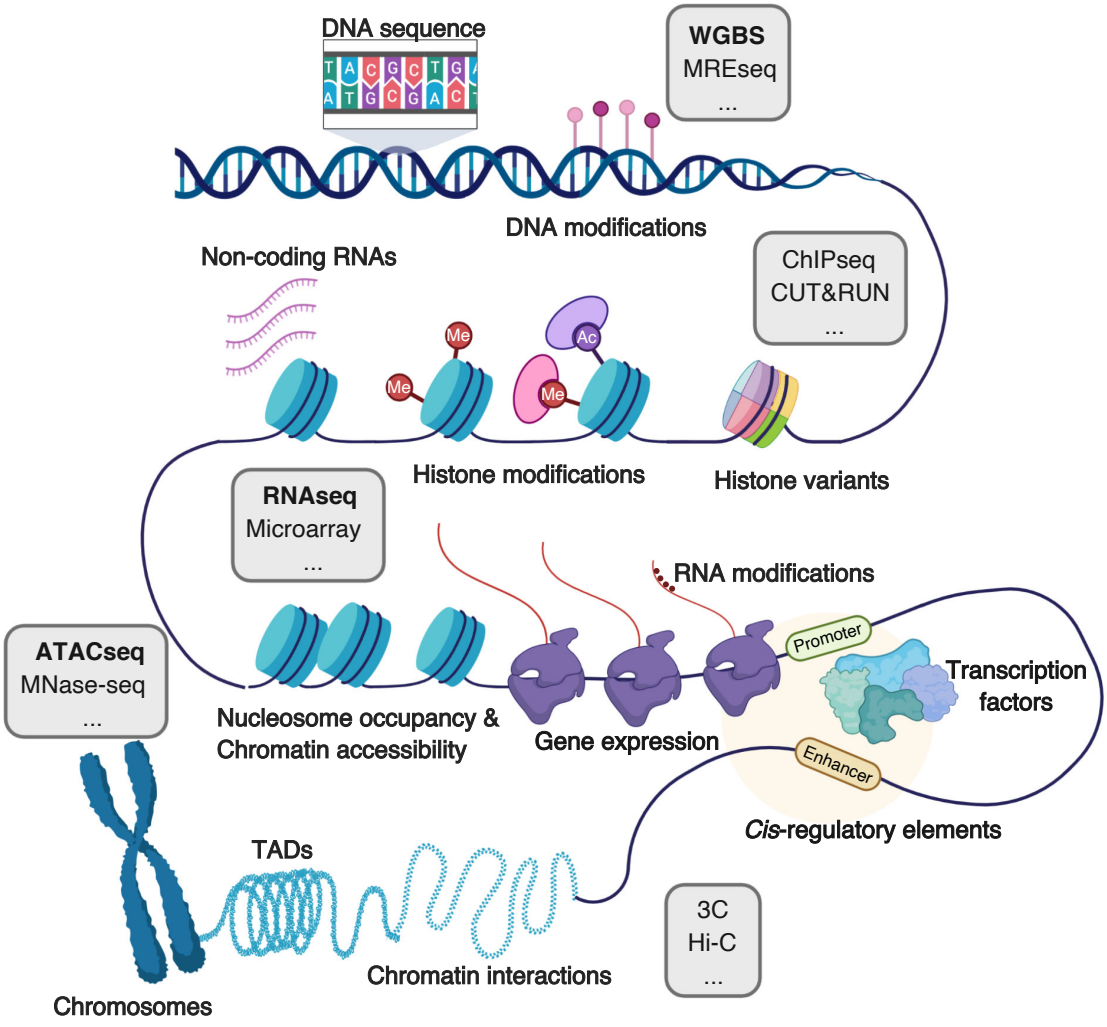

Figure 1.1: The multiple layers of the epigenome. Genomic DNA is packed into the nucleus as chromatin, with nucleosomes as the basic structural unit. The complex composition of different modifications constitutes different cell types as well as a disease's unique epigenome. These epigenetic modifications concern DNA, chromatin-associated proteins, and non-coding RNAs and together affect nucleosome occupancy, chromatin interactions, and the overall three-dimensional chromatin structure, such as TADs. Examples of different profiling methods to investigate the multiple layers of the epigenome are highlighted in gray boxes. Methods used in the present thesis are shown in bold.

group at the carbon 5 (C5) position of cytosines (5-methylcytosine, 5-mC), further referred to as DNA methylation [285]. The role and function of DNA methylation as an epigenetic mark and gene-regulatory modification is discussed in detail in **section 1.1.2**.

Many post-translational histone modifications have been identified at the single nucleosome level, including methylation, acetylation, and phosphorylation of histone tails. Together with histone variants, histone modifications regulate DNA binding around the nucleosome core and influence the chromatin structure and accessibility. Additionally, histone variants and modifications allow the recruitment of the transcriptional machinery, including TFs [285]. They can be profiled by chromatin immunoprecipitation followed by sequencing (ChIPseq) as well as a variety of novel next-generation sequencing methods, such as CUT & RUN [278], which are based on similar principles.

At the chromatin level, nucleosome positioning affects the chromatin accessibility, which in turn regulates the transcription of genes at *cis*-regulatory elements. *Cis*-regulatory elements include gene-regulatory regions such as promoters and enhancers that play a central role during development and differentiation as well as disease initiation and progression. Chromatin accessibility can be profiled by the assay for transposase-accessible chromatin sequencing (ATACseq) [40]. Furthermore, techniques such as micrococcal nuclease digestion with deep sequencing (MNaseSeq) have been used since 2008 to profile nucleosome occupancy [267]. A detailed introduction to the chromatin architecture and accessibility can be found in **section 1.1.3**.

The three-dimensional organization of chromatin constitutes a pivotal role in gene regulation. Promoter-enhancer interactions and more global mechanisms such as chromatin compaction can control gene expression and major cellular functions. The chromatin's three-dimensional structure can be profiled with chromosome conformation capture assays, such as 3C [71]. The recently developed high-throughput variant Hi-C has enabled the examination of chromatin organization at the high spatial level and aided the discovery of topological associating domains (TADs) of self-interacting chromatin [184].

At the transcript level, a prominent roleof non-coding RNAs has been described in gene regulation [147]. Types of non-coding RNAs include transfer RNAs (tRNAs) and ribosomal RNAs (rRNAs), as well as a variety of sparser long and short non-coding RNAs (ncRNAs). Both the presence of the ncRNA itself as well as a large number of RNA modifications can

interfere with gene expression on transcriptional and post-transcriptional levels. According to the epigenome, the entirety of RNA modifications, which affect gene expression, has been named the epitranscriptome[322].

Epigenomic profiling has been the key to discover associations between DNA and chromatin features with genomic functions. These investigations shed light on molecular processes that have a crucial impact on cellular processes of any kind. That way, epigenetics facilitated the identification of phenotypic markers in diagnostics and prognostics and will drive the discovery of novel treatment options for chronic pathologies such as muco-obstructive lung diseases and cancer[24].

1.1.2 DNA methylation

Arguably the most studied epigenetic layer is DNA methylation. It was discovered by Hotchkiss in 1948[149] and proposed as a putative epigenetic mark with a role in gene regulation by Holliday, Pugh, and Riggs in 1975[145]. DNA methylation describes a DNA molecule's covalent and reversible modification with a methyl group[81]. It occurs mainly on cytosines in the context of cytosine-phosphate-guanine dinucleotides (CpG) and is mediated via so-called DNA methyltransferases (DNMTs)[224]. While passive demethylation describes the gradual loss of DNA methylation during cell division, active demethylation requires the enzymatic machinery of ten-eleven translocation (TET) family proteins[152]. The interplay between these different active and passive methylating and demethylating forces eventually determines the DNA methylation landscape of a cell, also called the methylome.

In somatic cells, the methylome follows a bimodal distribution. Around 80% of the 28 million CpGs in the human genome and 21 million CpGs in the murine genome are methylated[279]. CpG-dense regions can be found in so-called CpG islands (CGis) that frequently overlap with active transcriptional start sites and remain mainly resistant to methylation. On average, CGis show DNA methylation levels of 10%, and *cis*-regulatory elements, such as enhancers, depict methylation levels ranging from 10% to 50%[191,282]. Under homeostasis, about 15% to 21% of all CpGs dynamically change methylation in the context of development[281,349]. On the contrary, pronounced aberrations of the DNA methylation landscape can be found in chronic malignancies, such as cancer[254].

Early studies of the epigenome showed a correlation between DNA methylation and gene silencing. Correspondingly, DNA methylation has been linked to X-chromosome inactivation, genetic imprinting, and gene silencing[23,181,210]. Although DNA methylation is widely recognized as a repressive epigenetic mark, the relationship between DNA methylation and gene expression is undoubtedly more complex than initially proposed. For instance, CpGs in gene bodies of transcribed genes are usually methylated, and some TFs can bind methylated DNA and induce transcription[334].

To understand these biological processes, DNA methylation profiling technologies are necessary. Over the past decades, a multitude of methodologies has been developed, including DNA methylation assays based on methylation-sensitive restriction enzymes (e.g., MREseq), 5-mC-specific antibodies (e.g., MeDIPseq), or bisulfite conversion-based techniques (e.g., Infinium MethylationEPIC Bead Chip and whole-genome bisulfite sequencing (WGBS)) that enable genome-wide DNA methylation profiling at single CpG resolution[336]. Nowadays, WGBS is accepted as the gold standard for DNA methylation profiling, but classical WGBS requires large amounts of DNA (>1 μg). This has been drastically reduced with the introduction of tagmentation-based methods, such as tagmentation-based WGBS (tWGBS) (requiring ∼20 ng of genomic DNA)[319] or post-bisulfite adaptor tagging (PBAT) WGBS that allows the generation of DNA methylation profiles of single cells[54]

1.1.3 Chromatin architecture and accessibility

To efficiently pack the genome, DNA is wrapped around histones, the building blocks of eukaryotic nucleosomes. These nucleosomes are the major component of chromatin that dynamically adapts its structure throughout cell cycle stages. Each nucleosome consists of two DNA turns, spanning 145-147 base pairs (bps), and the histone octamer, mainly composed of two copies of the core histone proteins H2A, H2B, H3, and H4[133,189]. These core histone proteins can be replaced with non-canonical variants[296] or be modified at various histone tail positions[343]. Post-translational histone modifications include methylation, phosphorylation, acetylation, ubiquitylation, and sumoylation and affect their biochemical properties[302]. Thereby, they affect diverse biological processes such as transcriptional activation and inactivation, chromosome packaging, as well as DNA damage and repair.

A well-studied example of histone modifications is the histone tails' acetylation on lysine residues. Histone acetylation can directly affect the chromatin architecture by weakening the DNA binding to the histone core[207]. The process of histone acetylation is mediated via histone acetylases, enzymes belonging to the group of epigenetic writers. Together with readers and editors, these enzymes establish and modify the histone code[207]. Post-translational histone modifications frequently correlate with chromatin accessibility and reflect certain functionalities of genomic regions related to gene expression regulation[207]. In addition to the recruitment of TFs to chromatin, active remodeling, for example, via the SWI/SNF complex, can alter nucleosome occupancy or completely evict nucleosomes from the chromatin[53]. Initial changes in chromatin accessibility are frequently caused by the binding of so-called pioneer TF factors that can recruit additional TFs to stabilize a nucleosome-depleted region[342]. Since active *cis*-regulatory DNA elements, such as promoters and enhancers, are generally accessible, profiling the chromatin accessibility can be used to identify gene-regulatory regions involved in cell type identity or disease development[226,275].

Many methods have been developed to profile chromatin accessibility, such as the genome-wide profiling technique ATAC that relies on the enzymatic cleavage of accessible chromatin and DNA transposition followed by sequencing[207]. This approach, combined with additional profiling methods, can lead to accurate gene expression models concerning enhancer-promoter interaction, TF binding, and other gene regulatory functions.

1.2 Ontogeny and functions of macrophages

1.2.1 Ontogeny of macrophages and its implication in inflammation and disease

Macrophages, first discovered by Metchnikoff in the late 1800s, are tissue-resident innate immune cells and contribute to homeostasis and disease[283]. They are found in most metazoan and are characterized by their ability to ingest dying cells, noxious particles, and pathogens, such as microbes and viruses. Furthermore, they are involved in regulating tissue growth and homeostasis as well as host protection[64]. Therefore, substantial work has gone into discovering their origins (summarized in **Fig. 1.2**) and functions in tissues at homeostasis, inflammation, and in sterile inflammatory conditions, such as cancer or atherosclerosis[330].

Tissue-resident macrophages were previously thought to be derived entirely from the adult hematopoietic system, with stem cells in the bone marrow differentiating to monocytic precursors in the blood. However, this hypothesis has been abandoned due to the development of genetic mouse and lineage tracing models. These experiments demonstrated that tissue-resident macrophages at steady-state do not require input from the blood but rather originate from early embryonic precursors and maintain their populations through proliferation[87,115,118,141,159,263,268,298]. However, certain populations of tissue-resident macrophages require to be replenished via monocytes, e.g., macrophages in the dermis, intestine, mammary gland, and a subpopulation of the heart require bloodborne precursors to preserve their pool[11,87,103,155,297,348]. Simultaneously, tissues such as the lung, brain, and liver maintain their populations independently from adult monocytes at steady-state[87].

Macrophages originate from multiple sources during embryonic development[225]. In mice, primitive hematopoiesis begins in the yolk sac with the emergence of early erythro-myeloid progenitors (EMPs)[140]. The second, transient hematopoietic wave, is defined by late EMPs and lymphomyeloid progenitors from the yolk sac, traveling to the fetal liver and giving rise to fetal liver monocytes[99,185,228]. The third and final wave of hematopoiesis starts with the emergence of hematopoietic stem cells from the para-aortic splanchnopleura. Hematopoietic stem cells seed the fetal liver before migrating to the spleen and bone marrow[162,263]. All other lineages of the hematopoietic system arise from the bone marrow, including

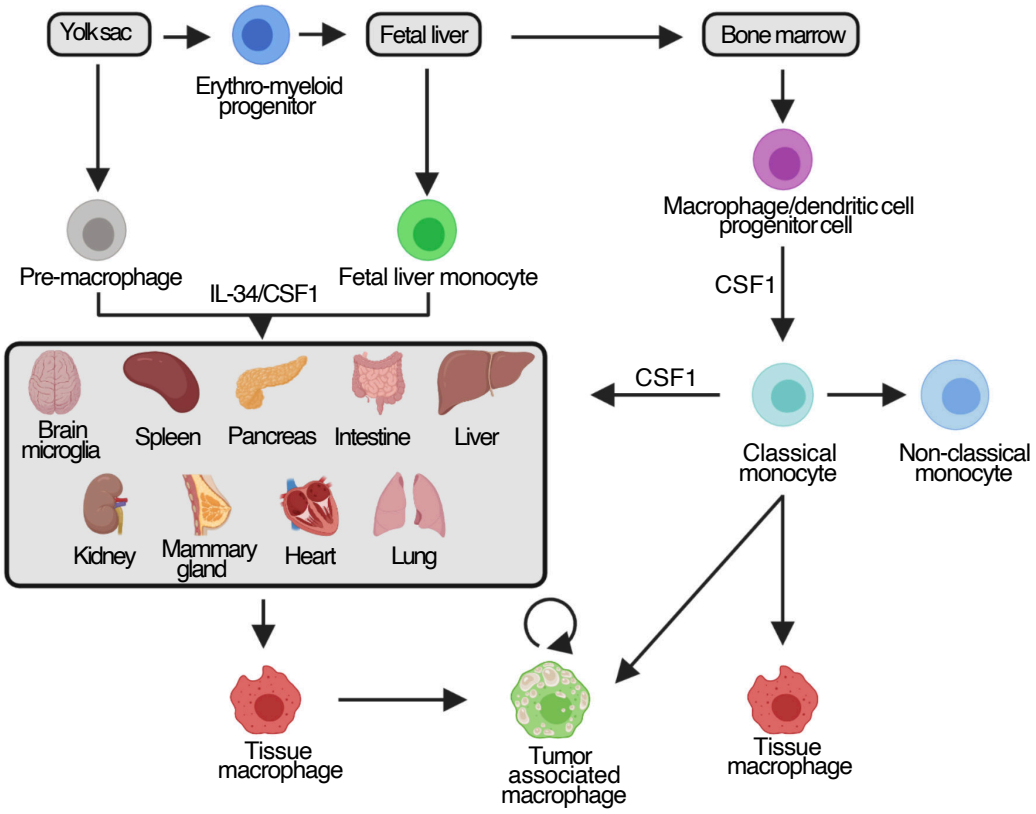

Figure 1.2: Macrophage lineages and TAM origin. Macrophages originate from at least three different embryonic sources: (i) EMPs in the yolk sac and (ii) fetal liver, which give rise to fetal liver monocytes, as well as (iii) macrophage/dendritic cell progenitor cells from the bone marrow. According to their origin, macrophage precursors differentiate into tissue-resident macrophages that populate almost all tissues. Most tissue-resident macrophages maintain themselves at a steady-state but can be replenished in response to macrophage depletion or inflammation. TAMs can arise from tissue-resident macrophages, but in most cancers, monocytes are the primary origin of TAMs. In response to tumor growth, monocytes undergo a distinct differentiation to TAMs. Figure adapted from Cassetta and Pollard, 2018[47].

macrophage/dendritic cell progenitor cells that differentiate into classical monocytes. Thus, lineage tracing has indicated that tissue-resident macrophages originate from three different embryonic sources, according to their origin: (i) EMP in the yolk sac and (ii) fetal liver, and (iii) macrophage/dendritic cell progenitor cells in the bone marrow[176,235].

The diversity of tissue-resident macrophages is mediated through unique gene regulatory mechanisms and distinct epigenomic landscapes[177,268]. The latter also provides a means for their plasticity and allows for crosstalk between the tissue niche's microenvironment and tissue-specific macrophage functions. This has been comprehensively shown by Lavin et al., 2014, who defined the vast enhancer landscape of tissue-resident macrophages associated with unique gene expression profiles[177]. The prominent role of the microenvironment in the epigenetic landscape and macrophages' high plasticity has been further investigated by transplanting bone marrow precursors and terminally differentiated macrophages into a different microenvironment. The new tissue niche was sufficient to completely reshape their expression profiles[177]. These results indicate the possibility of specific tissue-resident macrophage populations to serve as a therapeutic source of macrophages and the potential of macrophage deregulation by an altered microenvironment in chronic diseases[223,293].

Besides macrophage heterogeneity, the dominant receptor of almost all macrophage differentiation and survival processes is the colony-stimulating factor 1 (CSF1) receptor (CSF1R)[48]. Genetic deletion or pharmaceutical inhibition leads to the dramatic depletion of almost all macrophages in mice, except in the lung, in which macrophages are regulated via CSF2. However, additional tissue-specific cytokines and growth factors are dictated by the microenvironment to maintain macrophages' local identity[223].

Even though many tissues do not rely on monocyte input at steady-state, monocytes are significant contributors to the myeloid cell pool during inflammation[134]. This is possible due to the variety of monocytes' chemokine receptors, making them susceptible to signals from damaged or infected tissues. Amongst others, the following scenarios have been observed in which monocyte recruitment to macrophage compartments occurs, even in tissues that generally maintain their macrophage pool independently: Atherosclerosis[256,294], spinal cord and skeletal muscle injury[6,274], regression of fibrosis[209,249], and allergic skin[85]. Furthermore, following macrophage depletion (e.g., influenza infection of the lung), the proliferation of tissue-resident macrophages is observed to repopulate the niche[134]. Whether age plays a

relevant role in the expansion of tissue-resident macrophages or recruitment of monocytes remains to be examined in detail [134].

In addition to infectious diseases, tumor growth poses a unique challenge to the host, as it is both sterile yet pathogenic. In most solid tumors, macrophages are the predominant myeloid cell population [66,246]. Tumor-associated macrophages (TAMs) of most cancer entities were found to have a monocytic origin in experiments using transplanted fluorescently labeled bone marrow [68,67]. However, this was revisited upon recent findings that tissue-resident macrophages have a dual source. Together, two possible routes of TAM development in a given tissue have been suggested: (i) Tissue-resident macrophages of monocytic or embryonic origin change their phenotype during carcinogenesis and become TAMs. (ii) Recruited monocytes that undergo a distinct differentiation step become TAMs in response to tumor initiation and growths. The majority of findings related to TAMs have been made in mouse tumor models of the breast or lung [103,66,246], where major TAM populations are thought to be monocyte-derived [103]. For instance, a breast cancer mouse model demonstrated that the monocyte to TAM differentiation requires Notch signaling through the TF RBPJ [103]. This represented the first study to show a distinct differentiation pathway of TAMs compared to recruited tissue-resident macrophages. However, its role in other mouse models and different tumor types remains unknown [101,102]. Other studies identified ß-catenin–mediated transcriptional activation of FOS-like antigen 2 (FOSL2) and repression of the AT-rich interaction domain 5A (ARID5A) to drive reprogramming of TAMs from a tumor-suppressing into a tumor-supporting phenotype [264].

The distinct differentiation trajectories of macrophages explain why meaningful TAM-expression signatures used i.a. as prognostic biomarkers have only been generated comparing TAMs with healthy tissue-resident counterparts [46,308]. Comparison with macrophages or monocytes derived from other tissues such as the spleen or bone marrow captures developmental aspects of monocyte to macrophage differentiation instead of the disease-specific alterations of interest [308]. These findings emphasize macrophages' plasticity and show that the global transcriptome is mainly defined by tissue-specific signals that can be further disturbed by tumor development or other alterations in the microenvironment. In addition, these results highlight the importance of a proper experimental system when investigating TAM functions and reprogramming.

Yet, the exact mechanisms by which macrophages and monocytes evolve into TAMs and further support tumor development remain largely unknown. In particular, the underlying epigenetic modifications involved in TAM reprogramming have not been addressed by the current literature yet.

1.2.2 Functions and models of macrophage activation

In steady-state, macrophages perform a variety of functions to maintain tissue homeostasis. These functions include the removal of apoptotic cells, a process called efferocytosis, regulation of angiogenesis, as well as extracellular matrix, and tissue remodeling[138,242,329]. Moreover, macrophages can execute specialized functions depending on their tissue, such as recycling heme by red pulp macrophages in the spleen[167] and postnatal synapse remodeling of microglia in the brain[229,265]. Distinct phenotypes and functions of macrophages further suggest the importance of microenvironmental signals in macrophage programming[109,121,177].

However, one of the most prominent functions of macrophages is their role as gatekeepers in defending the host against infections and injury. Therefore, macrophages participate in defense responses, surveying most organs for a sign of infection. The recognition of pathogen-associated molecular patterns via pattern-recognition receptors, including Toll-like receptors (TLRs) involved in detecting lipopolysaccharide (LPS), is the basis to mount antimicrobial effector functions. This includes the uptake of microbes, in a process called phagocytosis, the release of effector molecules, and the recruitment of other innate and adaptive immune players to mount a full immune response[229,265]. Furthermore, the detection of danger-associated molecular patterns released by apoptotic and necrotic cells can trigger macrophage responses and cause sterile inflammation[119].

The process by which macrophages adopt functional programs in response to a cytokine milieu of a particular microenvironment is named macrophage polarization[213]. Although not unique among immune cells, a simplified classification of macrophage phenotypes, derived from in vitro experiments, has divided them into two groups[215]: classically (M1) and alternatively (M2) activated macrophages (**Fig. 1.3.a**). M1 macrophages are polarized by LPS exposure, similarly to macrophages that arise in response to Interferon-gamma (IFN-γ)

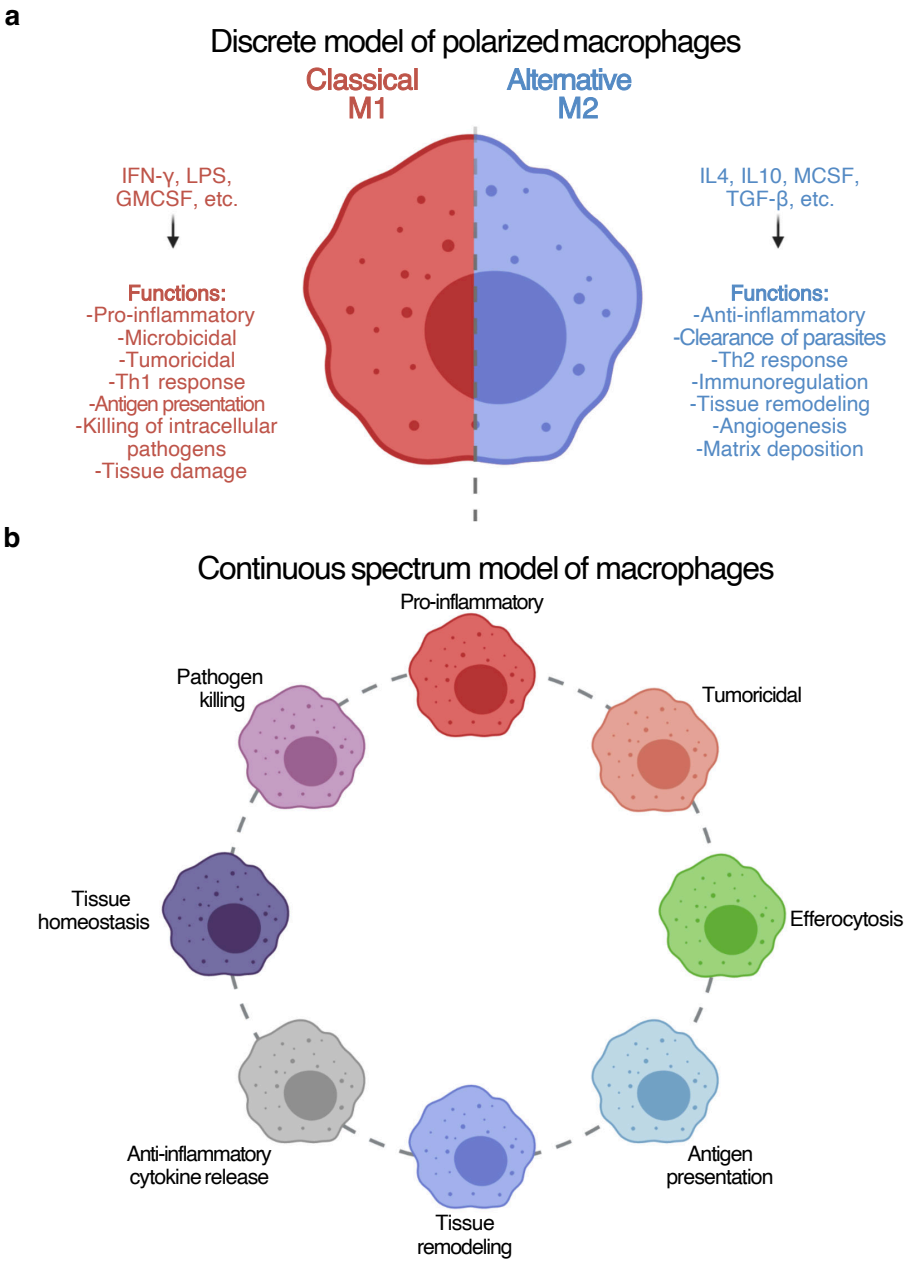

Figure 1.3: Models of macrophage activation. (**a**) Model of discrete macrophage activation. Simplified macrophage classification in classically (M1) and alternatively (M2) activated macrophages. Different chemicals or cytokines can stimulate macrophage polarization in vitro. (**b**) Continuous spectrum model of macrophage activation, in which macrophage programming and functions are recognized as multidimensional and dynamic, which can't be simplified into a bipolar scheme. Represents different phenotypes of macrophages identified in vivo. Figure adapted from Guilliams and van de Laar, 2015 [125].

production during Th1 responses (Type I). Accordingly, certain functions such as pathogen killing and antigen presentation have been assigned to M1 macrophages. On the contrary, M2 macrophages respond to cytokines characteristic of Th2 responses (Type II), such as IL-4 and IL-13. M2 macrophages fulfill anti-inflammatory functions such as wound healing and tissue remodeling[120].

However, while significant to the extreme in vitro settings or during acute inflammation, the strict bimodal macrophage polarization model is not transferable to the complex immune responses observed in vivo[213]. Recent efforts to further characterize the heterogeneity of macrophage's activation states gave rise to a spectrum model (**Fig. 1.3.b**), which includes bacterial-killing, wound healing, antigen presentation, and many more functional modules of macrophages[125,331]. Distinct macrophage functions are not necessarily mutually exclusive and can co-occur within the same population. Furthermore, recent in vivo studies of primary TAMs have shown that the original classification of pro-tumoral M2 and anti-tumoral M1 TAMs are not observed when comparing TAMs from breast cancer patients to appropriate healthy references[46].

1.3 Muco-obstructive lung disease

1.3.1 Causes and consequences of mucociliary dysfunction and airway muco-obstruction

A spectrum of chronic lung diseases, sharing the fundamental hallmarks of mucus obstruction and chronic airway inflammation, can be classified as muco-obstructive lung disease. Among them are rare mono-genetic conditions like cystic fibrosis (CF) and primary ciliary dyskinesia, as well as common complex lung diseases such as chronic obstructive pulmonary disease (COPD), non–cystic fibrosis bronchiectasis, and asthma[35,347,92]. Clinical features of muco-obstructive lung disease include cough, sputum overproduction, episodic exacerbations, alveolar destruction (emphysema), and inflammation of the bronchial tubes (chronic bronchitis, also known as bronchiolitis)[157].

In healthy persons, the mucus layer lining the surface of the airways is well-hydrated and allows rapid mucus transport from distal airways towards the trachea. This transport is possible due to a balanced ion transport: Cl^- secretion via the cystic fibrosis transmembrane conductance regulator (CFTR) and Na^+ absorption via the epithelial sodium channel (ENaC), allowing a balanced water transport by airway epithelia[143]. Furthermore, airway surface-hydration is monitored by cilial mechanosensing of mucus concentrations. This results in a mucus layer consisting of 2% solids and 98% water in healthy airways[137,161] (**Fig. 1.4.a**).

In contrast, in muco-obstructive lung diseases, abnormal epithelial fluid absorption causes depletion of the airways surface liquid, increased mucus concentrations, and enhanced osmotic pressure in the mucus layer[35]. In pathological conditions, mucus concentrations of around 8% solids are sufficient to cause muco-obstructive lung disease[137,161]. However, already moderately hyper-concentrated mucus (>2%) is associated with compressed cilia and reduced mucus transport in vivo. Severe hyper concentration causes complete flattening of cilia and eventually mucostasis and adhesion. Static mucus can be expectorated by coughing as a backup mechanism. However, mucus in small airways accumulates and causes airflow obstruction, favoring infection and inflammation[42,179] (**Fig. 1.4.b**).

In healthy conditions, airway mucus comprises approximately 98% water, 0.9% salt, 0.8%

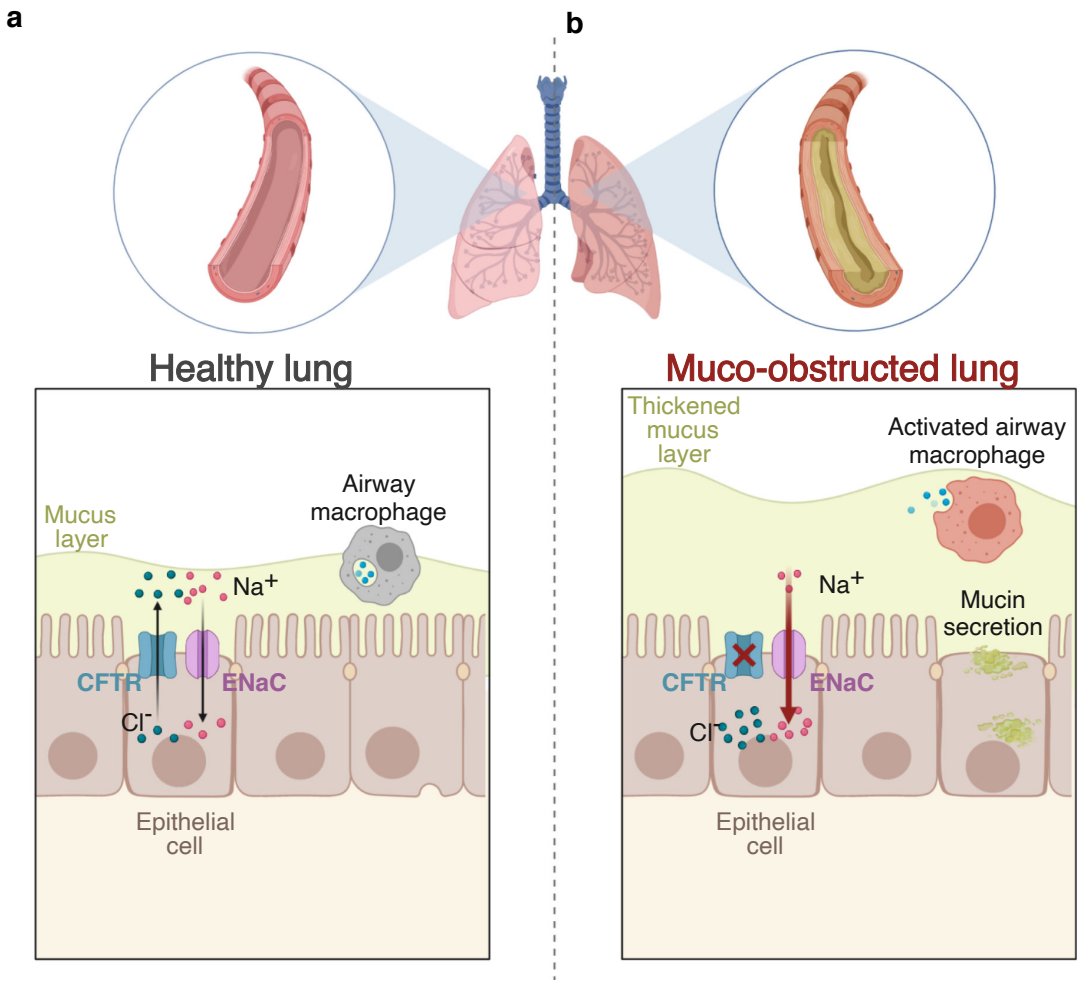

Figure 1.4: Muco-obstructive lung disease. (**a**) In the healthy lung, a well-balanced epithelial sodium (Na^+) absorption via ENAC, as well as secretion of chloride (Cl^-) via CFTR, leads to a hydrated airway surface. This enables mucociliary clearance of inhaled particles and pathogens. (**b**) In patients with muco-obstructive lung disease, an imbalanced ion transport (impaired Cl^- secretion and increased Na^+ absorption) combined with mucin hypersecretion leads to hyper-concentrated and dehydrated mucus. Eventually, this causes impairment of mucociliary clearance and accumulation of mucus, which precipitates infection and inflammation (e.g., activated AMs).

globular proteins, and 0.3% high-molecular-weight mucin polymers[257]. Its hydration status can be determined as the ratio between wet to dry mucus content or by measuring mucin concentration[137,161]. MUC5B and MUC5A are the two major synthesized and secreted respiratory mucins and form a mesh-like gel with many concentration-dependent features affecting mucociliary transport[93]. Mucin concentrations are raised in muco-obstructive lung diseases and correlate with disease pathogenesis. Although MUC5AC and MUC5B concentrations are elevated, MUC5B is the dominant mucin by concentration (10:1 over MUC5AC) in normal human lower and diseased airways. Mucus hyper concentration can be further enhanced by mucin hypersecretion, for example, caused by cigarette smoke[35,161].

Although muco-obstructive lung diseases are very heterogenous, a unifying aspect is an early manifestation of the disease in the small airways (bronchioles). Airways are defended against infections via mechanical clearance of mucus and pathogens, as well as the release of antimicrobial proteins and peptides secreted by the airway epithelium and immune cells[218]. In animal models, reduced mucus clearance and eventual formation of mucus plaques within airway lumens can induce the full spectrum of muco-obstructive lung diseases, including airflow obstruction and inflammation. Thus, plug formation is often associated with bacterial or viral infections, further enhancing mucin secretion. However, recent studies of experimental mouse models indicate that mucus per se can trigger key symptoms of muco-obstructive lung diseases, such as chronic airway inflammation and emphysema-like structural lung damage, even in the absence of bacterial infection[106,164,187,197,259].

Further unifying features of muco-obstructive lung diseases are exacerbations. Exacerbations are defined as a change in the patient's perception of well-being associated with seeking health care or an alteration in the patient's medical regime. They substantially impact the overall disease progression rate and severity, including the loss of lung functions[93]. Recent findings indicate that the spread of muco-obstructive lung disease to previously unaffected regions causes exacerbations[78]. A putative trigger for the spread of the disease are bacteria or viruses aspirated from the upper airways into the lung rather than a change in the overall microbiome composition. This concept is supported by a similar microbiome detected before and during exacerbations[60,309]. Exacerbations must be treated sturdily to prevent permanent lung function loss[42,137].

The most extensively studied muco-obstructive lung disease is CF. The increased mucus

concentrations and excessive mucus accumulation in CF patients' lungs are due to an autosomal recessive genetic disorder mediated via CFTR[251]. Nearly 1,700 CF-causing mutations have been described[63]. In addition, a deregulated Na^+ absorption by ENaC has been reported in CF patients, indicating coregulation of the two ion channels[25]. CF affects several body systems, but morbidity and mortality are mainly caused by bronchiectasis, small airway obstruction, and progressive respiratory impairment. Mucus extracted from CF patients at lung transplantation had solid concentrations ranging from 10-15%[42,137,161]. Interestingly, enhanced mucin concentrations and inflammatory cell numbers preceded bacterial infections in a pediatric CF cohort, emphasizing the inflammatory potential of mucus per se[90].

Perhaps the mildest example of mucin hyper concentration in the group of muco-obstructive lung diseases is one of the most common respiratory diseases, COPD[129,142,247]. COPD is the fourth leading cause of death worldwide, and patients manifest non-reversible, long-term breathing problems and airflow obstruction[247]. Epidemiological data suggest that cigarette smoke exposure correlates with mucin concentrations and is the primary cause of COPD[161]. In addition, other environmental factors, such as air pollution, dust fumes, and chemicals, as well as genetic predispositions, like α-1 antitrypsin deficiency, might influence COPD risk[15]. Furthermore, previous studies showed that mucin hyper concentration was associated with disease severity, increased airflow obstruction, and higher exacerbation rates. The epithelial defects in the airways of COPD patients, causing mucus hyper concentration, are complex and still an ongoing area of research. Cigarette smoke exposure may cause abnormalities in CFTR-mediated secretion of Cl^- and amplifies hypersecretion of MUC5AC and MUC5B[44,55,142].

The most direct approach to treat muco-obstructive lung diseases is the rehydration of mucus to reduce pathological concentrations. This is achieved by the inhalation of osmotically active aerosols, such as hypertonic saline or mannitol. Inhalation agents are shown to reduce the frequency of exacerbation and increase mucociliary clearance in patients with CF[4,79]. Current clinical developments focus on direct modulators of ion transport that might redirect Cl^- absorption to secretion, leading to a restored airway-surface hydration[92]. However, at the moment, the only disease-specific therapy available is Ivacaftor. This drug potentiates residual CFTR function and is approved for CF patients with specific CFTR

mutations[250].

Although epigenetic regulation behind mucus hypersecretion and the consequences on structural or inflammatory cells could offer an appealing therapeutic strategy for reversing altered cellular functions in muco-obstructive lung diseases, it is largely unexplored. Existing studies on CF, COPD, and asthma were frequently restricted to array-based approaches or lacked cellular resolution. Thus, most studies have been performed with samples from airway epithelium, blood, or even whole lung[41,50,193,212,280,291,337]. To provide a comprehensive, unbiased, and genome-wide epigenetic characterization, multi-omics profiling of isolated lung cell types must be performed, and functional consequences need to be addressed in detail.

1.3.2 Airway macrophages in muco-obstructive lung diseases

AMs are essential for lung homeostasis and host protection. They reside in the lumen of the conducting airways and at the distal airspaces. Like most macrophage populations, AMs have a high degree of plasticity, retaining adequate immune responses to invading pathogens while preventing pro-inflammatory responses to cellular debris or inhaled particles. Previous s´tudies have shown that in muco-obstructive lung diseases, AMs are activated, dysfunctional, and often correlate with disease pathogenesis and severity[43]. Changes in AM functions include impairments in efferocytosis and phagocytosis capacities, lysosomal killing, and increased release of inflammatory mediators, causing impaired tissue homeostasis and reduced barrier functions[14,104,180,306].

In COPD, enrichment of pigmented macrophages was identified around small airways and was associated with peribronchiolar fibrosis[98]. A key hallmark of COPD is emphysema, which is caused by infiltrating immune cells with a prominent role of macrophages and neutrophils. Their recruitment is most likely due to released cytokines from injured epithelial cells[70,73]. Infiltrating macrophages and neutrophils are the central effector cells, contributing to emphysema by releasing proteolytic enzymes like neutrophil and macrophage elastases[94]. Matrix metallopeptidase 12 (MMP12) is the key contributor to lung destruction in smoke-induced airway inflammation and muco-obstructive mouse models[135,306]. Moreover, a recent single-cell transcriptome study of a small cohort of COPD patients confirmed transcriptional

plasticity and macrophages' heterogeneity in the alveolar space. It revealed signatures associated with reduced cellular motility, altered lipid metabolism, and mitochondrial dysfunction of macrophages in COPD[16].

Like COPD, CF is associated with airway inflammation and an increased influx of neutrophils and macrophages[56]. These innate immune cells are thought to release proteases that damage the respiratory epithelium causing progressive structural lung damage. Furthermore, impairment of essential macrophage functions, such as reduced recognition of pathogens and decreased phagocytic capacity, can cause chronic airway infections in patients with CF[2,169,262]. The unique role of CFTR dysfunction and the muco-obstructive microenvironment on macrophage functions has not been addressed today.

As mentioned in **section 1.2.2**, recent work points to an epigenetic regulation in the activation of macrophages with the lung microenvironment playing a central role in shaping distinct transcriptional and epigenetic patterns[109,113,121,177]. This was demonstrated by replacing tissue-resident lung macrophages with bone marrow-derived monocytes (BMDMs)[293]. The transplanted BMDMs acquired a lung-specific gene expression profile and functioned similarly to lung macrophages. Also, completely differentiated peritoneal macrophages transferred into the lung upregulated AM-specific genes, demonstrating the microenvironment's ability to modify and reprogram macrophage identity independent of developmental origins[177].

1.3.3 *Scnn1b*-transgenic mouse model of airway muco-obstruction

Although muco-obstruction is a common hallmark of many chronic lung diseases, the mechanism causing disease phenotype and pathogenesis has received little attention. To gain in vivo knowledge of disease pathogenesis, mouse models can help to recapitulate and understand known disease hallmarks. The creation of mouse models mimicking the CF phenotype was already attempted in the early 90s by generating mouse strains with mutations in the *Cftr* locus using homologous recombination[257]. These *Cftr*$^{-/-}$ mice, as well as further attempts, exhibited defects in intestinal Cl^- secretion, producing a severe CF-like gastrointestinal phenotype. However, *Cftr*$^{-/-}$ mice did not develop muco-obstructive

lung disease, and no airway mucus plugging, goblet cell metaplasia, or spontaneous airway inflammation were observed[323].

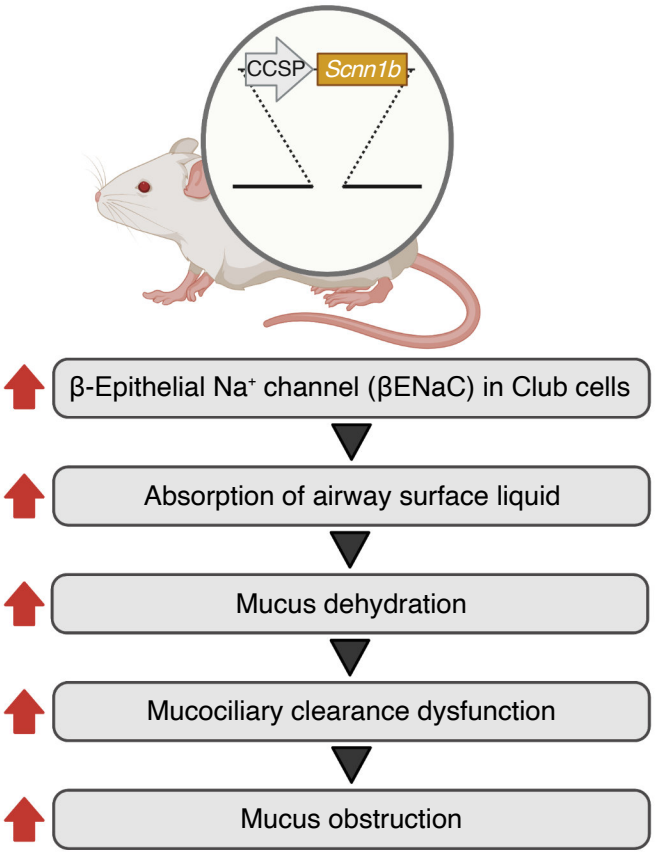

Figure 1.5: Scnn1b-Tg mouse model of airway muco-obstruction. Graphical representation of the mechanism causing muco-obstruction in the *Scnn1b*-Tg mouse model. Overexpression of the *Scnn1b*-Tg under a Club cell-specific promoter causes elevated βENaC expression in the airways. Increased Na^+ uptake leads to heightened absorption of airway surface liquid and mucus dehydration. Pathological mucus concentrations compress the periciliary layer and abolish mucociliary clearance and eventually elicit muco-obstructive disease hallmarks.

As an alternative approach, our collaborators Mall et al. generated a transgenic mouse model (**Fig. 1.5**) with an airway-specific overexpression of the b-subunit (*Scnn1b*, sodium channel epithelial 2 beta subunit) of EnaC to mimic CF ion transport pathophysiology in the lung of affected patients (in addition to impaired CFTR function, airways of CF

patients show an increased ENaC activity)[195]. The increased Na^+ absorption in the airways of *Scnn1b*-transgenic (Tg) mice resulted in the first animal model with spontaneous muco-obstruction, mimicking a CF-like lung disease with airway mucus obstruction, goblet cell metaplasia, mucus hypersecretion, chronic airway inflammation, reduced clearance of bacterial pathogens, and high pulmonary mortality[107,196,195,197]. The studies of the *Scnn1b*-Tg mouse phenotype provided a proof-of-concept that airway surface liquid depletion, induced by increased Na^+ absorption, causes mucociliary dysfunction, initiating a CF/COPD-like lung disease and muco-obstruction in vivo.

1.4 Tumor-associated macrophages in breast cancer

1.4.1 Breast cancer

Breast cancer is the most frequent malignancy and the leading cause of mortality in women worldwide. Most breast cancer patients are above the age of fifty, but younger women and rarely men are diagnosed with breast cancer as well [165,292].

Early stages of breast cancer, defined by cancer in the breast with or without axillary lymph node spread, are curable in most cases (70-80%) due to improvements in multimodal therapies. In contrast, advanced breast cancer, that metastasized to other organs is not considered curable using current approaches. Control of symptoms and survival prolongation are the main goals of treatment. Nowadays, breast cancer treatment decisions, mainly consisting of locoregional and systemic therapy, are primarily influenced by histological and molecular characteristics [132].

Although all breast cancers arise in the terminal duct lobular units of the collecting duct, breast cancer is considered a heterogeneous disease. Breast cancers are separated into preinvasive and invasive lesions on a histological level, with ductal carcinoma and lobular carcinoma being the most frequent subtypes. In 2000, Perou et al. reported an intrinsic classification system consisting of gene expression patterns of 496 genes, enabling the classification of breast cancer in four subtypes [236]: Luminal A and luminal B (expressing the estrogen receptor (ER)), basal-like, and human epidermal growth factor receptor 2 (HER2)-enriched (without ER expression). Other studies have repeatedly identified these subtypes with varying genes included in the diagnostic signature [150]. The classification system has evolved into a 50-gene classifier (PAM50) introducing the claudin-low subtype, largely carved out of the basal-like group [28]. The PAM50 classifier contains hormone receptor and proliferation-related genes, as well as genes with myoepithelial and basal features and a significant prognostic and predictive value for breast cancer patients [1,28,116,150].

Widely used in a clinical setting are the five surrogate intrinsic subtypes [132]: Luminal A-like, luminal B-like $HER2^-$, luminal B-like $HER2^+$, HER2-enriched, and triple-negative breast cancer (TNBC). Those subtypes are based on histology and immunohistochemistry of essential proteins, such as ER, progesterone receptor (PR), HER2, and the proliferation

marker Ki67. Tumors expressing ER or PR are called hormone receptor-positive breast cancers and allow endocrine therapy to block tumor growth. In general, the five surrogate intrinsic subtypes are clinically valuable and imply distinct treatment options[61,270]. Luminal A-like tumors show low-risk features such as low grade, high ER and PR expression, and low proliferation. In contrast, luminal B-like subtypes express ER and, to a lesser extent, PR, show high grade and high proliferation risk. HER2-positive tumors show more frequently intermediate or high histological grade features and have a low or absent expression of ER and PR, as well as medium to high proliferation. No surrogate biomarker was identified for the claudin-low intrinsic transcriptomic subtype associated with poor survival and increased expression of an epithelial-to-mesenchymal gene signature. TNBC, not expressing ER, PR, nor HER2, as well as non-luminal types, reveal aggressive features such as high grade and high proliferation. Since TNBC does not respond to hormonal therapy, it is considered the most aggressive and has a worse prognosis than other types of breast cancer[190,270].

Before recent technological advances in DNA methylation profiling, epigenetic breast cancer studies were restricted to a small number of genes[27,76,88]. For instance, the tumor suppressor gene breast cancer gene 1 (*BRCA1*), involved in DNA repair mechanisms, is associated with an increased risk of developing breast cancer as well as other cancer entities and was shown to be regulated via DNA methylation[151,170]. Furthermore, these studies demonstrated that the overall DNA methylation varies in different tumor subtypes and between cancerous and stromal tissues. The progress of superior next-generation sequencing technologies and improved bioinformatic analysis enabled genome-wide investigation of DNA methylation patterns in breast cancer. In 2012, The Cancer Genome Atlas (TCGA) network assayed the so far largest breast cancer DNA methylation cohort, consisting of 802 breast tumors[165]. DNA methylation profiling on bulk tumor samples was performed by Infinium DNA HM450 methylation arrays, in addition to copy number, gene expression, exome-sequencing and microRNA profiling. Using ER-positive tumors from the TCGA breast cancer cohort, an integrative analysis of DNA methylation and transcriptomic landscapes was performed by Koboldt et al. in 2012[165]. They identified several epigenetic hotspots functionally deregulated in ER-positive tumors as well as further epigenetic alterations in luminal-B tumors. Integration of gene expression and DNA methylation by Bell et al., 2019 revealed three TNBC sub-clusters with distinct prognoses[22]. Also, the role of

DNA methylation, along with copy number alterations in regulating microRNA expression, has been shown in the TCGA breast cancer cohort[9].

Overall, a multitude of breast cancer methylomes has been published. A shortcoming of them has been listed above. The vast majority of these breast cancer DNA methylation studies focused on promoter regions due to their established gene regulatory role. However, more recent studies have progressed to gene body methylation[95] and gene regulatory regions such as enhancers[96,139]. An overall positive correlation between DNA methylation in the gene body region and gene expression was observed. At *cis*-regulatory elements, such as enhancers, decreased DNA methylation was associated with increased TF-binding and enhanced transcription. Additionally, a study by Holm et al. included several normal cell types instead of bulk tissues as healthy references and thereby identified seven breast cancer clusters with distinct DNA methylation landscapes[146]. The dominant DNA methylation patterns were shown to reflect the tissue of origin, in addition to specific DNA methylation patterns driving cancer-specific gene expression.

Further generation of whole-genome methylomes of breast cancers, as demonstrated in the dissertation of R. Batra, who utilized the METABRIC breast cancer cohort, will highlight the role of DNA methylation and intratumor heterogeneity in epithelial tumor evolution[18]. In addition, complementary studies focusing on the epigenetic dissection of individual cell types are essential to understand distinct mechanisms of reprogramming and variations within the tumor microenvironment.

1.4.2 The role of tumor-associated macrophages in breast cancer

Though initially studied as a clonal disease, it is now widely accepted that tumors are evolving ecosystems, consisting of tumor, stromal, and infiltrating immune cells, as well as extracellular matrix components. It has been shown that genomically stable, non-cancerous cells, including stromal and infiltrating immune cells, are recruited by the tumor and undergo reprogramming to support tumor progression. Among the stromal cell types that have been identified in the tumor microenvironment are endothelial cells, which compose the blood and lymphatic circulatory system, pericytes, and cancer-associated fibroblasts (CAFs). The immune cell types combine various innate and adaptive immune cells, including T-cells, B-

cells, natural killer cells, dendritic cells, neutrophils, eosinophils, mast cells, and TAMs[158] (**Fig. 1.6.a**).

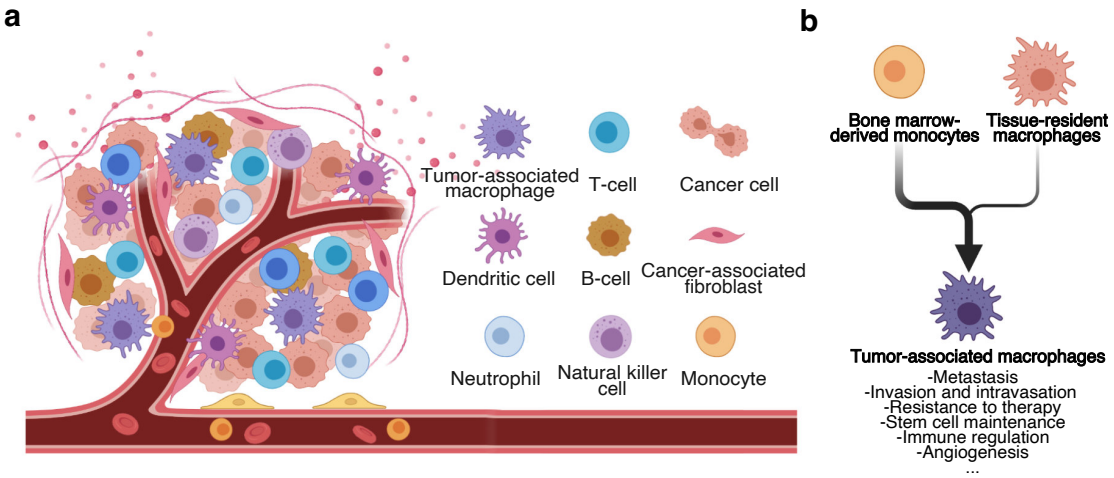

Figure 1.6: The tumor microenvironment and TAMs at a glance. (**a**) A simplified overview of the cellular components of the tumor microenvironment. Tumors consist of cancer and stromal cells (e.g., CAFs and pericytes) as well as immune infiltrates of the adaptive (e.g., T-cells and B-cells) and innate (e.g., TAMs, neutrophils, and eosinophils) immune system. (**b**) TAMs can originate from tissue-resident macrophages but primarily develop from recruited bone marrow-derived monocytes. TAMs drive tumor progression through various pro-tumoral functions, including the support of metastasis, invasion, and intravasation, resistance to therapy, stem cell maintenance, immune regulation, and angiogenesis.

In particular, in solid tumors, such as breast cancer, immune cells can constitute up to 50% of the entire tumor mass, with TAMs being the most frequent immune infiltrate[47]. Initially, these infiltrating immune cells were thought to be part of the body's immune response to fight tumors, which is still proposed for tumor onset today. In these early stages, the adaptive and innate immune systems react to proliferating tumor cells and can reduce cancer incidence[82]. However, it is now widely accepted that upon tumor development, the tumor microenvironment is reprogrammed to support tumor progression, while immune-cell mediated cytotoxicity is being suppressed. Substantial clinical and experimental evidence indicate that TAMs have a significant role in tumor progression and are often associated with poor overall prognosis as well as resistance to therapy[200].

As described in detail in **section 1.2.1**, TAMs primarily originate from BMDMs, recruited through inflammatory signaling of tumor cells as well as other players within the tumor microenvironment. As shown in mouse models of breast cancer, recruited

BMDMs develop via a distinct differentiation step into TAMs (e.g., by RBPJ activity) and facilitate tumor progression[7,103,245]. However, in glioblastoma and pancreatic ductal adenocarcinoma, TAMs originate from EMPs developed in the embryonic stage's yolk sac[36,51,305] (**Fig. 1.6.b**). Nevertheless, tumors promote TAM progenitors' recruitment and induce differentiation into tumor-associated phenotypes[46,308]. Chemoattractants with a prominent role in monocyte recruitment include chemokines such as CCL2, CCL5, IL34, VEGF, and CSF1 [13,198,199], as well as components of the complement system [34].

In addition to their role as chemotactic factors, these chemokines have been shown to activate unique transcriptional programs involved in the functional skewing of macrophages towards a pro-tumoral macrophage phenotype[163]. In particular, CSF1 has been described as a potent monocyte attractant, macrophage survival factor, and activation signal, promoting immunosuppressive TAMs[244]. In addition to signals originating from tumor cells (such as CSF1 and tumor growth factor beta (TGF-β)), additional components of the tumor microenvironment, such as T-cells[74,233,277], and eosinophils (e.g., IL4 and IL13) (Kratochvill et al. 2015), as well as stromal cells (e.g., IL1 and TGF-β) can secrete factors associated with the skewing and subversion of macrophage functions[168]. An essential role of the Th2 environment, including chemokines and growth factors such as IL4, CSF2, TGFB1, and ARG1, has been shown to contribute to an immunosuppressive reprogramming of TAMs[74,117,287]. Overall, distinct pathways of TAM reprogramming between different tumor entities and subtypes have been described.

A diversity of TAM functions supporting tumor development, including the promotion of angiogenesis, tissue invasion, intravasation, and metastasis, as well as the induction of resistance to cancer therapy, stem cell maintenance, and immune regulation, have been illustrated (**Fig. 1.6.b**). For example, the secretion of growth factors such as EGF has been shown to directly stimulate cancer cells' proliferation[131]. The secretion of proteases by TAMs can cause the digestion of extracellular matrix components, promoting tumor dissemination[46]. Production of reactive oxygen and nitrogen species can cause genetic instability[34], a hallmark of cancer, which further enables resistance to chemo- and radiotherapy. Moreover, TAMs can promote an immunosuppressive phenotype of regulatory T-cells. This is possible due to the production of immunosuppressive chemokines, such as IL10 and TGF-β[186,317], as well as through the presentation of inhibitory

transmembrane proteins, such as PD-L1 [208,289,317]

The contribution of genetic and epigenetic changes as well as specific molecular pathways involved in the rewiring of cancer cells into their malignant state have been well studied. Yet, we lack an overarching view of the alterations and molecular pathways orchestrating macrophage function in tumors. So far, a prominent role has been assigned to several TFs, including STAT, NF-κB, FOS, IRF, and TFs of the bHLH TF-family [175,198]. Among the bHLH TF-family, the oncogene c-MYC has been shown to, directly and indirectly, regulate pro-tumoral genes, such as *VEGF*, *MMP9*, *HIF-1α*, and *TGF-β* in TAMs [234]. Since c-MYC is also involved in cancer cells' proliferation, it represents a promising target for tumor therapies [202,204]. Furthermore, a recent publication focusing on lung cancer showed a prominent role of β-catenin–mediated transcriptional activation of FOSL2 and repression of ARID5A in TAM reprogramming [264].

Despite the accepted function of epigenetic regulation in macrophage development and inflammation, its role in TAM reprogramming is not well understood. A comprehensive appreciation of alterations in the DNA methylation landscape, and the functional consequences of TAM reprogramming, are urgently needed to drive the development of prognostic and diagnostic markers, as well as anti-cancer therapies reversing the tumor-promoting functions of TAMs in breast cancer.

2

Aims

Apart from their diverse functions in health, macrophages have a pivotal role in many inflammatory and non-inflammatory diseases. Due to their immense plasticity, macrophages can respond to various signals within their tissue niche. Understanding the epigenetic and gene-regulatory mechanism of macrophage reprogramming in response to an altered microenvironment may enable improved prognosis and treatment of patients with various diseases. The present thesis aimed to comprehensively characterize the epigenome of macrophages and monocytes in muco-obstructive lung disease and breast cancer, two chronic diseases with a worldwide health burden. Additionally, we evaluated how these epigenetic alterations and coinciding transcriptional programs influence macrophage-specific phenotypes and functions.

2.1 Investigating the epigenetic reprogramming of airway macrophages in muco-obstructive lung disease

Many chronic lung diseases, such as CF and COPD, are characterized by mucus obstruction and airway inflammation, although their mechanistic link remains largely elusive [35,92,347]. The first part of the present thesis focused on the role of the mucostatic airway microenvironment on epigenetic reprogramming of AMs and resulting transcriptomic and phenotypic changes. Therefore, the *Scnn1b*-Tg mouse, sharing critical features with CF and COPD, such as mucus plugging, emphysema-like structural lung damage, and chronic airway inflammation, was utilized [106,164,187,197,259]. The primary aims were:

1. Identify and characterize genome-wide alterations in the DNA methylation, chromatin accessibility, and transcriptome landscape of AMs from muco-obstructed and healthy mice.
2. Integrate epigenetic alterations with gene expression profiles to investigate models of macrophage activation.
3. Examine heterogeneity of macrophage activation on the level of single-cell surface markers.
4. Investigate monocyte recruitment to the muco-obstructed lung.
5. Test the function of mucus per se as an immunomodulatory stimulus of AMs.
6. Investigate functional impairment of AMs from muco-obstructive lungs by testing their efferocytosis and phagocytosis capacities.
7. Compare LPS responses on the level of chromatin accessibility, gene, and protein expression in AMs from *Scnn1b*-Tg, *Cftr*$^{-/-}$, and wild type (WT) mice.

The characterization and understanding of phenotypical and functional changes in AMs regarding the underlying epigenetic and transcriptomic mechanisms will support therapeutic approaches in patients with muco-obstructive lung disease.

2.2 Determining the cancer-specific DNA methylation landscape of tumor-associated macrophages and monocytes in breast cancer

In the tumor microenvironment of breast cancer, TAMs are the most frequent immune cell infiltrates[47]. They can regulate primary tumor growth, vascularization, metastatic spread, and tumor therapy[47,200]. It has been shown that TAMs provide these tumor-promoting functions by a unique transcriptome and phenotype compared to healthy references, making them an attractive target for novel therapeutic approaches[46,264,308]. However, the epigenetic mechanisms involved in TAM reprogramming are not well studied and were the central objective of the second part of this thesis. The 4T1 orthotopic breast cancer mouse model was utilized to isolated macrophage and monocyte populations from the breast and bone marrow. Specific aims included:

1. Identify and characterize genome-wide alterations in the DNA methylation and transcriptome profiles of macrophages and monocytes in breast cancer.
2. Dissect the epigenetic reprogramming of TAMs into BMDM-derived and TAM-specific changes.
3. Integrate epigenetic alterations with gene expression profiles to define DNA methylation-dependent gene expression changes.
4. Identify and characterize cancer-specific transcriptional alterations and define transcriptional immune signatures as prognostic and diagnostic markers for breast cancer patients.
5. Investigate cell-to-cell interactions within the tumor microenvironment that drive epigenetic reprogramming of TAMs.
6. Deconvolute DNA methylation profiles and define a TAM DNA methylation signature as a prognostic and diagnostic marker for patient stratification.

The resulting epigenetic and transcriptional blueprint of macrophages and monocytes in breast cancer will significantly impact the understanding of TAM reprogramming and indicate relevant signaling pathways, therapeutic approaches, as well as prognostic markers.

3 Results

3.1 Epigenetic reprogramming of airway macrophages drives polarization and inflammation in muco-obstructive lung disease

3.1.1 Airway macrophages from mice with muco-obstructive lung disease are epigenetically distinct

AMs exhibit a high level of plasticity, and recent studies indicate that the lung microenvironment plays an essential role in shaping the epigenetic landscape of tissue-resident AMs. In the present thesis, we investigated DNA methylation (tWGBS), chromatin accessibility (ATACseq), and gene expression (RNA sequencing (RNAseq)) of AMs to improve our understanding of the function of the muco-obstructive airway microenvironment on the epigenetic landscape of AMs and its role in the regulation of gene

expression (**Fig. 3.1.a**).

AMs were isolated from *Scnn1b*-Tg and WT mice by fluorescence-activated cell sorting (FACS) (**Fig. 3.1.b**). Sorted cells reached >95% purity as confirmed by back-sorting. No differences between the total number of AMs from *Scnn1b*-Tg and WT lungs were observed (**Fig. 3.1.c**). We further stained AMs from *Scnn1b*-Tg and WT mice with fluorescently labeled antibodies against SCNN1B and the macrophage-specific receptor MerTK to show that transgenic overexpression of *Scnn1b*, under the control of the club cell secretory protein (CCSP) promoter, is not present in AMs. Fluorescence microscopy analysis confirmed the absence of SCNN1B in *Scnn1b*-Tg and WT MerTK$^+$ AMs. In comparison, cultured murine tracheal epithelial cells (mTEC), used as controls, showed a strong signal for SCNN1B (**Fig. 3.1.d**). Consequently, alterations in the epigenome and transcriptome of AMs from muco-obstructive lungs can be attributed to an altered airway microenvironment of *Scnn1b*-Tg mice.

tWGBS provided robust DNA methylation profiles at single CpG resolution, as shown by following quality control criteria. A merged genome-wide CpG coverage of at least 15x per group, a coverage of >95% of all CpGs, and a bisulfite conversion rate, as determined by CH (where H corresponds to adenine, thymine, or cytosine) methylation levels of chromosome 19, of >98%, were observed. As expected for homogenous cell populations, global DNA methylation analysis revealed a similar bimodal β-value distribution in *Scnn1b*-Tg and WT AMs (**Fig. 3.1.e**). No genome-wide DNA methylation changes (average CpG β-value =0.73) were observed, comparing both genotypes.

To define discrete alterations of DNA methylation, differential methylation analysis between *Scnn1b*-Tg and WT AMs was performed and revealed 1,926 differentially methylated regions (DMRs, **Fig. 3.2.a**). These DMRs were associated with 1,625 genes, and the majority (1,404) showed hypomethylation in *Scnn1b*-Tg AMs. The comparison of chromatin accessibility at identified ATACseq peaks revealed 390 differentially accessible regions (DARs) associated with 312 genes (**Fig. 3.2.d**). The majority of them showed increased accessibility in *Scnn1b*-Tg AMs (339 DARs). As expected, hierarchical clustering of the identified epigenetic alterations segregated AMs according to their genotypes (**Fig. 3.2.b** and **c**), confirming *Scnn1b*-Tg specific modifications in the DNA methylation and chromatin accessibility landscape. Region overlap and enrichment analysis of DMRs revealed

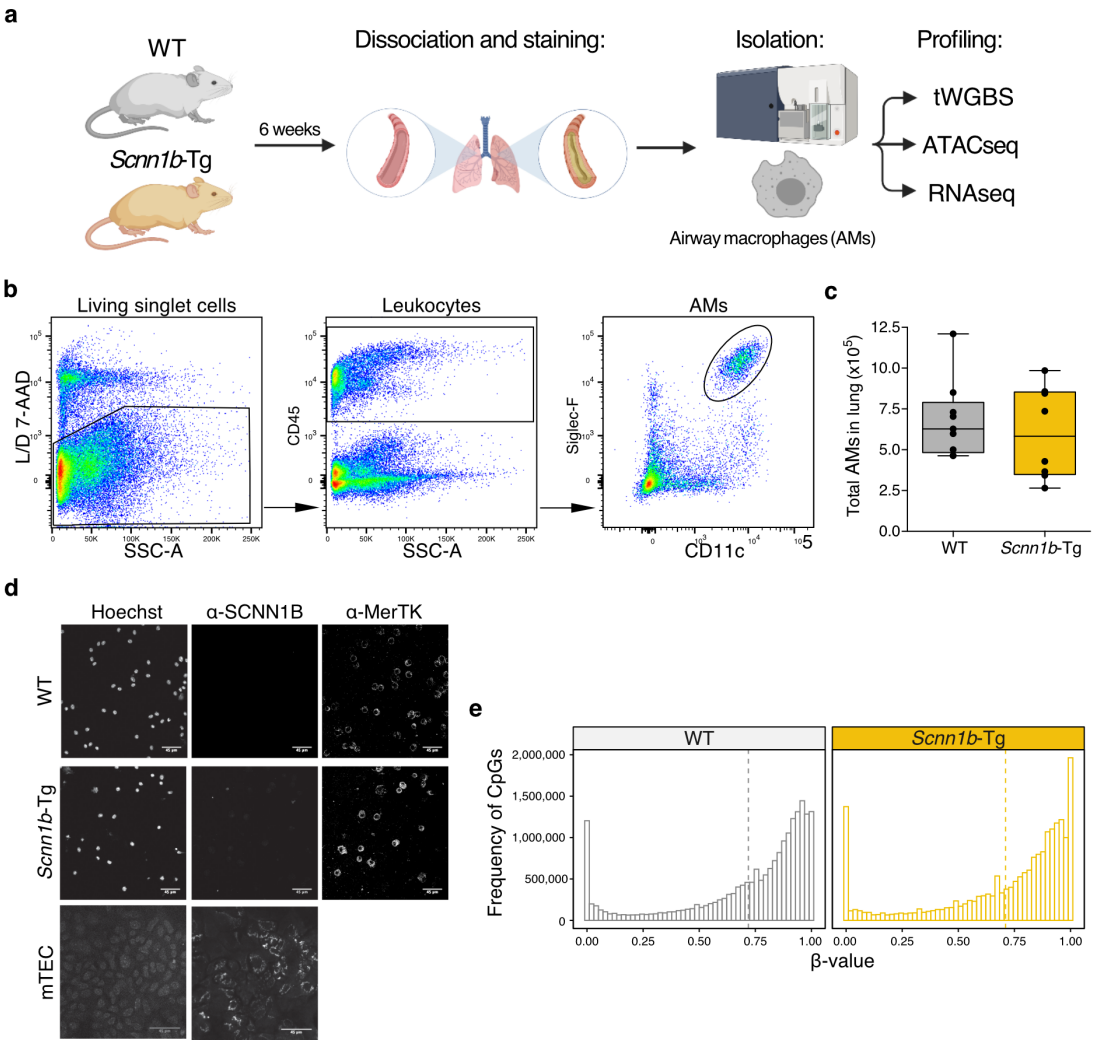

Figure 3.1: Purified AMs from muco-obstructive mice do not overexpress *Scnn1b*-Tg. (**a**) Graphical representation of the experimental workflow to characterize the epigenome (tWGBS and ATACseq) and transcriptome (RNAseq) of *Scnn1b*-Tg and WT AMs. (**b**) Gating strategy for sorting of AMs from dissociated lungs. (**c**) Quantification of the total number of AMs in the lung of *Scnn1b*-Tg and WT mice. The data show mean ±SEM of n =8-9 for each group. (**b**) Representative images of SCNN1B and MerTK expression on AMs and mTECs by immunofluorescence microscopy (n =3). (**e**) Histogram of the β-value distribution and mean DNA methylation levels in *Scnn1b*-Tg (n =3) and WT AMs (n =4).

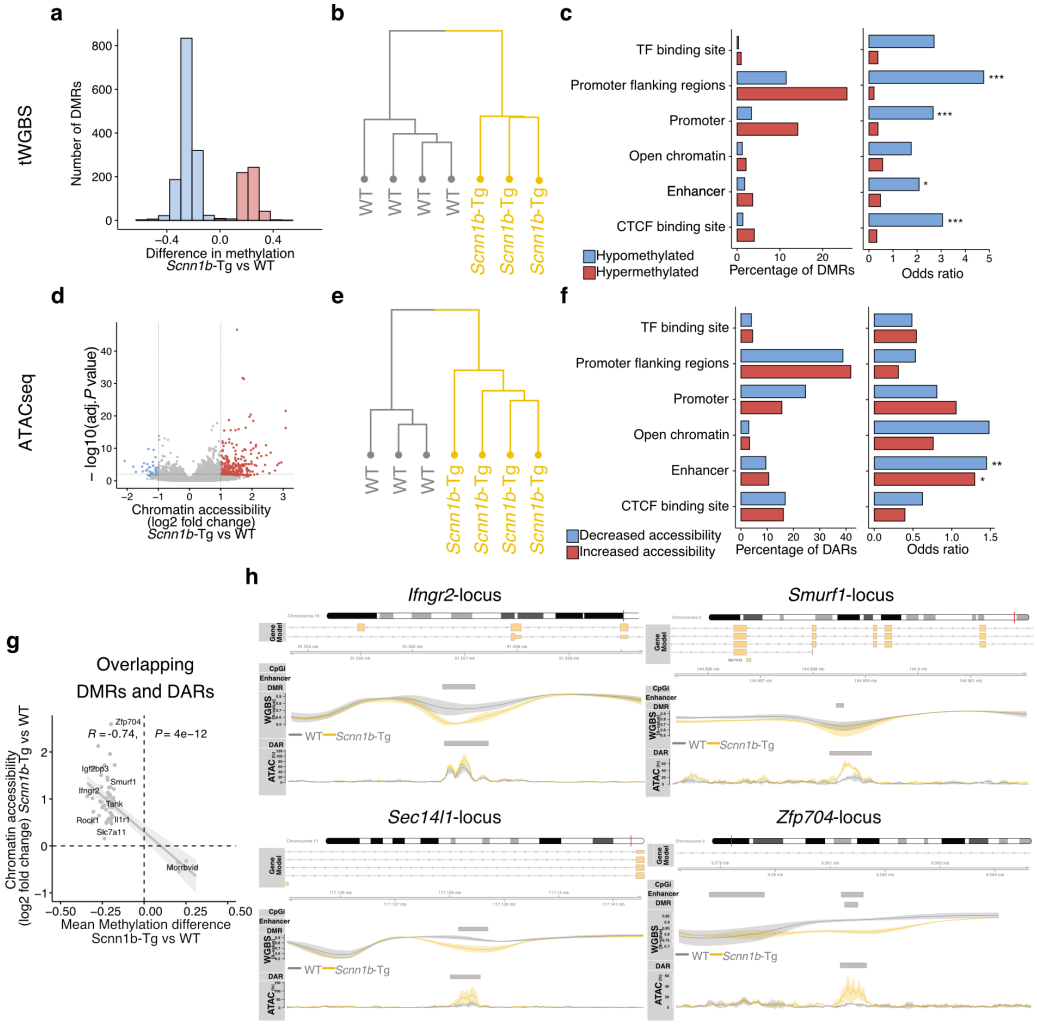

Figure 3.2: AMs from mice with muco-obstructive lung disease are epigenetically distinct from WT AMs. (**a**) Distribution of DNA methylation differences in *Scnn1b*-Tg (n =3) vs WT AMs (n =4) DMRs. DMRs are defined by at least three CpGs with adjusted *P* value <0.05, width of >50 bps, and an average change of DNA methylation >0.1. (**b** and **e**) Hierarchical clustering based on (**b**) DMRs methylation and (**e**) DARs accessibility. (**d**) Volcano plot of the differential chromatin accessibility analysis of *Scnn1b*-Tg (n =4) vs WT AMs (n =3). DARs are defined by an adjusted *P* value <0.05 and absolute log2 fold change >1. Red dots: DARs with increased accessibility in *Scnn1b*-Tg AMs; blue dots: DARs with reduced accessibility in *Scnn1b*-Tg AMs. (**c** and **f**) Annotation and enrichment of (**c**) DMRs and (**f**) DARs to gene regulatory regions stratified in hypo- and hypermethylated DMRs, and open and closed DARs, respectively. LOLA enrichment analysis: *, *P* value <0.05; **, *P* value <0.01; ***, *P* value <0.001. (**g**) Integrated analysis of overlapping DARs and DMRs. *P* values were calculated by Pearson correlation coefficient. The gray diagonal represents the linear regression. Shaded areas are the confidence interval of the correlation coefficient at 95%. (**h**) Locus plots of selected DMRs and DARs showing average DNA methylation and chromatin accessibility of *Scnn1b*-Tg and WT AMs. Shaded areas indicate 95% confident intervals. The gray boxes indicate CGis, enhancers, DMRs, and DARs (from top to bottom).

hypomethylated DMRs enriched in promoters, promoter flanking regions, enhancers, and CTCF-binding sites (**Fig. 3.2.c**). DARs depicted a similar pattern of enrichment in enhancers and open chromatin regions (**Fig. 3.2.f**), highlighting a potential gene-regulatory role of the identified epigenetic alterations.

To elucidate the interconnection of decreased DNA methylation and open chromatin and vice versa, an integrated analysis of DMRs and DARs was performed. 63 overlapping regions were identified that showed a strong inverse correlation (**Fig. 3.2.g**; Pearson correlation: R= -0.74; P value <0.001). These regions included coherently hypomethylated loci with increased accessibility in *Scnn1b*-Tg AMs that were associated with 58 genes. Amongst others, genes involved in cytokine signaling, such as *Il1r1*, *Tank*, and *Smurf1*, were identified. Additionally, multi-omics integration depicted genes like *Infgr2*, *Zfp704*, and *Sec14l*, previously associated with chronic lung diseases (**Fig. 3.2.g** and **h**)[41,239,241].

To address the functional significance of the identified DMRs and DARs on TF binding and their role in gene regulation, we characterized *Scnn1b*-Tg-specific alterations in the epigenome for enrichment in TF binding motifs. Regions with decreased DNA methylation and increased chromatin accessibility in *Scnn1b*-Tg AMs were enriched for TF motifs with a known role in inflammatory responses and macrophage polarization. For example, highly enriched motifs for the TFs C/EBP, IRF2, IRF3, and STAT6 were identified in hypomethylated *Scnn1b*-Tg vs WT DMRs (**Fig. 3.3.a**) and motifs for the inflammation-associated TFs JUNB, FRA1, NFκB-p65 (RELA), as well as the M2 polarizing TF ATF3 in DARs with increased accessibility in *Scnn1b*-Tg compared WT AMs (**Fig. 3.3.b**)[37,80,97,126,272]. Furthermore, we were interested in potential regulators of the observed changes in chromatin accessibility. Upstream regulator analysis identified cytokines, such as TGF-β, TNF-α, IFN-γ, IL-4, and bacterial-derived LPS, as activators in *Scnn1b*-Tg AMs. These upstream regulators confirm the abovementioned TFs (**Fig. 3.3.a** and **b**) involved in their signaling pathways[201].

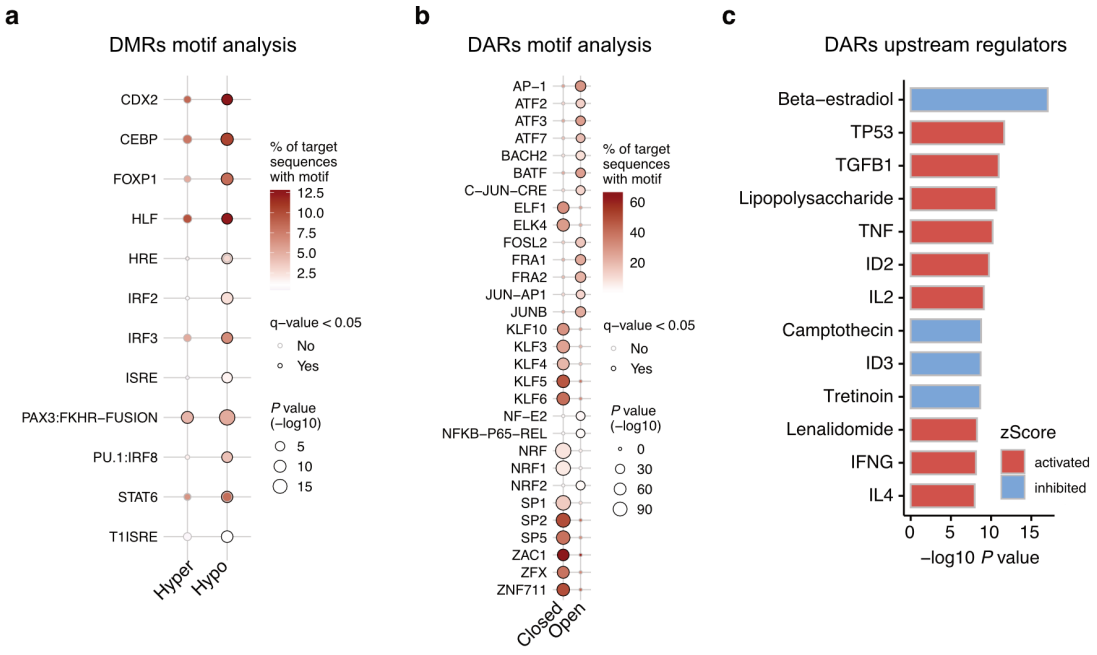

Figure 3.3: Epigenetic alterations in *Scnn1b*-Tg AMs are associated with inflammatory responses and macrophage polarization. (**a** and **b**) Motif enrichment of (**a**) DMRs and (**b**) DARs (adjusted *P* value <0.05) stratified in hypo- (hypo) and hypermethylated (hyper) DMRs and DARs with decreased (closed) and increased (open) accessibility in *Scnn1b*-Tg vs WT AMs, respectively. (**c**) Upstream regulator analysis of chromatin accessibility changes.

3.1.2 Epigenetic patterns of reduced DNA methylation and increased chromatin accessibility coincide with transcriptional activation of *Scnn1b*-transgenic airway macrophages

DNA methylation, chromatin accessibility, and TF binding are key regulators of gene expression. To examine the effect of the identified epigenetic changes on the transcriptional activity of AMs from muco-obstructive lungs, RNAseq of *Scnn1b*-Tg and WT AMs was performed.

Unsupervised hierarchical clustering of the gene expression profiles segregated *Scnn1b*-Tg and WT AMs (**Fig. 3.4.a**), suggesting an interconnection of gene expression, DNA methylation, and chromatin accessibility in AMs. Overall, differential gene expression analysis comparing *Scnn1b*-Tg with WT AMs, revealed 117 upregulated and 46 downregulated differentially expressed genes (DEGs) (**Fig. 3.4.b**). Loss of DNA methylation

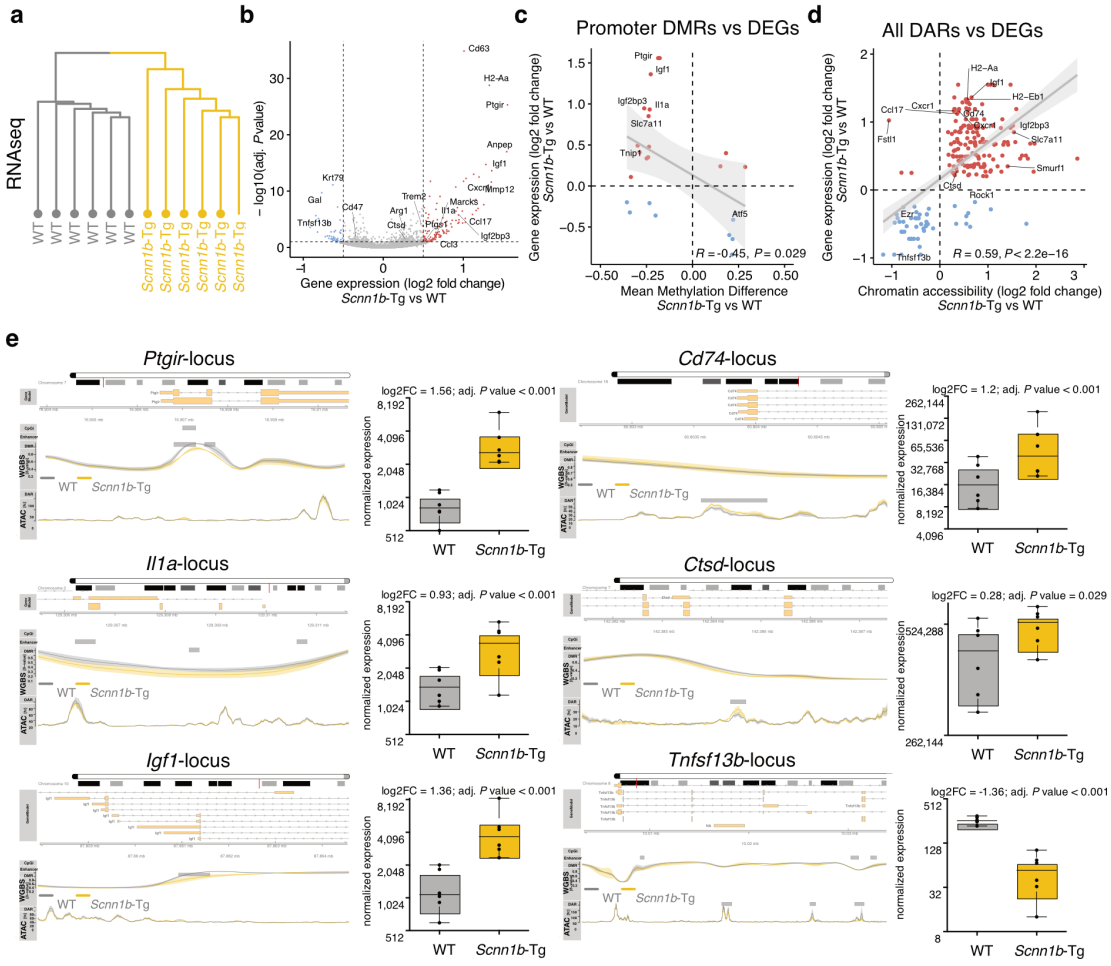

Figure 3.4: Epigenetic patterns of reduced DNA methylation and increased chromatin accessibility coincide with transcriptional activation of *Scnn1b*-Tg AMs.(**a**) Unsupervised hierarchical clustering of gene expression in *Scnn1b*-Tg and WT AMs (n =6). (**b**) Volcano plot of differential gene expression analysis. DEGs are defined by an adjusted *P* value <0.1, absolute log2 fold change >0.5. Red dots: increased expression in *Scnn1b*-Tg AMs; blue dots: reduced expression in *Scnn1b*-Tg AMs. (**c**) Integrated visualization of gene expression and promoter DNA methylation changes. DNA methylation differences of promoter DMRs (<5kbs from transcriptional start sites) vs gene expression changes of the corresponding DEGs (adjusted *P* value <0.1). *P* values were calculated by Pearson correlation coefficient. The gray diagonal represents the linear regression. Shaded areas are the confidence interval of the correlation coefficient at 95%. (**d**) Integrated analysis of chromatin accessibility and gene expression changes. Log2 fold change of DARs (adjusted *P* value <0.05) and DEGs (adjusted *P* value <0.1). *P* values were calculated by Pearson correlation coefficient. The The gray diagonal represents the linear regression. Shaded areas are the confidence interval of the correlation coefficient at 95%. (**e**) Locus plots of selected DMRs and DARs showing average DNA methylation and chromatin accessibility of *Scnn1b*-Tg and WT AMs. Shaded areas indicate 95% confident intervals. The gray boxes indicate CGis, enhancers, DMRs, and DARs (top to bottom). Normalized gene expression for the respective genes is plotted alongside the locus plots. *P* values were determined by differential gene expression analysis with DESeq2.

at promoter DMRs was associated with increased gene expression levels. In contrast, a gain of DNA methylation was commonly associated with decreased transcription. An overall inverse correlation (Pearson correlation: R =-0.45; P value <0.05) of promoter methylation and gene expression was shown (**Fig. 3.4.c**). For chromatin accessibility, the reverse pattern was observed. DARs with increased accessibility were associated with increased gene expression and vice versa. An overall positive correlation (Pearson correlation: R =0.59; P value <0.001) was shown for DARs annotated to the closest gene (**Fig. 3.4.d**). Interleukin 1 alpha (*Il1a*) and insulin-like growth factor 1 (*Igf1*) were two prominent examples of promoter hypomethylation with increased gene expression in *Scnn1b*-Tg AMs. *Il1α* is a cytokine that has previously been shown to contribute to sterile inflammation and tissue damage in children with CF[12,31,106,211]. *Igf1* is a pleiotropic growth factor linked to lung formation, tissue remodeling, and inflammation in a variety of lung diseases such as CF, COPD, asthma, and acute lung injury (**Fig. 3.4.c-e**)[321]. Furthermore, genes associated with macrophage polarization (*Cd17*, *Cxcr1*, *H2-Aa*, *H2-Ab1*), inflammation (*Ezr*, *CD74*), and remodeling (*Ctsd*) were identified by the integration of chromatin accessibility and gene expression (**Fig. 3.4.d** and **e**). In macrophages, *Ezr* (ezrin) is required for Toll-like receptor (*TLR*) 4-mediated LPS signaling and bacterial host defense[75]. Cathepsin D (*Ctsd*) is associated with emphysema in smoke models[344], and the AM surface marker *Cd74* contributes to neutrophil aggregation in the airways[295].

Notably, changes in DNA methylation or chromatin accessibility did not always correlate with gene expression, showing the complex interaction of certain epigenetic marks and transcription. DNA methylation does not always act as a repressive mark, and induction of gene expression is not always guaranteed for genes associated with open cis-regulatory regions. These results support the view that epigenetic patterns do not necessarily translate into transcriptional regulation but rather facilitate the recruitment of additional factors that can induce or repress gene expression.

3.1.3 Airway macrophages from muco-obstructive lungs are activated and proinflammatory

To assess the biological significance of the identified transcriptional changes, we performed pathway and gene ontology enrichment analysis using the 163 *Scnn1b*-Tg vs WT DEGs. This analysis revealed an overrepresentation of gene ontology terms associated with migration (e.g., leukocyte migration and cell migration regulation), immune processes (e.g., chemokine signaling pathway, neutrophil degranulation, and cytokine production), and tissue remodeling (**Fig. 3.5.a**) – all previously identified hallmarks of the *Scnn1b*-Tg mouse model and muco-obstructive lung diseases [106,197,306,347].

We further applied gene sets, relevant for lung diseases and cell physiology to obtain a comprehensive impression of the complex biological pathways implicated in AM alterations [261]. Gene set enrichment analysis (GSEA) showed the enhanced activation of pathways associated with AM activation, plasticity, and adaptation to environmental perturbations or disease pathogenesis (**Fig. 3.5.b**). Frequently, these pathways are deregulated in chronic diseases, such as cancer [341], atherosclerosis [284], or rheumatoid arthritis [108]. In detail, both M1 and M2 macrophage activation signatures were upregulated in *Scnn1b*-Tg compared to WT AMs. Besides, gene sets derived from human expression signatures of different muco-obstructive lung diseases, such as CF, COPD, and asthma, were strongly enriched in the gene expression profile of *Scnn1b*-Tg AMs. Differential expression of M1- and M2-polarization markers (e.g., M1: *Ptgir*, *Cd86*; M2: *Arg1*, *Mmp12*, *Ccl17*, *Cxcr1*, *Ccl22*, *Trem2*, *Ptgs1*) and genes implicated in muco-obstructive diseases were independently verified by qPCR (**Fig. 3.5.c**). Similar to the upstream regulator analysis of chromatin accessibility, activators involved in the induction of both type I (LPS, TNF, IFN-γ) and type II immunity (IL-4) were identified as upstream regulators of *Scnn1b*-Tg vs WT AM gene expression changes. Additionally, IFNAR, IKBKB, and IL-1β were identified as activators of *Scnn1b*-Tg AMs (**Fig. 3.5.d**).

Together, these results suggest that the muco-obstructive microenvironment drives epigenetic changes on both DNA methylation and chromatin accessibility level. Moreover, a strong association between epigenetic changes and transcriptional activation of *Scnn1b*-Tg AMs, affecting immune processes and tissue remodeling, was observed.

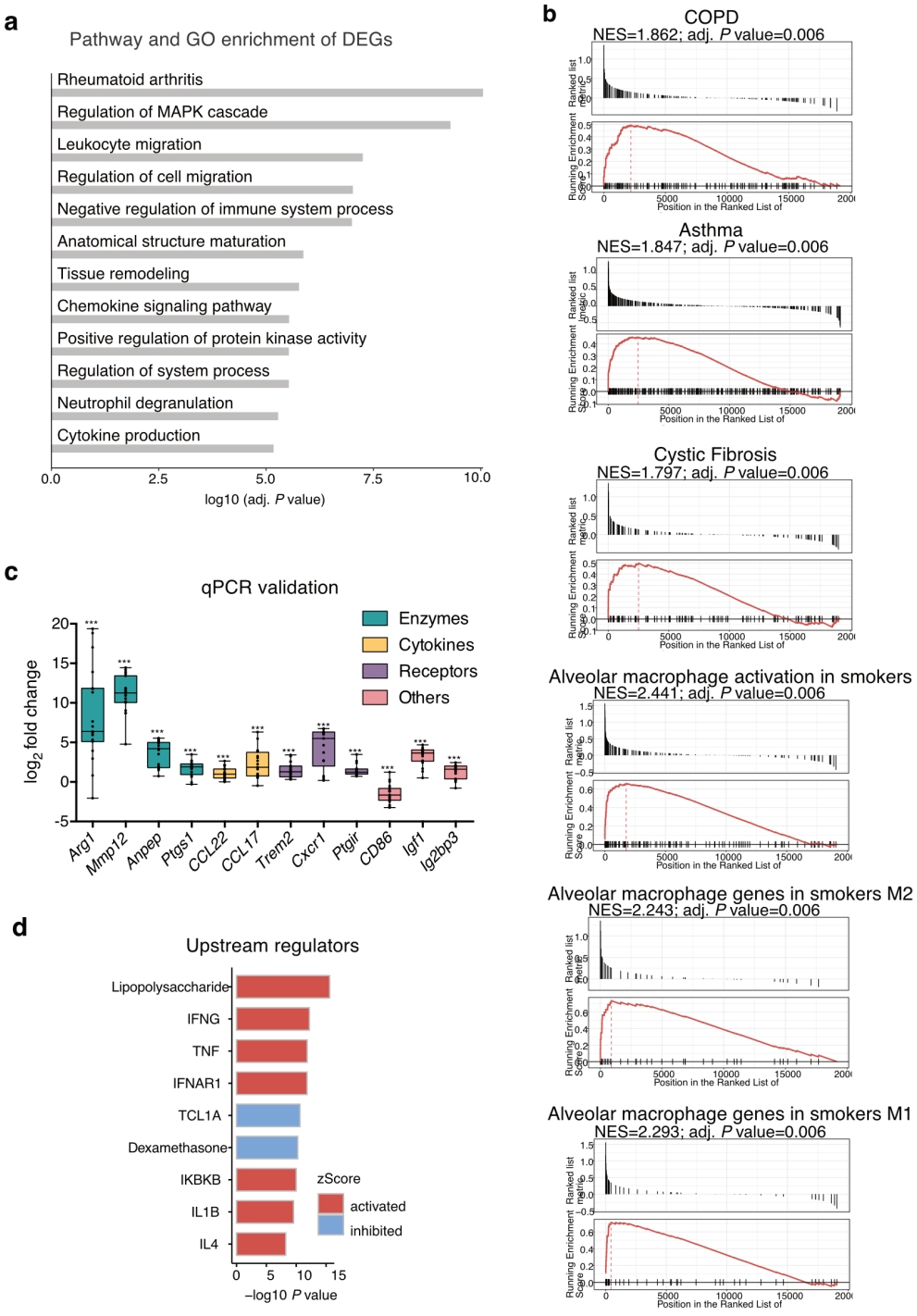

Figure 3.5: Transcriptome of *Scnn1b*-Tg AMs is enriched for proinflammatory pathways and macrophage polarization.

Figure 3.5: Transcriptome of *Scnn1b*-Tg AMs is enriched for proinflammatory pathways and macrophage polarization. (**a**) Overrepresentation analysis of *Scnn1b*-Tg vs WT AMs DEGs (adjusted *P* value <0.1, absolute log2 fold change >0.5) with pathways and gene ontologies. (**b**) Barcode plots of significantly enriched gene sets in *Scnn1b*-Tg AMs. Gene sets relevant to lung diseases and cellular physiology are defined by Saini et al., 2014. NES: normalized enrichment score. (**c**) qPCR validation of *Arg1*, *Mmp12*, *Anpep*, *Ptgs1*, *Ccl22*, *Ccl17*, *Trem2*, *Cxcr1*, *Ptgir*, *Cd86*, *Igf1*, and *Ig2bp3* gene expression changes. The data show log2 fold change ±SEM of n =17-20 per group. Unpaired, two-tailed Mann-Whitney U test: *, *P* value <0.05; **, *P* value <0.01; ***, *P* value <0.001. (**d**) Upstream regulator analysis of *Scnn1b*-Tg vs WT AMs gene expression changes.

Next, we validated the enhanced activation of AMs from muco-obstructive mice and addressed the question of AM heterogeneity on a single-cell level. Therefore, we stained cell type-specific markers (CD45.2, Siglec-F, CD11c, CD64, MerTK, and CD163), in addition to macrophage activation markers (M1: CD11b, CD86, MHCII, CD68, and CD38; M2: CD206, CD163, CD200R, CD209A, MGL2, and CLEC7A), and performed high-dimensional flow cytometry of *Scnn1b*-Tg and WT lungs. Quantification of the surface markers revealed an increased frequency of $CD11b^+$ and $MHCII^+$ AMs in *Scnn1b*-Tg compared to WT lungs (**Fig. 3.6.a** and **b**). To further distinguish different populations of the innate and adaptive immune response, uniform manifold approximation and projection (UMAP) was performed on gated leukocytes (**Fig. 3.6.c**). No cluster of cells unique for *Scnn1b*-Tg or WT lungs was identified. However, differential surface marker expression showed the downregulation of Siglec-F and upregulation of CLEC7a, CD11b, and CD68 on *Scnn1b*-Tg compared to WT AMs (**Fig. 3.6.d**).

To further assess AM heterogeneity, we divided *Scnn1b*-Tg and WT AMs into four sub-clusters and investigated their surface marker expression (**Fig. 3.6.e**). Notably, all sub-clusters were contributed by *Scnn1b*-Tg and WT AMs and represented by M1 and M2 activation markers (**Fig. 3.6.f**), indicating a mixed phenotype of AMs. An exclusive presentation of MHCII was shown for cluster 4, and cluster 1 was represented by CD163 expressing AMs. According to the overall increase of $MHCII^+$ AMs in the lungs of *Scnn1b*-Tg mice, an increased abundance of cluster4 AMs was observed in *Scnn1b*-Tg lungs (**Fig. 3.6.g**).

Collectively, these results confirm an increased activation of AMs in muco-obstructive disease and show a mixed phenotype of AMs. They further support the idea that in vivo macrophage phenotypes are multidimensional and cannot be categorized into binary states[201,331].

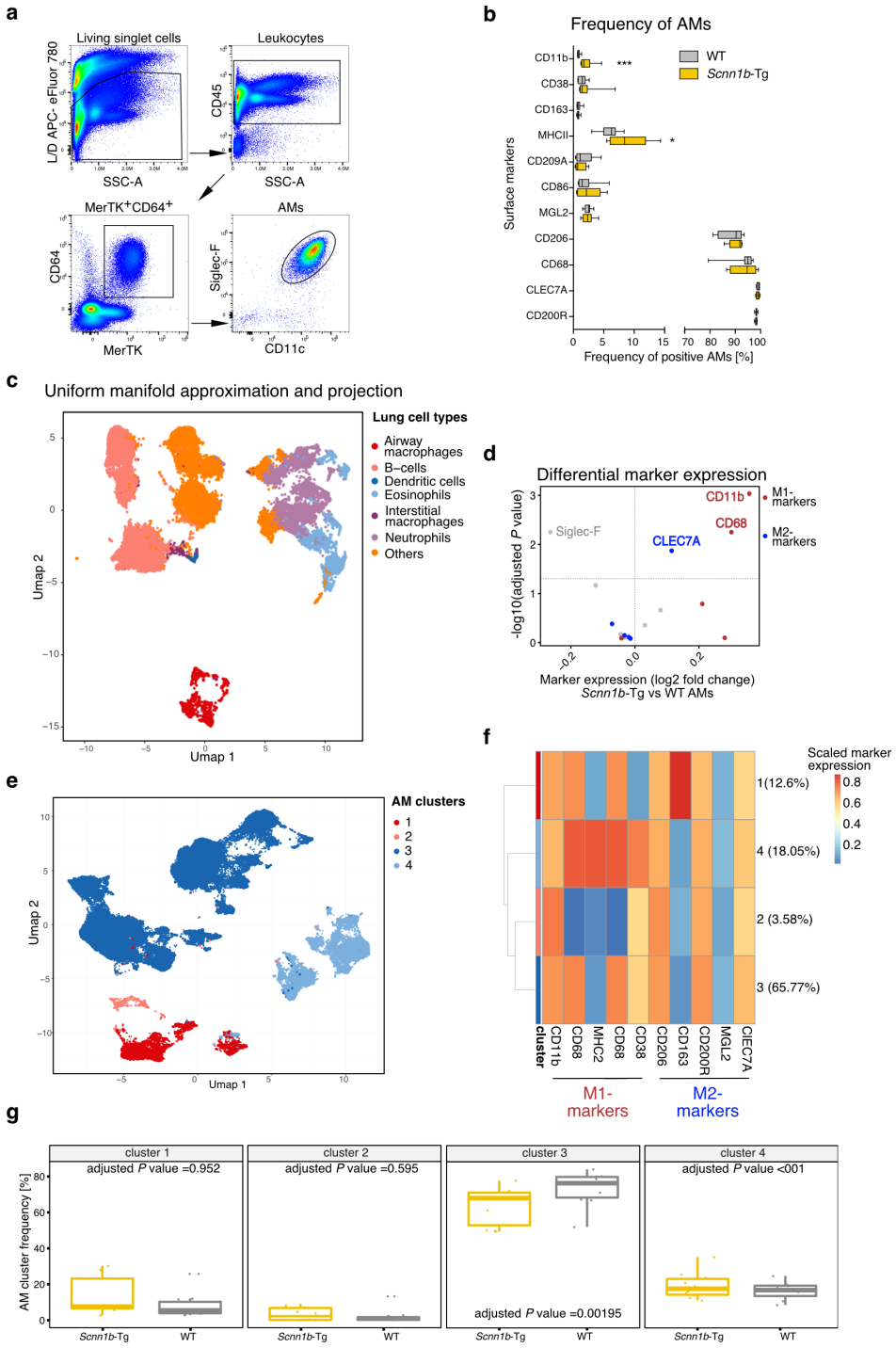

Figure 3.6: Single-cell analysis of macrophage surface marker expression validates enhanced activation of *Scnn1b*-Tg AMs.

Figure 3.6: Single-cell analysis of macrophage surface marker expression validates enhanced activation of *Scnn1b*-Tg AMs. (**a**) Gating strategy to identify leukocytes and AMs from *Scnn1b*-Tg and WT dissociated lungs. (**b**) Frequency of AMs with indicated surface marker expression, defined by back gating. The data show mean ±SEM of n =10 per group. Unpaired, two-tailed Mann-Whitney U test: *, *P* value <0.05; **, *P* value <0.01; ***, *P* value <0.001. (**c**) UMAP of 50,000 randomly sampled *Scnn1b*-Tg and WT leukocytes. (**d**) Differential surface marker expression of *Scnn1b*-Tg vs WT AMs, defined by cluster analysis. Red dots: surface markers for classical macrophage polarization (M1); blue dots: surface markers for alternative macrophage polarization (M2). (**e**) UMAP of 50,000 randomly sampled *Scnn1b*-Tg and WT AMs. (**f**) Scaled M1 and M2 surface marker expression of AM clusters. (**g**) Differential AM cluster abundance. *P* values were generated by fitting a linear model. n =10 per group.

3.1.4 Monocytes do not contribute to the macrophage pool in muco-obstructive lungs

Most tissue-resident macrophage populations, including AMs in the lung, are self-renewing. They arise from fetal progenitors and require minimal input from monocytes in homeostasis[124,134]. However, in response to inflammation and macrophage depletion, monocytes can be recruited to the lung, where the microenvironment eventually shapes them into cells that closely resemble tissue-resident AMs[173,335].

We applied a computational deconvolution method to evaluate if recruited monocytes play a substantial role in muco-obstructive lung disease and constitute the AM pool. Multi-Subject Single-Cell deconvolution (MuSiC) allows the characterization of cell type compositions from bulk RNAseq data by utilizing cell type-specific gene expression from single-cell RNAseq (scRNAseq) references[320]. First, we used macrophage and monocyte populations from the single-cell atlas of the aging lung as a reference[5]. As observed by the flow cytometry analysis in **Fig. 3.1**, deconvolution revealed a homogenous cell type composition of above 99% AMs in all samples (**Fig. 3.7.a**). No differences between *Scnn1b*-Tg and WT AMs were observed. To exclude potential biases in the cell type estimation by only using a reference of homeostatic lungs, we further utilized a scRNAseq dataset that characterized the inflammatory macrophage heterogeneity on a single-cell level[214]. Mould et al. collected AMs during health, peak inflammation, and resolution of inflammation. In doing so, the authors defined fetal-derived tissue-resident AMs (enriched in clusters 1 and 2) and bone marrow-derived recruited AMs (enriched in clusters 3, 4, and 5). Deconvolution of our bulk RNAseq data showed a homogenous composition of all our *Scnn1b*-Tg and WT samples of cluster 1 tissue-resident AMs (**Fig. 3.7.b**).

Finally, comparison of *Scnn1b*-Tg vs WT AMs gene expression changes with transcriptional alterations of fetal-derived tissue-resident vs recruited bone-marrow-derived AMs, generated in a bleomycin-induced lung fibrosis model[209], showed no correlation (Pearson correlation: R =0.03) and a neglectable overlap of differentially expressed genes (**Fig. 3.7.c**).

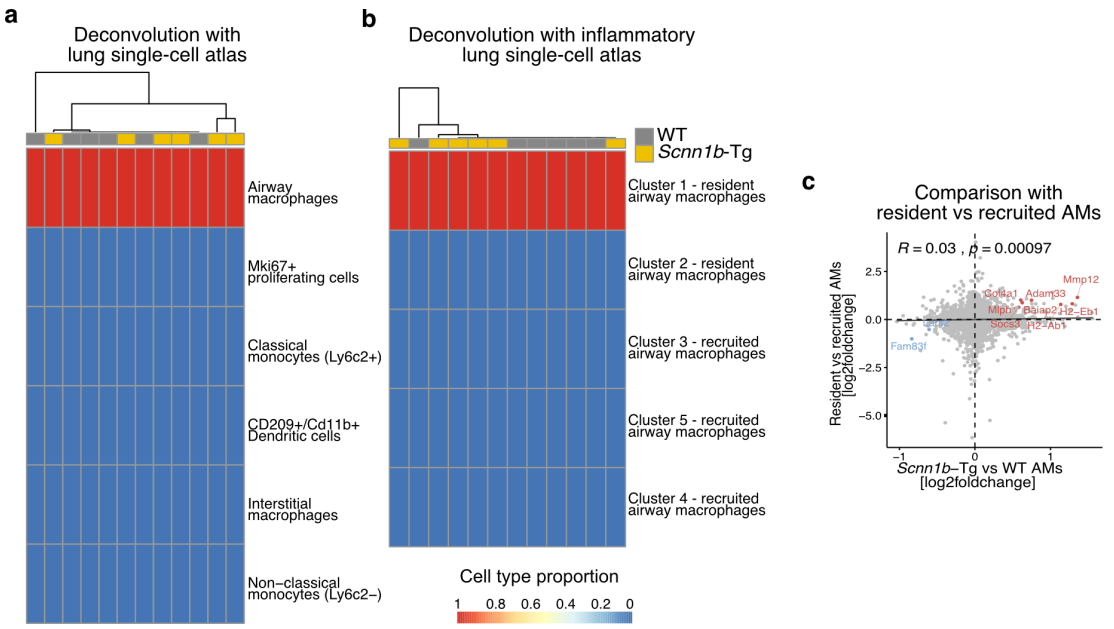

Figure 3.7: Monocytes do not replenish AMs in muco-obstructive lungs. (**a** and **b**) Deconvolution of *Scnn1b*-Tg and WT AM bulk transcriptomes with (**a**) scRNAseq of macrophage and monocyte populations, selected from the single-cell atlas of the aging lung and (**b**) scRNAseq of AM clusters, identified in homeostatic and inflammatory mouse lungs, reflecting the cellular origin of AMs. (**c**) Comparison of gene expression changes in *Scnn1b*-Tg vs WT AMs with resident vs recruited AMs, identified in Misharin et al., 2017. Red dots: significant upregulation in both datasets; blue dots: significant downregulation in both datasets. P values were calculated by Pearson correlation coefficient. The gray diagonal represents the linear regression. Shaded areas are the confidence interval of the correlation coefficient at 95%.

Overall, these results indicate that monocyte-derived AMs play an insignificant role in the *Scnn1b*-Tg mouse model. In case monocyte recruitment to the muco-obstructive lung has taken place at an earlier time point, the differences with fetal-derived tissue-resident AMs are not detectable anymore and don't contribute to the activated state of AMs in the muco-obstructed lung.

3.1.5 Mucus stimulates immune responses in airway macrophages

Various stimuli in the airway can potentially alter the phenotype of macrophages and cause epigenetic and transcriptional changes[110,113,121,177]. We stimulated primary AMs from WT mice with multiple concentrations and durations of native mucus to test its effect on macrophage activation. Therefore, the expression of genes associated with AM plasticity (*Ccl22*, *Ccl17*, *Mmp12*, and *Arg1*) and inflammation in chronic lung diseases (*Il1a* and *Il1b*) were evaluated 6, 12, and 24 hours (hrs) post mucus stimulation. Concentrations ranging from 0.1-10% mucus were applied. All tested genes showed induction post mucus treatment, similar to the changes detected in freshly sorted *Scnn1b*-Tg compared to WT AMs (**Fig. 3.8**). Induction of *Ccl17*, *Ccl22*, and *Il1b* gene expression was transient, with a peak 6 hrs post mucus treatment. For *Il1a* and *Mmp12*, we observed a sustained induction at most time points. Further concentration-dependent induction for *Mmp12* was shown. *Arg1* was the only gene that displayed a delayed induction with transcripts detectable 24 hrs post mucus treatment.

These results show that mucus has the direct potential to activate AMs and induce gene expression patterns involved in inflammation and macrophage polarization. Since mucus concentrations are abnormally raised in many chronic lung diseases[35], this finding has possible implications for disease pathogenesis and treatment options.

3.1.6 Muco-obstructive lung disease impairs macrophage-specific functions

To prevent the release of danger-associated molecular patterns and secondary necrosis from dying cells in chronically inflamed airways, clearance of apoptotic cells by a process called efferocytosis is indispensable[266]. To study in vivo efferocytosis capacities of *Scnn1b*-Tg and WT AMs, we performed intratracheal instillation of apoptotic cells labeled with a pH-sensitive dye (pHRodo). Under acidic conditions, as found in the lysosome of AMs, pHRodo emits fluorescence that can be measured via flow cytometry post isolation of AMs via lavage. Analysis of pHRodo-positive AMs showed a reduction in the clearance of apoptotic cells in *Scnn1b*-Tg compared to WT AMs, revealing reduced efferocytosis capacities of AMs in muco-obstructive lung disease (**Fig. 3.9.a**).

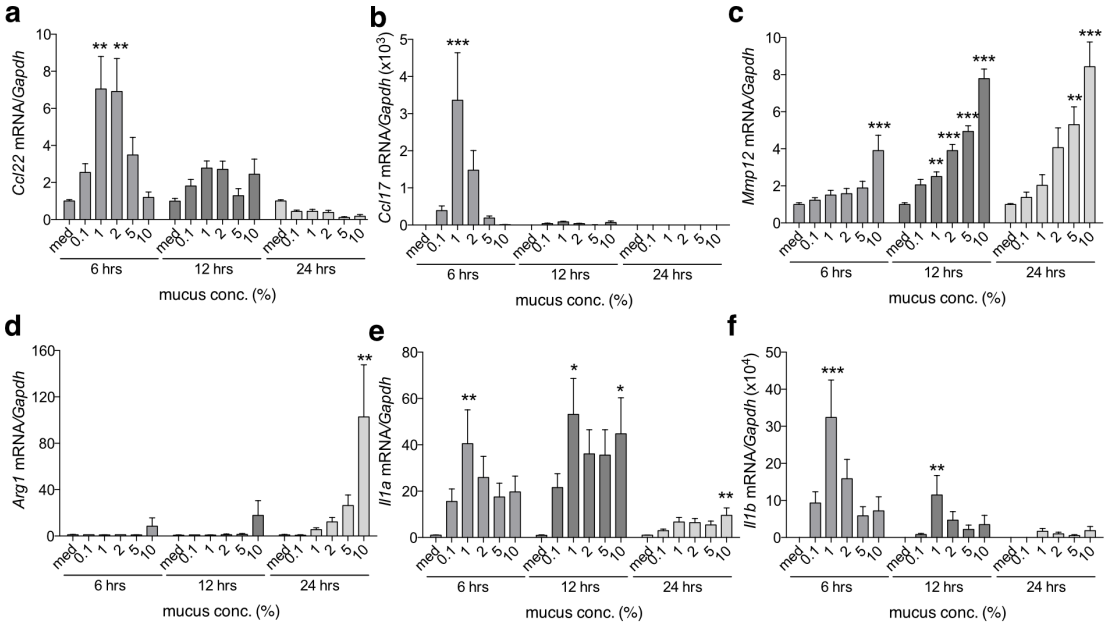

Figure 3.8: Mucus stimulates immune responses in WT AMs. (**a**-**f**) Gene expression levels of (**a**) *Ccl2*, (**b**) *Ccl17*, (**c**) *Mmp12*, (**d**) *Arg1*, (**e**) *Il1a* and (**f**) *Il1b* in WT AMs treated with incrasing mucus concentrations or medium (med) control for 6, 12 and 24 hrs, respectively. Gene expression levels were asessed via qPCR. The data show mean ± SEM of n =10 per group. One-way ANOVA with Tukey's test: *, *P* value <0.05; **, *P* value <0.01; ***, *P* value <0.001 compared to medium.

Furthermore, muco-obstructive lung disease is characterized by bacterial airway infections that can trigger acute exacerbations and heavily influence the overall rate of disease progression, including patient survival[271]. To evaluate the role of AMs in muco-obstructive lung diseases during bacterial infections, we assessed the phagocytic capacities of AMs ex vivo, using *E. coli* particles labeled with pHRodo. Flow cytometry showed reduced uptake of *E. coli* particles in *Scnn1b*-Tg AMs than WT AMs, reflecting a phagocytosis impairment (**Fig. 3.9.b**).

To assess the role and response of AMs to bacterial stimulation, we treated primary AMs from *Scnn1b*-Tg and WT mice ex vivo with bacteria-derived LPS for 6, 12, and 24 hrs. Baseline expression of the proinflammatory cytokines *Il1b*, *Il6*, *Il12b*, and *Tnf* was not significantly changed in AMs from the different genotypes (**Fig. 3.10.a**; *Nos2* was undetectable, data not shown). LPS treatment preceded a robust inflammatory response of *Scnn1b*-Tg and WT AMs on mRNA and protein levels. Comparable expression of *Nos2*, *Il6*,

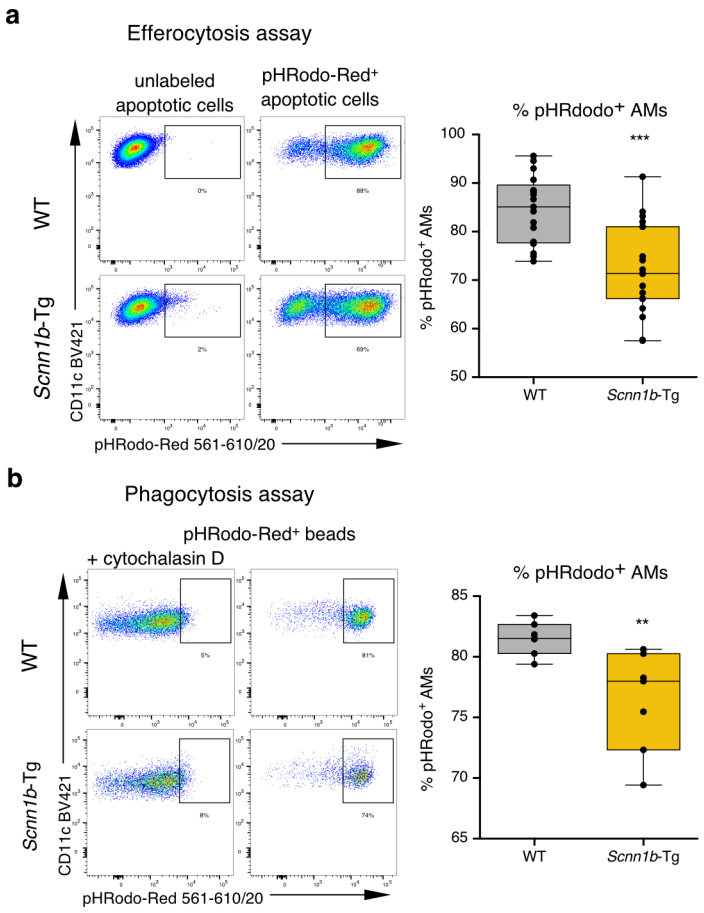

Figure 3.9: Scnn1b-Tg AMs are impaired in efferocytosis and phagocytosis capacities. (**a** and **b**) Analysis of (**a**) efferocytosis and (**b**) phagocytosis capacities of *Scnn1b*-Tg and WT AMs. Representative flow cytometry plots (left panels) and the proportion of pHRodo-positive AMs (right panels) are shown. The data show mean ±SEM of (**a**) n =17-19 and (**b**) n =7. Unpaired, two-tailed Mann-Whitney U test: **, *P* value <0.01; ***, *P* value <0.001.

Il1b, and *Il12b* on mRNA (**Fig. 3.10.b**) and IL-6 and IL-23 on protein level (**Fig. 3.10.c**) were detected 6 hrs post LPS treatment. mRNA levels for *Mmp12* and protein levels for IL-1β and CCL2 were already significantly upregulated in Scnn1b-Tg AMs at 6 hrs. IL-1β and IL-12 protein levels were below the detection limit.

Immune responses are tightly regulated and self-limiting to reduce excessive inflammation and tissue damage in the affected organ[216]. Accordingly, a substantial reduction in gene and protein expression was observed for most analyzed genes 12 hrs post

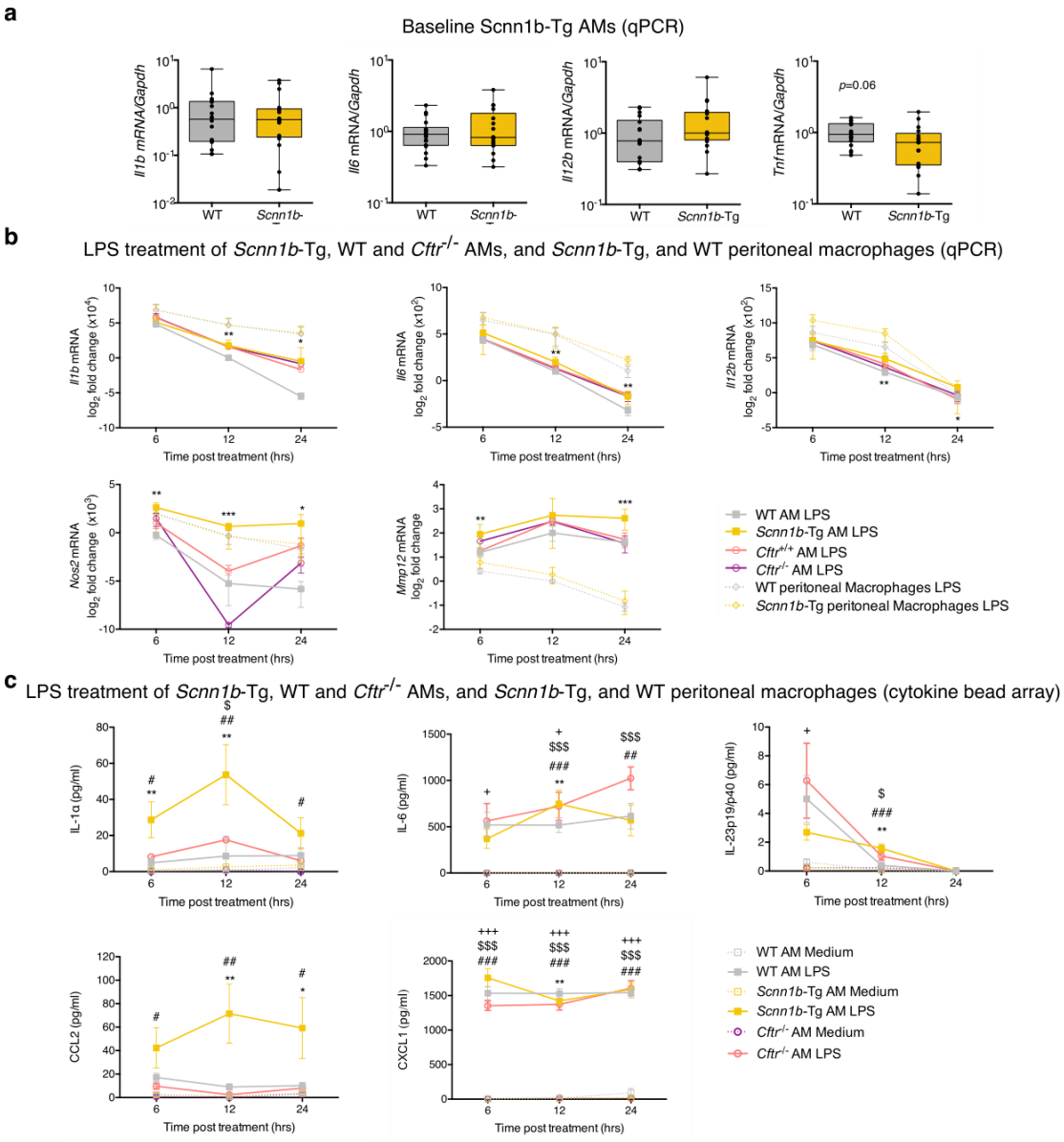

Figure 3.10: The muco-obstructive lung microenvironment in *Scnn1b*-Tg mice induces prolonged and hyperinflammatory immune responses in AMs.

Figure 3.10: The muco-obstructive lung microenvironment in *Scnn1b*-Tg mice induces prolonged and hyperinflammatory immune responses in AMs. (**a**) Gene expression, assessed by qPCR, of *Il1b*, *Il6*, *Il12b*, and *Tnf* in AMs from primary uncultured *Scnn1b*-Tg and WT mice at baseline. *P* values were determined by unpaired, two-tailed Mann-Whitney U test. (**b**) Gene expression of *Nos2*, *Il6*, *Il1b*, *Il12b*, and *Mmp12* from *Scnn1b*-Tg and WT AMs, *Scnn1b*-Tg, and WT peritoneal macrophages, as well as *Cftr*$^{-/-}$, and *Cftr*$^{+/+}$ AMs, at indicated time points post LPS treatment, assessed by qPCR. Gene expression was normalized to medium-teated samples. Unpaired, two-tailed Mann-Whitney U test: *, *P* value <0.05; **, *P* value <0.01; ***, *P* value <0.001. ND, not detectable. (**c**) Protein expression of IL-1α, IL-6, IL-23p40/p19, CCL2, and CXCL1, at indicated time points, post-medium and LPS treatment of *Scnn1b*-Tg, *Cftr*$^{-/-}$, and WT AMs. Protein levels were assessed by cytokine bead array. One-way ANOVA with Tukey's test: */#/$/+, *P* value <0.05; **/##/$$/++, *P* value <0.01; ***/###/$$$/++, *P* value <0.001. *, *Scnn1b*-Tg LPS vs WT LPS; #, *Scnn1b*-Tg medium vs *Scnn1b*-Tg LPS; $, *Cftr*$^{-/-}$ medium vs *Cftr*$^{-/-}$ LPS; +, WT medium vs WT LPS. The data show mean ±SEM of (**a**) n =17-18, (**b**-**c**) n =8-10 for *Scnn1b*-Tg and WT AMs, n =4 for peritoneal macrophages, and n =6-12 for *Cftr*$^{-/-}$ AMs.

LPS treatment (**Fig. 3.10.b**). However, a considerable upregulation was still shown for all measured genes (*Nos2*, *Il6*, *Il1b*, *Il12b*, and *Mmp12*) and the majority of measured proteins (IL-1β, IL-6, IL-23, and CCL2) in *Scnn1b*-Tg compared to WT AMs (**Fig. 3.10.b** and **c**). Only the chemokine CXCL1 showed increased induction in WT AMs 12 hrs post LPS treatment. Still, 24 hrs post LPS treatment, a prolonged and increased response of the genes *Il6*, *Nos2*, *Il12b*, and *Mmp12* and the proteins IL-1β, IL-6, and CCL2 were observed in *Scnn1b*-Tg compared to WT AMs.

In contrast, macrophages obtained from the peritoneum of *Scnn1b*-Tg and WT mice showed no differences in gene expression patterns post LPS treatment (**Fig. 3.10.b**), highlighting a lung-specific macrophage phenotype induced by the muco-obstructive microenvironment. To further validate the role of the airway microenvironment on AM responses, we utilized mice deficient in the cystic fibrosis transmembrane conductance regulator (*Cftr*$^{-/-}$). *Cftr*$^{-/-}$ causes CF in humans but fails to produce a muco-obstructive lung disease in knock-out mice[123]. Similar to macrophages from the peritoneum, no differences in LPS responses between *Cftr*$^{-/-}$ and WT AMs were detected (**Fig. 3.10.b** and **c**). Together, these results show the clear role of the local muco-obstructive microenvironment in shaping proinflammatory and prolonged immune responses of AMs to LPS.

To get an in-depth understanding of the proinflammatory and prolonged immune response of AMs from muco-obstructive lungs, paired RNAseq and ATACseq on LPS and medium-treated AMs were performed. The 12 hrs time point was used to capture the most pronounced alterations. Dimensionality reduction by principal component (PC) analysis

(PCA) of the whole transcriptome and chromatin accessibility landscape revealed segregation of LPS from medium-treated cells in PC1, explaining 73% and 71% of the variability, respectively (**Fig. 3.11.a** and **b**). Segregation of the mouse genotypes was shown in PC2, explaining about 7% of the assays' overall variability. As expected, overrepresentation analysis of the top 100 genes explaining the variability found in PC1 depicted pathways and gene ontologies involved in immune responses (e.g., response to LPS), immune activation, and host defense (**Fig. 3.11.c**). Similar pathways and gene ontologies associated with immune responses, such as interferon, cytokine, and anti-viral responses, were further enriched in PC2. These results validate the hyperinflammatory immune responses of *Scnn1b*-Tg compared to WT AMs, detected by qPCR and cytokine bead array, and indicate mediation of this process via enhanced interferon signaling. Accordingly, inflammatory regulators, such as LPS and the TFs NFκB, IFN-γ and STAT6, were predicted activators in the upstream regulator analysis of gene expression changes comparing *Scnn1b*-Tg with WT AMs post LPS treatment (**Fig. 3.11.f**).

In total, 246 DEGs (**Fig. 3.11.d**) and 897 DARs (**Fig. 3.11.e**) were identified, indicating transcriptional reprogramming and a rearrangement of the chromatin architecture in LPS-treated AMs from muco-obstructive lungs. Furthermore, DARs with increased accessibility in *Scnn1b*-Tg AMs were strongly enriched for TF motifs regulating inflammatory responses (e.g., IRF1, IRF2, IRF3, IRF8, NFY, and NFκB-p65; data not shown; detailed interference of TF activity in **Fig. 3.12.a**).

To evaluate epigenetic differences of *Scnn1b*-Tg compared to WT AMs, in relationship to differences in chromatin accessibility of regions responsive to LPS treatment, we defined LPS-responsive DARs (**Fig. 3.11.g**) and compared their accessibility in *Scnn1b*-Tg and WT AMs (**Fig. 3.11.h**). This revealed increased accessibility of LPS-responsive regions in LPS-treated *Scnn1b*-Tg compared to LPS-treated WT AMs (**Fig. 3.11.h**; top panel). Notably, already in primary uncultured *Scnn1b*-Tg AMs, a pattern of increased accessibility was depicted in *Scnn1b*-Tg AMs (**Fig. 3.11.h**; bottom panel). These results indicate proinflammatory epigenetic priming of AMs in muco-obstructive lung disease, which emerges as an enhanced immune response upon exposure to a pathophysiological relevant stimulus like LPS.

Gene expression is essentially determined by the activity of distinct TFs that can bind alone or cooperatively to their respective motif at accessible chromatin within gene regulatory

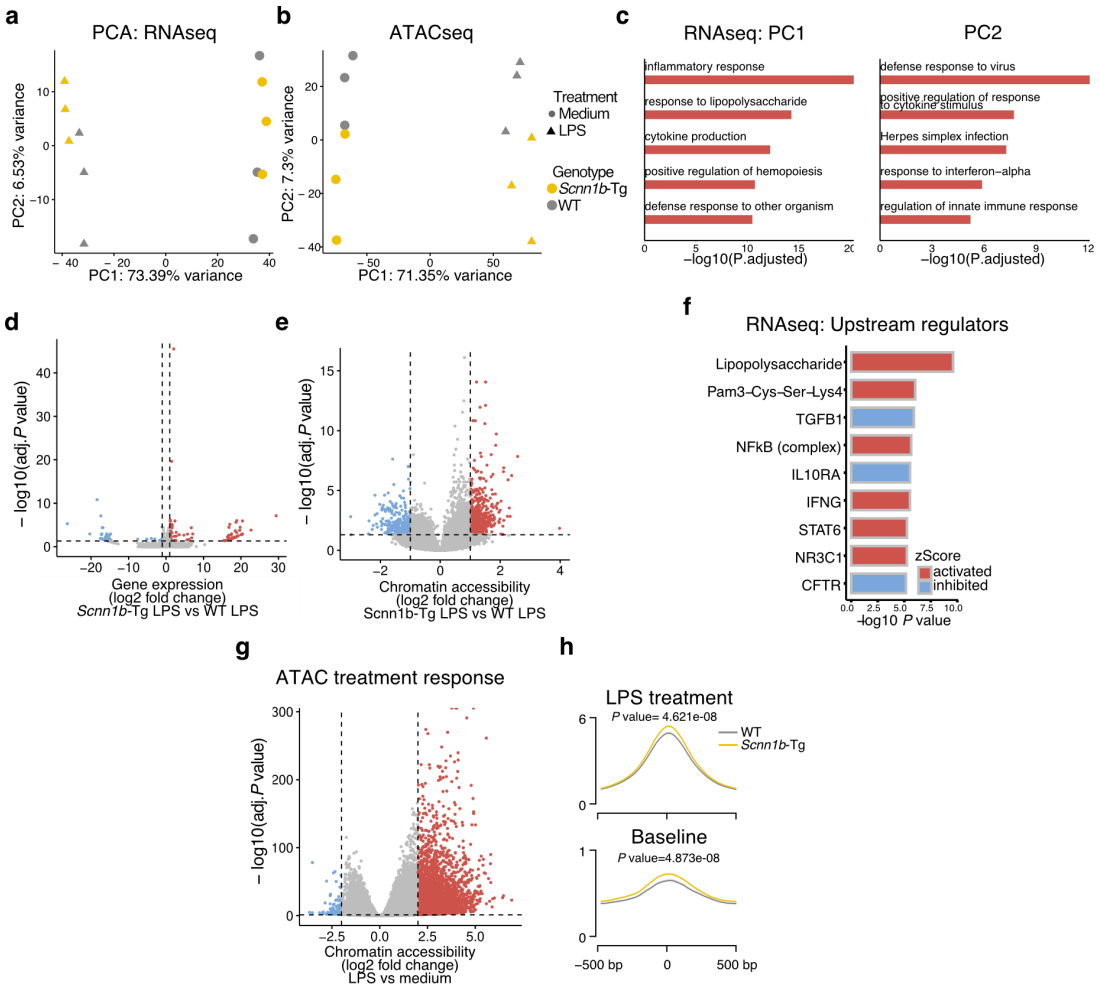

Figure 3.11: Genome-wide profiling confirms hyperinflammatory responses and indicates epigenetic priming of *Scnn1b*-Tg AMs. (**a** and **b**) Unsupervised PCA of (**a**) RNAseq (n =3) and (**b**) ATACseq (n =3) data from *Scnn1b*-Tg and WT AMs post LPS treatment for 12 hrs. (**c**) Enrichment of pathways and gene ontologies of the top 100 genes explaining PC1 (left panel) and PC2 (right panel) of RNAseq data. (**d** and **e**) Volcano plot visualizing the LPS response in *Scnn1b*-Tg vs WT AMs on (**d**) gene expression level (DEG: adjusted *P* value <0.05; log2 fold change >1; red dots: significantly upregulated genes in *Scnn1b*-Tg AMs; blue dots: significantly upregulated genes in WT AMs) and (**d**) chromatin accessibility level (DAR: adjusted *P* value <0.05; absolute log2 fold change >2; red dots: increased accessibility in *Scnn1b*-Tg AMs treated with LPS; blue dots: increased accessibility in WT AMs treated with LPS). (**f**) Upstream regulator analysis of gene expression changes in *Scnn1b*-Tg vs WT AMs, treated for 12 hrs with LPS. (**g**) Volcano plot visualizing the treatment response (LPS vs medium) of AMs on chromatin accessibility level. DAR: adjusted *P* value <0.05; absolute log2 fold change >2; red dots: increased accessibility in LPS treated AMs; blue dots reduced accessibility in LPS treated AMs. (**h**) Profile plot of LPS responsive DARs, visualized for LPS treated *Scnn1b*-Tg and WT AMs (top panel) and primary uncultured *Scnn1b*-Tg and WT AMs at baseline (lower panel). *P* values were determined by student's t-test.

regions. To study the role of specific TFs on the hyperinflammatory immune responses of *Scnn1b*-Tg AMs, we performed multi-omics integration of the RNAseq and ATACseq data from LPS-treated AMs. Prediction of TF activity was performed using the software diffTF[26]. A total of 80 differentially active TFs were identified, of which 60% showed increased activity in *Scnn1b*-Tg AMs (**Fig. 3.12.a**). Integration of gene expression data allows diffTF to classify TFs in transcriptional repressors and activators. 38% and 45% of the differentially active TFs were predicted as activators and repressors, respectively. For 17%, no definite status was assigned (undetermined). The estimated TF activity strongly correlated (Pearson correlation: R =0.45, P value =3.1x10^{-5}) with mean TF target gene expression changes, defined by the respective TF binding motif's presence within the promoter region (**Fig. 3.12.b**).

Next, we clustered highly significant TFs based on their position weight matrix, which resulted in the grouping of TFs based on their TF-family, with an overall consistent change of TF activity. TFs with increased or decreased activity in *Scnn1b*-Tg AMs post LPS treatment clustered together. The cluster of TFs with the most robust TF activity in *Scnn1b*-Tg AMs belonged to the interferon response factor (IRF) family, including IRF1, IRF2, IRF3, IRF7, IRF8, and IRF9 (**Fig. 3.12.c**). In addition to the enhanced TF activity, *Irf1* was induced on gene expression level in LPS-treated samples and further upregulated in LPS-treated *Scnn1b*-Tg AMs (P value <0.05; **Fig. 3.12.d**). These results imply a significant role of IRF1 in orchestrating proinflammatory and prolonged LPS responses in AMs from muco-obstructive lung disease.

In addition to the LPS-treated samples, differential TF activity analysis was performed on *Scnn1b*-Tg, and WT AMs cultured in medium for 12 hrs (**Fig. 3.13.a**). Overall, very similar results were obtained. A comparison of TF-activity from both analyses revealed a strong correlation (Pearson correlation: R =0.53, P value =2e^{-05}) of the LPS- and medium-treated comparisons (**Fig. 3.13.b**).

These results further support the hypothesis that AMs from muco-obstructive airways are epigenetically primed for enhanced inflammatory responses. While much is known about how LPS-mediated signaling activates the IRF TF-family[240], little has been reported about its function in macrophages of the muco-obstructive airway microenvironment. Here, we show that the IRF TF family's activity, particularly IRF1, is increased in *Scnn1b*-Tg AMs and associated with increased expression of hyperinflammatory genes under inflammatory

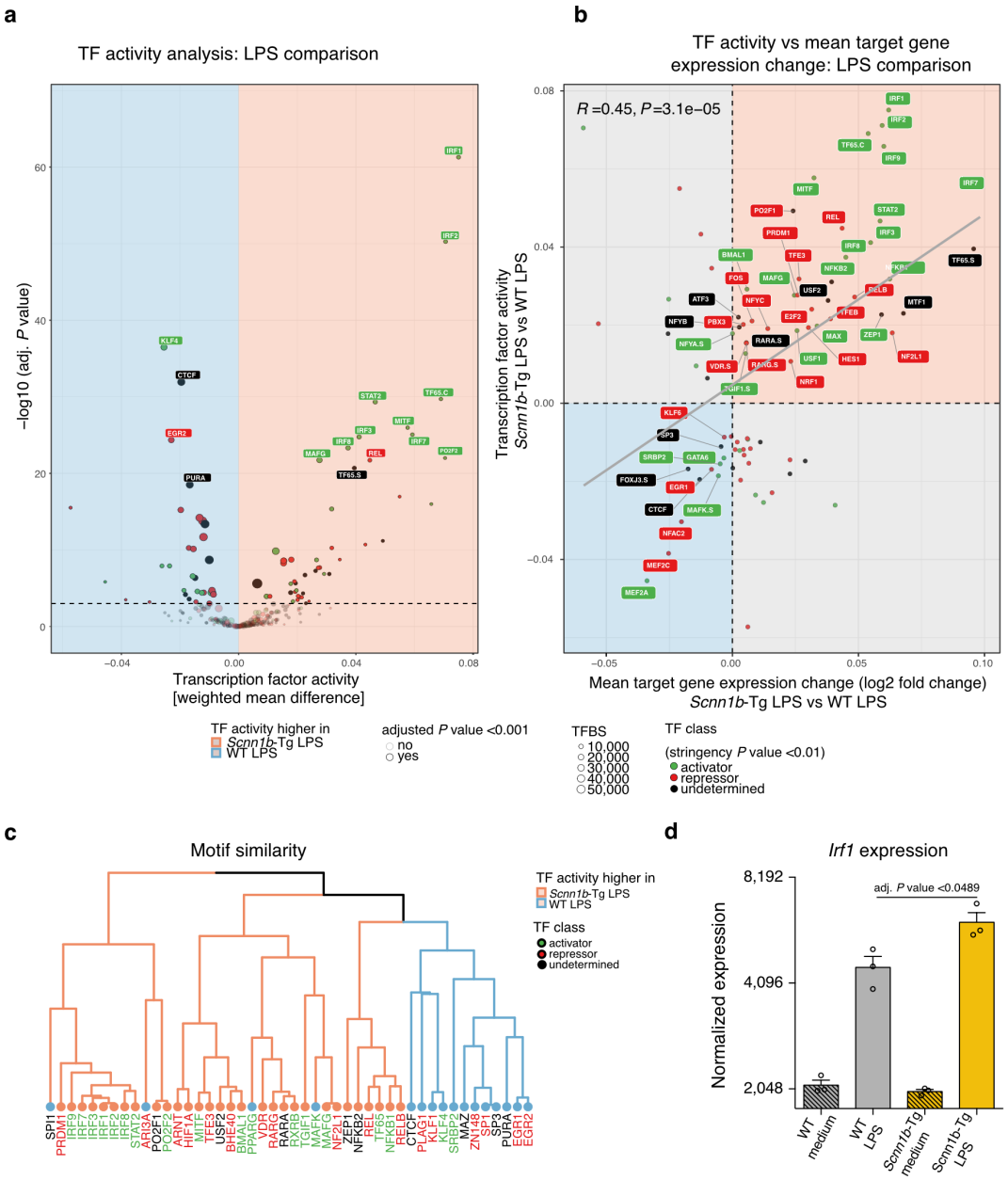

Figure 3.12: Multi-omics integration reveals enhanced TF activity of IRF1 in *Scnn1b*-Tg AMs post LPS treatment.

Figure 3.12: Multi-omics integration reveals enhanced TF activity of IRF1 in *Scnn1b*-Tg AMs post LPS treatment. (**a**) Differential TF activity analysis of *Scnn1b*-Tg vs WT AMs post 12 hrs of LPS treatment. TF activity and adjusted *P* values are visualized. Size represents the number of TF binding sites (TFBS). Green labeled TFs are predicted activators, red labeled TFs are predicted repressors, and black labeled TFs have no direction assigned. (**b**) Correlation of TF activity of significantly enriched TFs (adjusted *P* value <0.001) in *Scnn1b*-Tg vs WT AMs treated with LPS and mean target gene expression change. The gray diagonal indicates the linear regression. (**c**) Clustering of significantly activated TFs (adjusted *P* value <10e^{-6}) based on their position weight matrixes' similarity. Coloring of tree leaves based on TF activity. Color of labels defined by TF class. (**d**) Normalized *Irf1* gene expression obtained by RNAseq (*Scnn1b*-Tg LPS vs WT LPS) in treated and untreated *Scnn1b*-Tg and WT AMs. The data show mean ± SEM of n =3. *P* values were determined by differential gene expression analysis with DESeq2.

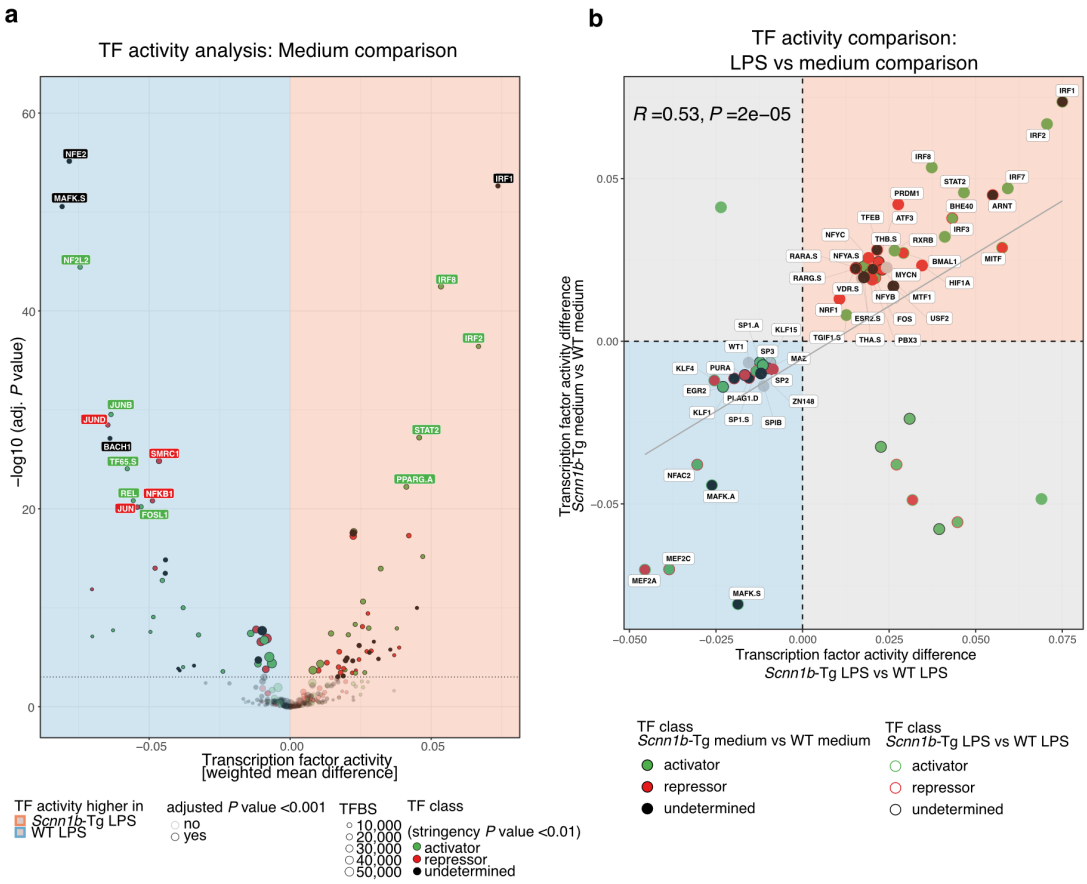

Figure 3.13: Hyperinflammatory responses are primed in *Scnn1b*-Tg AMs. (**a**) Differential TF activity analysis of medium treated *Scnn1b*-Tg vs WT AMs. TF activity and adjusted *P* values are visualized. Size represents the number of TFBS. Green labeled TFs are predicted activators, red labeled TFs are predicted repressors, and black labeled TFs have no direction assigned. (**b**) Incorporation of significantly enriched TFs (adjusted *P* value <0.05) of the LPS (**Fig. 3.12**) and medium comparison of *Scnn1b*-Tg vs WT AMs. The gray diagonal indicates the linear regression.

conditions. Future experiments will show if IRF1 inhibition provides a therapeutic approach for muco-obstructed patients suffering from bacterial exacerbations.

3.2 Cancer-specific DNA methylation landscape of macrophages and monocytes in breast cancer

3.2.1 Epigenetic profiling of macrophages and monocytes in breast cancer reveals cancer-specific DNA methylation landscape

To investigate the role of DNA methylation in cancer-specific reprogramming of macrophages, we isolated TAMs via FACS from primary BALB/c-derived 4T1 orthotopic tumors four weeks post 4T1 tumor cells injection. As normal references, tissue-resident mammary gland macrophages (MGs) were isolated from healthy mice. Previous studies in genetically engineered mouse models have suggested a monocytic origin of TAMs[7,245]. It was shown that monocyte recruitment from the bone marrow and further TAM differentiation is triggered by tumor development and utilizes distinct differentiation pathways compared to macrophage differentiation at a steady state[103]. Thus, we hypothesized that alterations in the DNA methylation landscape are already present in BMDMs from tumor-bearing mice (BMDM-T), which were consequently isolated via FACS as well. BMDMs from healthy mice (BMDM-H) were used as respective controls (**Fig. 3.14.a**).

WGBS by the low-input protocol, PBAT[232] yielded high bisulfite conversion rates and CpG coverages (>99% Bisulfite conversion rate; >15x genome-wide CpG coverage per replicate) with as little as 1000 cells/sample. Notably, analysis of global DNA methylation levels revealed an overall DNA hypomethylation in TAMs compared to MGs and BMDMs (**Fig. 3.14.b**). Differences in global DNA methylation are frequently observed in tumors but are uncommon for non-transformed cells[89]. However, whereas global DNA hypomethylation in cancer cells is often accompanied by CGi hypermethylation, no differences were observed for these regions between the investigated samples (**Fig. 3.14.c**). Unsupervised PCA of the 200,000 most variable CpGs segregated all groups, with PC1 separating macrophages from BMDMs and PC2 separating TAMs from MGs and BMDM-T from BMDM-H, indicating a unique DNA methylation profile of each group (**Fig. 3.14.d**).

As explained in detail in **section 1.2** meaningful conclusions can only be generated when comparing TAMs with MGs, their healthy tissue-resident counterparts[46,308]. Therefore, DMR calling between TAMs and MGs was performed to define coherent changes in DNA

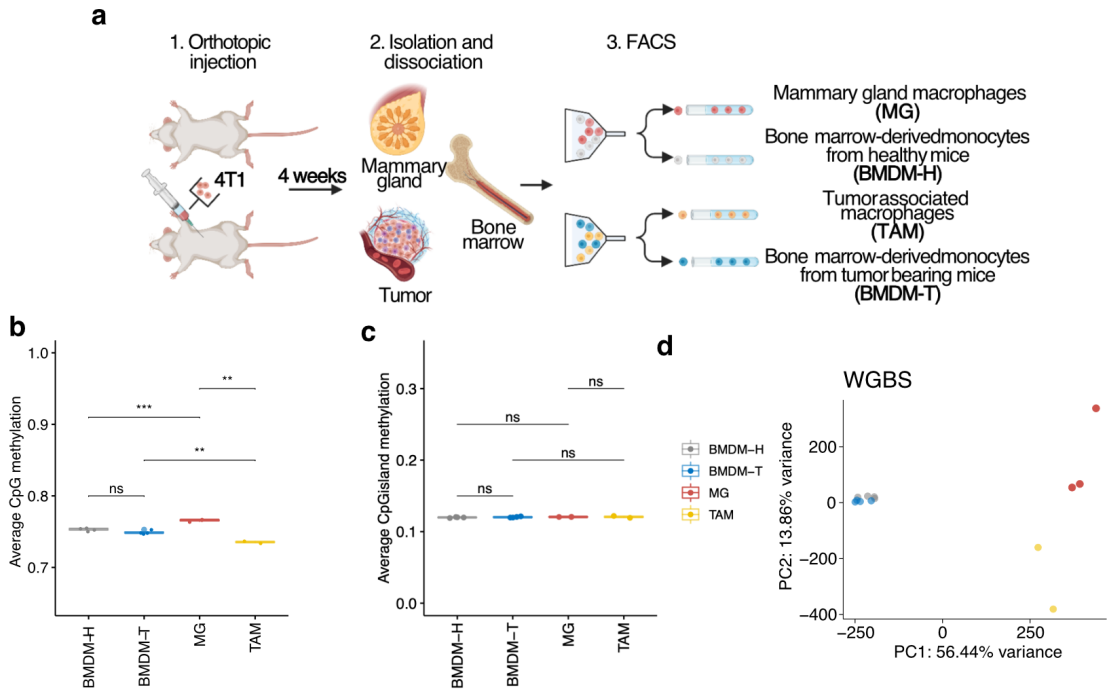

Figure 3.14: WGBS profiling of macrophages and monocytes in the 4T1 orthotopic breast cancer mouse model. (**a**) Graphical representation of the experimental workflow. (**b** and **c**) Average (**b**) CpG and (**c**) CGis methylation per group. For exploratory analysis, only CpGs with a coverage <5 in at least two samples were used. (**b** and **c**) Student's T-test. ns, *P* value >0.05; **, *P* value <0.01; ***, *P* value <0.001, ns, *P* value >0.5. (**d**) PCA of the 200,000 most variable CpGs (WGBS) in TAMs (n =2), MGs (n =3), BMDM-T (n =4), and BMDM-H (n =4) samples.

methylation. This confirmed the global DNA methylation analysis and revealed pronounced alterations in the DNA methylation landscape. 7,042 hypo- and 2,860 hypermethylated TAM vs MG DMRs were identified (**Fig. 3.15.a**), enriched for gene regulatory regions such as promoter and promoter-flanking regions (**Fig. 3.15.b**). To gain insights into the potential role of these regions in regulating signaling pathways, we performed locus overlap, and Molecular Signatures Database (MSigDB) hallmarks enrichment analysis (**Fig. 3.15.c**). MsigDB hallmarks are a collection of annotated gene sets, representing well-defined biological states and processes[288]. Enrichment analysis showed a clear overrepresentation of hypomethylated TAM vs MG DMRs, associated with inflammation (e.g., Il2/Stat5 signaling, Il6/JAK/Stat3 signaling, and IFN-γ response) and growth factor signaling (e.g., TGF-β signaling and TNF-α signaling via NFκB). These results were also reflected in the

enrichment of TF binding motifs (**Fig. 3.15.d** and **e**). Inflammation-associated TF families such as IRF (e.g., IRF8) and STAT (e.g., STAT1) were overrepresented in hypomethylated TAM vs MG DMRs. Furthermore, TF families associated with developmental processes (e.g., RUNT), macrophage polarization (e.g., STAT), and TGF-β signaling (e.g., bZIP) were among the most significantly enriched TF-families. Notably, the TFs *Runx3* (RUNT TF-family), *Stat1* (STAT TF-family), and *FosL2* (bHLH TF-family) exhibited promoter-flanking hypomethylation (**Fig. 3.15.f** and **g**), indicating a gene regulatory effect of these DMRs on TF expression. Further prominent examples of DMRs with a potential role in TAM reprogramming included the promoter-flanking hypomethylation of the transmembrane receptors *Tgfbr1* (**Fig. 3.15.h**) and *Ifngr1*.

In contrast to the pairwise comparison of TAMs vs MGs, we observed only minor differences in the DNA methylation landscape of BMDM-T compared to BMDM-H. In total, 179 hypo- and 79 hypermethylated DMRs were identified (**Fig. 3.16.a**). However, enrichment of similar immune-related MSigDB hallmarks (e.g., Il6/JAK/STAT3 signaling, IFN-α, and IFN-γ response) were shown within hypomethylated BMDM-T vs BMDM-H DMRs (**Fig. 3.16.b**), indicating a BMDM trajectory towards the TAM DNA methylation landscape. Correspondingly, the TF motif analysis revealed enrichment of STAT, RUNT, and bZIP TF-families in hypomethylated BMDM-T vs BMDM-H DMRs (**Fig. 3.16.c** and **d**).

Collectively, this WGBS data represent the first comprehensive characterization of the DNA methylation landscape in TAMs and BMDM-T of breast cancer and cancer in general. Utilizing a recently developed low-input DNA methylation profiling method, we were able to produce high-quality references of healthy tissue-resident MGs and BMDM-H. Comparison of TAMs and MGs disclosed a cancer-specific DNA methylation landscape. It highlighted known tumor microenvironment drivers, such as the TF FOSL2, previously reported in the reprogramming of macrophages by lung cancer [17,128]. In addition, novel putative drivers of the TAMs epigenome, like the TF RUNX3, were identified. The recognized TFs can be further exploited to generate prognostic signatures and develop novel drugs, explicitly targeting these TFs. In addition, an early effect of breast cancer on the epigenome of BMDMs was shown, demonstrating a systemic impact of breast cancer progression and an early reprogramming of TAM progenitors.

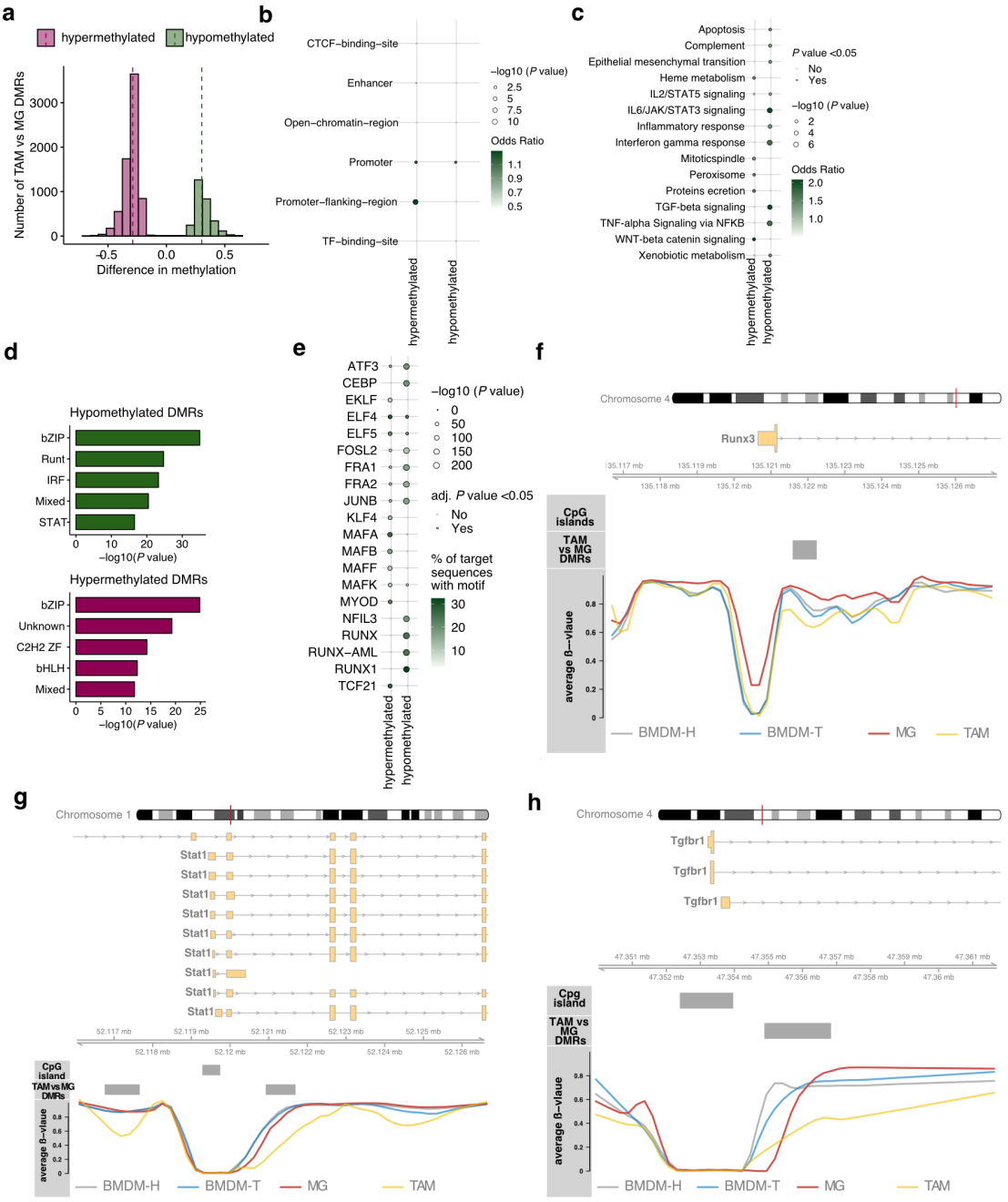

Figure 3.15: Cancer-specific DNA methylation landscape of TAMs in breast cancer.

Figure 3.15: Cancer-specific DNA methylation landscape of TAMs in breast cancer. (**a**) Distribution of DNA methylation differences in TAM (n =2) vs MG (n =3) DMRs. DMRs are defined by at least three CpGs with an adjusted *P* value <0.05, a width of >50 bp, and an average change of DNA methylation >0.1. (**b**) Annotation and enrichment of TAM vs MG DMRs to gene regulatory regions, stratified in hypo- and hypermethylated regions. (**c**) MSigDB hallmarks enrichment of TAM vs MG DMRs stratified in hypo- and hypermethylated regions. (**d** and **e**) TF motif enrichment of TAM vs MG DMRs stratified in hypo-and hypermethylated regions. (**d**) TF motifs were grouped by TF-family. (**f**-**h**) Locus plots of selected DMRs, annotated to the (**f**) *Runx3*, (**g**) *Stat1*, and (**h**) *Tgfbr1* locus, showing average DNA methylation of TAMs, MGs, BMDM-T, and BMDM-H. The gray boxes indicate CGis (top) and TAM vs MG DMRs (bottom).

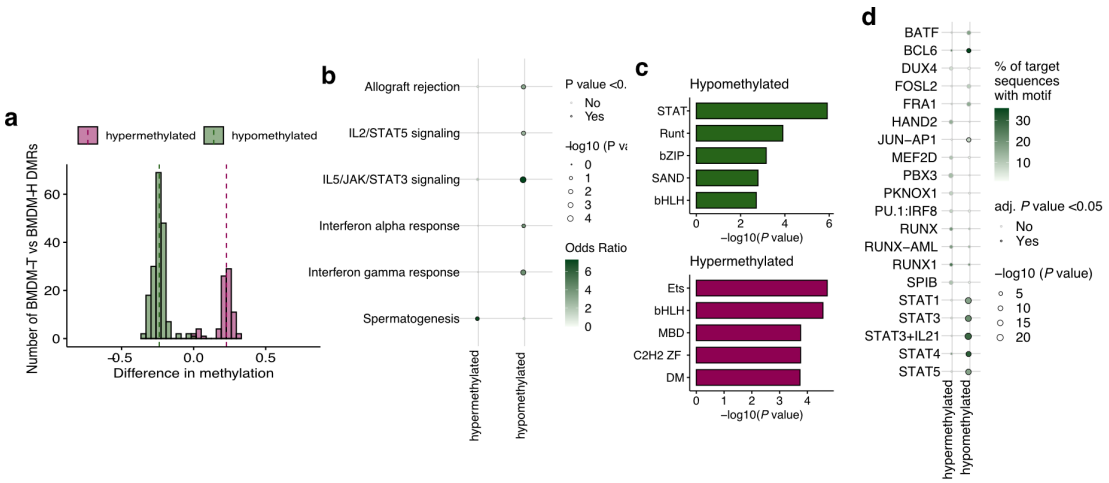

Figure 3.16: BMDMs in breast cancer reveal minor alterations in the DNA methylation landscape. (**a**) Distribution of DNA methylation differences in BMDM-T (n =4) vs BMDM-H (n =4) DMRs. DMRs are defined by at least three CpGs with an adjusted *P* value <0.05, a width of >50 bp, and an average change of DNA methylation >0.1. (**b**) MSigDB hallmarks enrichment of BMDM-T vs BMDM-H DMRs stratified in hypo-and hypermethylated regions. (**c** and **d**) TF motif enrichment of BMDM-T vs BMDM-H DMRs stratified in hypo-and hypermethylated regions. (**c**) TF motifs were grouped by TF family.

To further dissect the DNA methylation differences between TAMs and MGs, we performed hierarchical clustering on the DNA methylation levels of the 9,902 identified TAM vs MG DMRs in all samples. Hierarchical clustering segregated the DNA methylation profiles of each group, with TAMs forming an independent cluster together with BMDMs (**Fig. 3.17.a**). Further k-means clustering of the DMRs, identified 6 DMR clusters that depicted a unique methylation profile within the different groups (**Fig. 3.17.b**). Clusters 4 and 6 were identified as specifically hypomethylated in TAMs compared to MGs and BMDMs, indicating TAM-specific alterations in the DNAm landscape. Similarly, cluster 5

revealed an intermediate methylation level in TAMs compared to BMDMs and MGs. The remaining clusters 1, 2, and 3 showed similar methylation levels in TAMs and BMDMs compared to MGs. Similar methylation levels in these clusters indicate the putative cellular origin of TAMs, which are BMDMs[7,245]. In detail, clusters 1 and 2 were hypomethylated, and cluster 3 was hypermethylated in TAMs and BMDMs compared to MGs.

To functionally interpret these unique DNA methylation programs, we performed TF motif enrichment of the identified DMR clusters and applied the enrichment results to a hierarchical cluster analysis (**Fig. 3.17.c**). TF motif analysis depicted a similar enrichment of TFs in DMR clusters with comparable methylation levels in the different groups. Clusters 1 and 2, hypomethylated in TAMs and BMDMs, showed the most substantial enrichment for TF motifs within the RUNT TF-family (e.g., RUNX). Also, TF motifs of CEBP and NFIL3 were strongly enriched. Cluster 4 and 6, specifically hypomethylated in TAMs, showed the most substantial enrichment for TF motifs from the bZIP TF-family, such as FRA1, FRA2, and FOSL2. Notably, TF motifs strongly enriched in clusters 1 and 2 were also identified to a lesser extend in cluster 6. Cluster 3, hypermethylated in TAMs and BMDMs, showed enrichment for different TFs of the MAF TF-family and the TF TCF21.

Further characterization of the DNA methylation programs of TAMs by MSigDB hallmarks enrichmentc explained which DMR clusters contributed to the overall identified signaling pathways of TAM vs MG DMRs in **Fig. 3.15.c**. Notably, cluster 4, specifically hypomethylated in TAMs, was uniquely enriched for TGF-β signaling. Additionally, enrichment of epithelial to mesenchymal transition, Il6/JAK/STAT3, TNF-α signaling, and IFN-γ response was found in cluster 4. Similar hallmarks were identified in the TAM and BMDM hypomethylated clusters 2 and 6. Cluster 1, hypomethylated in TAMs and BMDMs, was enriched for IL2/STAT5 and Notch signaling. WNT-β catenin signaling was attributed to the TAM and BMDM hypermethylated cluster 3.

Overall, these results show how the DNA methylation landscape of TAMs can be dissected into different DNA methylation programs. We identified programs unique for TAMs (TAM-specific) and DNA methylation programs reminiscent of their monocytic origin. Most TFs and MSigDB hallmarks identified in the overall TAM vs MG comparison (**Fig. 3.15**) were attributed to one of the 6 DMR clusters, further disentangling the function and origin of cancer-specific alterations in the DNA methylation landscape of TAMs.

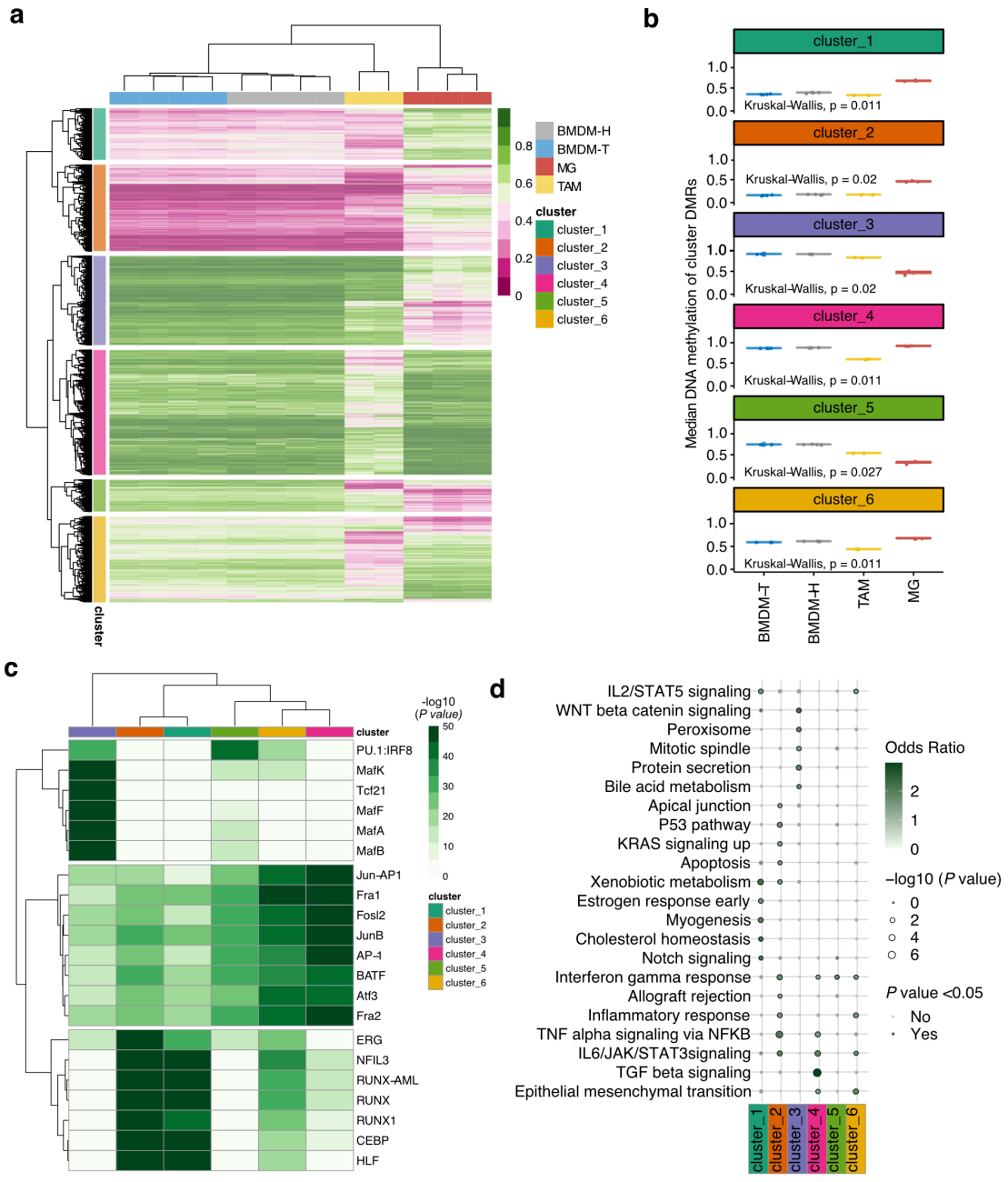

Figure 3.17: Dissection of the TAM DNA methylation landscape reveals BMDM-derived epigenetic patterns and TAM-specific alterations. (**a**) Hierarchical clustering of TAM vs MG DMRs in all samples. DMR clusters were identified by k-means clustering (k =6). (**b**) Median DNA methylation of each cluster in every group of samples. (**c**) Hierarchical clustering of TF motif enrichment results for DMRs in every cluster. *P* values are set to a maximum of -log10(*P* value) =50. (**d**) MsigDB hallmarks enrichment of DMRs in every cluster. Rows are ordered by hierarchical clustering.

3.2.2 Epigenetic reprogramming of macrophages and monocytes in breast cancer is correlated with cancer-specific transcriptional profiles

DNA methylation is a known regulator of gene expression, and transcriptional reprogramming of macrophages by breast cancer has been described in previous studies[46,308]. To explore functional consequences of the identified cancer-specific DNA methylation landscape, RNAseq of TAMs, MGs, BMDM-T, and BMDM-H was performed.

Similar to the described WGBS data, unsupervised PCA of the 5,000 most variably expressed genes revealed segregation of all groups (**Fig. 3.18.a**). Macrophages and BMDMs were separated in PC1, and PC2 separated TAMs and BMDM-T from MGs and BMDM-Hs, respectively, indicating a strong impact of breast cancer on the transcriptional landscape of macrophages and monocytes.

Next, differential gene expression analysis in a group-wise manner was executed for all comparisons (TAM vs MG, BMDM-T vs BMDM-H, BMDM-H vs MG, BMDM-T vs TAM, BMDM-T vs MG, and BMDM-H vs TAM). Hierarchical clustering of the union set of 47,562 DMRs from all comparisons (**Fig. 3.18.b**) exposed the same arrangements as the hierarchical clustering of all 5,919 identified DEGs (**Fig. 3.18.c**). Each group formed its own cluster, and further separation of BMDMs from macrophages was depicted. These clustering results show a significant effect of the tissue niche (macrophages in the breast vs monocytes in the bone marrow) that is further perturbed by cancer-specific signals (BMDM-T vs BMDM-H and TAMs vs MGs). Additionally, similar clustering of DMRs and DEGs suggested an interconnection of DNA methylation and gene expression in macrophages and monocytes. Indeed, Pearson correlation analysis of DMR methylation levels and gene expression of their annotated genes revealed an overall inverse correlation (median Pearson correlation estimate =-0.32; **Fig. 3.18.d**). A total of 6,985 significantly correlating DMRs/gene pairs (Pearson correlation P value <0.05) associated with 3,254 different genes was identified. This substantial number of correlating DMR/gene pairs depicts an essential role of DNA methylation in the gene regulation of macrophages and monocytes. It also shows their immense plasticity in adjusting to different tissue niches and environmental stimuli, as provided by the tumor microenvironment.

Notably, a large proportion of correlating DMR/gene pairs depicted differential

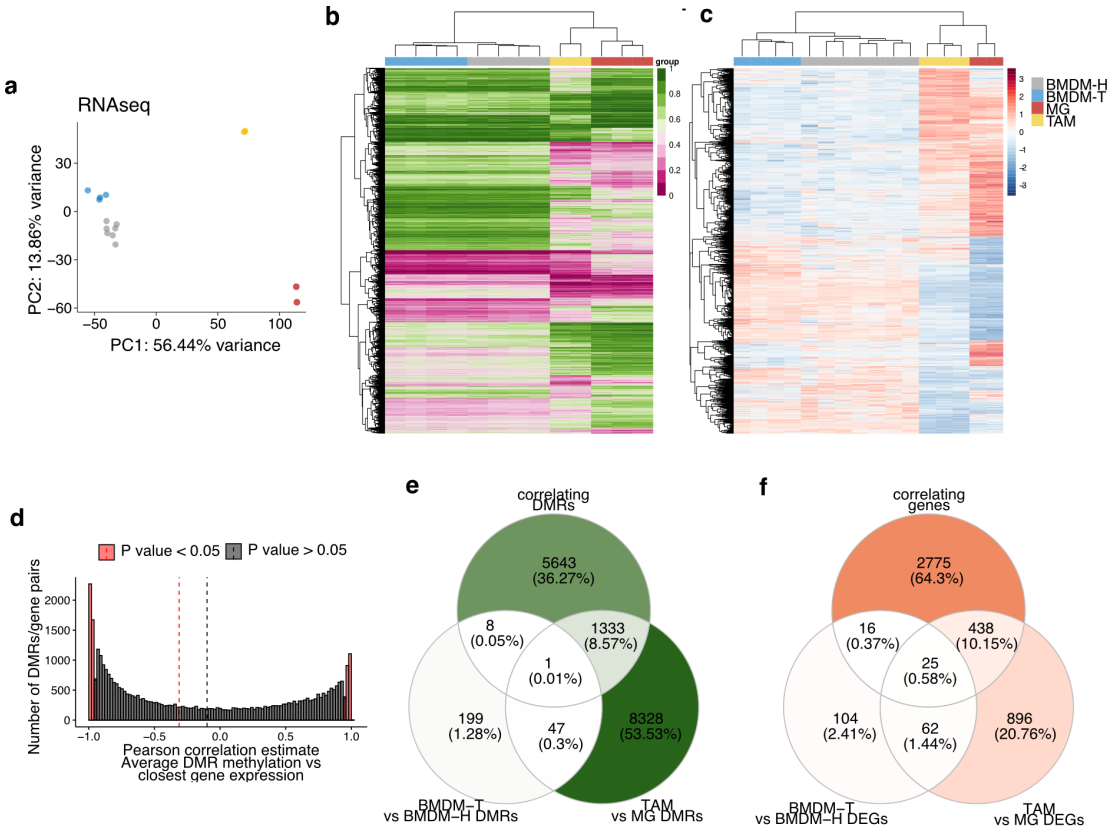

Figure 3.18: Cancer-specific DNA methylation landscape of macrophages and monocytes is correlated with transcriptional alterations. (**a**) PCA of the 5,000 most variable genes (RNAseq) in TAMs (n =3), MGs (n =2), BMDM-T (n =4), and BMDM-H (n =7). (**b** and **c**) Hierarchical clustering of (**b**) a union set of 47,562 DMRs and (**c**) 5, 919 DEGs from all comparisons (TAM vs MG, BMDM-T vs BMDM-H, BMDM-H vs MG, BMDM-T vs TAM, BMDM-T vs MG, and BMDM-H vs TAM). DMRs are defined by at least three CpGs with an adjusted *P* value <0.05, a width of >50 bp, and an average change of DNA methylation >0.1. DEGs are defined by an adjusted *P* value <0.05 and an absolute log2 fold-change >1. (**d**) Pearson correlation of DMR methylation levels and gene expression of annotated genes (DMRs are annotated to the overlapping or closest gene with a maximum distance of <10 kbs). Average DMR methylation and gene expression per group is used. (**e**) Venn diagram of TAM vs MG and BMDM-T vs BMDM-H DMRs, overlapping with correlating DMRs (Pearson correlation with gene expression, *P* value < 0.05). (**f**) Venn diagram of TAM vs MG and BMDM-T vs BMDM-H DEGs, overlapping with correlating genes (Pearson correlation with DMR methylation; *P* value < 0.05).

expression and methylation in the TAM vs MG comparison (1,336 DMRs (**Fig. 3.18.e**) and 463 DEGs (**Fig. 3.18.f**). Aligned visualization of DNA methylation and gene expression depicted the robust correlation of many DMR/gene pairs (**Fig. 3.19.a**). Most frequently an inverse correlation was identified: DMR hypomethylation correlated with gene induction and DMR hypermethylation with gene repression (**Fig. 3.19.b**). The hypomethylated fraction of functional TAM vs MG DMRs revealed enrichment for TGF-β and TNF-α signaling as well as IFN-γ response, indicating an apparent effect of the cancer-specific DNA methylation on TAM transcriptional profiles (**Fig. 3.19.c**). Further overrepresentation of leukocyte-related processes and inflammation was shown for the overlapping DEGs (**Fig. 3.19.e** and **f**). Again, TFs of the STAT and RUNT TF-families were found to be enriched in hypomethylated TAM vs MG DMRs correlating with gene expression (**Fig. 3.19.d**). Examples of correlating DMR/gene pairs with significant expression induction in TAMs included the transcription factor *Runx3*, the checkpoint inhibitor *Cd247*, the transmembrane receptor *Tgfbr1*, and the class II major histocompatibility complex gene *H2-Eb1* (**Fig. 3.19.g**).

Complementing our previous analysis, the multi-omics integration depicted a clear role of DNA methylation in the transcriptional reprogramming of TAMs. Particularly, pathways driven by microenvironmental stimuli, such as TGF-β, TNF-α, and IFN-γ, were enriched in the fraction of hypomethylated TAM vs MG DMRs that correlated with a cancer-specific transcriptome of TAMs. Putative drivers of TAM reprogramming, such as *Runx3*, and TAM effector genes with an immunosuppressive function on the tumor microenvironment, like *Cd274*, seemed to be regulated via DNA methylation.

Due to overall minor differences in the BMDM-T vs BMDM-H comparison, a small subset of 41 DEGs (**Fig. 3.18.f**) and 9 DMRs (**Fig. 3.18.e**) were overlapping with the correlating DMR/gene pairs. Similar to the TAM vs MG comparison, the majority of correlating DMR/gene pairs depicted an inverse correlation (**Fig. 3.20.a** and **b**). Notably, the overlapping fraction of DEGs induced in BMDM-T was associated with processes involved in leukocyte adhesion (**Fig. 3.20.c**). Adhesion of leukocytes to the vascular epithelium is crucial during BMDM recruitment to the tumor microenvironment and a prerequisite for TAM expansion.

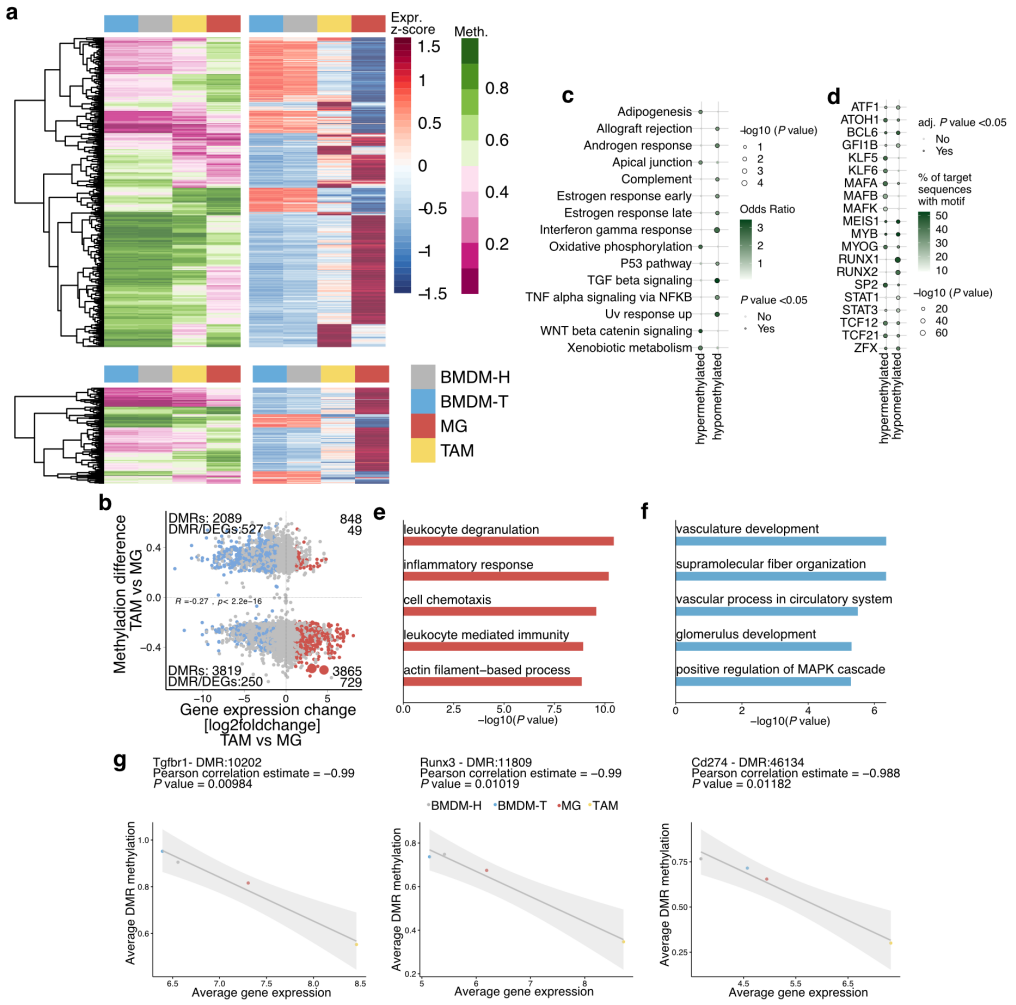

Figure 3.19: Epigenetic reprogramming of TAMs in breast cancer is correlated with a cancer-specific transcriptional profile. (**a**) Hierarchical clustering of correlating DMR/gene pairs overlapping with TAM vs MG DEGs (left; Pearson correlation with gene expression, *P* value < 0.05). DMR/gene pairs with a negative (top) and positive (bottom) Pearson estimate are visualized separately. Average DMR methylation (left) and gene expression (right) per group are visualized. Rows are ordered by hierarchical clustering of DNA methylation levels. (**b**) Scatterplot of TAM vs MG DMR methylation differences and gene expression changes. DMRs are annotated to the overlapping or closest gene with a maximum distance of <10 kbs. Red dots: genes significantly upregulated in TAMs vs MGs; blue dots: genes significantly downregulated in TAMs vs MGs. (**c**) MSigDB hallmarks enrichment of TAM vs MG DMRs, overlapping with correlating DMRs (Pearson correlation with gene expression, *P* value <0.05), stratified in hypo- and hypermethylated DMRs. (**d**) TF motif enrichment of TAM vs MG DMRs, overlapping with correlating DMRs (Pearson correlation with gene expression, *P* value <0.05), stratified in hypo- and hypermethylated DMRs. (**e** and **f**) Pathway and gene ontology enrichment of TAM vs MG genes, overlapping with DMR/gene pairs, stratified in (**e**) up- (left) and (**f**) downregulated genes (right). (**g**) Examples of correlating DMR/gene pairs. Average gene expression and DMR methylation are visualized on the x- and y-axis, respectively. *P* values were calculated by Pearson correlation coefficient. The gray diagonal represents the linear regression. Shaded areas are the confidence interval of the correlation coefficient at 95%.

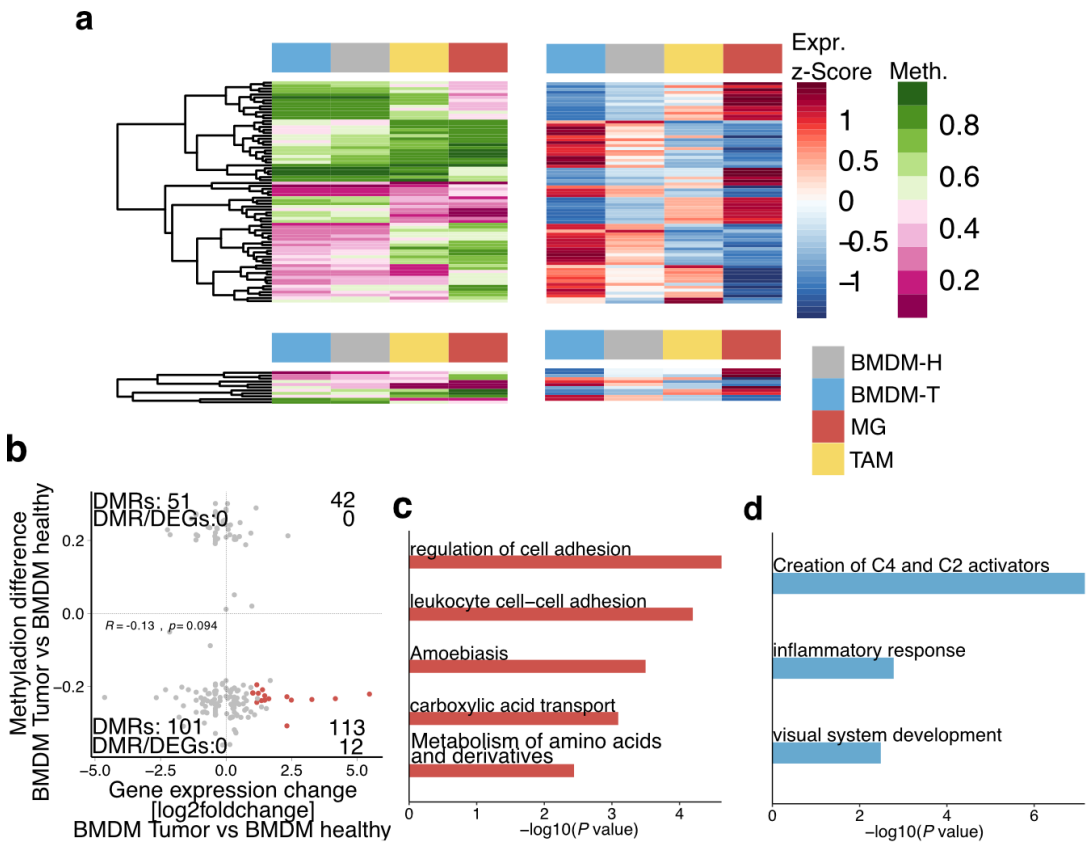

Figure 3.20: Epigenetic reprogramming of BMDMs in breast cancer is correlated with transcriptional changes involved in leukocyte recruitment. (**a**) Hierarchical clustering of correlating DMR/gene pairs that overlap with BMDM-T vs BMDM-H DEGs (left; Pearson correlation with gene expression, *P* value < 0.05). DMR/gene pairs with a negative (top) and positive (bottom) Pearson correlation estimate are visualized separately. Average DNA methylation (left) and gene expression (right) per group are visualized. Rows are ordered by hierarchical clustering of DMR methylation levels. (**b**) Scatterplot of BMDM-T vs BMDM-H DMR methylation differences and gene expression changes. DMRs are annotated to an overlapping or closest gene with a maximum distance of <10 kbs. Red dots: genes significantly upregulated in BMDM-T vs BMDM-H. (**c** and **d**) Pathway and gene ontology enrichment of BMDM-T vs BMDM-H genes, overlapping with correlating DMR/gene pairs, stratified in (**c**) up- (left) and (**d**) downregulated genes (right).

3.2.3 Cancer-specific transcriptional profile of tumor-associated macrophages is associated with breast cancer subgroups and poor clinical outcomes in breast cancer patients

To further characterize the identified cancer-specific transcriptional alterations of TAMs, we defined upstream regulators of the 1,421 TAM vs MG DEGs (**Fig. 3.21.a** and **b**). Similar to the MSigDB enrichment results of TAM vs MG DMRs, upstream regulator analysis identified IFN-γ, TNF-α, TGFB1 as key activators of gene expression. In addition, the major macrophage growth factors CSF1 (**Fig. 3.25.f**) and CSF2 (**Fig. 3.21.b**) were determined as upstream activators. The identification of CSF1 validates the prominent role of this growth factor in monocyte recruitment and TAM reprogramming[77]. Moreover, the results show the multifunctional role of TGFB1 in the suppression of immunosurveillance by the tumor microenvironment[300].

We further assessed the prognostic relevance of our findings for human breast cancer patients. Therefore, we utilized the largest human breast cancer gene expression cohort METABRIC[62], and explored a TAM-specific expression signature. Upregulated DEGs in TAMs compared to MGs, which were highly expressed in breast cancer samples, defined this signature. A previous breast cancer study identified a CSF1 response signature linked to higher tumor grade and decreased ER and PR expression[20]. In addition, tumors with a high CSF1 signature expression revealed an increased mutation rate. Applying this CSF1 response signature, we stratified the METABRIC breast cancer cohort into CSF1-high, CSF1-mid, and CSF1-low groups and evaluated TAM signature expression. This showed an increased expression in the CSF1-high compared to CSF1-mid and CSF1-low groups (**Fig. 3.21.c**). According to the role of CSF1 in monocyte recruitment, a strong overall correlation (**Fig. 3.21.d**; Pearson correlation: R =0.43, P value <0.001) of the TAM signature expression and macrophage infiltration of the different breast cancer samples, predicted via CIBERSORT, was observed[217].

Next, we assigned the tumor samples to breast cancer molecular subtypes based on the PAM50 classification system[28]. The highest expression of the TAM signature was shown in the aggressive claudin-low, HER2, and basal compared to luminal A or B breast cancer subtypes (**Fig. 3.21.e**). Together, these results validate the association of TAMs

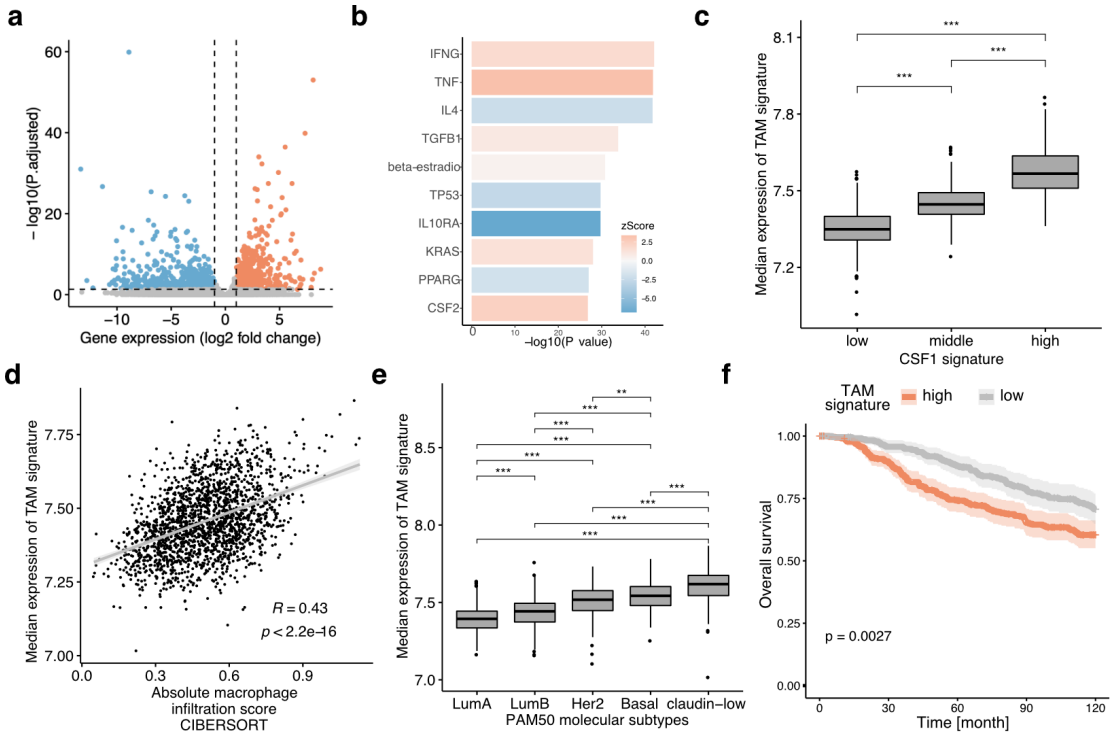

Figure 3.21: The cancer-specific transcriptional profile of TAMs is associated with breast cancer subgroups and poor clinical outcomes in breast cancer patients. (**a**) Volcano plot of TAM vs MG differential gene expression analysis. DEGs are defined by an adjusted *P* value <0.05, absolute log2 fold change >1. Red dots: increased expression in TAMs; blue dots: reduced expression in TAMs. (**b**) Upstream regulator analysis of TAM vs MG gene expression changes. The bar's color indicates the activation (red) or repression (blue) of genes regulated by the identified upstream regulators. (**c**) Median expression of the TAM signature in the human breast cancer cohort, METABRIC, stratified by CSF1 signature expression. TAM signature was compiled of highly expressed (>0.05 quantile) and significantly upregulated TAM vs MG DEGs (adjusted *P* value <0.05 and log2 fold change > 1) that are expressed in the METABRIC cohort. (**d**) Correlation of TAM signature expression with macrophage infiltration score in the METABRIC cohort, predicted by CIBERSORT. *P* values were calculated by Pearson correlation coefficient. The gray diagonal represents the linear regression. Shaded areas are the confidence interval of the correlation coefficient at 95%. (**e**) Median expression of the TAM signature in the human breast cancer cohort, METABRIC, stratified by the molecular PAM50 classifier. (**f**) Cancer-specific survival of the METABRIC cohort according to TAM signature expression (+/-1SD of median TAM signature expression). (**c** and **e**) One-way ANOVA with Tukey's post hoc multiple comparisons test. **, *P* value <0.01; ***, *P* value <0.001.

with aggressive breast cancers and depict the significance of the 4T1 breast cancer mouse model in the study of breast cancer TAMs. Therefore, we continued investigating whether the identified TAM signature was associated with clinical outcomes in the METABRIC cohort. Consistently with our previous findings, high expression of the TAM signature was associated with a shortened cancer-specific survival (**Fig. 3.21.f**).

To understand which genes contribute to worse clinical outcomes in breast cancer patients, k-means clustering on all TAM vs MG DEGs, identified in the 4T1 orthotopic mouse model, was performed (**Fig. 3.22.a**). A comparable clustering result as shown in the TAM vs MG DMRs analysis of **Fig. 3.17** was revealed. TAMs clustered together with BMDM samples, and 6 DEG clusters with different expression levels in the distinct groups were identified (**Fig. 3.22.b**). All clusters with increased gene expression in TAMs compared to MGs (clusters 1, 2, and 3) were associated with a shorter cancer-specific survival (**Fig. 3.22.c**). Additionally, these clusters were enriched for pathways involved in inflammatory processes, such as IFN-γ signaling, positive regulation of cell migration and Neutrophil degranulation (**Fig. 3.22.d**). Strikingly, the most prominent effect on patient survival was obtained with cluster 3 DEGs that showed decreased expression in MGs compared to TAMs compared to BMDMs. Since previously published studies used BMDMs or other macrophage populations as healthy references[32,222], the identified genes in cluster 3 with a critical role in patient survival were missed in their TAM signatures. Cluster 5 DEGs, with decreased gene expression in TAMs and BMDMs, compared to MGs, had the opposite effect on patient survival. Increased expression was associated with an increase in cancer-specific survival.

Overall, these results show that pathways identified in the DNA methylation landscape of TAMs are reflected in the cancer-specific transcriptome of TAMs, associated with aggressive breast cancer subtypes and poor clinical survival. Additionally, these results further emphasize the role of BMDM gene expression patterns in TAMs.

To elaborate the transcriptional alterations in the monocytic origin of TAMs, differential expression analysis between BMDM-T and BMDM-H was performed. 111 in BMDM-T upregulated, and 96 downregulated DEGs were identified (**Fig. 3.23.a**). Although overall differences were minor compared to the TAM vs MG comparison, similar upstream regulators of transcription, such as IFN-γ, TNF-α, and CSF2, were identified (**Fig. 3.23.b**).

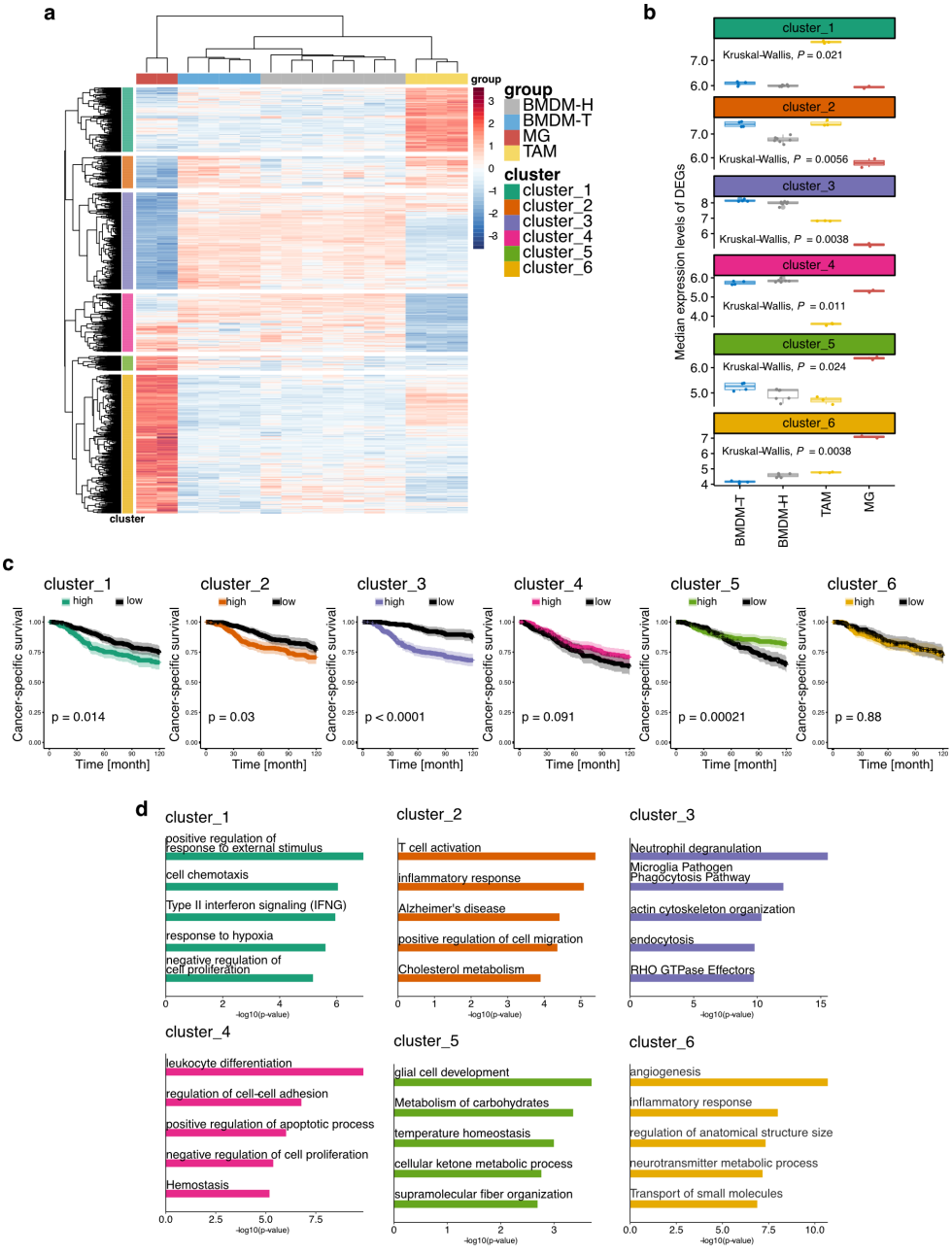

Figure 3.22: Cluster analysis reveals a TAM transcriptional program with high expression in BMDMs and strong effect on patient survival. (**a**) Hierarchical clustering of TAM vs MG DEGs in all samples. DEG clusters were identified by k-means clustering (k =6). (**b**) Median gene expression of each cluster in every group. (**c**) Cancer-specific survival of the METABRIC cohort according to the expression of genes identified in every cluster (+/-1SD of median cluster DEGs expression). (**d**) Enrichment of pathways and gene ontologies of DEGs, identified in the different clusters.

These findings reflect a cancer-specific effect on gene expression patterns in BMDMs and support our results of transcriptional and epigenetic reprogramming in the monocyte to TAM trajectory.

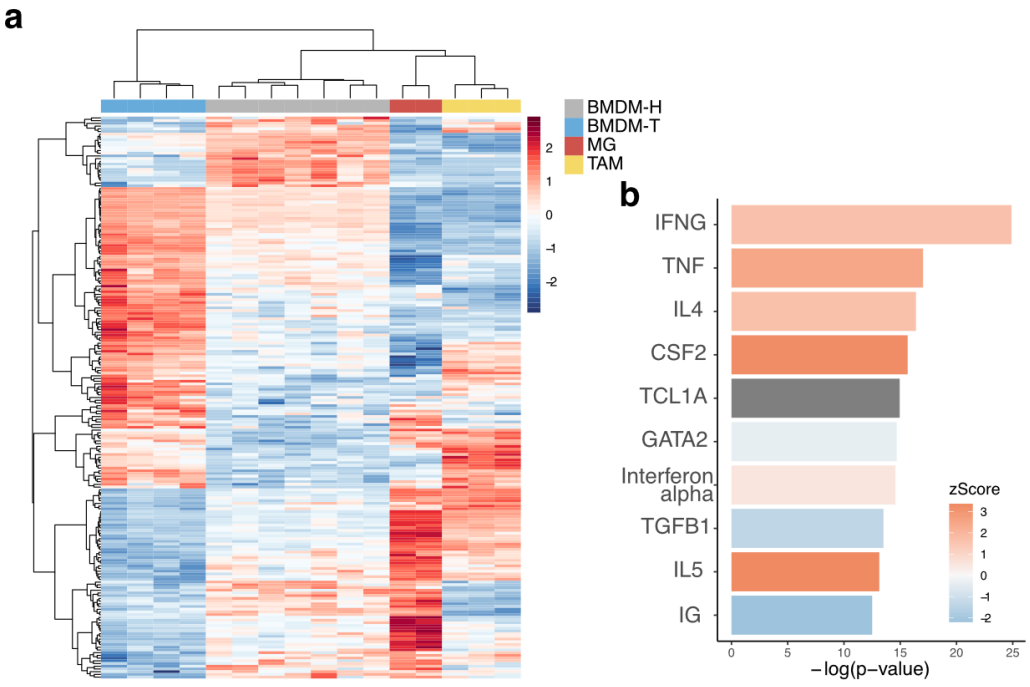

Figure 3.23: Characterization of cancer-specific transcriptional alterations of BMDMs in breast cancer. (**a**) Hierarchical clustering of BMDM-T vs BMDM-H DEGs in all samples. DEGs are defined by an adjusted *P* value <0.05, absolute log2 fold change >1. (**b**) Upstream regulator analysis of BMDM-T vs BMDM-H gene expression changes. The bar's color indicates the activation (red) or repression (blue) of genes regulated by the identified upstream regulators.

3.2.4 Complex signaling within the tumor microenvironment is associated with the cancer-specific DNA methylation landscape of tumor-associated macrophages

The central pathways and upstream activators regulating the identified DEGs and DMRs (e.g., IFN-γ, TGF-β, CSF1, and TNF-α) suggested microenvironmental signals to be drivers of TAM reprogramming. We, therefore, utilized a publicly available scRNAseq dataset of BALB/c-derived 4T1 orthotopic tumors[269] to understand the origin of these microenvironmental signals. Using Seurat[286], we identified 14 clusters assigned to their

putative cell type identity by cross-referencing cluster-specific marker genes with published resources. Eight different cell types of the tumor microenvironment, in addition to cancer cells of epithelial origin, were depicted (**Fig. 3.24.a**). Overall, macrophages accounted for >60% of all sequenced cells (**Fig. 3.4.b**), confirming previous reports that identified macrophages as the most prominent immune cell infiltrate of breast cancer[47,314]. On the contrary, only around 25% of all cells accounted for cancer cells.

Next, we applied a model for predicting cell-to-cell interactions based on known ligand/receptor pairs (CellPhoneDB)[84]. Network construction of the cell-to-cell interactions within the 4T1-single-cell dataset revealed CAFs and cancer/epithelial cells to be the major interaction hub of macrophages (**Fig. 3.24.c**). In total, over 400 interactions of macrophages with other cell types of the tumor microenvironment were identified (**Fig. 3.24.d**), validating the abundant interactions of TAMs[111]. The crosstalk included the interaction of the inhibitory molecule CD274 on macrophages with PDCD1 on T-cells, and CD80 on B-cells, macrophages, and neutrophils. Also, the inhibitory receptor CTLA4, expressed by NK- and T-cells, was predicted to interact with CD80 and CD86 on macrophages, indicating the diverse immune checkpoints of the tumor microenvironment.

Although CellPhoneDB models potential ligand/receptor interactions based on their expression, it does not account for downstream transcriptional or epigenetic effects in the interacting cell type of interest. To determine the ligand/receptor interactions with the most substantial impact on TAM reprogramming, we further prioritized ligands based on their capacity to activate TFs, identified in the TAM DNA methylation landscape (**Fig. 3.25.b**). We specifically investigated the intersection (**Fig. 3.25.a**) of predicted ligand/receptor interactions (**Fig. 3.25.c**), overlapping with cytokines and growth factors that have the potential to activate TFs[243] (**Fig. 3.25.d**) determined in the TF motif analysis of hypomethylated TAM vs MG DMRs (**Fig. 3.25.e**). Utilizing this approach, we identified seven key ligands (TGFB3, TGFB1, IFN-γ, CSF3, CSF1, CCL4, and CCL2), signaling via six receptors (TGFBR1, IFNGR, CSF3R, SIRPA, CCR5, and CCR2) and 12 TFs (STAT4, STAT3, STAT1, RUNX, NFκB-P65-REL, NFKB-P50, FOSL2, FLI1, ATF3, ATF2, and AP-1) that explain TAM reprogramming in breast cancer. Noteworthy, 6 of the 7 identified ligands were also predicted as upstream regulators in the TAM vs MG expression analysis (TGFB3, TGFB1, IFN-γ, CSF3, CSF1, and CCL2), confirming the critical role of these

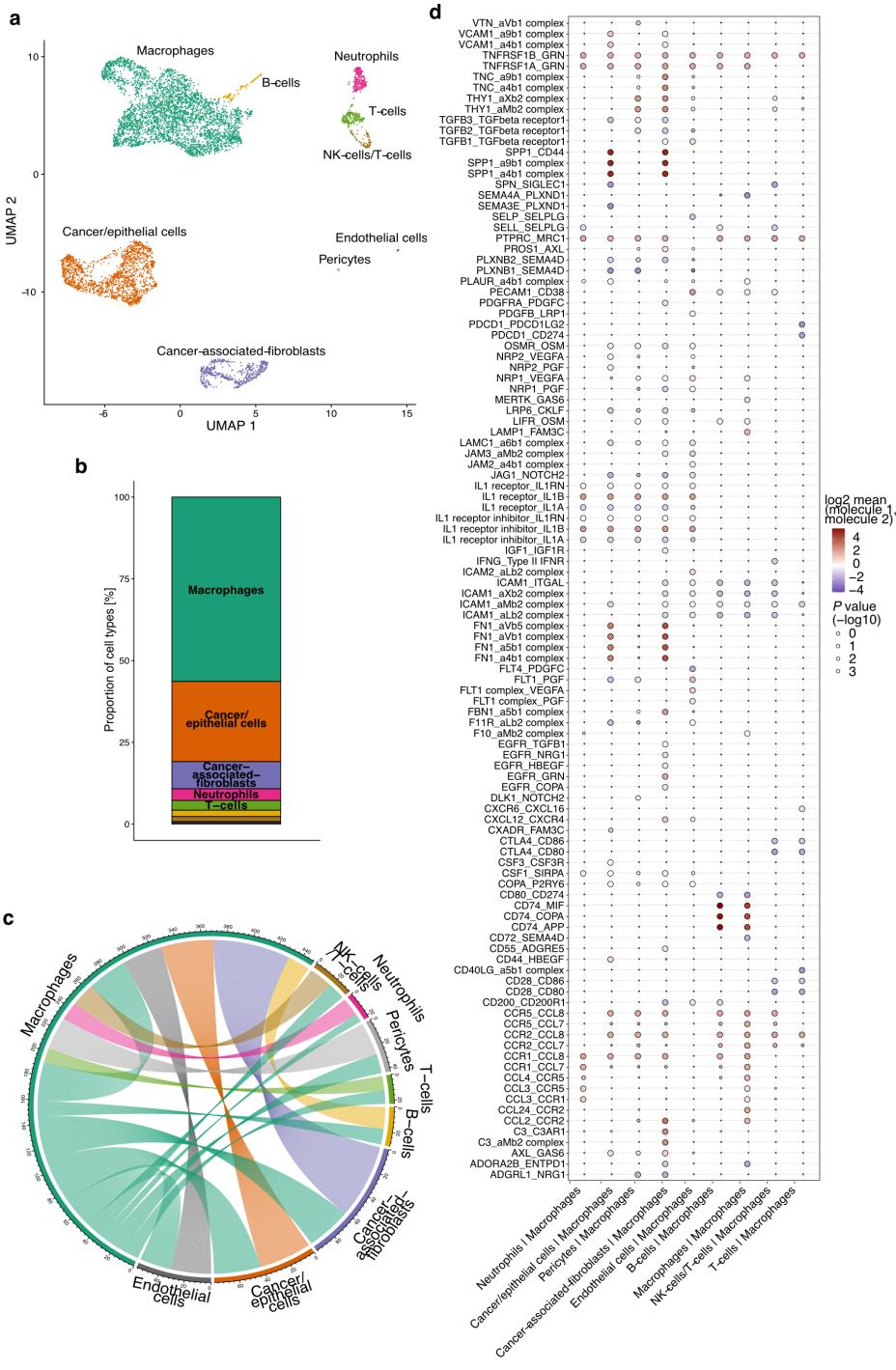

Figure 3.24: scRNAseq reveals complex signaling of macrophages within the tumor microenvironment.

Figure 3.24: scRNAseq reveals complex signaling of macrophages within the tumor microenvironment. (**a**) UMAP representation of breast cancer, obtained from scRNAseq of the 4T1 orthotopic breast cancer mouse model. Data was acquired from Sebastian et al., 2020. The color labeling indicates annotated cell types. (**b**) Proportions of the different cell types, identified via scRNAseq. (**c**) Chord diagram of predicted ligand/receptor interactions of macrophages with cell types specified in the scRNAseq of the 4T1 orthotopic mouse model. Ligand/receptor interactions were predicted via CellphoneDB. Macrophage interactions with a *P* value <0.05 are visualized. (**d**) Dot plot of all ligand/receptor interactions of macrophages with a *P* value <0.05.

ligands and their effect on DNA methylation in TAM reprogramming (**Fig. 3.25.f**).

Among these ligands, we were able to show that TGFB3 was released by CAFs, cancer cells, and pericytes and interacted via TGFBR1, which was predicted to activate FOSL2 in TAMs. Similarly, TGFB1 had a dual-source from CAFs and endothelial cells and interacted via TGFBR1, leading to the activation of FOSL2 and STAT3. In contrast, IFN-γ was shown to be secreted by NK-/T-cells and interacted via Type II IFNR. Downstream of IFNγ, a multitude of TFs (STAT4, STAT1, RUNX1, RUNX, NFκB-P65-REL, and AP-1) were activated and enriched in hypomethylated TAM vs MG DMRs. Furthermore, the major macrophage growth factor, CSF1, was shown to have various sources in the tumor microenvironment. Interaction with SIRPA led to the proposed activation of NFκB-P65-REL and NFvB-P50 in TAMs. Supporting the central role of the identified TFs in the cancer-specific reprogramming of TAMs, *Stat1*, *Runx3*, and *FosL2* gene expression was found to be significantly induced in TAMs compared to MGs and BMDMs (**Fig. 3.25.g**).

In summary, within a highly complex signaling network of the tumor microenvironment in breast cancer, we were able to identify prominent microenvironmental regulators of TAM DNA methylation and transcription. We were able to specify their source within the tumor microenvironment and designated the involved receptors and TFs causing the transcriptional and epigenetic switch in TAMs.

3.2.5 Tumor-associated macrophage DNA methylation signature is associated with breast cancer subgroups and poor clinical outcomes in breast cancer patients

Differential methylation signals can potentially arise from cell type compositions of the analyzed samples. To a certain extent, this bias was avoided by fluorescently activated cell sorting of macrophage and monocyte populations by specific surface markers. However,

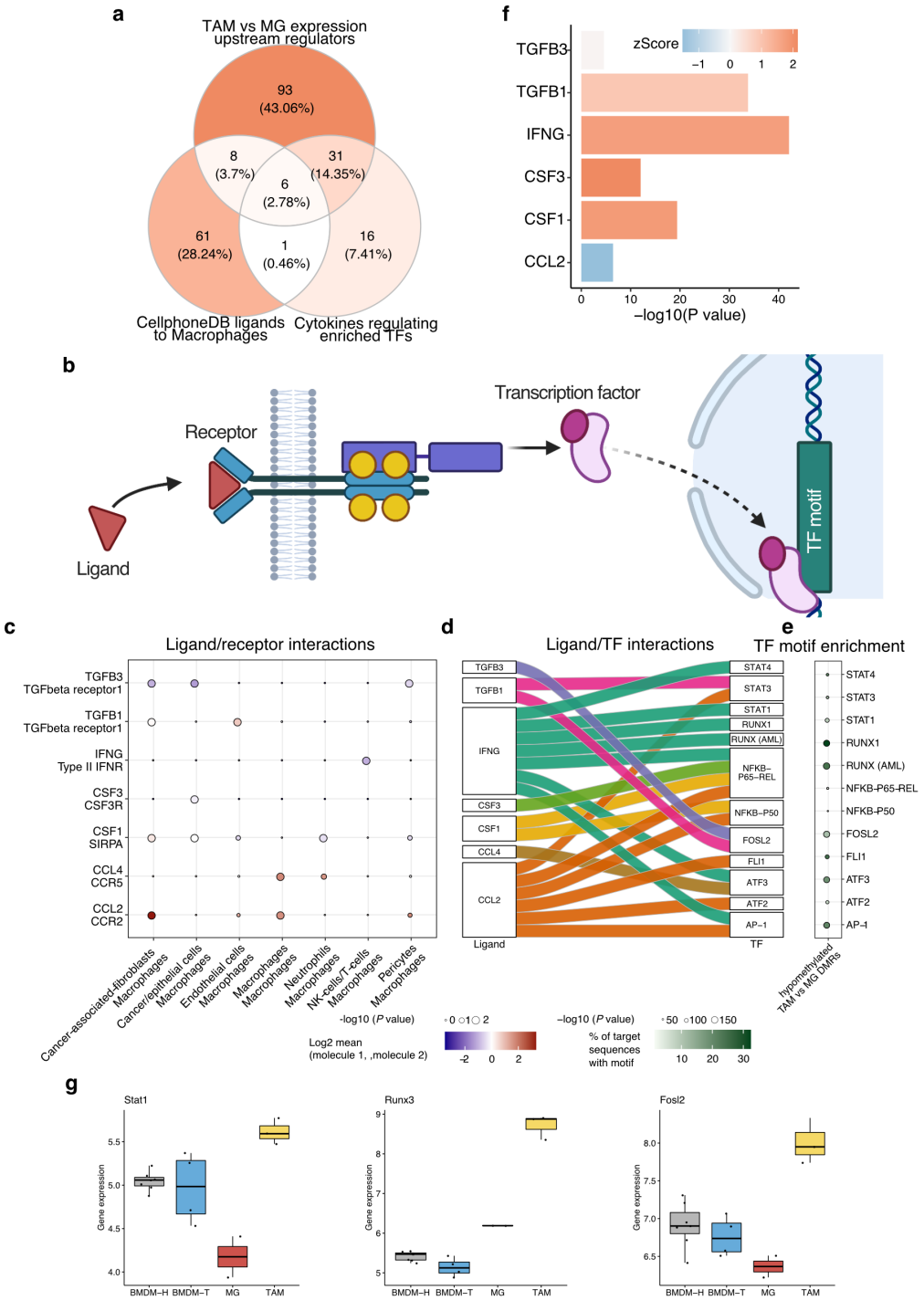

Figure 3.25: Epigenetic reprogramming of TAMs can be linked to specific ligand/receptor interactions within the tumor microenvironment.

Figure 3.25: Epigenetic reprogramming of TAMs can be linked to specific ligand/receptor interactions within the tumor microenvironment. (**a**) Venn diagram of ligands predicted to interact with macrophages, ligands identified as upstream regulators of TAM vs MG gene expression changes, and ligands with an activating effect on TFs, identified in the TF motif analysis of hypomethylated TAM vs MG DMRs. Ligand/receptor interactions were predicted via CellphoneDB. (**b**) Dot plot of prioritized ligand/receptor interactions. Ligand/receptor interactions were prioritized by an overlap of ligands predicted to interact with macrophages, and ligands with an activating effect on TFs, identified in hypomethylated TAM vs MG DMR TF motif enrichment. (**c**) Graphical representation of the data integration and ligand prioritization workflow. Ligand/receptor interactions are integrated with ligand/TF activation and TF motif information. (**d**) Alluvial plot indicating the selected ligands and their impact on TF activity. (**e**) Selected TFs identified in the TF motif enrichment of hypomethylated TAM vs MG DMRs. (**f**) Selected upstream regulators identified in the TAM vs MG comparison, overlapping with ligands predicted to interact with macrophages, and ligands with an effect on TF activity, identified in the TF motif analysis of hypomethylated TAM vs MG DMRs. (**g**) Gene expression of TFs identified as differentially expressed (adjusted *P* value <0.05 and absolute log2 fold change >1) in the TAM vs MG comparison.

further heterogeneity might be present on an epigenetic level, or cancer-specific alterations are not present in all sampled cells (e.g., unchanged MGs or BMDMs within the TAM samples).

To control for this bias, we performed reference-free deconvolution with MeDeCom that allows the decomposition of DNA methylomes into latent methylation components (LMCs) and their respective proportions in each sample [192]. The resulting LMCs correspond to the underlying sources of variation in the bulk methylomes, and the proportions quantify their relative contribution to each bulk sample.

In total, five LMCs, explaining the methylation levels of a union set of DMRs from all comparisons, were identified, and a differential enrichment in the distinct groups was observed (**Fig. 3.26.a** and **b**): LMC1 was uniquely enriched in TAMs and depleted in MGs and BMDMs; LMC2 was enriched in MGs and depleted in TAMs; LMC3 was enriched in BMDM-T and TAMs, and depleted in MGs; LMC4 was enriched in MGs and depleted in BMDMs; LMC5 was enriched in BMDM-H and depleted in TAMs and MGs. These deconvolution results confirmed our prior assumption of the sampled TAM methylomes being composed mainly out of a unique TAM DNA methylation signature (LMC1) and to a lesser extend of BMDM-T (LMC3) and MG methylomes (LMC4).

To functionally annotate these LMCs, we determined the DMRs specifically hypomethylated in one LMC compared to the average methylation of the DMRs in the remaining LMCs. By using a very stringent cutoff (delta >0.7), we treated the obtained

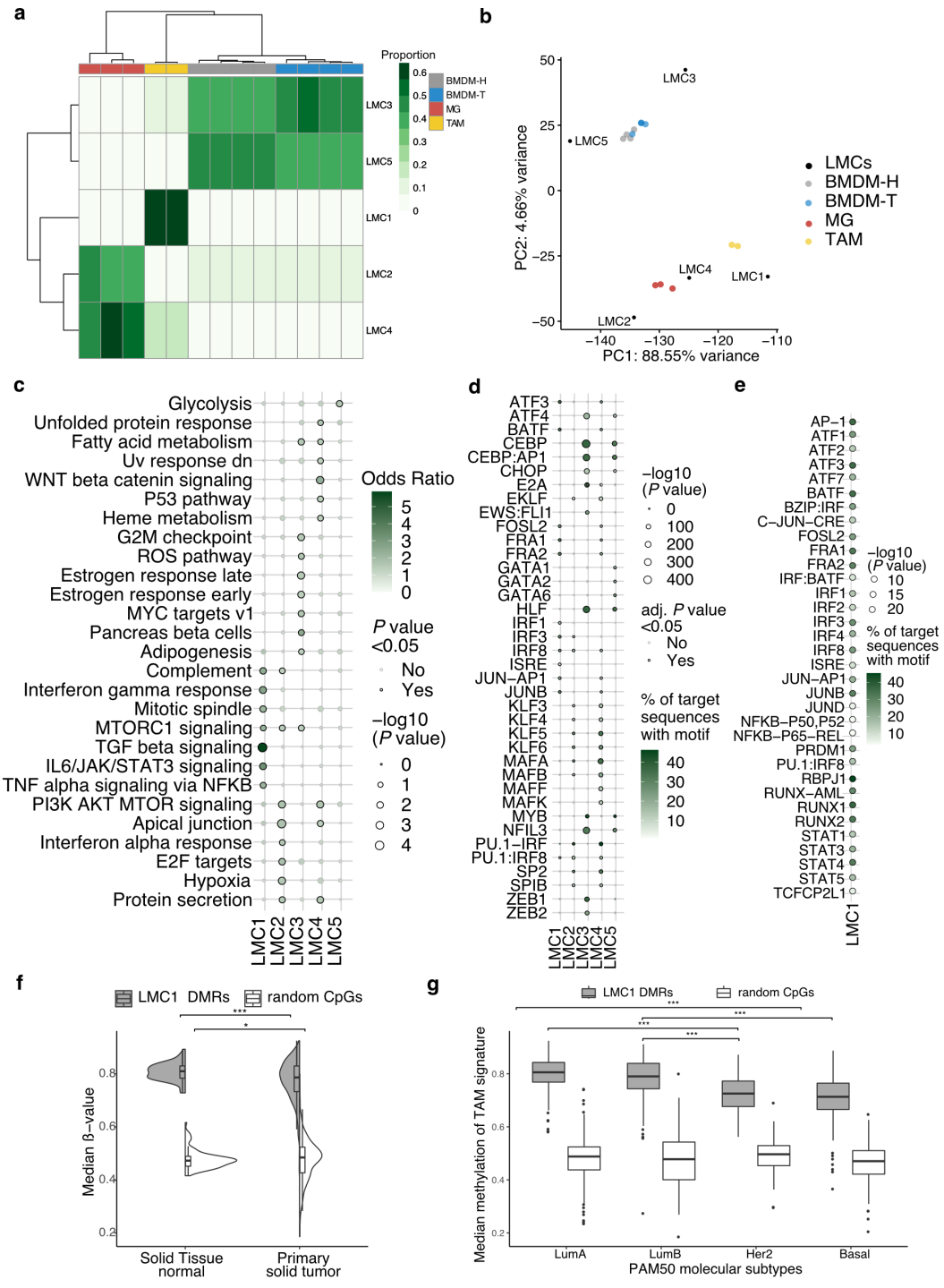

Figure 3.26: Deconvolution of DNA methylation landscapes identifies a unique TAM signature associated with cancer-specific pathways and breast cancer subtypes.

Figure 3.26: Deconvolution of DNA methylation landscapes identifies a unique TAM signature associated with cancer-specific pathways and breast cancer subtypes. (**a**) Hierarchical clustering of recovered LMC proportions in each sample, identified by reference-free deconvolution using MeDeCom (k =5 and λ =0.01). Methylation levels of a union track of DMRs from all comparisons (TAM vs MG, BMDM-T vs BMDM-H, BMDM-H vs MG, BMDM-T vs TAM, BMDM-T vs MG, and BMDM-H vs TAM) were used for deconvolution analysis. (**b**) PCA of DNA methylation levels of DMRs from all comparisons and the DNA methylation levels of DMRs annotated to the different LMCs. (**c**) MSigDB hallmarks enrichment of DMRs associated with the identified LMCs. All MSigDB hallmarks with a *P* value <0.05 are shown. (**d** and **e**) TF motif enrichment of DMRs associated with LMCs. (**d**) Top 10 TF motifs per LMC and (**e**) all LMC1 TF motifs with an adjusted *P* value < 0.05 are shown. (**f**) Median DNA methylation of LMC1 DMRs in primary solid tumors and normal tissue of the TCGA breast cancer cohort. (**g**) Median DNA methylation of LMC1 DMRs in the TCGA breast cancer cohort, stratified by the PAM50 molecular classifier. (**f** and **g**) One-way ANOVA with Tukey's post hoc multiple comparisons test. *, *P* value <0.05; ***, *P* value <0.001.

sites as LMC-specific and further used them for MsigDB hallmarks enrichment (**Fig. 3.26.c**) and TF motif analysis (**Fig. 3.26.d**). Specifically, the 333 LMC1 DMRs were of interest, since LMC1 was uniquely enriched in TAMs and therefore depicted a cancer-specific TAM DNA methylation signature. Exclusive enrichment of TGF-β, TNF-α, IFN-γ, and Il6/JAK/STAT3 signaling and the MSigDB hallmark mitotic spindle was observed for LMC1 DMRs (**Fig. 3.26.c**). Furthermore, the MsigDB hallmarks complement system and MTORC1 signaling were enriched in these regions. Accordingly, hypomethylated LMC1 DMRs showed enrichment for TF motifs belonging to the BZIP (e.g., FOSL2, FRA1, and FRA2), IRF (e.g., IRF1, IRF3, and IRF8), RUNT (e.g., RUNX), and STAT (e.g., STAT1, STAT3, STAT4, and STAT5) TF-family. Also, RBPJ1, the transcriptional regulator of Notch signaling and a TF essential for monocyte to TAM differentiation in a transgenic mouse model of breast cancer [103], showed robust enrichment in LMC1 DMRs (**Fig. 3.26.e**).

Previous studies [46,308] as well as our own findings (**Fig. 3.21**) demonstrate the suitability of TAM expression signatures as prognostic and diagnostic markers for breast cancer. However, DNA methylation-based immune signatures have not been purposed for this analysis, yet. Therefore, we sought to utilize the identified LMC1 signature in a large DNA methylation cohort of breast cancer [165]. We investigated LMC1 DMRs that overlapped with 450k Illumina probes of the TCGA-breast cancer cohort post lift-over from the mm10 to the hg19 reference genome. This revealed reduced DNA methylation of LMC1 DMRs in primary solid tumors than solid normal breast tissue (**Fig. 3.26.f**). Furthermore, we assigned patient samples to their respective breast cancer molecular subtypes, based on the PAM50

classification, and investigated LMC1 DNA methylation (**Fig. 3.26.g**). Patient samples from the basal and Her2 PAM50 molecular subtypes revealed lower DNA methylation compared to luminal A or B samples. For a random set of CpGs, no significant differences between tumor and normal and within the different PAM50 molecular subtypes were identified, indicating an LMC1-specific instead of a genome-wide hypomethylation in tumors and aggressive breast cancer subtypes.Together, these results emphasize an association of the TAM DNA methylation signature, driven by tumor microenvironmental-derived stimuli like TGF-β, TNF-α, and IFN-γ, as well as TFs, such as RUNX3, FosL2, STAT1, and RBPJ1 with more aggressive breast cancer subtypes.

Gene annotation of the TAM DNA methylation signature showed an association of LMC1 DMRs with 44 TAM vs MG DEGs. The majority of them (40 DEGs) were significantly upregulated (adjusted *P* value <0.05; log2 fold change >1) in TAMs (**Fig. 3.27.a**). Notably, the signature contained surface-membrane receptors (e.g., *Tgfbr1* and *Ifngr2*) and TFs (e.g., *Runx3* and *Stat1*) with a role in TAM reprogramming. Also, the immune inhibitory ligand, *Cd274*, was identified within these DEGs. Consistent with the TAM expression signature of **Fig. 3.21**, stratification of the METABRIC breast cancer cohort with annotated LMC1 DMRs that overlapped with upregulated TAM vs MG DEGs showed increased expression levels in claudin-low and basal compared to luminal A or B breast cancer subtypes (**Fig. 3.27.b**)). Also, stratification based on the CSF1 signature expression[20] revealed an increased LMC1 signature expression in CSF1-high compared to CSF1-mid and -low groups (**Fig. 3.27.c**). Accordingly, a significant correlation between the LMC1 signature expression and macrophage infiltration was observed (**Fig. 3.27.d**). Furthermore, patients with a high LMC1 signature expression also had a substantial decrease in cancer-specific survival (**Fig. 3.27.e**).

Overall, such data reinforces the necessity of homogenous reference samples for computational deconvolution analysis and the concept of TAMs in promoting cancer progression. They will further guide the identification of unique TAM DNA methylation and expression markers that provide the possibility for new therapeutic approaches as well as diagnostic and prognostic marker discovery.

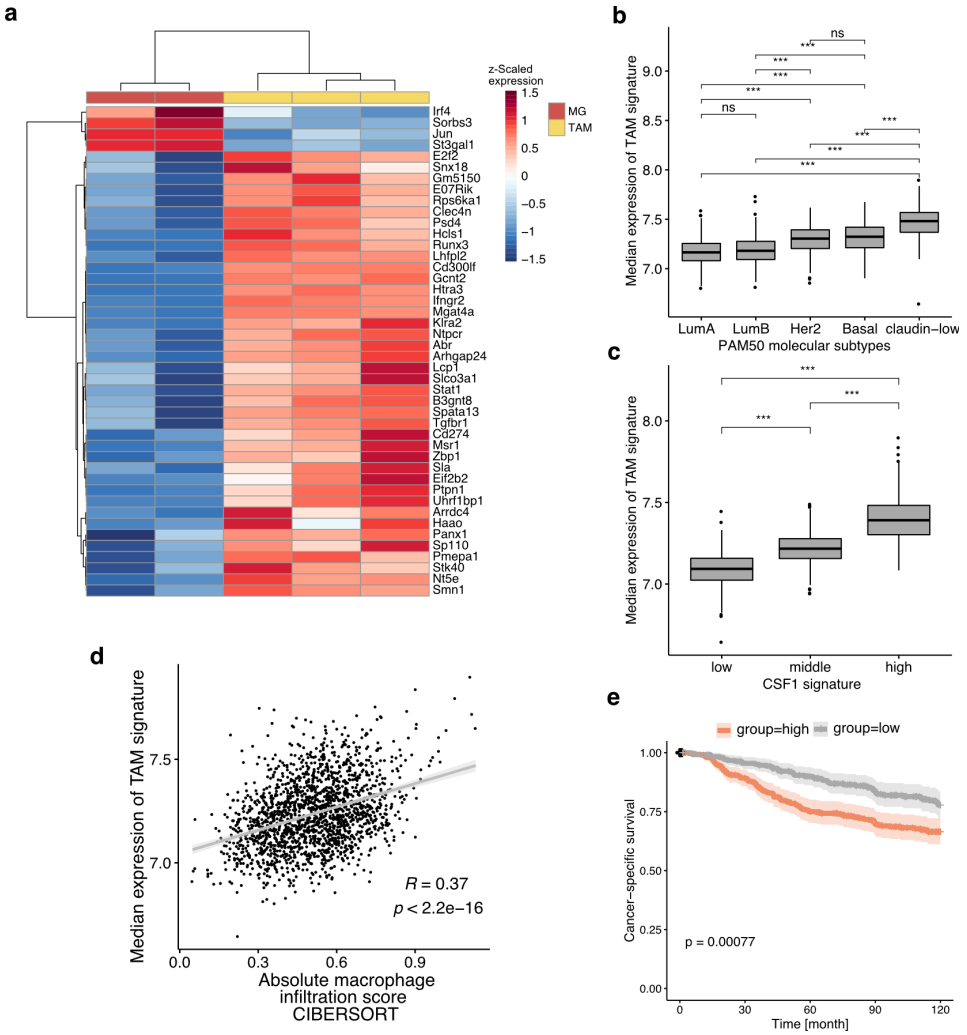

Figure 3.27: Genes annotated to TAM DNA methylation signature are associated with poor clinical outcomes in breast cancer patients and confirm the role of *Runx3* and *Stat1* in TAM reprogramming. (**a**) Hierarchical clustering of TAM vs MG DEGs (adjusted *P* value <0.05 and absolute log2 fold change >1), annotated to LMC1 DMRs. LMC1 DMRs are annotated to an overlapping or closest gene with a maximum distance of <10 kbs. (**b** and **c**) Median expression of genes significantly upregulated in the TAM vs MG comparison (adjusted *P* value <0.05 and log2 fold change >1) and annotated to LMC1 DMRs, in human breast cancer cohort METABRIC, stratified by (**b**) the PAM50 molecular classifier and (**c**) CSF1 signature expression. (**d**) Correlation of the expression of genes, significantly upregulated in TAM vs MG (adjusted *P* value <0.05 and log2 fold change >1) and annotated to LMC1 DMRs, with macrophage infiltration in patients of the METABRIC cohort. The macrophage infiltration score was calculated by the sum of M0, M1, and M2 macrophages predicted by CIBERSORT. *P* values were calculated by Pearson correlation coefficient. The gray diagonal represents the linear regression. Shaded areas are the confidence interval of the correlation coefficient at 95%. (**e**) Cancer-specific survival of the METABRIC cohort according to the expression of genes significantly upregulated in TAM vs MG (adjusted *P* value <0.05 and log2 fold change >1) and annotated to LMC1 DMRs (+/- 1 SD of median TAM signature expression). (**b** and **c**) One-way ANOVA with Tukey's post hoc multiple comparisons test. ns, *P* value >0.05; ***, *P* value <0.001.

4

Discussion

4.1 Epigenetic reprogramming of airway macrophages drives polarization and inflammation in muco-obstructive lung disease

Using WGBS and ATACseq, we demonstrated that the altered airway microenvironment in muco-obstructive lung disease causes proinflammatory changes in the epigenetic landscape of AMs. We revealed that *Scnn1b*-Tg AMs are deregulated in the DNA methylation and chromatin accessibility level, with alterations enriched for gene-regulatory regions such as promoters and enhancers. Those changes favor the binding of TFs involved in inflammation and macrophage polarization and correlate with the induction of a transcriptional program enriched for macrophage activation, inflammatory processes, and tissue remodeling. Activation of AMs in muco-obstructive lungs was confirmed via high-dimensional single-cell analysis of protein surface markers and showed a mixed phenotype of classical and alternative macrophage activation. Deconvolution of RNAseq data revealed

that monocyte recruitment to the muco-obstructed lung plays a neglectable role in the *Scnn1b*-Tg model of muco-obstructive lung disease. On the contrary, stimulation of WT AMs with native mucus induced a transcriptional program reminiscent of the one observed in *Scnn1b*-Tg AMs, showing the direct immunomodulatory effect of mucus. Moreover, functional consequences of the epigenetic modifications in *Scnn1b*-Tg AMs were shown by impaired efferocytosis and phagocytosis, and a prolonged hyperinflammatory response upon LPS challenge was depicted. Impaired LPS responses on transcriptional and chromatin accessibility levels were linked to increased TF activity of the IRF TF-family in *Scnn1b*-Tg AMs. These findings will guide the development and improvement of immunomodulatory therapies for muco-obstructive lung diseases, such as CF and COPD.

AMs reside in different airway niches of the lung and are exposed to unique environmental signals. In muco-obstructive lung disease, these niches include regions of dehydrated and excess mucus, as well as mucus plugging, causing local hypoxia, increased apoptosis, necrosis, infection, and inflammation[35]. Our findings show that AMs undergo epigenetic reprogramming due to sustained exposure to signals provided by the microenvironment of muco-obstructed airways. Reduced DNA methylation and increased chromatin accessibility of gene regulatory regions and TF-binding motifs that play a crucial role in macrophage activation, plasticity, and inflammation (e.g., IRF2/3, ATF3, NFKB, AP-1, CEBP, and STAT6) were observed. Different gene-regulatory roles can be assigned to the identified TFs. IRF2/3 and ATF3 suppress macrophage inflammation, while NFKB and AP-1 stimulate inflammatory responses[80,126,153]. Classical macrophage activation is promoted by NFκB and AP-1, while alternative activation is stimulated by CEBP, STAT6, and ATF3[307]. Additionally, some of the discovered TFs have been previously linked to chronic lung diseases. AMs from CF patients show increased nuclear translocation of NFκB, and increased NFκB expression has been demonstrated in the airways of patients with COPD and asthma[83,311]. STAT6 is involved in the IL-33-induced release of IL-13, which plays a critical role in type II inflammation of the airways[105,172,325]. Modifications in other epigenetic layers have been previously shown in AMs from COPD patients. Increased acetylation of histones within promoter regions was linked to enhanced baseline expression of inflammatory markers. Notably, this hyperinflammatory phenotype persisted even after prolonged ex vivo culture[105,172,325]. Correspondingly, AMs from patients with asthma

revealed increased expression of inflammatory genes linked to repressed histone deacetylase activity augmented by the increased enzymatic activity of histone acetylases. These alterations weren't observed in asthmatic patients' peripheral blood mononuclear cells, emphasizing the role of the local muco-obstructive microenvironment in AM function[59].

According to the epigenetic alterations in *Scnn1b*-Tg AMs, transcriptional profiling showed coinciding changes in gene expression. Significant upregulation of classical (e.g., *Ccl2*, *Ptgir*, *Ccl9*, *Il1a*, *Marcks*, *H2-Aa*, and *H2-Eb1*) and alternative markers of macrophage activation (e.g., *Mmp12*, *Arg1*, *Trem2*, *Ccl22*, *Ccl17*, and *Ptgs1*) were observed. Upstream regulator analysis of the transcriptome and chromatin accessibility predicted the respective stimuli for classical (IFN-γ and LPS) and alternative (IL-4) macrophage activation. In fact, the muco-obstructive microenvironment of *Scnn1b*-Tg lungs supports AM activation in both directions. Increased expression of IL-4, IL-13, and TNF-α as well as a higher bacterial burden has been shown in previous studies[105,187,197]. Together, these findings suggest the presence of AM subtypes or a mixed AM phenotype in *Scnn1b*-Tg mice. Instead of the emergence of novel AM subpopulations in *Scnn1b*-Tg compared to WT mice, analysis of AM heterogeneity by high-dimensional single-cell flow cytometry revealed activation of already existing AM subpopulations in muco-obstructive lungs (decreased expression of Siglec-F and increased expression of CLEC7A, CD68, CD11B in *Scnn1b*-Tg AMs). The single-cell analysis also showed the presence of classical and alternative macrophage markers on the same AM populations. These results indicate a mixed phenotype of AMs in *Scnn1b*-Tg lungs and emphasize a spectrum model of macrophage activation. In contrast to the simplified classification of macrophages into pro- (M1) and anti-inflammatory (M2) functions, macrophages can acquire multiple tasks, reflecting cellular adaptations to environmental perturbations[125,331]. These results align with a recent scRNAseq study of COPD patients, confirming the absence of novel AM subpopulations in the muco-obstructed lung[16]. The study further confirmed AM plasticity and heterogeneity and revealed the difficulty of inter-patient heterogeneity in COPD, emphasizing the role of mouse models for the basic molecular understanding of muco-obstructive lung disease.

In contrast to common mouse models of induced lung fibrosis and acute lung inflammation, monocyte recruitment to the muco-obstructed lung plays a neglectable role in *Scnn1b*-Tg mice[209,214]. In both previous studies, the authors have demonstrated that

recruited monocytes express higher levels of proinflammatory and profibrotic genes than resident AMs. However, fate mapping also revealed that recruited mfonocytes commit to an AM fate over time. Utilizing these references, we have demonstrated that AMs in the muco-obstructed lung resemble tissue-resident AMs. Furthermore, the data indicates that no monocyte recruitment occurs at six weeks of age. If monocyte recruitment to the lung has taken place at an earlier time point, they have completely adapted to the transcriptional phenotype of AMs from *Scnn1b*-Tg lungs.

Many immunomodulatory factors in chronic obstructive lung diseases may interact with AMs and drive proinflammatory epigenetic reprogramming. Mucus is one putative immunomodulatory factor, as it can directly bind to leukocyte receptors through mucin glycans[164,273]. Ex vivo stimulation of WT AMs with native mucus showed upregulation of genes (e.g., *Arg1*, *Mmp12*, *Il1a*, *Ccl17*, and *Ccl22*), reminiscent of the *Scnn1b*-Tg AM phenotype. These results imply the direct interaction of mucin glycoproteins with AM receptors in muco-obstructive lungs. In line with this interaction, binding of MUC5B to Siglec-F on lung eosinophils has been shown previously[164,273]. This interaction induced the apoptosis of eosinophils in allergic inflammation, although an effect on AMs expressing Siglec-F was not observed. MUC2 expression has been shown to repress inflammation in the gut and further induce tolerance in DCs[273]. Further understanding of the interaction between mucus/mucins and AM dysfunction will help develop new therapeutic approaches targeting the underlying cause of many chronic lung diseases.

For AMs, the identified disease-related epigenetic alterations had marked functional implications. Crucial AM functions, such as efferocytosis and phagocytosis, were decreased, and treatment of *Scnn1b*-Tg AMs with LPS induced significantly more cytokines than LPS-treaded WT AMs. The enhanced and prolonged LPS-response of *Scnn1b*-Tg AMs was shown on mRNA and protein levels. A clear role of the muco-obstructed microenvironment in priming hyperinflammatory responses was given, as *Scnn1b*-Tg macrophages from the peritoneum or AMs from $Cftr^{-/-}$ mice ($Cftr^{-/-}$ mice do not develop a muco-obstructive lung phenotype) responded similarly to WT controls. Infections with gram-negative bacteria like *P. aeruginosa* are common in CF and other muco-obstructive lung diseases. The resulting excessive inflammatory responses can harm the host's tissue integrity and homeostasis[29,86].

Integrated analysis of the chromatin accessibility and transcriptome data of LPS

treated AMs revealed the IRF transcription factor family and especially IRF1 as mediators of prolonged and hyperinflammatory LPS responses. In addition, previous research has indicated that IRF1 plays a vital role in LPS-induced acute lung injury[328]. Together, these results suggest that increased IRF1 signaling in AMs from muco-obstructed lungs might lead to the high morbidity and mortality seen in patients with CF and COPD, who frequently experience acute pulmonary exacerbations[29,86,311,315].

Recent advancements in epigenetic inhibitors targeting the bromodomains and extra terminal domain (BET) family of proteins have shown their therapeutic potential in cancer, inflammatory, and autoimmune diseases[21,114,219]. In particular, their function to counter immunoinflammatory damage via the regulation of enhancer activity has been described. Therefore, we postulate a BET-targeted therapy in modulating macrophages' inflammatory responses in chronic lung diseases to refine the overall therapeutic strategies of muco-obstructed lung diseases.

4.2 Cancer-specific DNA methylation landscape of tumor-associated macrophages and monocytes in breast cancer

Utilizing a low-input WGBS protocol, we provided the first comprehensive characterization of the DNA methylation landscape of TAMs and BMDM-T in breast cancer and cancer in general. By comparing TAMs from the 4T1 orthotopic breast cancer mouse model with their healthy counterpart, MGs, we were able to show massive alterations in the TAM epigenome on a global and focal level. We defined known as well as novel putative tumor microenvironment drivers and showed the fundamental involvement of DNA methylation in the process of TAM reprogramming. Even in the bone marrow compartment, epigenetic reprogramming of monocytes by breast cancer was exposed. Further dissection of TAM alterations identified TAM-specific epigenetic programs as well as DNA methylation patterns originating from their monocytic progenitors. Alterations in the DNA methylation landscape were correlated to a cancer-specific transcriptome of TAMs and BMDM-Ts, associated with aggressive breast cancer subtypes, macrophage infiltration, and poor clinical outcomes in a human cohort of breast cancer patients. Further dissection of the cancer-specific signature established the significance of BMDM-originating transcriptional patterns in the outcomes of breast cancer patients. By integrating scRNAseq data of the breast cancer mouse model, we mapped microenvironmental stimuli within the tumor microenvironment, responsible for TAM reprogramming, and identified critical TFs involved in this process. Using a reference-free deconvolution approach, we further detected a unique TAM DNA methylation signature. Differential methylation of the TAM signature was associated with aggressive breast cancer subtypes and high tumor grade in human breast cancer patients. Collectively, our results highlight the TFs, STAT1, RUNX3, and FOSL2 in TAM reprogramming and as potential targets for TAM-based therapeutic interventions. Along with recent evidence of the role of TAMs in chemo- and immunotherapy resistance [221], our study pinpoints the need to investigate the epigenetic landscape of TAMs in human cancers and identify markers and mechanisms for TAM-specific targeting.

Previous studies in cancer mouse models have shown that TAMs are of monocytic origin in most cancer entities, and further TAM expansion via proliferation is possible [103,66,246]. In breast cancer, a cancer-specific reprogramming of monocytes to TAMs upon macrophage

differentiation has been indicated[7,103,102,245]. However, clinical translation of TAM transcriptome signatures has only been achieved upon comparing TAMs with their healthy tissue counterpart – MGs[308]. This discrepancy emphasizes the high plasticity of macrophages and their potential to quickly adapt to a specific microenvironment[109,121,177]. In the case of TAMs, recruited monocytes adapt to the tissue niche and are further dictated by cancer-specific signals[46]. Accordingly, we performed a comprehensive comparison of TAMs with MGs and identified massive alterations in the DNA methylation landscape. Genome-wide hypomethylation, in addition to focal changes, enriched for gene-regulatory regions such as promoters were identified. Furthermore, TF-binding motifs (e.g., ATF3, CEBP, FRA1, FRA2, FOSl2, JUNB, NFIL3, and RUNX) and pathways involved in macrophage polarization and inflammation (e.g., IFN-γ response, IL2/STAT5 signaling, IL6/STAT3/signaling), as well as tumor-specific reprogramming of macrophages (e.g., TGF-β signaling, TNF-α signaling via NFκB), frequently associated with alternative macrophage polarization, were shown.

Further dissection of the TAM DNA methylation landscape revealed distinct epigenetic programs with a dual origin. A subset of DMRs showed similar methylation levels to BMDMs, whereas the remaining regions showed TAM-specific DNA methylation changes. These results emphasize a monocytic origin of TAMs in the 4T1 orthotopic breast cancer mouse model. In addition, further complementation of the TAM DNA methylation landscape by cancer-specific differentiation was shown. BMDM-originating patterns showed the most significant enrichment for inflammatory pathways such as IFN-γ response, TNF-α, and IL6/JAK/STAT3 signaling, as well as developmentally associated TFs, such as CEBP, RUNX, and NFIL3[65,160,340]. In contrast, TAM-specific alterations were explicitly enriched for tumor-microenvironment-associated pathways, including the signaling via the anti-inflammatory cytokine TGF-β[238]. Accordingly, enrichment of TF-binding motifs, previously assigned to the alternative polarization of macrophages, such as ATF3 and FOSL2, were identified in the TAM-specific DNA methylation programs[264,307].

Macrophage polarization has been classified into proinflammatory M1 and anti-inflammatory M2 states[201], and TAM phenotypes have often been described as M2-like in the case of tumor-supporting, immunosuppressive TAMs[65]. However, the beforementioned TFs and pathways support TAM polarization in both directions: TAM-specific programs

enriched for pathways and TFs known to regulate M2 functions; BMDM-originating programs enriched for pathways and TFs known to regulate M1 functions. These results reinforce the current trend in macrophage biology that states that macrophage phenotypes are more complex and cannot be classified into binary states[125,331]. Additionally, it validates a recent transcriptome study that showed no preferential enrichment neither of M2- nor M1-associated genes in TAMs of human breast and endometrial cancer[46].

Transcriptional profiling and multi-omics integration of TAMs, MGs, and BMDMs depicted a strong correlation between DNA methylation and gene expression. In particular, alterations in the DNA methylation landscape between TAMs and MGs were inversely correlated with a cancer-specific transcriptional program. Similar to previous studies, we were able to identify a TAM expression signature and showed its association with high tumor grade and poor clinical outcomes in human breast cancer patients[46,112]. Furthermore, our TAM signature's highest expression was observed in the most aggressive breast cancer subtypes and within a CSF1-high group, previously associated with higher tumor grade[20]. Corresponding to the role of CSF1 in monocyte recruitment and differentiation[77], TAM signature expression was correlated with the overall macrophage infiltration in human breast tumors, validating macrophage density as a predictor of poor survival[47]. These results demonstrate that an appropriate cancer mouse model, such as the 4T1 orthotopic breast cancer model, can directly lead to clinically translatable results. Generation of prognostic signatures based on TAM transcriptomes could be tested in prospective clinical trials (especially when targeting the tumor microenvironment, as done by CSF1 inhibition[231,299,332]) to assess treatment performance.

As shown for the DNA methylation landscape, the monocytic origin of TAMs was also reflected within distinct transcriptional programs. Notably, TAM vs MG DEGs with an intermediate expression level in TAMs compared to BMDMs and MGs allowed the most substantial segregation in patient survival. Patients with a high expression of these genes showed the worst cancer-specific survival. Since these highly predictive DEGs would have been missed comparing TAMs with BMDMs, these results emphasize the necessity of comparing TAMs with their healthy tissue counterparts when investigating TAM-related gene expression changes and functions. Macrophage phenotypes are strongly dictated by their tissue niche, albeit of potential differences in their ontogeny[46,308].

A distinct transcriptional program of monocytes has been reported in human renal carcinoma, as well as colorectal and breast cancer[46,52]. Accordingly, we were able to show that BMDMs from the 4T1 mouse model respond to breast cancer with a tumor-specific program on the level of gene expression and DNA methylation. Epigenetic and transcriptional alterations of BMDMs highlight the systemic effect of cancer and an early reprogramming of TAM progenitors. Although overall changes were weaker in comparison to the alterations identified in TAMs, enrichment of similar pathways (e.g., IFN-γ response, Il5/JAK/STAT3 signaling), upstream regulators (e.g., IFN-γ, TNF, CSF1, and CSF2), and TFs (e.g., STAT1) were identified. The enrichment of STAT1 TF motifs validates the prominent role of CSF1 in the recruitment and reprogramming of BMDMs to TAMs. It has been demonstrated that CSF1 is the key chemoattractant of monocytes and activates STAT1 TF-activity[20,310]. In addition, CSF1R inhibition delays mammary tumor growth in murine models[102,174]. Collectively, these results highlight the potential in reducing tumor progression by inhibiting monocyte to TAM reprogramming as early as in the bone marrow compartment[200]. The present dissertation shows a novel function of DNA methylation in regulating these processes and could help identify therapeutic approaches targeting the epigenome.

To elucidate the crosstalk between TAMs and the tumor microenvironment, we utilized a publicly available scRNAseq dataset of the 4T1 orthotopic breast cancer mouse model[269]. Notably, TAMs were the strongest infiltrate within the tumor microenvironment and accounted for more sequenced cells than cancer cells. We were able to define ligand/receptor interactions of TAMs with cancer cells as well as other components of the tumor microenvironment. Most frequently, interactions of TAMs with cancer-associated fibroblasts and cancer cells were identified, but further interactions with most tumor microenvironment components were shown. This highlights the complex interplay of the tumor microenvironment involved in TAM reprogramming. It also depicts the difficulties in developing in vitro models to study TAM differentiation: cancer-cell conditioned media or co-culture with cancer cells might not provide all the necessary signals to induce TAM differentiation as observed in vivo.

Further integration of the ligand/receptor interaction results with publicly available ligand/TF interaction data[243], together with our multi-omics characterization, allowed the definition of crucial tumor microenvironment signals (TGFB3, TGFB1, IFN-IFN-γ,

CSF3, CSF1, CCL4, and CCl2) and TFs (STAT4, STAT3, STAT1, RUNX1, RUNX, NFκB-P65-REL, NFκB-P50, FOSL2, FLI1, ATF3, ATF2, and AP-1) responsible for TAM reprogramming. The identified TFs *Stat1*, *Runx3*, and *FosL2* also showed significant induction on gene expression level. STAT1 is a known regulator of IFN-γ signaling and, as mentioned, is activated upon CSF1 response[20,310]. Furthermore, the presence of STAT1-positive TAMs was an independent prognostic factor for shorter disease-specific survival in follicular lymphoma[3], and its role in inducing an immunosuppressive tumor microenvironment in breast cancer has been described[206]. The function of FOSL2 in TAM reprogramming has recently been reported for lung cancer[264]. Sarode et al. showed that beta-catenin-mediated transcriptional activation of FOSL2 and repression of ARID5A drive a gene regulatory switch in macrophages to tumor-promoting TAMs. Although our data indicate induction of FOSL2 via the growth factors TGFB1 and TGFB3, a general role of FOSL2 in TAM reprogramming across many cancer entities is conceivable. Notably, STAT1, RUNX3, and FOSL2 seemed to be induced via hypomethylation, further highlighting the gene-regulatory role of DNA methylation in TAM phenotypes.

In contrast to STAT1 and FOSL2, no function of RUNX3 has been described in TAM biology. However, the RUNT-related TF-family is evolutionarily conserved, and significant roles have been defined for many developmental and biological processes, e.g., the role of RUNX3 in the differentiation of CD8+ T-cells or the function of RUNX1 as a tumor suppressor gene in AML[10,326]. As previously reported, we identified the regulation of Runx3 by promoter hypomethylation[244]. In addition to the strong representation of RUNX motifs in hypomethylated TAM vs MG DMRs and induction of *Runx3* gene expression in TAMs, we were able to identify RUNX motifs within a functional DMR annotated to the *Cd274* locus. *Cd274* encodes for the inhibitory transmembrane protein PD-L1 and can trigger the inhibition of adaptive immune cells[290]. Indeed, ligand/receptor interaction analysis predicted the interaction of PD-L1 on TAMs with PDCD1 on T-cells and CD80 on B-cells. The expression of PD-L1 on tumor-infiltrating immune cells has previously been associated with an immunosuppressive macrophage phenotype and an aggressive malignant potential in patients with lung and ovarian cancer[122,289]. Cancer immunotherapy targeting PD-L1 and CTLA-4 has achieved remarkable success and has been approved by the Food and Drug Administration to treat solid tumors, including breast cancer[39]. Further investigation of the

epigenetic mechanism regulating *Cd274* in TAMs could help identify immune checkpoint blockade biomarkers for breast cancer.

In addition to a TAM gene expression signature, we generated a DNA methylation-based immune signature using the reference-free deconvolution method MeDeCom[192]. This approach reduced the overall number of 47,562 DMRs to 333 regions, specifically hypomethylated in an LMC only present within TAM samples. The presence of this LMC highlights the unique epigenetic immunoediting of TAMs. Additionally, differential hypomethylation of the TAM signature was found in human tumors compared to normal samples and in the most aggressive breast cancer subtypes. Methylation-based classifiers have already been generated for brain tumors and show the potential to transform tumor pathology in clinics due to the robust and reproducible profiling technology[45]. Future generations of large whole genome-bisulfite datasets of breast cancer patients with long-term follow-up data will help determine TAM DNA methylation signatures' prognostic and diagnostic potential in patient stratification.

Further characterization of the identified TAM DNA methylation signature validated signaling pathways (e.g., TGF-β, TNF-α, and INF-γ signaling), as well as crucial TFs (e.g., STAT1, FOSL2, and RUNX) involved in TAM reprogramming. Additionally, it showed enrichment for TF motifs of RBPJ1. A previous report revealed that monocyte to TAM differentiation in a genetic breast cancer mouse model requires Notch signaling through the transcriptional regulator RBPJ[103]. Confirmation of this finding emphasizes the potential of a conserved mechanism in TAM reprogramming and shows the strength of DNA methylation profiling techniques in identifying these processes.

Annotation of the TAM DNA methylation signature allowed us to evaluate patient survival in the human breast cancer expression cohort METABRIC[62]. Similar to the TAM expression signature, an association between TAM signature expression, macrophage infiltration, and patient survival was observed. In addition, the majority of genes annotated to the TAM DNA methylation signature showed a strong expression induction in TAMs and repeatedly identified the TFs *Stat1* and *Runx3*, highlighting their role in TAM reprogramming.

Overall, the present thesis reinforces the concept of TAMs in the promotion and progression of breast cancer and shows a fundamental role of DNA methylation in regulating

these processes. Furthermore, the investigation of DNA methylation and gene expression landscapes allows the identification of drivers in TAM reprogramming. Thus, it provides opportunities for new therapeutic targets and allows predictive as well as diagnostic marker discovery.

5

Conclusion and perspectives

The present doctoral thesis focused on macrophages, innate immune cells present in essentially all tissues. Macrophages play a primary role in tissue homeostasis, host defense, and the orchestration of immune responses[64]. On the contrary, dysfunctional macrophages have a significant pathophysiological impact and contribute to many inflammatory and non-inflammatory diseases . Although the respective tissue niche shapes diverse macrophage populations through distinct gene-regulatory mechanisms, common functionalities of macrophages are given [177,223,293]. These include efferocytosis and phagocytosis, as well as appropriate immune responses to pathological stimuli [138,242,329]. To mount an effective immune response upon pathogen infection, rapid induction of inflammatory signals and further self-limitation to reduce excessive inflammation and tissue damage must be assured[216]. However, inappropriate macrophage activation, mediated through specific signals within the altered microenvironment, induces uncontrolled macrophage responses, such as excessive inflammation, tissue remodeling, or the support of

tumor progression[29,47,86]. Therefore, macrophages' homeostatic, reparative, and protective functions are subverted, causing the association between macrophage states and disease progression.

The mechanisms behind macrophage reprogramming and dysfunction are frequently not understood. Potential causes can be presumed within an altered microenvironment, and consequences might be reflected in the macrophages' epigenetic and transcriptional landscapes. To exemplify these mechanisms and consequences of macrophage reprogramming, we characterized macrophages' and monocytes' epigenomes as well as coinciding transcriptional patterns in two chronic diseases. Collectively, we demonstrated epigenetic reprogramming of macrophages and monocytes by an altered microenvironment and proposed a direct impact on gene regulation and macrophage functions.

Muco-obstruction and breast cancer are two distinct diseases with a worldwide health burden, affecting different organs and diverse classes of tissue-resident macrophages. Yet, we were able to identify specific commonalities of macrophage reprogramming as well as alterations and mechanisms of macrophage recruitment. We generated a genome-wide epigenetic map of tissue-resident macrophages from both diseases and defined alterations in the epigenome and transcriptome compared to their healthy counterparts. In the case of the *Scnn1b*-Tg mouse model of muco-obstruction, changes of *Snn1b*-Tg compared to WT AMs were defined on chromatin accessibility, DNA methylation, and gene expression level. Additionally, alterations in essential macrophage functions, such as efferocytosis, phagocytosis, as well as in the responses to mucus and a pathophysiological relevant stimulus, LPS, were analyzed. For TAMs from the 4T1 orthotopic mouse model of breast cancer, we focused on alterations in the DNA methylation and transcriptome landscape compared to their healthy counterpart, MGs, and in relation to their cellular origin BMDMs.

Breast cancer heavily reprogrammed the DNA methylation landscape of TAMs compared to MGs on a global level. TAMs accumulate in the tumor microenvironment because of the recruitment and reprogramming of BMDMs[103,66,246]. Consequently, the monocytic origin was reflected in the DNA methylation landscape that depicted DNA methylation programs similar to those observed in BMDMs. In contrast, only focal changes in the DNA methylation level of *Scnn1b*-Tg compared to WT AMs were observed. Accordingly, further investigation excluded monocyte-recruitment to the muco-obstructive

lung and indicated the reprogramming of the local AM pool. Yet, these differences in ontogeny do not represent a tissue-specific phenomenon but are instead a disease-related characteristic. Previous studies have shown the recruitment of inflammatory monocytes to the lung upon inflammation in fibrosis or virus infection [209,249].

Although the distinct macrophage populations were reprogrammed to a different extend, we detected similar inflammatory signatures in tissue-resident macrophages from both chronic diseases. Most notably was the identified pro-inflammatory IFN-γ program. IFN-γ is a cytokine critical for innate and adaptive immune responses against viruses, bacteria, or other infections. In addition, it is associated with a variety of autoinflammatory and immune diseases. IFN-γ alone or in combination with LPS can induce a classically activated macrophage phenotype (M1)[213,215]. In combination with previous studies, our results indicate a different origin of the enriched IFN-γ programs. Whereas IFN-γ was shown to be secreted from NK-/T-cells within the tumor microenvironment of breast cancer, an increased bacterial burden could explain the M1 signature found enriched in *Scnn1b*-Tg AMs [105,187,197].

In addition to the pro-inflammatory M1 signature, *Scnn1b*-Tg AMs and TAMs from breast cancer were enriched for an alternatively activated macrophage (M2) program on an epigenetic and gene expression level (e.g., enrichment of TGF-β and IL-4 signatures). The presence of M1, together with M2 markers, contradicts the binary macrophage polarization system and indicates an immense complexity in the in vivo setting. The plasticity of macrophage phenotypes should be defined in a spectrum model since stimuli supporting the activation of macrophages into pro-and anti-inflammatory states can be present simultaneously [125,331]. For AMs from *Scnn1b*-Tg mice, the presence of diverse M1 or M2 polarized subpopulations was excluded via single-cell high-dimensional flow cytometry, and a mixed phenotype was shown. Also, for TAMs, the co-occurrence of M1 and M2 programs was indicated, by the presence of M1 and M2 pathways, in the same DNA methylation program, uniquely present within the TAM samples.

Future studies should dissect the phagocyte system on a single-cell level. These analyses will clearly show the presence of M1 and M2 subpopulations or a mixed phenotype within a diseased organ. In addition, a multimodal single-cell analysis will help to understand the identified gene-regulatory networks and indicate trajectories of macrophage reprogramming. Although modern computational methods can infer trajectories via pseudotime or velocity

analyses, time-resolved or linage tracing studies will be needed to comprehensively map the reprogramming of monocytes and macrophages in different chronic diseases.

In addition, future studies need to validate the identified alterations in human patient cohorts. Whereas large breast cancer multi-omics datasets already exist[62,165], isolated TAMs from human breast cancer patients have only been profiled on a transcriptional level[46]. Yet, we found differential transcription and methylation of in mice generated TAM signatures in severe breast cancer subtypes. Similarly, existing studies of muco-obstructive lung disease have primarily focused on mixed samples (whole lung tissue, epithelium, blood, lavage) and not on defined cell populations[41,50,193,194,212,280]. In addition, DNA methylation studies were frequently limited to a small set of patients or using array-based methods[50], restricting the epigenetic analysis to a selected part of the genome.

Ultimately, similar to the functional analysis of AMs from *Scnn1b*-Tg and WT mice, functional characterization of TAMs compared to MGs and BMDMs remains to be investigated in the context of epigenetic reprogramming by breast cancer. In the case of TAMs, the effect of epigenetic reprogramming on tumor progression is of central interest, and crosstalk between TAMs and cancer cells should be further investigated. This could be achieved by coculture assays, including TAMs and cancer cells, as well as the specific inhibition or knockdown of identified signals within the tumor microenvironment in vivo.

Albeit these remaining questions, the present thesis represents the first comprehensive genome-wide characterization of the DNA methylation landscape in AMs from muco-obstructive lung disease as well as TAMs in breast cancer. Our work highlights the benefit of analyzing isolated cell types instead of bulk tissues or tumors and emphasizes the specific effects of certain chronic diseases on the tissue-resident macrophage pool. It has shown the immense potential of genome-wide profiling methods in identifying epigenetic drivers and the discovery of disease markers that will provide novel diagnostic and prognostic approaches, as well as the possibility for new therapeutic options targeting macrophages.

6

Material and methods

6.1 Epigenetic reprogramming of airway macrophages drives polarization and inflammation in muco-obstructive lung disease

6.1.1 Mice

Scnn1b-Tg and *Cftr*$^{-/-}$ (gut-corrected) mice on a C57BL/6 background were bred in-house under pathogen-free conditions and genotyped as described previously[195,345]. 6-week old female mice were used for FACS sorting experiments. Gender-matched 6-week old mice were used in all further experiments. As control animals, WT littermates were used. All animal experiments have been reviewed and authorized by the local authorities (Regierungspräsidium Karlsruhe, Germany).

6.1.2 Isolation of airway macrophages by lavage

Mice were anesthetized by intraperitoneal injection of 120 mg/kg ketamine and 16 mg/kg xylazine (Sigma-Aldrich, Darmstadt, Germany) and further exsanguinated. Primary AMs were obtained by flushing the lungs three times with 800 µl PBS plus 5 mM EDTA (Sigma-Aldrich). The lavage was repeated twice. For ex vivo treatment experiments, 3-4 washes were pooled to maximize the number of AMs.

6.1.3 Isolation of peritoneal macrophages

Euthanization of mice was performed by cervical dislocation. Primary peritoneal macrophages were obtained by injecting 10 ml of PBS supplemented with 5 mM EDTA (Sigma-Aldrich) into the peritoneum and further fluid aspiration.

6.1.4 Culture and treatment of primary macrophages with lipopolysaccharide and mucus

For LPS treatment, collected cells were seeded into a flat-bottom 96-well plate in complete DMEM (1 g/L D-Glucose, L-Glutamine, Pyruvate; Gibco, Dreieich, Germany) containing 10% heat-inactivated FCS (Gibco), 1x penicillin-streptomycin (Gibco), and 2 mM L-glutamine (Gibco) to a final count of 100,000 AMs/well. For baseline gene expression analysis, adhering cells were resuspended in 200 µl Trizol (Thermo Fisher Scientific GmbH, Dreieich, Germany). For baseline gene expression, 1 hr post cell seeding at 37 °C, 5% CO_2, non-adherent cells were washed from the plate with prewarmed PBS. Adherent cells were resuspended in 200 µl Trizol (Thermo Fisher Scientific GmbH). For LPS treatment, adherent cells were exposed to 100 ng/ml LPS (*P. aeruginosa*) (Sigma-Aldrich) for 6, 12, and 24 hrs. Complete DMEM was used as control. For mucus treatment, AMs were cultured with different concentrations (0%, 0.1%, 1%, 2%, 5%, and 10%) of bovine submaxillary gland mucus (Merck Millipore, Darmstadt, Germany). Supernatants were collected, and adherent cells were resuspended in 200 µl Trizol (Thermo Fisher Scientific GmbH).

6.1.5 Primary mouse tracheal epithelial culture

To isolate the trachea, mice were anesthetized by intraperitoneal injection of 120 mg/kg ketamine and 16 mg/kg xylazine (Sigma-Aldrich) and exsanguinated. Tracheas were opened, washed in DMEM/F-12 (Gibco) containing 1% penicillin-streptomycin (Gibco), transferred into 20 ml dissociation medium containing 1.4 mg/ml protease E (Sigma-Aldrich) and 0.1 mg/ml DNase I (Roche Diagnostics GmbH, Mannheim, Germany), and incubated overnight at 37 °C. Heat-inactivated FCS (Gibco) was used to stop the enzymatic reaction. Cells were then resuspended through a 100 µm cell strainer (BD Biosciences, Heidelberg, Germany), resuspended in DMEM/F-12 supplemented with heat-inactivated FCS (Gibco), 4.4 µg/ml insulin (human recombinant zinc; Gibco), and 0.1 mg/ml primocin (InvivoGen, Toulouse, France), and seeded into bacterial culture dishes. 2 hrs post-incubation at 37 °C, non-adherent epithelial cells were seeded on transwell filters (Costar, Sigma-Aldrich), coated with collagen from human placenta (Sigma-Aldrich). The protocol from Horani et al., 2013 was adapted for submerged mouse tracheal epithelial culture (mTEC/Plus) and air-liquid interface culturing (ALI, mTEC/SF)[148]. The primary medium for both culturing approaches consists of DMEM/F-12 (Gibco) supplemented with 15 mM HEPES (Carl Roth GmbH & Co. KG, Karlsruhe, Germany), 3.6 mM $NaHCO_3$ (ApplieChem GmbH, Darmstadt, Germany), 4 mM L-glutamine (Gibco), and 1x penicillin-streptomycin (Gibco). The submerged culture medium was prepared as followed; primary medium was supplemented with 10 µg/ml insulin (human recombinant zinc, Gibco), 5 µg/ml transferrin (Sigma-Aldrich), 25 ng/ml recombinant human epidermal growth factor (EGF, Gibco), 30 µg/ml bovine pituitary gland extract (BPE, Sigma-Aldrich), 5% heat-inactivated FCS (Gibco). The ALI culture medium was prepared as followed; primary medium was supplemented with 5 µg/ml insulin (human recombinant zinc, Gibco), 5 µg/ml transferrin (Sigma-Aldrich), 5 ng/ml EGF (Gibco), 30 µg/ml BPE (Sigma-Aldrich) and 1 mg/ml BSA (SERVA Electrophoresis GmbH, Heidelberg, Germany) reconstituted in HBSS (Gibco). Before use, retinoic acid (RA, Sigma-Aldrich) was added to mTEC/Plus and mTEC/SF medium (final concentration $5x10^{-8}$ M). The submerged culture medium was modified after three days, and trans-epithelial resistance was assessed on day five. Cells were moved to ALI culture conditions using mTEC/SF medium-plus RA when a 1000 /cm2 was reached. Every

other day, a medium change was performed, and surfaces were washed with PBS.

6.1.6 Immunofluorescence microscopy

Cells were fixed for 10 minutes (mins) with 4% paraformaldehyde (Otto Fischer GmbH & Co. KG, Saarbrucken, Germany), permeabilized for 8 min with 0.2% Triton X-100 (ApplieChem GmbH), and blocked for 15 min with 1% BSA (SERVA Electrophoresis GmbH). Staining was performed for 60 min at 37 °C with rabbit anti-mouse-SCNN1B (1:200, kindly provided by Prof. Dr. C. Korbmacher, University Erlangen-Nuremberg), rat anti-mouse-MerTK (1:20; R&D Systems Inc., Wiesbaden, Germany) and mouse anti-mouse-acetylated-α-tubulin (1:200; Life Technologies, Dreieich, Germany). Next, the respective secondary (ab')2 fragment goat anti-rabbit IgG (AF647, 1:200, Life Technologies), F(ab')2 fragment goat anti-rat IgG (AF488, 1:300, Life Technologies), F(ab')2 fragment goat anti-mouse IgG (AF488, 1:200, Life Technologies), and Hoechst 33258 (1:20000, Life Technologies) were applied for 2 hrs at room temperature. Images were acquired with a Leica TCS SP8 camera (Leica Microsystems, Wetzlar, Germany) and analyzed with the LASX v3.5.19976 software.

6.1.7 Fluorescence-activated cell sorting of airway macrophages for sequencing

For FACS, 1 ml dispase (BD Biosciences) was intratracheally instilled into the lungs and plugged by instillation of 300 µl low melting agarose (1%). When agarose was solidified, the whole lung, including the tracheobronchial tree, was extracted and incubated in 2 ml dispase for 35 min at room temperature. To stop the reaction, complete DMEM was added, lungs were mashed with a plunger, the tracheobronchial tree was removed, and the cell suspension was pushed through a 100 µm cell strainer (BD Biosciences). Following red blood cell lysis (RBC lysis buffer, eBiosciences, Dreieich, Germany), the cell suspension was enriched using $CD45^+$ magnetic beads separation, according to the manufacturer's instructions (Miltenyi Biotech, Bergisch Gladbach, Germany). After positive selection, cells were counted, and antibody concentrations were calculated based on the collected cell numbers and initial antibody titration (**Table 6.1**). Following staining with fluorochrome-conjugated antibodies against murine CD45.2, Siglec-F, and CD11c, cells were incubated for 5 min with purified rat

IgG2b anti-mouse CD16/CD32 receptor antibody (BD Biosciences, Heidelberg, Germany) in FACS buffer containing 1% BSA (SERVA Electrophoresis GmbH, Heidelberg, Germany) and 5 mM EDTA (Sigma-Aldrich). 5 min before sorting samples were stained with 7-AAD (0.25 µg/ml per $1x10^6$ cells; Biolegend, London, UK) to exclude dead cells. Sorting was performed at the EMBL Flow Core Facility, Heidelberg, Germany. A standard BD Fusion, equipped with 100 -mW 405 -nm, 100 -mW 488 -nm, 80 -mW 561 -nm, 80 -mW 640 -nm lasers, and an ND2.0 filter in front of the FSC photodiode, a nozzle size of 100 µm, and corresponding BD FACSFlow sheath pressure of 20 psi, matched with a transducer frequency of 32 kHz, was used for AM sorting. The input pressure was changed to ensure that an event populated every fifth to the sixth drop. A purity check of sorted cells was done on selected samples from each run. Purities were ranging from 95% to 99%. Sorted AMs were either immediately processed or treated with 100 ng LPS for 12 hrs for nucleic acid isolation and sequencing.

Table 6.1: Antibody panels used for efferocytosis and phagocytosis assays, high-dimensional flow cytometry, as well as FACS.

Efferocytosis and Phagocytosis				
Antibody	**Clone**	**Fluorophor**	**Dilution for BAL cells**	**Supplier**
Siglec-F	E50-2440	BUV395	1:400	BD Biosciences
CD11c	N418	BV421	1:400	BD Biosciences
CD45.2	104	AF700	1:400	BD Biosciences
Surface stain				
Antibody	**Clone**	**Fluorophor**	**Concentration 1x106 cells**	**Supplier**
CD206	C068C2	PE-Cy7	1 mg/ml	Biolegend
CD301b (MGL2)	URA-1	PE-Dazzle 594	2 mg/ml	Biolegend
CD369 (CLEC7A)	bg1fpj	PerCp-eFluor710	1 mg/ml	eBiosciences

CD64	X54-5/7.1	BV711	1 mg/ml	Biolegend
MerTK	2B10C42	PE	1 mg/ml	Biolegend
MHCII	M5/114.15.2	BV510	0.25 mg/ml	Biolegend
CD200R	OX110	AF647	2 mg/ml	BD Biosciences
CD38	90	Pacific Blue	1 mg/ml	Biolegend
CD86	GL-1	PerCp-Cy5.5	2 mg/ml	Biolegend
CD68	FA-11	APC	1 mg/ml	Biolegend
CD163	TNKUPJ	Super Bright 436	2 mg/ml	eBiosciences
CD209a	5H10	BV786	2 mg/ml	BD Biosciences
CD11b	M1/70	BV605	0.25 mg/ml	Biolegend
CD11c	N418	BV421	0.5 mg/ml	BD Biosciences
CD45.2	104	AF700	0.5 mg/ml	BD Biosciences
Siglec-F	E50-2440	BB515	0.25 mg/ml	BD Biosciences
FACS				
Antibody	**Clone**	**Fluorophor**	**Concentration 1x106 cells**	**Supplier**
CD11c	N418	BV421	0.5 mg/ml	BD Biosciences
Siglec-F	E50-2440	PE	0.25 mg/ml	BD Biosciences
CD45.2	104	AF700, APC, PE-Cy7	0.5 mg/ml	BD Biosciences

6.1.8 Staining and flow cytometry for surface marker expression analysis

To obtain a single-cell suspension, lungs were perfused with PBS and digested with 1 mg/ml Collagenase D (Roche Diagnostics GmbH, Mannheim, Germany) and 30 µg/ml DNAse I (Roche Diagnostics GmbH). After 1 hr incubation at 37 °C on a shaker, the digested lungs were mechanically placed through a 100 µm cell strainer (BD Biosciences, Heidelberg, Germany). After 1 hr at 37 °C on a shaker, red blood cell lysis was performed

(RBC lysis buffer, eBiosciences), and two million cells were used for further staining. In FACS buffer containing 1% BSA (SERVA Electrophoresis GmbH), 5 mM EDTA (Sigma-Aldrich), and 0.05% sodium azide (Sigma-Aldrich), cells were incubated for 5 min with purified rat IgG2b anti-mouse CD16/CD32 receptor antibody (BD Biosciences), followed by staining with fluorochrome-conjugated antibodies against murine CD45.2, Siglec-F, CD11b, CD11c, CD64, MerTK, CD200R, CD206, CD163, CD38, CD86, CD68, MHCII, MGL2, CLEC7A, and CD209A (**Table 6.1**) in brilliant stain buffer (BD Biosciences) for 25 min at 4 °C. Next, the APC-eFlour780 live/dead fixable dye was applied for 30 minutes at 4 °C (1:1000; eBiosciences). Samples were measured on a standard 405/488/561/640 nm laser engine CYTEK Aurora (Cytekbiosciences, Freemont CA, USA). Data were preprocessed and analyzed for frequencies using the FACSDiva software and FlowJo 10.4 (BD Biosciences). Cell-types were defined by the expression of specific surface markers: Alveolar macrophages (AM): $CD45.2^+$, $CD64^+$, $MerTK^+$, $CD11c^+$, and $SiglecF^+$; Interstitial macrophages (IM): $CD45.2^+$, $CD64^+$, $MerTK^+$, $MHCII^+$, and $SiglecF^-$; Dendritic cell cluster 1 (DC1): $CD45.2^+$, $CD64^-$, $MerTK^-$, $SiglecF^-$, $MHCII^+$, $CD11c^+$, and $CD11b^+$; Dendritic cell cluster 2 (DC2): $CD45.2^+$, $CD64^-$, $MerTK^-$, $SiglecF^-$, $MHCII^+$, $CD11c^+$, and $CD11b^-$; Neutrophils: $CD45.2^+$, $CD64^-$, $MerTK^-$, $CD11b^+$, $SiglecF^-$, and $MHCII^-$; Eosinophils: $CD45.2^+$, $CD64^-$, $MerTK^-$, $CD11b^+$, and $SiglecF^+$; B-cells (BC): $CD45.2^+$, $CD64^-$, $MerTK^-$, $SiglecF^-$, $MHCII^+$, and $CD38^+$; structural cells: $CD45.2^-$.

6.1.9 Staining and flow cytometry for efferocytosis and phagocytosis assays

Murine LA4 ATCC CCL-196 cells ($5x10^5$ cells/ml; ATCC, Wesel, Germany) were used for the efferocytosis assay. Apoptosis was induced by incubating LA4 ATCC CCL-196 cells for 3 hrs with 1 μM staurosporine (Enzo Life Sciences (ELS) AG, Lausen, Switzerland). According to the manufacturer's instructions, apoptotic cells were labeled with an equimolar solution of Annexin V-Biotin (Biolegend) and pHRodo Red Avidin (Thermo Fisher Scientific GmbH) in Annexin V staining buffer (Biolegend). After 15 min at room temperature, a total of 1x106 apoptotic cells were resuspended in 50 μl PBS and intratracheally administered into mice anesthetized with isoflurane. 2-3 hrs post-administration, mice were sacrificed, and airway macrophages were isolated by lavage.

For the phagocytosis assay, AMs were obtained by lavage and incubated for 1 hr with or without the phagocytosis inhibitor Cytochalasin D (10 μM, Sigma-Aldrich) in complete DMEM. pHRodo Red *E. coli* bioparticles (Thermo Fisher Scientific GmbH) were added and incubated for 1 hr, according to the manufacturer's instructions. Staining was performed with purified rat IgG2b anti-mouse CD16/CD32 receptor antibody (BD Biosciences) in FACS buffer containing 1% BSA (SERVA Electrophoresis GmbH), 5 mM EDTA (Sigma-Aldrich), and 0.05% sodium azide (Sigma-Aldrich) for 5 min. Next, fluorochrome-conjugated antibodies against murine Siglec-F, CD45.2, and CD11c (**Table 6.1**) were added for 25 min at 4 °C in the dark. After washing, cells were incubated for 30 min at 4 °C with APC-eFlour780 (1:1000; eBiosciences). Data were acquired on a BD LSRFortessa equipped with 20 -mW 355 -nm, 50 -mW 405 -nm, 50 -mW 488 -nm, 50 -mW 561 -nm, 40 -mW 640 -nm lasers, and an ND1.0 filter in front of the FSC photodiode. Internalization of LA4 cells and *E. coli* bioparticles in AMs was followed with the pHrodo dye. Further analysis was performed using the FACSDiva and FlowJo 10.4 software (BD Biosciences).

6.1.10 RNA isolation and quantitative PCR

Trizol (Thermo Fisher Scientific GmbH) and RNeasy Mini Kit (Qiagen, Düsseldorf, Germany) were applied according to the manufacturer's instructions to extract RNA. cDNA was generated by reverse transcription (Superscript III, Invitrogen, Dreieich, Germany) and used for quantification by qPCR. Thermo Fischer Scientific probes to assay *Il1b*, *Il12b*, *Mmp12*, *Arg1*, *Ccl22*, *Ccl17*, *CD86*, *Cxcr1*, *Trem2*, *Ptgs1*, *Ptgir*, *Anpep*, *Igf1*, and *Igf2bp3* together with *Gapdh* (primer limited) were used in duplex runs.
For *Il6*, the following primers and probe were applied:
fwd, 5′-GAGGATACCACTCCCAACAGACC-3',
rev, 5′-AAGTGCATCATCGTTGTTCATACA-3′;
probe, 5′-FAM-CAGAATTGCCATTGCACAA-TAMRA-3′;
and for Tnf:
fwd, 5′-CATCTTCTCAAAATTCGAGTGACAa-3′;
rev, 5′-TGGGAGTAGACAAGGTACAACCC-3′;

probe 5′-FAM-CACGTCGTAGCAAAC-3′ (Eurofins Genomics GmbH, Ebersberg, Germany).
Gapdh was used as a reference, and fold induction was calculated by the 7500 Real-Time PCR System SDS Software (Applied Biosystems, Dreieich, Germany).

6.1.11 Chemokine and cytokine detection

The cytometric bead array (BD Biosciences) was used according to manufacturer's instructions to analyze supernatants obtained from medium and LPS treated AMs for IL-6, IL-1α, IL-23, TNF-α, CCL2, CCL3, and CXCL1. Quantification was performed on a BD FortessaLSR according to a standard curve with the BD Cytometric Bead Array FCAP Array Software v3 (BD Biosciences).

6.1.12 Nucleic acid isolation for sequencing

According to the manufacturer's instructions, DNA and RNA were isolated using Trizol reagent (Thermo Fisher Scientific GmbH) following AllPrep DNA/RNA Mini Kit (Qiagen). For RNA isolation, DNAse I (RNase-free DNAse set, Qiagen) digestion was performed. For RNA and DNA isolation, Proteinase K (Puregene Proteinase K, Qiagen) digestion was performed. Agilent Bioanalyzer (Agilent Technologies Germany GmbH & Co. KG, Waldbronn, Germany) was used to determine DNA and RNA quality. All RNA samples used for sequencing required an RNA integrity number (RIN) >8.5. Quantification was performed by Qubit fluorometry (Thermo Fisher Scientific GmbH).

6.1.13 Tagmentation-based whole-genome bisulfite sequencing library preparation

tWGBS was performed as previously described with 20 ng DNA per sample[319]. Each tagmentation reaction was split into four sequencing libraries with different barcodes and then pooled in equimolar amounts to reach a final concentration of 10 nM. Libraries were sequenced at the DKFZ Genomics and Proteomics Core Facility (Heidelberg, Germany) using paired-end, 125 bps, on one lane of a HiSeq2000 v4 sequencer (Illumina, San Diego, CA, USA) per sample.

6.1.14 Assay for transposase-accessible chromatin sequencing library preparation

ATACseq libraries were prepared according to the Omni-ATAC protocol[58]. 50,000 viable cells/sample were used. The tagmentation reaction was stopped by the addition of 20 µl of 5 M Guanidinium thiocyanate (Sigma-Aldrich), and transposed chromatin was purified using 30 µl of AMPure XP beads (Beckman Coulter, Brea, CA, USA) and 110 µl of PEG buffer containing 2.5 M NaCl and 20% PEG 8000 (Sigma-Aldrich). Post library amplification, DNA was purified with a left-sided size selection applying 1.4x of AMPure XP beads (Beckman Coulter), which were finally resuspended in 1x elution buffer (Qiagen). Library size distribution was checked by Agilent Bioanalyzer (Agilent Technologies Germany GmbH & Co. KG), and concentrations were measured by Qubit fluorometry (Thermo Fisher Scientific GmbH). Multiplexes of 4 samples per lane were sequenced at the DKFZ Genomics and Proteomics Core Facility using a HiSeq 2000 v4, paired-end, 125 bps platform (Illumina).

6.1.15 RNA sequencing library preparation

The DKFZ Genomics and Proteomics Core Facility prepared paired-end sequencing libraries of baseline, LPS-, and medium-treated samples from total RNA using the SMART-Seq v4 Ultra Low Input RNA Kit (Takara Bio, Saint-Germain-en-Laye, France). Sequencing was performed at the DKFZ Genomics andProteomics Core Facility on a HiSeq 2000 v4, paired-end, 125 bps platform (Illumina). EMBL Genomics Core Facility (Heidelberg, Germany) prepared single-end sequencing libraries of baseline samples from total RNA using the NEBNext Ultra II Directional RNA Library Prep Kit from Illumina. Sequencing was performed at EMBL Genomics Core Facility on a NextSeq 500, single-end, 75 bps platform (Illumina).

6.1.16 Tagmentation-based whole-genome bisulfite sequencing data processing

tWGBS reads were trimmed using Trimmomatic[33] v0.36 and aligned against the mouse reference genome mm10 using bwa mem[182] v0.7.8, invoking the parameter "-T 0". Alignment duplicates were marked with Picard[38] v1.125 *MarkDuplicates*. Methylation calling was performed with MethylDackel[Ryan] v0.3.0, and M-bias was removed by excluding

the five base pairs at the two ends of the reads from methylation calling. Samples used for downstream analysis had a bisulfite conversion rate >98%, and more than 95% of all reference CpGs were covered. Each *Scnn1b*-Tg and WT group of replicates had a genome-wide CpG coverage of >20x.

6.1.17 Assay for transposase-accessible chromatin sequencing data processing

ATACseq reads were processed using the ENCODE ATACseq pipeline with default parameters[156]. Mm10 was used as a reference genome. Samples applied for downstream analysis achieved >50 million non-duplicated, non-mitochondrial reads, an irreproducible discovery rate <2, and a fraction of reads in peaks >0.5.

6.1.18 RNA sequencing data processing

RNAseq data were processed with the nf-core RNAseq pipeline[91] v1.2 using default parameters. Reads were aligned to the mouse reference genome mm10 by applying the software HISAT2, with *-unstranded* option. For single-end data, the *-singleEnd* option was used. Transcripts were assembled with StringTie and the gene code gene annotation release M20[100]. Stringties'[237] prepDE.py script (setting: *-eb*) was applied to generate gene counts.

6.1.19 DNA methylation smoothing and differential DNA methylation analysis

The R package Bsseq[130] v1.20.0 was used to smooth (*bsmooth*) the DNA methylation profiles with default parameters. DMRs between *Scnn1b*-Tg and WT AMs were called in a pair-wise comparison using DSS[230] v2.32.0. Regions with >3 CpGs, a length of >50 bps, a delta of >0.1, and a Benjamin-Hochberg corrected *P* value <0.05 were selected as statistically significant.

6.1.20 Differential chromatin accessibility analysis

The R package DiffBind[281] v2.14.0 was used to perform differential accessibility analysis. A common peak set was defined by the presence of a peak in at least two samples. edgeR was applied[255] as the statistical method of differential accessibility analysis. For the LPS

treatment experiment, the date of library preparation was included as a blocking factor to adjust for batch effects. The LPS treatment effect was identified by extracting count values for consensus peaks and defining a multi-factor design including the batch, genotype, treatment, and genotype/treatment interaction (~ *batch* + *genotype* + *treatment* + *genotype: treatment*), using DESeq2 [188] v1.26.0. The treatment covariate was extracted using the following contrast: *c("treatment", "medium", "LPS")*. LPS responsive regions with an adjusted *P* value <0.05 and a log2 fold-change >2 were considered significantly more accessible in LPS vs medium-treated samples. Annotation of differentially accessible regions was performed using the R package ChIPseeker [339] v1.22.1 and TxDb.Mmusculus.UCSC.mm10.knownGene [19] v3.10.0.

6.1.21 Differential gene expression analysis

Identification of differentially expressed genes was performed with the R package DESeq2 [188] v1.26.0. For the group-wise comparison of baseline replicates, the littermate was included in the design formula to adjust for batch effects. For the analysis of the LPS stimulation experiment, the library preparation date was included as a covariate. Adjusted *P* values and log2 fold changes to fulfill statistical significance are mentioned in the respective figure legends.

6.1.22 Enrichment of gene regulatory regions

The R package LOLA [276] v 1.16.0 was used to enrich DMRs and DARs with multi-cell gene regulatory regions from Ensembl [333]. DMRs and DARs with an adjusted *P* value <0.05 were stratified in hypo- and hypermethylated and increased and decreased accessibility in *Scnn1b*-Tg vs WT AMs, respectively. Enrichment was performed against a random background of DMRs or the consensus peak set of DARs.

6.1.23 Hierarchical cluster analysis

Hierarchical cluster analysis of DNA methylation levels was performed by calculating the Manhattan distance of all DMRs and performing a complete linkage clustering. Similarly, Euclidean distance of TMM normalized counts of DARs was used for chromatin accessibility [258,282]. For gene expression, regularized log-transformed gene counts were

calculated using DESeq2[188] v1.26.0 and applied to batch removal with the limma[253] v3.42.2 function *removeBatchEffect*. z-Scaled values were used to calculate Euclidean distance, and clustering was performed with the Ward's method.

6.1.24 Transcription factor motif analysis of differentially methylated and differentially accessible regions

DNA motif enrichment was performed using the command-line tool Homer[136] v4.9.1 and the parameter *-size_given*. All DMRs and DARs with an adjusted *P* value <0.05 were stratified in hypo- and hypermethylated or opened and closed regions.

6.1.25 Locus plot

The R package gviz[127] v1.30.3 was used to generate locus plots.

6.1.26 Upstream regulator analysis

According to the developer's manual, upstream regulator analysis with a prediction of the activation state was done using QIAGEN's Ingenuity Pathway Analysis. Upstream regulator analysis is based on prior knowledge of expected effects between transcriptional regulators, such as TFs, cytokines, and receptors, and their target genes stored in the Ingenuity Knowledge Base. Upstream regulator analysis of chromatin accessibility was performed with genes annotated to DARs. For this purpose, the R package ChIPseeker[339] v1.22.1 and TxDb.Mmusculus.UCSC.mm10.knownGene[19] v3.10.0 was applied.

6.1.27 Gene set enrichment analysis

GSEA with custom gene sets, obtained from Saini et al.[261], was performed using the R package clusterProfiler[338] v3.12.0. The fgsea algorithm was applied as the statistical method of choice.

6.1.28 Overrepresentation analysis of pathways and gene ontologies

Overrepresentation analysis of pathways and gene ontologies was performed using the webtool Metascape[346]. For the baseline expression analysis, all DEGs with an adjusted *P* value <0.1 were used. For the LPS stimulation analysis, the top 100 genes explaining the variance in PC1 and PC2 were applied.

6.1.29 Analysis of surface marker expression

Flow cytometry data were preprocessed using FACSDiva software and FlowJo 10.4 (BD Biosciences). Leukocytes were defined based on the expression of CD45.2. Fluorescence intensities were exported for further analysis according to the workflow described by Nowicka et al.[220]. In short, fluorescence intensities were transformed with the arcsine-square-root transformation, and cell clustering was performed with the R packages FlowSOM[312] v1.18.0 and ConsensusClusterPlus[324] v1.50.0. 20 meta clusters were defined that were assigned to cell types based on the expression of specific surface markers: Airway macrophages: $CD45.2^+$, $CD64^+$, $MerTK^+$, $CD11c^+$, and $SiglecF^+$; Interstitial macrophages: $CD45.2^+$, $CD64^+$, $MerTK^+$, $MHCII^+$, and $SiglecF^-$; Dendritic cells: $CD45.2^+$, $CD64^-$, $MerTK^-$, $SiglecF^-$, $MHCII^+$, and $CD11c^+$; Neutrophils: $CD45.2^+$, $CD64^-$, $MerTK^-$, $CD11b^+$, $SiglecF^-$, and $MHCII^-$; Eosinophils: $CD45.2^+$, $CD64^-$, $MerTK^-$, $CD11b^+$, and $SiglecF^+$; B-cells: $CD45.2^+$, $CD64^-$, $MerTK^-$, $SiglecF^-$, $MHCII^+$, and $CD38+^+$ Visual representation with UMAP was performed by subsampling 5,000 cells per sample and the R package umap[304] v0.2.4.1. To perform differential surface marker expression, stratified by cell types, a linear mixed model was applied, including the flow cytometry experiments' date as a covariate. Differentially expressed surface markers were defined by an adjusted *P* value <0.05. Similarly, differential cluster abundancy was performed on the frequency of AM sub-clusters by applying a linear mixed model including the flow cytometry experiments' date as a covariate. The differential abundance of AM sub-clusters was defined by an adjusted *P* value <0.05.

6.1.30 Deconvolution of RNA sequencing data

Deconvolution of bulk RNAseq with scRNAseq datasets was done with the R package MuSiC[318] v0.1.1. Processed and annotated scRNAseq from the single-cell atlas of the aging lung[5] and single-cell atlas of inflammatory airspace macrophages[214] were kindly provided by the authors. Only macrophage and monocyte clusters were used for the deconvolution with the single-cell atlas of the aging lung. All clusters were used for cell type estimation with the single-cell atlas of inflammatory airspace macrophages.

6.1.31 Principal component analysis

For gene expression analysis, batch removed regularized log-transformed values were applied to the base R function *promp*. In the case of ATACseq data, log-transformed normalized counts per consensus peaks were generated with the R package DiffBind[282] v2.14.0 and the DESeq2[188] v1.26.0 function *rlog*, further applied to *prcomp*.

6.1.32 Profile plots

The R package peakSeason[203] v0.1.0 was used to visualize profile plots. *P* values were determined with the student's t-test after a Shapiro test verified the normal distribution.

6.1.33 Transcription factor activity analysis

Differential transcription factor activity was assessed by diffTF[26] v1.3.3, using ATACseq and RNAseq data. Analytical mode with default parameters, comparing *Scnn1b*-Tg and WT AMs treated with LPS or medium, was applied. As a reference, in silico predicted transcription factor binding sites for 442 mouse transcription factors were used[171]. The transcription factor class (activator, repressor, or undetermined) was determined by integrating gene expression data of matching samples. Mean target gene expression was calculated for transcription factors with an adjusted *P* value < 0.001 by taking the average expression log2 fold change for each gene with the respective transcription factor motif <1,500 bps away from the transcriptional start site.

6.1.34 Hierarchical cluster analysis of transcription factors motifs

Differentially active TFs (adjusted *P* value <0.001) were clustered based on their position weight matrix similarity. For this purpose, clustering results from the RSAT suite were acquired[205].

6.1.35 Code and data availability

All data analysis is based on publicly available software and is described in **section 6**. The generated sequencing data have been deposited in the NCBI Gene Expression Omnibus under the accession number GSE154808.

6.1.36 Statistical analysis

Statistical analyses were performed using R[301] v3.6 or GraphPad Prism 6 (GraphPad Software Inc., San Diego, USA). For qPCR and cytokine bead array results, two-group comparisons were performed using unpaired, two-tailed Mann-Whitney U test, and multi-group comparisons were performed using one-way ANOVA with Tukey's or Bonferroni's multiple comparison test.

6.1.37 Custom schematics

Custom schematics were created with BioRender and Affinity Designer.

6.2 Cancer-specific DNA methylation landscape of macrophages and monocytes in breast cancer

6.2.1 Mice

BALB/c mice were maintained under specific pathogen-free conditions at the Weizmann Institute of Science (WIS, Rehovot, Israel) animal facility. All animal experiments were performed according to institutional guidelines and approved by the local ethics committee at the WIS (IACUC 40471217- 2).

6.2.2 4T1 cancer cell line culture

4T1 cells stably expressing firefly luciferase (pLVX-Luc) were kindly provided by Z. Granot (HUJI, Jerusalem, Israel). The cancer cell line was cultured in DMEM with 10% fetal bovine serum (FBS) (Invitrogen). The medium was exchanged every other day.

6.2.3 Orthotopic injection of 4T1 cells to the mammary fat pad

Eight weeks old BALB/c female mice were injected under anesthesia with 100,000 4T1 cells expressing luciferase reporter (4T1-Luc) in 50 µl PBS to the mammary fat pad.

6.2.4 Isolation of mammary gland macrophages and bone marrow-derived monocytes from healthy mice

Euthanization of mice was performed by cervical dislocation of 12 weeks old Blab/c mice to extract the mammary fat pad. The mammary fat pad was minced and dissociated with 5 ml gentleMACS dissociation buffer consisting of DMEM (Biological Industries, Cromwell, CT, USA), 0.02 g collagenase II (Merck Millipore), 0.02 g collagenase IV (Merck Millipore), and 0.005 g deoxyribonuclease (Invitrogen). The reaction was stopped by 20 ml of complete DMEM medium (DMEM, 10% FBS, and 1% Penicillin-Streptomycin) added to the dissociation buffer followed by filtration through a 70 µm strainer. Red blood cell lysis was performed with red blood cell lysis buffer (Biolegend), and cells were centrifuged for 5 min at 350 g, and 4 °C. Tissue-resident macrophages were enriched via positive selection

for F4/F80. Therefore, the pellet was resuspended in MACS buffer containing PBS, 0.5% BSA (Merck Millipore), and 250 mg EDTA (J.T.Beaker, Phillipsburg, New Jersey, USA) and further incubated with anti-F4/80 MicroBeads (Miltenyi Biotech). According to the manufacturer's instructions, tissue-resident macrophage enrichment was performed.

From the same mice, Tibia and Femur leg bones were dissected to isolate BMDM from healthy mice. Bones were flushed with MACS buffer using a 5 ml syringe with a 25 G needle. The flushed cells from the bone marrow were then centrifuged at 500 g for 5 min and resuspended in red blood cell lysis buffer.

6.2.5 Isolation of tumor-associated macrophages and bone marrow-derived monocytes from tumor-bearing mice

Four weeks post 4T1-Luc cells injection, mice were sacrificed via cervical dislocation. Tumors were isolated from the mammary fat pad, minced, and digested in 5 ml digestion buffer, consisting of 5 ml RPMI (Biological Industries), 0.005 g deoxyribonuclease (Invitrogen), and 15 mg collagenase A (Sigma-Aldrich) using a gentleMACS dissociator (Milteny Biotech) with the default program for solid tumors. The dissociated cells were strained through a 70 µm cell strainer and centrifuged for 7 min at 350 g. Red blood cells were lysed using a red blood cell lysis buffer. Immune cells were enriched via the surface marker CD45. Therefore, the pellet was resuspended in MACS buffer and incubated with anti-CD45 MicroBeads (Milteny Biotech). Immune cell enrichment was performed according to the manufacturer's instructions.

BMDM isolation of tumor-bearing mice was performed as described for BMDM from healthy mice in **section 6.2.4**.

6.2.6 Fluorescence-activated cell sorting of tumor-associated macrophages, mammary gland macrophages, and bone marrow-derived monocytes

Isolated cells were incubated with TrueStain FcX™ anti-mouse CD16/32 (Biolegend) for 10 min on ice to perform FC receptor blockage. TAMs and BMDMs were incubated in MACS buffer for 30 min at 4 °C and stained with fluorochrome-conjugated antibodies (**Table 6.2**) against murine CD11b, F4/F80, Gr1, and the live/dead staining DRAQ7TM

(Biolegend). A similar approach was used for mammary gland macrophages. Staining was performed without the anti-Grl antibody. Following staining, cells were washed with MACS buffer. Cells were gated based on marker expression. BMDMs: DRAQ7^{-}, CD11b^{+}, Gr1^{+}, and F4/80^{low}; MGs: DRAQ7^{-}, CD11b^{+}, and F4/F80^{+}; TAMs: DRAQ7^{-}, CD11b^{+}, Gr1^{-}, and F4/F80^{+}. Cells were sorted using FACSAria III (BD Biosciences) into Eppendorf tubes containing 40 µl of lysis/binding buffer of Dynabeads mRNA DIRECT Purification Kit (Thermo Fisher Scientific) for RNA isolation. The remaining cells were collected for DNA isolation into FACS tubes containing 1ml complete DMEM media.

Table 6.2: Antibody panels used for FACS.

Antibody	Clone	Fluorophor	Concentration per 100 µl	Supplier
CD11b	M1/70	PB	1 µl	Biolegend
F4/80	BM8	FITC	1 µl	Biolegend
Gr1	RB6-8C5	PerCP-Cy5.5	1 µl	Biolegend

6.2.7 DNA isolation for sequencing

Isolation of DNA from sorted cells was performed with the DNeasy Blood & Tissue Kits (Qiagen) according to the manufacturer's instructions. DNA was eluted in 30 µl DNase/RNase-free water, and DNA concentrations were detected by Qubit fluorometry (Invitrogen).

6.2.8 Whole-genome bisulfite sequencing by post-bisulfite adaptor tagging library preparation

The single-cell bisulfite sequencing protocol, utilizing PBAT, was applied to generate WGBS data of low input material[54]. As input, 6 ng of purified DNA or 1,000 cells, which were directly sorted into RLT Plus buffer (Qiagen), were used. A total of 10 µl of cell suspension was applied to the protocol, including the following changes: A single preamplification step was performed for 90 min at 37 °C. 14 cycles of library amplification were conducted with default PCR parameters. Libraries were purified by applying a 0.7x SPRI selection

using Ampure XP beads (Agencourt). The libraries' molarities were calculated based on concentrations measured with the Qubit dsDNA Assay (Thermo Fisher Scientific) and fragment size distribution, measured with the high sensitivity D5000 Assay for the Agilent Tapestation (Agilent Technologies Germany GmbH & Co. KG). A second round of 0.7x beads purification was applied to the libraries. Libraries were sequenced using paired-end, 150 bps, on one lane per sample of a HiSeq X sequencer (Illumina) at the DKFZ Genomics and Proteomics Core Facility.

6.2.9 RNA sequencing library preparation

For the preparation of RNAseq libraries, 1,000 cells from each population were sorted into 40 µl of lysis buffer (Thermo Fisher Scientific). mRNA was captured with 15 µl of Dynabeads oligo(dT) (Thermo Fisher Scientific), washed, and eluted at 85 °C with 10 µl of 10 mM Tris-Cl (pH 7.5). A derivation of the MARSseq protocol described by Jaitin et al. was used to prepare RNAseq libraries[154]. Sequencing was performed at WIS on a NextSeq 500, paired-end, 75 bps platform (Illumina).

6.2.10 Whole-genome bisulfite sequencing by post-bisulfite adaptor tagging data processing

WGBS data, generated with the PBAT protocol, was processed by the Omics IT and Data Management Core Facility (DKFZ, Heidelberg). Preprocessing of the reads was performed according to Delacher et al., 2017[72]. Reads were aligned using an updated version of the pipeline published by[319], which was implemented as a Roddy Workflow in the automated One Touch Pipeline[252]. Briefly, adaptor sequences of raw reads were trimmed using Trimmomatic[33]. Sequencing reads were then in silico bisulfite-converted (C>T for the first read in the pair, G>A for the second). The software BWA-MEM[182] was used with default parameters to align the converted reads to the in silico bisulfite-converted reference genome mm10, extended with the PhiX and lambda phage sequences. After alignment, reads were converted back to their original state, considering reads with a mapping quality ≥25 and nucleotides with a Phred-scaled quality score ≥25. PCR duplicate removal was performed per library using Picard[38]. Methylation calling and M-bias QC

was performed using MethylDackel[314] v0.4.0 and the parameters *–OT 6,0,6,140 –OB 2,145,12,150*, according to M-bias plot quality control.

6.2.11 RNA sequencing data processing

RNAseq data were processed by the LSCF Bioinformatics pipeline of the WIS as described in Kohen et al., 2019[166]. The mouse reference genome mm10 was used, and reads with multiple mappings were excluded.

6.2.12 Differential DNA methylation analysis

Methylation profiles of all samples were imported with the R package Bsseq[130] v1.20.0. DMRs of all comparisons (TAM vs MG, BMDM-T vs BMDM-H, BMDM-H vs MG, BMDM-T vs TAM, BMDM-T vs MG, and BMDM-H vs TAM) were called in a pair-wise comparison with DSS[230] v2.32.0. Regions with >3 CpGs, a length of >50 bps, a delta of >0.1, and a Benjamin-Hochberg corrected *P* value <0.05 were selected as DMRs.

6.2.13 Principal component analysis

For PCA and further exploratory analysis of WGBS data, CpGs were filtered by a coverage >5 in >2 samples from the same group and a coverage <0.99 percentile of all CpG coverages. Methylation levels of the 200,000 most variable methylated CpGs were applied to the R base function *prcomp*. For RNAseq data, variance stabilizing transformation (*vst*) was applied to normalized gene counts, using DESeq2[188] v1.26.0, further applied to batch removal with the limma[253] v3.42.2 function *removeBatchEffect*. Finally, the base R function *prcomp* was used on the 5,000 most variably expressed genes.

6.2.14 Enrichment of gene regulatory regions and Molecular Signatures Database hallmarks

The R package LOLA[276] v 1.16.0 was used to enrich DMRs with multi-cell gene regulatory regions from Ensembl[100] and MSigDB hallmark gene sets[183]. DMRs of each comparison were stratified in hypo- and hypermethylated regions and enriched to a background

containing a union set of DMRs from all comparisons. The LOLA database of MSigDB hallmarks was generated by annotating the gene sets' promoter and gene body regions using the R package TxDb.Mmusculus.UCSC.mm10.knownGene[19] v3.10.0.

6.2.15 Transcription factor motif enrichment by transcription factor families

The command-line tool GimmeMotifs[313] v0.14.4 was used to define enriched DNA TF motifs by TF-family. GimmeMotif was applied with default options on DMRs, stratified in hypo- and hypermethylated regions. TF motifs were grouped by TF-family. The most significant *P* value per TF-family was visualized.

6.2.16 Transcription factor motif enrichment of differentially methylated regions

Transcription factor motif analysis was performed as described in **section 6.1.24**.

6.2.17 Differential gene expression analysis

DEGs were identified using the R package DESeq2[188] v1.26.0. Group-wise comparisons (TAM vs MG, BMDM-T vs BMDM-H, BMDM-H vs MG, BMDM-T vs TAM, BMDM-T vs MG, and BMDM-H vs TAM) were performed by creating a design formula, including the group and date of library preparation, to adjust for batch effects. DEGs were defined by an adjusted *P* value <0.05 and an absolute log2 fold change >1.

6.2.18 Locus plot

Locus plots were generated as described in **section 6.1.25**.

6.2.19 Hierarchical cluster analysis

Hierarchical cluster analysis of DMRs, DEGs, TF motif enrichments, and LMC proportions was performed using the R package Pheatmap[248] v1.0.12. Complete-linkage clustering was applied on the Euclidean distance of absolute methylation values, z-scaled gene expression[188], -log10(*P* values) of enriched TF motifs[136], and LMC proportions. In detail, for the hierarchical cluster analysis of gene expression, *vst* function was applied to normalized

gene counts, using the R package DESeq2[188] v1.26.0. These were further used for batch removal with the limma[253] v3.42.2 function *removeBatchEffect* before z-scaling. For the cluster analysis of DMRs and DEGs, the resulting tree was cut into six clusters using the Pheatmap[248] v1.0.12 function *cutree* (k=6).

6.2.20 Integration of whole-genome bisulfite sequencing and RNA sequencing data

For the integration of DNA methylation and gene expression, average DMR methylation per group was calculated and annotated to genes with the R package ChIPseeker[339] v1.22.1 and TxDb.Mmusculus.UCSC.mm10.knownGene[19] v3.10.0. Average gene expression per group was calculated post variance stabilizing transformation (*vst*) of normalized gene counts[188], which were further used for batch removal using limma[253] v3.42.2 function *removeBatchEffect*. As a batch, the date of library preparation was specified. DMR/gene pairs were further integrated via Pearson correlation. Correlating DMR/gene pairs were defined by a *P* value <0.05. Overlap analysis with DMRs from the TAM vs MG or BMDM-T vs BMDM-H comparison was performed with the *findOverlaps* function from the R package GenomicRanges[178] v1.38.0. For the joined visualization of DMR methylation differences and gene expression changes in a scatter plot, delta methylation values from the differential methylation analysis with DSS[230] v2.32.0 and log2 fold changes from the differential gene expression analysis with DESeq2[188] v1.26.0 were used.

6.2.21 Overrepresentation analysis of pathways and gene ontologies

Overrepresentation analysis of pathways and gene ontologies was performed as described in **section 6.1.28**.

6.2.22 Upstream regulator analysis

Upstream regulator analysis was performed as described in **section 6.1.26**.

6.2.23 Utilized publicly available datasets

Following publicly available datasets were used for the analysis in **section 3.1.2**:

(a) METABRIC cohort[62]: METABRIC gene expression data and associated clinical information were obtained from the cBioPortal for cancer genomics database[49]. Non-classified molecular subtypes and normal samples were removed from the analysis. For survival analysis, events were limited to 120 months of overall survival and censored based on cancer-related deaths (died of cancer = 1; living or died of other causes = 0).

(b) TCGA (breast cancer) cohort[165]: TCGA breast cancer Illumina Human Methylation 450k array data were obtained using the R package TCGAbiolinks[57] v2.14.0. Probes were transferred from hg19 to mm10 reference genome via the R package liftOver[30] v1.10.0. Overlaps with LMC1 DMRs were identified with the *findOverlaps* function from the R package GenomicRanges[178] v1.38.0.

(c) 4T1 orthotopic mouse model scRNAseq[269]: The raw count matrix was obtained from DRYAD. The analysis was performed with the R package Seurat[286] v 3.2.2. Cells with fewer than 200 detected genes per cell and genes expressed by fewer than two cells were removed. Normalization was performed using the LogNormalize method and a scaling factor of 1,000. Clusters were defined by constructing a k-nearest-neighbor graph based on the Euclidean distance in PCA space (dimensions =1:20) using the *FindNeighbors* function. Clusters were then applied to the Louvain algorithm to iteratively group cells together by the *FindClusters* function (resolution =0.5). A total of 14 clusters were identified in the 4T1 scRNAseq data assigned to 8 different cell types by cross-referencing cluster-specific marker genes to published resources.

6.2.24 Tumor-associated macrophages expression signature

The TAM expression signature was defined by selecting DEGs that were upregulated in TAMs compared to MGs (adjusted *P* value <0.05 and log2 fold change >1) and expressed >0.05 percentile of all genes. The gene list was further filtered based on co-expression in the METABRIC cohort by selecting genes with a human ortholog[62].

6.2.25 Survival analysis

For survival analysis using the TAM expression signature, TAM vs MG DEG clusters, or the TAM methylation signature, annotated to upregulated TAM vs MG DEGs (adjusted *P* value

<0.05 and log2 fold change >1), average signature expression per patient in the METABRIC cohort was calculated[62]. Patients were assigned to the high or low expression group by having a higher or lower mean signature expression than the median +/-1 SD of all patients. Cancer-specific survival was used as an endpoint. The analysis was performed with the R package survival[303] v3.1.8.

6.2.26 Uniform manifold approximation and projection

Visual representation of the scRNAseq 4T1 breast cancer dataset was performed with Seurat's[286] v 3.2.2 *RunUMAP* function, using the first 20 dimensions. PCA was used as the dimensional reduction method for UMAP input.

6.2.27 Prediction of ligand/receptor interactions

To study cell-to-cell interactions in the 4T1 scRNAseq dataset, normalized gene counts were exported, and mouse gene symbols were converted to the human HUGO gene nomenclature. Ligand/receptor interactions were investigated using CellPhoneDB[84] v2.1.4. Prioritization of ligand/receptor interactions was done by examining the overlap of predicted ligands with ligands that can activate identified TFs in the TF motif enrichment of TAM vs MG hypomethylated DMRs. Therefore, a database curated by Pro et al.,2018 was applied[243], and functionally validated mouse ligand/TF interactions were selected. Further overlap with upstream regulators (*P* value <0.05) from the TAM vs MG comparison and the molecular type cytokine or growth factors was visualized.

6.2.28 Deconvolution of DNA methylation landscapes

Latent methylation components were identified using MeDeCom[192] v0.3.0. MeDeCom was applied on the union track of DMRs from all comparisons (TAM vs MG, BMDM-T vs BMDM-H, BMDM-H vs MG, BMDM-T vs TAM, BMDM-T vs MG, and BMDM-H vs TAM) using the following parameters: NINIT=10, NFOLDS=10, ITERMAX=300. The model was optimized using cross-validation error (CVE), with different λ values and a diverse number of components. Parameters were selected based on a stabilized CVE at k =5 and λ =0.01. DMRs, specifically hypomethylated in an LMC, were identified by comparing

the average methylation of the remaining LMCs, using a cutoff delta >0.7. LMC1 DMRs were used to define the TAM methylation signature. To investigate the TAM methylation signature in the METABRIC expression cohort, the signature was further subsetted by selecting DMRs that were annotated to genes upregulated in the TAM vs MG comparison (adjusted *P* value <0.05 and log2 fold change >1)[62].

6.2.29 Code

All data analysis is based on publicly available software and is described in **section 6**.

6.2.30 Statistical analysis

Statistical analyses were performed using R[301] v3.6.

6.2.31 Custom schematics

Custom schematics were created with BioRender and Affinity Designer.

Abbreviations

Table 6.3: List of abbreviations.

	Abbreviation	Definition
	%	Percentage
	5-methylcytosine; 5-mC	Carbon 5 position of cytosines
A	ARID1A	AT-rich interaction domain 5A
	ATACseq	Assay for transposase-accessible chromatin sequencing
B	BMDM	Bone marrow-derived monocyte
	BMDM-H	Bone marrow-derived monocyte from healthy mice
	BMDM-T	Bone marrow-derived monocyte from tumor-bearing mice
	bp	base pair
C	C5	Carbon 5
	CCSP	Club cell secretory protein
	cDNA	Complementary DNA
	CF	Cystic fibrosis
	CFTR	Cystic fibrosis transmembrane conductance regulator
	CGi	Cytosine-phosphate-guanine dinucleotide island
	ChIPseq	Chromatin immunoprecipitation followed by sequencing
	chr	Chromosome
	COPD	Chronic obstructive pulmonary disease
	CpG	Cytosine-phosphate-guanine dinucleotide
	CSF1	Colony-stimulating factor 1

	CSF1R	Colony-stimulating factor 1 receptor
	Ctsd	Cathepsin D
D	DAR	Differentially accessible region
	DEG	Differentially expressed gene
	DMR	Differentially methylated region
	DNA	Deoxyribonucleic acid
	DNMT	DNA methyltransferase
	dNTP	Deoxynucleoside triphosphate
E	EDTA	Ethylenediaminetetraacetic acid
	EMP	Erythro-myeloid progenitor
	ENaC	Epithelial sodium channel
	ER	Estrogen receptor
	Ezr	Ezrin
F	FACS	Fluorescence-activated cell sorting
	FOSL2	FOS-like antigen 2
	FSC	Forward Scatter
G	GSEA	Gene set enrichment analysis
H	H_2O	Water
	H3K27ac	Histone H3 lysine 27 acetylation
	HER2	Human epidermal growth factor receptor 2
	HOMER	Hypergeometric Optimization of Motif EnRichment
	hr	Hour
	HSC	Hematopoietic stem cell
I	IFN-γ	Interferon-gamma
	Igf1	Insulin-like growth factor 1
	Il1a	Interleukin 1 alpha
	IRF	Interferon respose factor
K	kg	Kilogram
L	LMC	Laten methylation component
	LPS	Lipopolysaccharide
M	M	Molar

	med	Medium
	MG	Mammary gland macrophage
	min	Minute
	mm	Mus musculus
	MMP12	Matrix metallopeptidase 12
	MNaseSeq	Micrococcal nuclease digestion with deep sequencing
	MSigDB	Molecular Signatures Database
	mTEC	Murine tracheal epithelial cells
	MuSiC	MUlti-Subject Single-Cell deconvolution
N	n	Number of replicates
	ncRNA	Non-coding RNA
	ng	Nanograam
P	PBAT	Post-bisulfite adaptor tagging
	PBS	Phosphate buffered saline
	PC	Principal component
	PCA	Principal component analysis
	PCR	Polymerase chain reaction
	PR	Progesterone receptor
R	RNA	Ribonucleic acid
	RNAseq	RNA sequencing
	rRNA	Ribosomal RNA
S	*Scnn1b*	Sodium channel epithelial 2 beta subunit
	scRNAseq	Single-cell RNA sequencig
	SSC	Side scatter
T	TAD	Topological associating domain
	TAM	Tumor-associated macrophage
	TCGA	The Cancer Genome Atlas
	TET	Ten-eleven translocation
	TF	Transcription factor
	TFBS	Transcription factor binding sites

	Tg	Transgenic
	TLR4	Toll-like receptor 4
	TNBC	Triple-negative breast cancer
	tRNA	Transfer RNA
	tWGBS	Tagmentation-based whole-genome bisulfite sequencing
U	UMAP	Uniform manifold approximation and projection
W	WGBS	Whole-genome bisulfite sequencing
	WT	Wild type

List of figures

List of tables

References

[1] Ades, F., Zardavas, D., Bozovic-Spasojevic, I., Pugliano, L., Fumagalli, D., De Azambuja, E., Viale, G., Sotiriou, C., & Piccart, M. (2014). Luminal B breast cancer: Molecular characterization, clinical management, and future perspectives.

[2] Alexis, N. E., Muhlebach, M. S., Peden, D. B., & Noah, T. L. (2006). Attenuation of host defense function of lung phagocytes in young cystic fibrosis patients. *Journal of Cystic Fibrosis*, 5(1), 17–25.

[3] Álvaro, T., Lejeune, M., Camacho, F. I., Salvadó, M. T., Sánchez, L., García, J. F., Lopez, C., Jaén, J., Bosch, R., Pons, L. E., Bellas, C., & Piris, M. A. (2006). The presence of STAT1-positive tumor-associated macrophages and their relation to outcome in patients with follicular lymphoma. *Haematologica*, 91(12), 1605–1612.

[4] Anderson, S. D., Daviskas, E., Brannan, J. D., & Chan, H. K. (2018). Repurposing excipients as active inhalation agents: The mannitol story. *Advanced Drug Delivery Reviews*, 133, 45–56.

[5] Angelidis, I., Simon, L. M., Fernandez, I. E., Strunz, M., Mayr, C. H., Greiffo, F. R., Tsitsiridis, G., Ansari, M., Graf, E., Strom, T.-M., Nagendran, M., Desai, T., Eickelberg, O., Mann, M., Theis, F. J., & Schiller, H. B. (2019). An atlas of the aging lung mapped by single cell transcriptomics and deep tissue proteomics. *Nature Communications*, 10(1), 963.

[6] Arnold, L., Henry, A., Poron, F., Baba-Amer, Y., Van Rooijen, N., Plonquet, A., Gherardi, R. K., & Chazaud, B. (2007). Inflammatory monocytes recruited after skeletal

muscle injury switch into antiinflammatory macrophages to support myogenesis. *Journal of Experimental Medicine*, 204(5), 1057–1069.

[7] Arwert, E. N., Harney, A. S., Entenberg, D., Wang, Y., Sahai, E., Pollard, J. W., & Condeelis, J. S. (2018). A Unidirectional Transition from Migratory to Perivascular Macrophage Is Required for Tumor Cell Intravasation. *Cell Reports*, 23(5), 1239–1248.

[8] Atlasi, Y. & Stunnenberg, H. G. (2017). The interplay of epigenetic marks during stem cell differentiation and development. *Nature Reviews Genetics*, 18(11), 643–658.

[9] Aure, M. R., Leivonen, S. K., Fleischer, T., Zhu, Q., Overgaard, J., Alsner, J., Tramm, T., Louhimo, R., Alnæs, G. I., Perälä, M., Busato, F., Touleimat, N., Tost, J., Børresen-Dale, A. L., Hautaniemi, S., Troyanskaya, O. G., Lingjærde, O. C., Sahlberg, K. K., & Kristensen, V. N. (2013). Individual and combined effects of DNA methylation and copy number alterations on miRNA expression in breast tumors. *Genome Biology*, 14(11), R126.

[10] Bae, S. C. & Choi, J. K. (2004). Tumor suppressor activity of RUNX3. *Oncogene*, 23(24), 4336–4340.

[11] Bain, C. C., Bravo-Blas, A., Scott, C. L., Gomez Perdiguero, E., Geissmann, F., Henri, S., Malissen, B., Osborne, L. C., Artis, D., & Mowat, A. M. I. (2014). Constant replenishment from circulating monocytes maintains the macrophage pool in the intestine of adult mice. *Nature Immunology*, 15(10), 929–937.

[12] Balázs, A. & Mall, M. A. (2019). Mucus obstruction and inflammation in early cystic fibrosis lung disease: Emerging role of the IL-1 signaling pathway. *Pediatric Pulmonology*, 54(S3), S5–S12.

[13] Balkwill, F., Charles, K. A., & Mantovani, A. (2005). Smoldering and polarized inflammation in the initiation and promotion of malignant disease. *Cancer Cell*, 7(3), 211–217.

[14] Barnes, P. J. (2008). The cytokine network in asthma and chronic obstructive pulmonary disease. *The Journal of clinical investigation*, 118(11), 3546–56.

[15] Barnes, P. J., Burney, P. G., Silverman, E. K., Celli, B. R., Vestbo, J., Wedzicha, J. A., & Wouters, E. F. (2015). Chronic obstructive pulmonary disease. *Nature Reviews Disease Primers*, 1(1), 1–21.

[16] Baßler, K., Fujii, W., Kapellos, T. S., Horne, A., Reiz, B., Dudkin, E., Luecken, M., Reusch, N., Osei-Sarpong, C., Warnat-Herresthal, S., Wagner, A., Bonaguro, L., Guenther, P., Pizarro, C., Schreiber, T., Becker, M., Haendler, K., Wohnhaas, C. T., Baumgartner, F., Koehler, M., Theis, H., Kraut, M., Wadsworth, M. H., Hughes, T. K., Ferreira, H. J. G., Schulte-Schrepping, J., Hinkley, E., Kaltheuner, I. H., Geyer, M., Thiele, C., Shalek, A. K., Feisst, A., Thomas, D., Dickten, H., Beyer, M., Baum, P., Yosef, N., Aschenbrenner, A. C., Ulas, T., Hasenauer, J., Theis, F. J., Skowasch, D., & Schultze, J. L. (2020). Alterations of multiple alveolar macrophage states in chronic obstructive pulmonary disease. *bioRxiv*, (pp. 2020.05.28.121541).

[17] Batlle, E. & Massagué, J. (2019). Transforming Growth Factor-β Signaling in Immunity and Cancer. *Immunity*, 50(4), 924–940.

[18] Batra, R. N. (2018). *Decoding the regulatory role and epiclonal dynamics of DNA methylation in 1482 breast tumours*. PhD thesis, University of Cambridge.

[19] BC, T. (2019). TxDb.Mmusculus.UCSC.mm10.knownGene: Annotation package for TxDb object(s). R package version 3.4.7.

[20] Beck, A. H., Espinosa, I., Edris, B., Li, R., Montgomery, K., Zhu, S., Varma, S., Marinelli, R. J., Van Rijn, M. D., & West, R. B. (2009). The macrophage colony-stimulating factor 1 response signature in breast carcinoma. *Clinical Cancer Research*, 15(3), 778–787.

[21] Belkina, A. C., Nikolajczyk, B. S., & Denis, G. V. (2013). BET Protein Function Is Required for Inflammation: Brd2 Genetic Disruption and BET Inhibitor JQ1 Impair Mouse Macrophage Inflammatory Responses. *The Journal of Immunology*, 190(7), 3670–3678.

[22] Bell, C. G., Lowe, R., Adams, P. D., Baccarelli, A. A., Beck, S., Bell, J. T., Christensen, B. C., Gladyshev, V. N., Heijmans, B. T., Horvath, S., Ideker, T., Issa, J.-P. J., Kelsey, K. T.,

Marioni, R. E., Reik, W., Relton, C. L., Schalkwyk, L. C., Teschendorff, A. E., Wagner, W., Zhang, K., & Rakyan, V. K. (2019). DNA methylation aging clocks: challenges and recommendations. *Genome Biology*, 20(1), 249.

[23] Ben-Hattar, J. & Jiricny, J. (1988). Methylation of single CpG dinucleotides within a promoter element of the Herpes simplex virus tk gene reduces its transcription in vivo. *Gene*, 65(2), 219–227.

[24] Benayoun, B. A., Pollina, E. A., & Brunet, A. (2015). Epigenetic regulation of ageing: Linking environmental inputs to genomic stability. *Nature Reviews Molecular Cell Biology*, 16(10), 593–610.

[25] Berdiev, B. K., Qadri, Y. J., & Benos, D. J. (2009). Assessment of the CFTR and ENaC association. *Molecular BioSystems*, 5(2), 123–227.

[26] Berest, I., Arnold, C., Reyes-Palomares, A., Palla, G., Rasmussen, K. D., Helin, K., & Zaugg, J. B. (2019). Quantification of differential transcription factor activity and multiomics-based classification into activators and repressors: diffTF. *bioRxiv*.

[27] Berman, H., Zhang, J., Crawford, Y. G., Gauthier, M. L., Fordyce, C. A., McDermott, K. M., Sigaroudinia, M., Kozakiewicz, K., & Tlsty, T. D. (2005). Genetic and epigenetic changes in mammary epithelial cells identify a subpopulation of cells involved in early carcinogenesis. *Cold Spring Harbor Symposia on Quantitative Biology*, 70, 317–327.

[28] Bernard, P. S., Parker, J. S., Mullins, M., Cheung, M. C., Leung, S., Voduc, D., Vickery, T., Davies, S., Fauron, C., He, X., Hu, Z., Quackenhush, J. F., Stijleman, I. J., Palazzo, J., Matron, J. S., Nobel, A. B., Mardis, E., Nielsen, T. O., Ellis, M. J., & Perou, C. M. (2009). Supervised risk predictor of breast cancer based on intrinsic subtypes. *Journal of Clinical Oncology*, 27(8), 1160–1167.

[29] Bhatt, J. M. (2013). Treatment of pulmonary exacerbations in cystic fibrosis. *European Respiratory Review*, 22(129), 205–216.

[30] Bioconductor (2020). liftOver: Changing genomic coordinate systems with rtracklayer::liftOver.

[31] Birket, S. E. & Rowe, S. M. (2019). Revealing the molecular signaling pathways of mucus stasis in cystic fibrosis. *Journal of Clinical Investigation*, 129(10), 4089–4090.

[32] Biswas, S. K., Gangi, L., Paul, S., Schioppa, T., Saccani, A., Sironi, M., Bottazzi, B., Doni, A., Vincenzo, B., Pasqualini, F., Vago, L., Nebuloni, M., Mantovani, A., & Sica, A. (2006). A distinct and unique transcriptional program expressed by tumor-associated macrophages (defective NF-κB and enhanced IRF-3/STAT1 activation). *Blood*, 107(5), 2112–2122.

[33] Bolger, A. M., Lohse, M., & Usadel, B. (2014). Trimmomatic: A flexible trimmer for Illumina sequence data. *Bioinformatics*, 30(15), 2114–2120.

[34] Bonavita, E., Galdiero, M. R., Jaillon, S., & Mantovani, A. (2015). Phagocytes as Corrupted Policemen in Cancer-Related Inflammation. In *Advances in Cancer Research*, volume 128 (pp. 141–171). Academic Press Inc.

[35] Boucher, R. C. (2019). Muco-obstructive lung diseases. *New England Journal of Medicine*, 380(20), 1941–1953.

[36] Bowman, R. L., Klemm, F., Akkari, L., Pyonteck, S. M., Sevenich, L., Quail, D. F., Dhara, S., Simpson, K., Gardner, E. E., Iacobuzio-Donahue, C. A., Brennan, C. W., Tabar, V., Gutin, P. H., & Joyce, J. A. (2016). Macrophage Ontogeny Underlies Differences in Tumor-Specific Education in Brain Malignancies. *Cell Reports*, 17(9), 2445–2459.

[37] Bradley, M. N., Zhou, L., & Smale, S. T. (2003). C/EBPβ Regulation in Lipopolysaccharide-Stimulated Macrophages. *Molecular and Cellular Biology*, 23(14), 4841–4858.

[38] Broad Institute (2018). Picard Tools.

[39] Bu, X., Yao, Y., & Li, X. (2017). Immune checkpoint blockade in breast cancer therapy. In *Advances in Experimental Medicine and Biology*, volume 1026 (pp. 383–402). Springer New York LLC.

[40] Buenrostro, J. D., Giresi, P. G., Zaba, L. C., Chang, H. Y., & Greenleaf, W. J. (2013). Transposition of native chromatin for fast and sensitive epigenomic profiling of open chromatin, DNA-binding proteins and nucleosome position. *Nature methods*, 10(12), 1213–8.

[41] Busch, R., Qiu, W., Lasky-Su, J., Morrow, J., Criner, G., & DeMeo, D. (2016). Differential DNA methylation marks and gene comethylation of COPD in African-Americans with COPD exacerbations. *Respiratory Research*, 17(1), 1–15.

[42] Button, B., Goodell, H. P., Atieh, E., Chen, Y. C., Williams, R., Shenoy, S., Lackey, E., Shenkute, N. T., Cai, L. H., Dennis, R. G., Boucher, R. C., & Rubinstein, M. (2018). Roles of mucus adhesion and cohesion in cough clearance. *Proceedings of the National Academy of Sciences of the United States of America*, 115(49), 12501–12506.

[43] Byrne, A. J., Mathie, S. A., Gregory, L. G., & Lloyd, C. M. (2015). Pulmonary macrophages: Key players in the innate defence of the airways. *Thorax*, 70(12), 1189–1196.

[44] Cantin, A. M., Bilodeau, G., Ouellet, C., Liao, J., & Hanrahan, J. W. (2006). Oxidant stress suppresses CFTR expression. *American Journal of Physiology - Cell Physiology*, 290(1).

[45] Capper, D., Jones, D. T., Sill, M., Hovestadt, V., Schrimpf, D., Sturm, D., Koelsche, C., Sahm, F., Chavez, L., Reuss, D. E., Kratz, A., Wefers, A. K., Huang, K., Pajtler, K. W., Schweizer, L., Stichel, D., Olar, A., Engel, N. W., Lindenberg, K., Harter, P. N., Braczynski, A. K., Plate, K. H., Dohmen, H., Garvalov, B. K., Coras, R., Hölsken, A., Hewer, E., Bewerunge-Hudler, M., Schick, M., Fischer, R., Beschorner, R., Schittenhelm, J., Staszewski, O., Wani, K., Varlet, P., Pages, M., Temming, P., Lohmann, D., Selt, F., Witt, H., Milde, T., Witt, O., Aronica, E., Giangaspero, F., Rushing, E., Scheurlen, W., Geisenberger, C., Rodriguez, F. J., Becker, A., Preusser, M., Haberler, C., Bjerkvig, R., Cryan, J., Farrell, M., Deckert, M., Hench, J., Frank, S., Serrano, J., Kannan, K., Tsirigos, A., Brück, W., Hofer, S., Brehmer, S., Seiz-Rosenhagen, M., Hänggi, D., Hans, V., Rozsnoki, S., Hansford, J. R., Kohlhof, P., Kristensen, B. W., Lechner, M.,

Lopes, B., Mawrin, C., Ketter, R., Kulozik, A., Khatib, Z., Heppner, F., Koch, A., Jouvet, A., Keohane, C., Mühleisen, H., Mueller, W., Pohl, U., Prinz, M., Benner, A., Zapatka, M., Gottardo, N. G., Driever, P. H., Kramm, C. M., Müller, H. L., Rutkowski, S., Von Hoff, K., Frühwald, M. C., Gnekow, A., Fleischhack, G., Tippelt, S., Calaminus, G., Monoranu, C. M., Perry, A., Jones, C., Jacques, T. S., Radlwimmer, B., Gessi, M., Pietsch, T., Schramm, J., Schackert, G., Westphal, M., Reifenberger, G., Wesseling, P., Weller, M., Collins, V. P., Blümcke, I., Bendszus, M., Debus, J., Huang, A., Jabado, N., Northcott, P. A., Paulus, W., Gajjar, A., Robinson, G. W., Taylor, M. D., Jaunmuktane, Z., Ryzhova, M., Platten, M., Unterberg, A., Wick, W., Karajannis, M. A., Mittelbronn, M., Acker, T., Hartmann, C., Aldape, K., Schüller, U., Buslei, R., Lichter, P., Kool, M., Herold-Mende, C., Ellison, D. W., Hasselblatt, M., Snuderl, M., Brandner, S., Korshunov, A., Von Deimling, A., & Pfister, S. M. (2018). DNA methylation-based classification of central nervous system tumours. *Nature*, 555(7697), 469–474.

[46] Cassetta, L., Fragkogianni, S., Sims, A. H., Coussens, L. M., Smith, H. O., Pollard Correspondence, J. W., Swierczak, A., Forrester, L. M., Zhang, H., Soong, D. Y., Cotechini, T., Anur, P., Lin, E. Y., Fidanza, A., Lopez-Yrigoyen, M., Millar, M. R., Urman, A., Ai, Z., Spellman, P. T., Hwang, E. S., Dixon, J. M., Wiechmann, L., Coussens, L. M., Smith, H. O., & Pollard, J. W. (2019). Human Tumor-Associated Macrophage and Monocyte Transcriptional Landscapes Reveal Cancer-Specific Reprogramming, Biomarkers, and Therapeutic Targets. *Cancer Cell*, 35(4), 588–602.e10.

[47] Cassetta, L. & Pollard, J. W. (2018). Targeting macrophages: therapeutic approaches in cancer. *Nature Reviews Drug Discovery*, 17(12), 887–904.

[48] Cecchini, M. G., Dominguez, M. G., Mocci, S., Wetterwald, A., Felix, R., Fleisch, H., Chisholm, O., Hofstetter, W., Pollard, J. W., & Stanley, E. R. (1994). Role of colony stimulating factor-1 in the establishment and regulation of tissue macrophages during postnatal development of the mouse. *Development*, 120(6), 1357–1372.

[49] Cerami, E., Gao, J., Dogrusoz, U., Gross, B. E., Sumer, S. O., Aksoy, B. A., Jacobsen, A., Byrne, C. J., Heuer, M. L., Larsson, E., Antipin, Y., Reva, B., Goldberg, A. P., Sander, C.,

& Schultz, N. (2012). The cBio Cancer Genomics Portal: An open platform for exploring multidimensional cancer genomics data. *Cancer Discovery*, 2(5), 401–404.

[50] Chen, Y., Armstrong, D. A., Salas, L. A., Hazlett, H. F., Nymon, A. B., Dessaint, J. A., Aridgides, D. S., Mellinger, D. L., Liu, X., Christensen, B. C., & Ashare, A. (2018). Genome-wide DNA methylation profiling shows a distinct epigenetic signature associated with lung macrophages in cystic fibrosis. *Clinical Epigenetics*, 10(1).

[51] Chen, Z., Feng, X., Herting, C. J., Garcia, V. A., Nie, K., Pong, W. W., Rasmussen, R., Dwivedi, B., Seby, S., Wolf, S. A., Gutmann, D. H., & Hambardzumyan, D. (2017). Cellular and molecular identity of tumor-associated macrophages in glioblastoma. *Cancer Research*, 77(9), 2266–2278.

[52] Chittezhath, M., Dhillon, M. K., Lim, J. Y., Laoui, D., Shalova, I. N., Teo, Y. L., Chen, J., Kamaraj, R., Raman, L., Lum, J., Thamboo, T. P., Chiong, E., Zolezzi, F., Yang, H., VanGinderachter, J. A., Poidinger, M., Wong, A. S., & Biswas, S. K. (2014). Molecular Profiling Reveals a Tumor-Promoting Phenotype of Monocytes and Macrophages in Human Cancer Progression. *Immunity*, 41(5), 815–829.

[53] Clapier, C. R., Iwasa, J., Cairns, B. R., & Peterson, C. L. (2017). Mechanisms of action and regulation of ATP-dependent chromatin-remodelling complexes. *Nature Reviews Molecular Cell Biology*, 18(7), 407–422.

[54] Clark, S. J., Smallwood, S. A., Lee, H. J., Krueger, F., Reik, W., & Kelsey, G. (2017). Genome-wide base-resolution mapping of DNA methylation in single cells using single-cell bisulfite sequencing (scBS-seq). *Nature Protocols*, 12(3), 534–547.

[55] Clunes, L. A., Davies, C. M., Coakley, R. D., Aleksandrov, A. A., Henderson, A. G., Zeman, K. L., Worthington, E. N., Gentzsch, M., Kreda, S. M., Cholon, D., Bennett, W. D., Riordan, J. R., Boucher, R. C., & Tarran, R. (2012). Cigarette smoke exposure induces CFTR internalization and insolubility, leading to airway surface liquid dehydration. *The FASEB Journal*, 26(2), 533–545.

[56] Cohen-Cymberknoh, M., Kerem, E., Ferkol, T., & Elizur, A. (2013). Airway inflammation in cystic fibrosis: Molecular mechanisms and clinical implications. *Thorax*, 68(12), 1157–1162.

[57] Colaprico, A., Silva, T. C., Olsen, C., Garofano, L., Cava, C., Garolini, D., Sabedot, T. S., Malta, T. M., Pagnotta, S. M., Castiglioni, I., Ceccarelli, M., Bontempi, G., & Noushmehr, H. (2016). TCGAbiolinks: An R/Bioconductor package for integrative analysis of TCGA data. *Nucleic Acids Research*, 44(8), e71.

[58] Corces, M. R., Trevino, A. E., Hamilton, E. G., Greenside, P. G., Sinnott-Armstrong, N. A., Vesuna, S., Satpathy, A. T., Rubin, A. J., Montine, K. S., Wu, B., Kathiria, A., Cho, S. W., Mumbach, M. R., Carter, A. C., Kasowski, M., Orloff, L. A., Risca, V. I., Kundaje, A., Khavari, P. A., Montine, T. J., Greenleaf, W. J., & Chang, H. Y. (2017). An improved ATAC-seq protocol reduces background and enables interrogation of frozen tissues. *Nature Methods*, 14(10), 959–962.

[59] Cosío, B. G., Mann, B., Ito, K., Jazrawi, E., Barnes, P. J., Chung, K. F., & Adcock, I. M. (2004). Histone Acetylase and Deacetylase Activity in Alveolar Macrophages and Blood Mononocytes in Asthma. *American Journal of Respiratory and Critical Care Medicine*, 170(2), 141–147.

[60] Cox, M. J., Turek, E. M., Hennessy, C., Mirza, G. K., James, P. L., Coleman, M., Jones, A., Wilson, R., Bilton, D., Cookson, W. O. C., Moffatt, M. F., & Loebinger, M. R. (2017). Longitudinal assessment of sputum microbiome by sequencing of the 16S rRNA gene in non-cystic fibrosis bronchiectasis patients. *PLOS ONE*, 12(2), e0170622.

[61] Curigliano, G., Burstein, H. J., Winer, E. P., Gnant, M., Dubsky, P., Loibl, S., Colleoni, M., Regan, M. M., Piccart-Gebhart, M., Senn, H.-j., André, F., Baselga, J., Bergh, J., Bonnefoi, H., Brucker, S. Y., Cardoso, F., Carey, L., Ciruelos, E., Cuzick, J., Denkert, C., Di Leo, A., Ejlertsen, B., Francis, P., Galimberti, V., Garber, J., Gulluoglu, B., Goodwin, P., Harbeck, N., Hayes, D. F., Huang, C.-s., Huober, J., Hussein, K., Jassem, J., Jiang, Z., Karlsson, P., Morrow, M., Orecchia, R., Osborne, K. C., Pagani, O., Partridge, A. H., Pritchard, K., Ro, J., T Rutgers, E. J., Sedlmayer, F., Semiglazov, V., Shao, Z., Smith, I.,

Toi, M., Tutt, A., Viale, G., Watanabe, T., Whelan, T. J., & Xu, B. (2017). De-escalating and escalating treatments for early-stage breast cancer: the St. Gallen International Expert Consensus Conference on the Primary Therapy of Early Breast Cancer 2017. *Annals of Oncology*, 28, 1700–1712.

[62] Curtis, C., Shah, S. P., Chin, S. F., Turashvili, G., Rueda, O. M., Dunning, M. J., Speed, D., Lynch, A. G., Samarajiwa, S., Yuan, Y., Gräf, S., Ha, G., Haffari, G., Bashashati, A., Russell, R., McKinney, S., Aparicio, S., Brenton, J. D., Ellis, I., Huntsman, D., Pinder, S., Murphy, L., Bardwell, H., Ding, Z., Jones, L., Liu, B., Papatheodorou, I., Sammut, S. J., Wishart, G., Chia, S., Gelmon, K., Speers, C., Watson, P., Blamey, R., Green, A., MacMillan, D., Rakha, E., Gillett, C., Grigoriadis, A., De Rinaldis, E., Tutt, A., Parisien, M., Troup, S., Chan, D., Fielding, C., Maia, A. T., McGuire, S., Osborne, M., Sayalero, S. M., Spiteri, I., Hadfield, J., Bell, L., Chow, K., Gale, N., Kovalik, M., Ng, Y., Prentice, L., Tavaré, S., Markowetz, F., Langerød, A., Provenzano, E., Purushotham, A., Børresen-Dale, A. L., & Caldas, C. (2012). The genomic and transcriptomic architecture of 2,000 breast tumours reveals novel subgroups. *Nature*, 486(7403), 346–352.

[63] Cystic Fibrosis Foundation (2021). Types of CFTR Mutations | CF Foundation.

[64] Davies, L. C., Jenkins, S. J., Allen, J. E., & Taylor, P. R. (2013). Tissue-resident macrophages. *Nature Immunology*, 14(10), 986–995.

[65] De Bruijn, M. & Dzierzak, E. (2017). Runx transcription factors in the development and function of the definitive hematopoietic system. *Blood*, 129(15), 2061–2069.

[66] De Palma, M. & Lewis, C. E. (2013). Macrophage regulation of tumor responses to anticancer therapies. *Cancer Cell*, 23(3), 277–286.

[67] De Palma, M., Venneri, M. A., Galli, R., Sergi, L. S., Politi, L. S., Sampaolesi, M., & Naldini, L. (2005). Tie2 identifies a hematopoietic lineage of proangiogenic monocytes required for tumor vessel formation and a mesenchymal population of pericyte progenitors. *Cancer Cell*, 8(3), 211–226.

[68] De Palma, M., Venneri, M. A., Roca, C., & Naldini, L. (2003). Targeting exogenous genes to tumor angiogenesis by transplantation of genetically modified hematopoietic stem cells. *Nature Medicine*, 9(6), 789–795.

[69] Deans, C. & Maggert, K. A. (2015). What Do You Mean, "Epigenetic"? *Genetics*, 199(4), 887–896.

[70] Decramer, M., Janssens, W., & Miravitlles, M. (2012). Chronic obstructive pulmonary disease. In *The Lancet*, volume 379 (pp. 1341–1351).: Elsevier B.V.

[71] Dekker, J., Rippe, K., Dekker, M., & Kleckner, N. (2002). Capturing chromosome conformation. *Science*, 295(5558), 1306–1311.

[72] Delacher, M., Imbusch, C. D., Weichenhan, D., Breiling, A., Hotz-Wagenblatt, A., Träger, U., Hofer, A. C., Kägebein, D., Wang, Q., Frauhammer, F., Mallm, J. P., Bauer, K., Herrmann, C., Lang, P. A., Brors, B., Plass, C., & Feuerer, M. (2017). Genome-wide DNA-methylation landscape defines specialization of regulatory T cells in tissues. *Nature Immunology*, 18(10), 1160–1172.

[73] Demedts, I. K., Bracke, K. R., Van Pottelberge, G., Testelmans, D., Verleden, G. M., Vermassen, F. E., Joos, G. F., & Brusselle, G. G. (2007). Accumulation of dendritic cells and increased CCL20 levels in the airways of patients with chronic obstructive pulmonary disease. *American Journal of Respiratory and Critical Care Medicine*, 175(10), 998–1005.

[74] DeNardo, D. G., Barreto, J. B., Andreu, P., Vasquez, L., Tawfik, D., Kolhatkar, N., & Coussens, L. M. (2009). CD4+ T Cells Regulate Pulmonary Metastasis of Mammary Carcinomas by Enhancing Protumor Properties of Macrophages. *Cancer Cell*, 16(2), 91–102.

[75] Di Pietro, C., Zhang, P. X., O'Rourke, T. K., Murray, T. S., Wang, L., Britto, C. J., Koff, J. L., Krause, D. S., Egan, M. E., & Bruscia, E. M. (2017). Ezrin links CFTR to TLR4 signaling to orchestrate anti-bacterial immune response in macrophages. *Scientific Reports*, 7(1), 1–11.

[76] Dickinson, R. E., Dallo, A., Bieche, I., Krex, D., Norton, D., Maher, E. R., & Latif, F. (2004). Epigenetic inactivation of SLIT3 and SLIT1 genes in human cancers. *British Journal of Cancer*, 91(12), 2071–2078.

[77] Ding, J., Guo, C., Hu, P., Chen, J., Liu, Q., Wu, X., Cao, Y., & Wu, J. (2016). CSF1 is involved in breast cancer progression through inducing monocyte differentiation and homing. *International Journal of Oncology*, 49(5), 2064–2074.

[78] Diseases, L. & Boucher, R. C. (2015). On the Pathogenesis of Acute Exacerbations of Mucoobstructive Lung Diseases. *Annals of the American Thoracic Society*, 12(November), S160–S163.

[79] Donaldson, S. H., Bennett, W. D., Zeman, K. L., Knowles, M. R., Tarran, R., & Boucher, R. C. (2006). Mucus Clearance and Lung Function in Cystic Fibrosis with Hypertonic Saline. *New England Journal of Medicine*, 354(3), 241–250.

[80] Dorrington, M. G. & Fraser, I. D. C. (2019). NF- κ B Signaling in Macrophages : Dynamics , Crosstalk , and Signal Integration. *Frontiers in Immunology*, 10(April), 705.

[81] Doskočil, J. & Šorm, F. (1962). Distribution of 5-methylcytosine in pyrimidine sequences of deoxyribonucleic acids. *Biochimica et Biophysica Acta*, 55(6), 953–959.

[82] Dunn, G. P., Old, L. J., & Schreiber, R. D. (2004). The three Es of cancer immunoediting. *Annual Review of Immunology*, 22, 329–360.

[83] Edwards, M. R., Bartlett, N. W., Clarke, D., Birrell, M., Belvisi, M., & Johnston, S. L. (2009). Targeting the NF-κB pathway in asthma and chronic obstructive pulmonary disease. *Pharmacology and Therapeutics*, 121(1), 1–13.

[84] Efremova, M., Vento-Tormo, M., Teichmann, S. A., & Vento-Tormo, R. (2020). CellPhoneDB: inferring cell–cell communication from combined expression of multi-subunit ligand–receptor complexes. *Nature Protocols*, 15(4), 1484–1506.

[85] Egawa, M., Mukai, K., Yoshikawa, S., Iki, M., Mukaida, N., Kawano, Y., Minegishi, Y., & Karasuyama, H. (2013). Inflammatory Monocytes Recruited to Allergic Skin Acquire

an Anti-inflammatory M2 Phenotype via Basophil-Derived Interleukin-4. *Immunity*, 38(3), 570–580.

[86] Eklöf, J., Sørensen, R., Ingebrigtsen, T. S., Sivapalan, P., Achir, I., Boel, J. B., Bangsborg, J., Ostergaard, C., Dessau, R. B., Jensen, U. S., Browatzki, A., Lapperre, T. S., Janner, J., Weinreich, U. M., Armbruster, K., Wilcke, T., Seersholm, N., & Jensen, J. U. (2020). Pseudomonas aeruginosa and risk of death and exacerbations in patients with chronic obstructive pulmonary disease: an observational cohort study of 22 053 patients. *Clinical Microbiology and Infection*, 26(2), 227–234.

[87] Epelman, S., Lavine, K. J. J., & Randolph, G. J. J. (2014). Origin and Functions of Tissue Macrophages. *Immunity*, 41(1), 21–35.

[88] Esteller, M. (2000). Promoter Hypermethylation and BRCA1 Inactivation in Sporadic Breast and Ovarian Tumors. *Journal of the National Cancer Institute*, 92(7), 564–569.

[89] Esteller, M. (2002). CpG island hypermethylation and tumor suppressor genes: A booming present, a brighter future. *Oncogene*, 21(35 REV. ISS. 3), 5427–5440.

[90] Esther, C. R., Muhlebach, M. S., Ehre, C., Hill, D. B., Wolfgang, M. C., Kesimer, M., Ramsey, K. A., Markovetz, M. R., Garbarine, I. C., Gregory Forest, M., Seim, I., Zorn, B., Morrison, C. B., Delion, M. F., Thelin, W. R., Villalon, D., Sabater, J. R., Turkovic, L., Ranganathan, S., Stick, S. M., & Boucher, R. C. (2019). Mucus accumulation in the lungs precedes structural changes and infection in children with cystic fibrosis. *Science Translational Medicine*, 11(486).

[91] Ewels, P. A., Peltzer, A., Fillinger, S., Patel, H., Alneberg, J., Wilm, A., Garcia, M. U., Di Tommaso, P., & Nahnsen, S. (2020). The nf-core framework for community-curated bioinformatics pipelines.

[92] Fahy, J. V. & Dickey, B. F. (2010). Airway Mucus Function and Dysfunction. *New England Journal of Medicine*, 363(23), 2233–2247.

[93] Fanucchi, S., Domínguez-Andrés, J., Joosten, L. A., Netea, M. G., & Mhlanga, M. M. (2020). The Intersection of Epigenetics and Metabolism in Trained Immunity. *Immunity*, 54(1), 32–43.

[94] Finkelstein, R., Fraser, R. S., Ghezzo, H., & Cosio, M. G. (1995). Alveolar inflammation and its relation to emphysema in smokers. *American Journal of Respiratory and Critical Care Medicine*, 152(5 I), 1666–1672.

[95] Fleischer, T., Edvardsen, H., Solvang, H. K., Daviaud, C., Naume, B., Børresen-Dale, A.-L., Kristensen, V. N., & Tost, J. (2014). Integrated analysis of high-resolution DNA methylation profiles, gene expression, germline genotypes and clinical end points in breast cancer patients. *International Journal of Cancer*, 134(11), 2615–2625.

[96] Fleischer, T., Tekpli, X., Mathelier, A., Wang, S., Nebdal, D., Dhakal, H. P., Sahlberg, K. K., Schlichting, E., Sauer, T., Geisler, J., Hofvind, S., Bathen, T. F., Engebraaten, O., Garred, Ø., Geitvik, G. A., Langerød, A., Kåresen, R., Mælandsmo, G. M., Russnes, H. G., Sørlie, T., Lingjærde, O. C., Skjerven, H. K., Park, D., Fritzman, B., Børresen-Dale, A. L., Borgen, E., Naume, B., Eskeland, R., Frigessi, A., Tost, J., Hurtado, A., & Kristensen, V. N. (2017). DNA methylation at enhancers identifies distinct breast cancer lineages. *Nature Communications*, 8(1), 1379–1379.

[97] Fontana, M. F., Baccarella, A., Pancholi, N., Pufall, M. A., Herbert, D. R., Kim, C. C., R, D. B., & Kim, C. C. (2016). JUNB is a Key Transcriptional Modulator of Macrophage Activation Mary. *J Immunol*, 194(1), 177–186.

[98] Fraig, M., Shreesha, U., Savici, D., & Katzenstein, A.-L. A. (2002). Respiratory Bronchiolitis. *The American Journal of Surgical Pathology*, 26(5), 647–653.

[99] Frame, J. M., McGrath, K. E., & Palis, J. (2013). Erythro-myeloid progenitors: "Definitive" hematopoiesis in the conceptus prior to the emergence of hematopoietic stem cells. *Blood Cells, Molecules, and Diseases*, 51(4), 220–225.

[100] Frankish, A., Diekhans, M., Ferreira, A. M., Johnson, R., Jungreis, I., Loveland, J., Mudge, J. M., Sisu, C., Wright, J., Armstrong, J., Barnes, I., Berry, A., Bignell, A.,

Carbonell Sala, S., Chrast, J., Cunningham, F., Di Domenico, T., Donaldson, S., Fiddes, I. T., García Girón, C., Gonzalez, J. M., Grego, T., Hardy, M., Hourlier, T., Hunt, T., Izuogu, O. G., Lagarde, J., Martin, F. J., Martínez, L., Mohanan, S., Muir, P., Navarro, F. C., Parker, A., Pei, B., Pozo, F., Ruffier, M., Schmitt, B. M., Stapleton, E., Suner, M. M., Sycheva, I., Uszczynska-Ratajczak, B., Xu, J., Yates, A., Zerbino, D., Zhang, Y., Aken, B., Choudhary, J. S., Gerstein, M., Guigó, R., Hubbard, T. J., Kellis, M., Paten, B., Reymond, A., Tress, M. L., & Flicek, P. (2019). GENCODE reference annotation for the human and mouse genomes. *Nucleic Acids Research*, 47(D1), D766–D773.

[101] Franklin, R. A. & Li, M. O. (2014). The ontogeny of tumor-associated macrophages: a new understanding of cancer-elicited inflammation. *OncoImmunology*, 3(9), e955346.

[102] Franklin, R. A. & Li, M. O. (2016). Ontogeny of Macrophages and Its Implication in Cancer Regulation. *TRENDS in CANCER*, 2(1), 20–34.

[103] Franklin, R. A., Liao, W., Sarkar, A., Kim, M. V., Bivona, M. R., Liu, K., Pamer, E. G., & Li, M. O. (2014). The cellular and molecular origin of tumor-associated macrophages. *Science*, 344(6186), 921–925.

[104] Fricker, M. & Gibson, P. G. (2017). Macrophage dysfunction in the pathogenesis and treatment of asthma. *European Respiratory Journal*, 50(3).

[105] Fritzsching, B., Hagner, M., Dai, L., Christochowitz, S., Agrawal, R., van Bodegom, C., Schmidt, S., Schatterny, J., Hirtz, S., Brown, R., Goritzka, M., Duerr, J., Zhou-Suckow, Z., & Mall, M. A. (2017). Impaired mucus clearance exacerbates allergen-induced type 2 airway inflammation in juvenile mice. *Journal of Allergy and Clinical Immunology*, 140(1), 190–203.e5.

[106] Fritzsching, B., Zhou-Suckow, Z., Trojanek, J. B., Schubert, S. C., Schatterny, J., Hirtz, S., Agrawal, R., Muley, T., Kahn, N., Sticht, C., Gunkel, N., Welte, T., Randell, S. H., Länger, F., Schnabel, P., Herth, F. J. F., & Mall, M. A. (2015). Hypoxic epithelial necrosis triggers neutrophilic inflammation via IL-1 receptor signaling in cystic fibrosis lung disease. *American Journal of Respiratory and Critical Care Medicine*, 191(8), 902–913.

[107] Frizzell, R. A. & Pilewski, J. M. (2004). Finally, mice with CF lung disease. *Nature Medicine*, 10(5), 452–454.

[108] Fukui, S., Iwamoto, N., Takatani, A., Igawa, T., Shimizu, T., Umeda, M., Nishino, A., Horai, Y., Hirai, Y., Koga, T., Kawashiri, S. Y., Tamai, M., Ichinose, K., Nakamura, H., Origuchi, T., Masuyama, R., Kosai, K., Yanagihara, K., & Kawakami, A. (2018). M1 and M2 Monocytes in rheumatoid arthritis: A contribution of imbalance of M1/M2 monocytes to osteoclastogenesis. *Frontiers in Immunology*, 8(JAN).

[109] Gautiar, E. L., Shay, T., Miller, J., Greter, M., Jakubzick, C., Ivanov, S., Helft, J., Chow, A., Elpek, K. G., Gordonov, S., Mazloom, A. R., Ma'Ayan, A., Chua, W. J., Hansen, T. H., Turley, S. J., Merad, M., Randolph, G. J., Best, A. J., Knell, J., Goldrath, A., Brown, B., Jojic, V., Koller, D., Cohen, N., Brenner, M., Regev, A., Fletcher, A., Bellemare-Pelletier, A., Malhotra, D., Jianu, R., Laidlaw, D., Collins, J., Narayan, K., Sylvia, K., Kang, J., Gazit, R., Garrison, B. S., Rossi, D. J., Kim, F., Rao, T. N., Wagers, A., Shinton, S. A., Hardy, R. R., Monach, P., Bezman, N. A., Sun, J. C., Kim, C. C., Lanier, L. L., Heng, T., Kreslavsky, T., Painter, M., Ericson, J., Davis, S., Mathis, D., & Benoist, C. (2012a). Gene-expression profiles and transcriptional regulatory pathways that underlie the identity and diversity of mouse tissue macrophages. *Nature Immunology*, 13(11), 1118–1128.

[110] Gautiar, E. L., Shay, T., Miller, J., Greter, M., Jakubzick, C., Ivanov, S., Helft, J., Chow, A., Elpek, K. G., Gordonov, S., Mazloom, A. R., Ma'Ayan, A., Chua, W. J., Hansen, T. H., Turley, S. J., Merad, M., Randolph, G. J., Best, A. J., Knell, J., Goldrath, A., Brown, B., Jojic, V., Koller, D., Cohen, N., Brenner, M., Regev, A., Fletcher, A., Bellemare-Pelletier, A., Malhotra, D., Jianu, R., Laidlaw, D., Collins, J., Narayan, K., Sylvia, K., Kang, J., Gazit, R., Garrison, B. S., Rossi, D. J., Kim, F., Rao, T. N., Wagers, A., Shinton, S. A., Hardy, R. R., Monach, P., Bezman, N. A., Sun, J. C., Kim, C. C., Lanier, L. L., Heng, T., Kreslavsky, T., Painter, M., Ericson, J., Davis, S., Mathis, D., & Benoist, C. (2012b). Gene-expression profiles and transcriptional regulatory pathways that underlie the identity and diversity of mouse tissue macrophages. *Nature Immunology*, 13(11), 1118–1128.

[111] Ge, Z. & Ding, S. (2020). The Crosstalk Between Tumor-Associated Macrophages (TAMs) and Tumor Cells and the Corresponding Targeted Therapy. *Frontiers in Oncology*, 10, 2404.

[112] Gentles, A. J., Newman, A. M., Liu, C. L., Bratman, S. V., Feng, W., Kim, D., Nair, V. S., Xu, Y., Khuong, A., Hoang, C. D., Diehn, M., West, R. B., Plevritis, S. K., & Alizadeh, A. A. (2015). The prognostic landscape of genes and infiltrating immune cells across human cancers. *Nature Medicine*, 21(8), 938–945.

[113] Gibbings, S. L., Goyal, R., Desch, A. N., Leach, S. M., Prabagar, M., Atif, S. M., Bratton, D. L., Janssen, W., & Jakubzick, C. V. (2015). Regular Article Transcriptome analysis highlights the conserved difference between embryonic and postnatal-derived alveolar macrophages. *Blood*, 126(11), 1357–1366.

[114] Gilan, O., Rioja, I., Knezevic, K., Bell, M. J., Yeung, M. M., Harker, N. R., Lam, E. Y., Chung, C., Bamborough, P., Petretich, M., Urh, M., Atkinson, S. J., Bassil, A. K., Roberts, E. J., Vassiliadis, D., Burr, M. L., Preston, A. G., Wellaway, C., Werner, T., Gray, J. R., Michon, A. M., Gobbetti, T., Kumar, V., Soden, P. E., Haynes, A., Vappiani, J., Tough, D. F., Taylor, S., Dawson, S. J., Bantscheff, M., Lindon, M., Drewes, G., Demont, E. H., Daniels, D. L., Grandi, P., Prinjha, R. K., & Dawson, M. A. (2020). Selective targeting of BD1 and BD2 of the BET proteins in cancer and immunoinflammation. *Science*, 368(6489), 387–394.

[115] Ginhoux, F., Greter, M., Leboeuf, M., Nandi, S., See, P., Gokhan, S., Mehler, M. F., Conway, S. J., Ng, L. G., Stanley, E. R., Samokhvalov, I. M., & Merad, M. (2010). Fate mapping analysis reveals that adult microglia derive from primitive macrophages. *Science*, 330(6005), 841–845.

[116] Gnant, M., Filipits, M., Greil, R., Stoeger, H., Rudas, M., Bago-Horvath, Z., Mlineritsch, B., Kwasny, W., Knauer, M., Singer, C., Jakesz, R., Dubsky, P., Fitzal, F., Bartsch, R., Steger, G., Balic, M., Ressler, S., Cowens, J. W., Storhoff, J., Ferree, S., Schaper, C., Liu, S., Fesl, C., & Nielsen, T. O. (2014). Predicting distant recurrence in receptor-positive breast cancer patients with limited clinicopathological risk: Using the

PAM50 Risk of Recurrence score in 1478 postmenopausal patients of the ABCSG-8 trial treated with adjuvant endocrine therapy alone. *Annals of Oncology*, 25(2), 339–345.

[117] Gocheva, V., Wang, H. W., Gadea, B. B., Shree, T., Hunter, K. E., Garfall, A. L., Berman, T., & Joyce, J. A. (2010). IL-4 induces cathepsin protease activity in tumor-associated macrophages to promote cancer growth and invasion. *Genes and Development*, 24(3), 241–255.

[118] Goldmann, T., Wieghofer, P., Müller, P. F., Wolf, Y., Varol, D., Yona, S., Brendecke, S. M., Kierdorf, K., Staszewski, O., Datta, M., Luedde, T., Heikenwalder, M., Jung, S., & Prinz, M. (2013). A new type of microglia gene targeting shows TAK1 to be pivotal in CNS autoimmune inflammation. *Nature Neuroscience*, 16(11), 1618–1626.

[119] Gong, T., Liu, L., Jiang, W., & Zhou, R. (2020). DAMP-sensing receptors in sterile inflammation and inflammatory diseases. *Nature Reviews Immunology*, 20(2), 95–112.

[120] Gordon, S. (2003). Alternative activation of macrophages. *Nature Reviews Immunology*, 3(1), 23–35.

[121] Gosselin, D., Link, V. M., Romanoski, C. E., Fonseca, G. J., Eichenfield, D. Z., Spann, N. J., Stender, J. D., Chun, H. B., Garner, H., Geissmann, F., & Glass, C. K. (2014). Environment Drives Selection and Function of Enhancers Controlling Tissue-Specific Macrophage Identities. *Cell*, 159(6), 1327–1340.

[122] Gottlieb, C. E., Mills, A. M., Cross, J. V., & Ring, K. L. (2017). Tumor-associated macrophage expression of PD-L1 in implants of high grade serous ovarian carcinoma: A comparison of matched primary and metastatic tumors. *Gynecologic Oncology*, 144(3), 607–612.

[123] Grubb, B. R. & Boucher, R. C. (1999). Pathophysiology of gene-targeted mouse models for cystic fibrosis. *Physiological Reviews*, 79(1 SUPPL. 1).

[124] Guilliams, M., De Kleer, I., Henri, S., Post, S., Vanhoutte, L., De Prijck, S., Deswarte, K., Malissen, B., Hammad, H., & Lambrecht, B. N. (2013). Alveolar macrophages

develop from fetal monocytes that differentiate into long-lived cells in the first week of life via GM-CSF. *Journal of Experimental Medicine*, 210(10), 1977–1992.

[125] Guilliams, M. & van de Laar, L. (2015). A hitchhiker's guide to myeloid cell subsets: Practical implementation of a novel mononuclear phagocyte classification system. *Frontiers in Immunology*, 6(JUL), 406.

[126] Günthner, R. & Anders, H.-J. (2013). Interferon-Regulatory Factors Determine Macrophage Phenotype Polarization. *Mediators of Inflammation*, 2013.

[127] Hahne, F. & Ivanek, R. (2016). Visualizing genomic data using Gviz and bioconductor. *Methods in Molecular Biology*, 1418, 335–351.

[128] Ham, B., Fernandez, M. C., D'Costa, Z., & Brodt, P. (2016). The diverse roles of the TNF axis in cancer progression and metastasis. *Trends in cancer research*, 11(1), 1–27.

[129] Han, M. L. K., Agusti, A., Calverley, P. M., Celli, B. R., Criner, G., Curtis, J. L., Fabbri, L. M., Goldin, J. G., Jones, P. W., MacNee, W., Make, B. J., Rabe, K. F., Rennard, S. I., Sciurba, F. C., Silverman, E. K., Vestbo, J., Washko, G. R., Wouters, E. F., & Martinez, F. J. (2010). Chronic obstructive pulmonary disease phenotypes: The future of COPD. *American Journal of Respiratory and Critical Care Medicine*, 182(5), 598–604.

[130] Hansen, K. D., Langmead, B., & Irizarry, R. A. (2012). BSmooth: from whole genome bisulfite sequencing reads to differentially methylated regions. *Genome Biology*, 13(10), 1–10.

[131] Haque, A. S., Moriyama, M., Kubota, K., Ishiguro, N., Sakamoto, M., Chinju, A., Mochizuki, K., Sakamoto, T., Kaneko, N., Munemura, R., Maehara, T., Tanaka, A., Hayashida, J. N., Kawano, S., Kiyoshima, T., & Nakamura, S. (2019). CD206+ tumor-associated macrophages promote proliferation and invasion in oral squamous cell carcinoma via EGF production. *Scientific Reports*, 9(1), 1–10.

[132] Harbeck, N., Penault-Llorca, F., Cortes, J., Gnant, M., Houssami, N., Poortmans, P., Ruddy, K., Tsang, J., & Cardoso, F. (2019). Breast cancer. *Nature Reviews Disease Primers*, 5(1), 1–31.

[133] Harp, J. M., Hanson, B. L., Timm, D. E., & Bunick, G. J. (2000). Asymmetries in the nucleosome core particle at 2.5 Å resolution. *Acta Crystallographica Section D: Biological Crystallography*, 56(12), 1513–1534.

[134] Hashimoto, D., Chow, A., Noizat, C., Teo, P., Beasley, M. B., Leboeuf, M., Becker, C. D., See, P., Price, J., Lucas, D., Greter, M., Mortha, A., Boyer, S. W., Forsberg, E. C., Tanaka, M., van Rooijen, N., García-Sastre, A., Stanley, E. R., Ginhoux, F., Frenette, P. S., & Merad, M. (2013). Tissue-resident macrophages self-maintain locally throughout adult life with minimal contribution from circulating monocytes. *Immunity*, 38(4), 792–804.

[135] Hautamaki, R. D., Kobayashi, D. K., Senior, R. M., & Shapiro, S. D. (1997). Requirement for macrophage elastase for cigarette smoke-induced emphysema in mice. *Science*, 277(5334), 2002–2004.

[136] Heinz, S., Benner, C., Spann, N., Bertolino, E., Lin, Y. C., Laslo, P., Cheng, J. X., Murre, C., Singh, H., & Glass, C. K. (2010). Simple Combinations of Lineage-Determining Transcription Factors Prime cis-Regulatory Elements Required for Macrophage and B Cell Identities. *Molecular Cell*, 38(4), 576–589.

[137] Henderson, A. G., Ehre, C., Button, B., Abdullah, L. H., Cai, L. H., Leigh, M. W., DeMaria, G. C., Matsui, H., Donaldson, S. H., Davis, C. W., Sheehan, J. K., Boucher, R. C., & Kesimer, M. (2014). Cystic fibrosis airway secretions exhibit mucin hyperconcentration and increased osmotic pressure. *Journal of Clinical Investigation*, 124(7), 3047–3060.

[138] Henson, P. M. & Hume, D. A. (2006). Apoptotic cell removal in development and tissue homeostasis. *Trends in Immunology*, 27(5), 244–250.

[139] Heyn, H., Vidal, E., Ferreira, H. J., Vizoso, M., Sayols, S., Gomez, A., Moran, S., Boque-Sastre, R., Guil, S., Martinez-Cardus, A., Lin, C. Y., Royo, R., Sanchez-Mut, J. V., Martinez, R., Gut, M., Torrents, D., Orozco, M., Gut, I., Young, R. A., & Esteller, M. (2016). Epigenomic analysis detects aberrant super-enhancer DNA methylation in human cancer. *Genome Biology*, 17(1).

[140] Hoeffel, G., Chen, J., Lavin, Y., Low, D., Almeida, F. F., See, P., Beaudin, A. E., Lum, J., Low, I., Forsberg, E. C., Poidinger, M., Zolezzi, F., Larbi, A., Ng, L. G., Chan, J. K., Greter, M., Becher, B., Samokhvalov, I. M., Merad, M., & Ginhoux, F. (2015). C-Myb+ Erythro-Myeloid Progenitor-Derived Fetal Monocytes Give Rise to Adult Tissue-Resident Macrophages. *Immunity*, 42(4), 665–678.

[141] Hoeffel, G., Wang, Y., Greter, M., See, P., Teo, P., Malleret, B., Leboeuf, M., Low, D., Oller, G., Almeida, F., Choy, S. H., Grisotto, M., Renia, L., Conway, S. J., Stanley, E. R., Chan, J. K., Ng, L. G., Samokhvalov, I. M., Merad, M., & Ginhoux, F. (2012). Adult Langerhans cells derive predominantly from embryonic fetal liver monocytes with a minor contribution of yolk sac-derived macrophages. *Journal of Experimental Medicine*, 209(6), 1167–1181.

[142] Hogg, J. C., Paré, P. D., & Hackett, T. L. (2017). The contribution of small airway obstruction to the pathogenesis of chronic obstructive pulmonary disease. *Physiological Reviews*, 97(2), 529–552.

[143] Hollenhorst, M. I., Richter, K., & Fronius, M. (2011). Ion transport by pulmonary epithelia. *Journal of Biomedicine and Biotechnology*, 2011, 16.

[144] Holliday, R. (1994). Epigenetics: An overview. *Developmental Genetics*, 15(6), 453–457.

[145] Holliday, R. & Pugh, J. E. (1975). DNA modification mechanisms and gene activity during development. *Science*, 187(4173), 226–232.

[146] Holm, K., Staaf, J., Lauss, M., Aine, M., Lindgren, D., Bendahl, P. O., Vallon-Christersson, J., Barkardottir, R. B., Höglund, M., Borg, Å., Jönsson, G., & Ringnér, M. (2016). An integrated genomics analysis of epigenetic subtypes in human breast tumors links DNA methylation patterns to chromatin states in normal mammary cells. *Breast Cancer Research*, 18(1).

[147] Holoch, D. & Moazed, D. (2015). RNA-mediated epigenetic regulation of gene expression. *Nature Reviews Genetics*, 16(2), 71–84.

[148] Horani, A., Dickinson, J. D., & Brody, S. L. (2013). Applications of mouse airway epithelial cell culture for asthma research. *Methods in Molecular Biology*, 1032, 91–107.

[149] HOTCHKISS, R. D. (1948). The quantitative separation of purines, pyrimidines, and nucleosides by paper chromatography. *The Journal of biological chemistry*, 175(1), 315–332.

[150] Hu, Z., Fan, C., Oh, D. S., Marron, J. S., He, X., Qaqish, B. F., Livasy, C., Carey, L. A., Reynolds, E., Dressler, L., Nobel, A., Parker, J., Ewend, M. G., Sawyer, L. R., Wu, J., Liu, Y., Nanda, R., Tretiakova, M., Orrico, A. R., Dreher, D., Palazzo, J. P., Perreard, L., Nelson, E., Mone, M., Hansen, H., Mullins, M., Quackenbush, J. F., Ellis, M. J., Olopade, O. I., Bernard, P. S., & Perou, C. M. (2006). The molecular portraits of breast tumors are conserved across microarray platforms. *BMC Genomics*, 7(1), 96.

[151] Huen, M. S., Sy, S. M., & Chen, J. (2010). BRCA1 and its toolbox for the maintenance of genome integrity. *Nature Reviews Molecular Cell Biology*, 11(2), 138–148.

[152] Ito, S., Shen, L., Dai, Q., Wu, S. C., Collins, L. B., Swenberg, J. A., He, C., & Zhang, Y. (2011). Tet proteins can convert 5-methylcytosine to 5-formylcytosine and 5-carboxylcytosine. *Science*, 333(6047), 1300–1303.

[153] Jadhav, K. & Zhang, Y. (2017). Activating transcription factor 3 in immune response and metabolic regulation. *Liver Research*, 1(2), 96–102.

[154] Jaitin, D. A., Kenigsberg, E., Keren-Shaul, H., Elefant, N., Paul, F., Zaretsky, I., Mildner, A., Cohen, N., Jung, S., Tanay, A., & Amit, I. (2014). Massively parallel single-cell RNA-seq for marker-free decomposition of tissues into cell types. *Science*, 343(6172), 776–779.

[155] Jakubzick, C., Gautier, E. L., Gibbings, S. L., Sojka, D. K., Schlitzer, A., Johnson, T. E., Ivanov, S., Duan, Q., Bala, S., Condon, T., VanRooijen, N., Grainger, J. R., Belkaid, Y., Ma'ayan, A., Riches, D. W., Yokoyama, W. M., Ginhoux, F., Henson, P. M., & Randolph, G. J. (2013). Minimal differentiation of classical monocytes as they survey steady-state tissues and transport antigen to lymph nodes. *Immunity*, 39(3), 599–610.

[156] Jin Lee, Grey Christoforo, Grey Christoforo, CS Foo, Chris Probert, Anshul Kundaje, M. D. (2016). kundajelab/atac$_{d}$nase$_{p}$ipelines : 0.3.0($Version$0.3.0).

[157] Jones, P. W. (2005). St. George's respiratory questionnaire: MCID. In *COPD: Journal of Chronic Obstructive Pulmonary Disease*, volume 2 (pp. 75–79).

[158] Joyce, J. A. & Pollard, J. W. (2009). Microenvironmental regulation of metastasis. *Nature Reviews Cancer*, 9(4), 239–252.

[159] Jung, S., Aliberti, J., Graemmel, P., Sunshine, M. J., Kreutzberg, G. W., Sher, A., & Littman, D. R. (2000). Analysis of Fractalkine Receptor CX3CR1 Function by Targeted Deletion and Green Fluorescent Protein Reporter Gene Insertion. *Molecular and Cellular Biology*, 20(11), 4106–4114.

[160] Keniry, M., Dearth, R. K., Persans, M., & Parsons, R. (2014). New Frontiers for the NFIL3 bZIP Transcription Factor in Cancer, Metabolism and Beyond. *Discoveries*, 2(2), e15.

[161] Kesimer, M., Ford, A. A., Ceppe, A., Radicioni, G., Cao, R., Davis, C. W., Doerschuk, C. M., Alexis, N. E., Anderson, W. H., Henderson, A. G., Barr, R. G., Bleecker, E. R., Christenson, S. A., Cooper, C. B., Han, M. K., Hansel, N. N., Hastie, A. T., Hoffman, E. A., Kanner, R. E., Martinez, F., Paine, R., Woodruff, P. G., O'Neal, W. K., & Boucher, R. C. (2017). Airway Mucin Concentration as a Marker of Chronic Bronchitis. *New England Journal of Medicine*, 377(10), 911–922.

[162] Kieusseian, A., de la Grange, P. B., Burlen-Defranoux, O., Godin, I., & Cumano, A. (2012). Immature hematopoietic stem cells undergo maturation in the fetal liver. *Development (Cambridge)*, 139(19), 3521–3530.

[163] Kitamura, T., Qian, B. Z., Soong, D., Cassetta, L., Noy, R., Sugano, G., Kato, Y., Li, J., & Pollard, J. W. (2015). CCL2-induced chemokine cascade promotes breast cancer metastasis by enhancing retention of metastasis-associated macrophages. *Journal of Experimental Medicine*, 212(7), 1043–1059.

[164] Kiwamoto, T., Katoh, T., Evans, C. M., Janssen, W. J., Brummet, M. E., Hudson, S. A., Zhu, Z., Tiemeyer, M., & Bochner, B. S. (2015). Endogenous airway mucins carry glycans that bind Siglec-F and induce eosinophil apoptosis. *Journal of Allergy and Clinical Immunology*, 135(5), 1329–1340.e9.

[165] Koboldt, D. C., Fulton, R. S., McLellan, M. D., Schmidt, H., Kalicki-Veizer, J., McMichael, J. F., Fulton, L. L., Dooling, D. J., Ding, L., Mardis, E. R., Wilson, R. K., Ally, A., Balasundaram, M., Butterfield, Y. S., Carlsen, R., Carter, C., Chu, A. A., Chuah, E., Chun, H. J. E., Coope, R. J., Dhalla, N., Guin, R., Hirst, C., Hirst, M., Holt, R. A., Lee, D., Li, H. I., Mayo, M., Moore, R. A., Mungall, A. J., Pleasance, E., Robertson, A. G., Schein, J. E., Shafiei, A., Sipahimalani, P., Slobodan, J. R., Stoll, D., Tam, A., Thiessen, N., Varhol, R. J., Wye, N., Zeng, T., Zhao, Y., Birol, I., Jones, S. J., Marra, M. A., Cherniack, A. D., Saksena, G., Onofrio, R. C., Pho, N. H., Carter, S. L., Schumacher, S. E., Tabak, B., Hernandez, B., Gentry, J., Nguyen, H., Crenshaw, A., Ardlie, K., Beroukhim, R., Winckler, W., Getz, G., Gabriel, S. B., Meyerson, M., Chin, L., Kucherlapati, R., Hoadley, K. A., Auman, J. T., Fan, C., Turman, Y. J., Shi, Y., Li, L., Topal, M. D., He, X., Chao, H. H., Prat, A., Silva, G. O., Iglesia, M. D., Zhao, W., Usary, J., Berg, J. S., Adams, M., Booker, J., Wu, J., Gulabani, A., Bodenheimer, T., Hoyle, A. P., Simons, J. V., Soloway, M. G., Mose, L. E., Jefferys, S. R., Balu, S., Parker, J. S., Hayes, D. N., Perou, C. M., Malik, S., Mahurkar, S., Shen, H., Weisenberger, D. J., Triche, T., Lai, P. H., Bootwalla, M. S., Maglinte, D. T., Berman, B. P., Van Den Berg, D. J., Baylin, S. B., Laird, P. W., Creighton, C. J., Donehower, L. A., Noble, M., Voet, D., Gehlenborg, N., Di Cara, D., Zhang, J. J., Zhang, H., Wu, C. J., Yingchun Liu, S., Lawrence, M. S., Zou, L., Sivachenko, A., Lin, P., Stojanov, P., Jing, R., Cho, J., Sinha, R. R., Park, R. W., Nazaire, M. D., Robinson, J., Thorvaldsdottir, H., Mesirov, J., Park, P. J., Reynolds, S., Kreisberg, R. B., Bernard, B., Bressler, R., Erkkila, T., Lin, J., Thorsson, V., Zhang, W., Shmulevich, I., Ciriello, G., Weinhold, N., Schultz, N., Gao, J., Cerami, E., Gross, B., Jacobsen, A., Sinha, R. R., Aksoy, B. A., Antipin, Y., Reva, B., Shen, R., Taylor, B. S., Ladanyi, M., Sander, C., Anur, P., Spellman, P. T., Lu, Y., Liu, W., Verhaak, R. R., Mills, G. B., Akbani, R., Zhang, N., Broom, B. M., Casasent, T. D., Wakefield, C., Unruh, A. K., Baggerly, K., Coombes, K., Weinstein, J. N., Haussler, D., Benz, C. C., Stuart, J. M.,

Benz, S. C., Zhu, J., Szeto, C. C., Scott, G. K., Yau, C., Paull, E. O., Carlin, D., Wong, C., Sokolov, A., Thusberg, J., Mooney, S., Ng, S., Goldstein, T. C., Ellrott, K., Grifford, M., Wilks, C., Ma, S., Craft, B., Yan, C., Hu, Y., Meerzaman, D., Gastier-Foster, J. M., Bowen, J., Ramirez, N. C., Black, A. D., Pyatt, R. E., White, P., Zmuda, E. J., Frick, J., Lichtenberg, T. M., Brookens, R., George, M. M., Gerken, M. A., Harper, H. A., Leraas, K. M., Wise, L. J., Tabler, T. R., McAllister, C., Barr, T., Hart-Kothari, M., Tarvin, K., Saller, C., Sandusky, G., Mitchell, C., Iacocca, M. V., Brown, J., Rabeno, B., Czerwinski, C., Petrelli, N., Dolzhansky, O., Abramov, M., Voronina, O., Potapova, O., Marks, J. R., Suchorska, W. M., Murawa, D., Kycler, W., Ibbs, M., Korski, K., Spychała, A., Murawa, P., Brzeziński, J. J., Perz, H., Łaźniak, R., Teresiak, M., Tatka, H., Leporowska, E., Bogusz-Czerniewicz, M., Malicki, J., Mackiewicz, A., Wiznerowicz, M., Van Le, X., Kohl, B., Viet Tien, N., Thorp, R., Van Bang, N., Sussman, H., Phu, B. D., Hajek, R., Hung, N. P., Phuong, T. V. T., Thang, H. Q., Khan, K. Z., Penny, R., Mallery, D., Curley, E., Shelton, C., Yena, P., Ingle, J. N., Couch, F. J., Lingle, W. L., King, T. A., Gonzalez-Angulo, A. M., Dyer, M. D., Liu, S., Meng, X., Patangan, M., Waldman, F., Stöppler, H., Rathmell, W. K., Thorne, L., Huang, M., Boice, L., Hill, A., Morrison, C., Gaudioso, C., Bshara, W., Daily, K., Egea, S. C., Pegram, M. D., Gomez-Fernandez, C., Dhir, R., Bhargava, R., Brufsky, A., Shriver, C. D., Hooke, J. A., Campbell, J. L., Mural, R. J., Hu, H., Somiari, S., Larson, C., Deyarmin, B., Kvecher, L., Kovatich, A. J., Ellis, M. J., Stricker, T., White, K., Olopade, O., Luo, C., Chen, Y., Bose, R., Chang, L. W., Beck, A. H., Pihl, T., Jensen, M., Sfeir, R., Kahn, A., Chu, A. A., Kothiyal, P., Wang, Z., Snyder, E., Pontius, J., Ayala, B., Backus, M., Walton, J., Baboud, J., Berton, D., Nicholls, M., Srinivasan, D., Raman, R., Girshik, S., Kigonya, P., Alonso, S., Sanbhadti, R., Barletta, S., Pot, D., Sheth, M., Demchok, J. A., Shaw, K. R., Yang, L., Eley, G., Ferguson, M. L., Tarnuzzer, R. W., Zhang, J. J., Dillon, L. A., Buetow, K., Fielding, P., Ozenberger, B. A., Guyer, M. S., Sofia, H. J., & Palchik, J. D. (2012). Comprehensive molecular portraits of human breast tumours. *Nature*, 490(7418), 61–70.

[166] Kohen, R., Barlev, J., Hornung, G., Stelzer, G., Feldmesser, E., Kogan, K., Safran, M., & Leshkowitz, D. (2019). UTAP: User-friendly Transcriptome Analysis Pipeline. *BMC Bioinformatics*, 20(1), 154.

[167] Kohyama, M., Ise, W., Edelson, B. T., Wilker, P. R., Hildner, K., Mejia, C., Frazier, W. A., Murphy, T. L., & Murphy, K. M. (2009). Role for Spi-C in the development of red pulp macrophages and splenic iron homeostasis. *Nature*, 457(7227), 318–321.

[168] Kratochvill, F., Neale, G., Haverkamp, J. M., Van de Velde, L. A., Smith, A. M., Kawauchi, D., McEvoy, J., Roussel, M. F., Dyer, M. A., Qualls, J. E., & Murray, P. J. (2015). TNF Counterbalances the Emergence of M2 Tumor Macrophages. *Cell Reports*, 12(11), 1902–1914.

[169] Krysko, O., Van Zele, T., Claeys, S., & Bachert, C. (2009). Comment on "Potent Phagocytic Activity with Impaired Antigen Presentation Identifying Lipopolysaccharide-Tolerant Human Monocytes: Demonstration in Isolated Monocytes from Cystic Fibrosis Patients". *The Journal of Immunology*, 183(8), 4831.1–4832.

[170] Kuchenbaecker, K. B., Hopper, J. L., Barnes, D. R., Phillips, K. A., Mooij, T. M., Roos-Blom, M. J., Jervis, S., Van Leeuwen, F. E., Milne, R. L., Andrieu, N., Goldgar, D. E., Terry, M. B., Rookus, M. A., Easton, D. F., & Antoniou, A. C. (2017). Risks of breast, ovarian, and contralateral breast cancer for BRCA1 and BRCA2 mutation carriers. *JAMA - Journal of the American Medical Association*, 317(23), 2402–2416.

[171] Kulakovskiy, I. V., Vorontsov, I. E., Yevshin, I. S., Soboleva, A. V., Kasianov, A. S., Ashoor, H., Ba-Alawi, W., Bajic, V. B., Medvedeva, Y. A., Kolpakov, F. A., & Makeev, V. J. (2016). HOCOMOCO: Expansion and enhancement of the collection of transcription factor binding sites models. *Nucleic Acids Research*, 44(D1), D116–D125.

[172] Kuperman, D. A., Huang, X., Koth, L. L., Chang, G. H., Dolganov, G. M., Zhu, Z., Elias, J. A., Sheppard, D., & Erle, D. J. (2002). Direct effects of interleukin-13 on epithelial cells cause airway hyperreactivity and mucus overproduction in asthma. *Nature Medicine*, 8(8), 885–889.

[173] Landsman, L. & Jung, S. (2007). Lung Macrophages Serve as Obligatory Intermediate between Blood Monocytes and Alveolar Macrophages. *The Journal of Immunology*, 179(6), 3488–3494.

[174] Lao, L., Fan, S., & Song, E. (2017). Tumor associated macrophages as therapeutic targets for breast cancer. *Advances in Experimental Medicine and Biology*, 1026, 331–370.

[175] Larionova, I., Kazakova, E., Patysheva, M., & Kzhyshkowska, J. (2020). Transcriptional, epigenetic and metabolic programming of tumor-associated macrophages. *Cancers*, 12(6), 1–40.

[176] Lavin, Y., Mortha, A., Rahman, A., & Merad, M. (2015). Regulation of macrophage development and function in peripheral tissues. *Nature Reviews Immunology*, 15(12), 731–744.

[177] Lavin, Y., Winter, D., Blecher-Gonen, R., David, E., Keren-Shaul, H., Merad, M., Jung, S., & Amit, I. (2014). Tissue-resident macrophage enhancer landscapes are shaped by the local microenvironment. *Cell*, 159(6), 1312–26.

[178] Lawrence, M., Huber, W., Pagès, H., Aboyoun, P., Carlson, M., Gentleman, R., Morgan, M. T., & Carey, V. J. (2013). Software for Computing and Annotating Genomic Ranges. *PLoS Computational Biology*, 9(8), e1003118.

[179] Leith, D. E. (1968). Cough. *Physical therapy*, 48(5), 439–447.

[180] Lévêque, M., Le, S., Del, P., & Martin-chouly, C. (2017). The impact of impaired macrophage functions in cystic fi brosis disease progression. *Journal of Cystic Fibrosis*, 16(4), 443–453.

[181] Li, E., Beard, C., & Jaenisch, R. (1993). Role for DNA methylation in genomic imprinting. *Nature*, 366(6453), 362–365.

[182] Li, H. (2013). Aligning sequence reads, clone sequences and assembly contigs with BWA-MEM.

[183] Liberzon, A., Subramanian, A., Pinchback, R., Thorvaldsdóttir, H., Tamayo, P., & Mesirov, J. P. (2011). Molecular signatures database (MSigDB) 3.0. *Bioinformatics*, 27(12), 1739–1740.

[184] Lieberman-Aiden, E., Van Berkum, N. L., Williams, L., Imakaev, M., Ragoczy, T., Telling, A., Amit, I., Lajoie, B. R., Sabo, P. J., Dorschner, M. O., Sandstrom, R., Bernstein, B., Bender, M. A., Groudine, M., Gnirke, A., Stamatoyannopoulos, J., Mirny, L. A., Lander, E. S., & Dekker, J. (2009). Comprehensive mapping of long-range interactions reveals folding principles of the human genome. *Science*, 326(5950), 289–293.

[185] Lin, Y., Yoder, M. C., & Yoshimoto, M. (2014). Lymphoid progenitor emergence in the murine embryo and yolk sac precedes stem cell detection. *Stem Cells and Development*, 23(11), 1168–1177.

[186] Liu, Z., Kuang, W., Zhou, Q., & Zhang, Y. (2018). TGF-β1 secreted by M2 phenotype macrophages enhances the stemness and migration of glioma cells via the SMAD2/3 signalling pathway. *International Journal of Molecular Medicine*, 42(6), 3395–3403.

[187] Livraghi-Butrico, A., Grubb, B. R., Kelly, E. J., Wilkinson, K. J., Yang, H., Geiser, M., Randell, S. H., Boucher, R. C., & O'Neal, W. K. (2012). Genetically determined heterogeneity of lung disease in a mouse model of airway mucus obstruction. *Physiological Genomics*, 44(8), 470–484.

[188] Love, M. I., Huber, W., & Anders, S. (2014). Moderated estimation of fold change and dispersion for RNA-seq data with DESeq2. *Genome Biology*, 15(12), 550.

[189] Luger, K., Mäder, A. W., Richmond, R. K., Sargent, D. F., & Richmond, T. J. (1997). Crystal structure of the nucleosome core particle at 2.8 Å resolution. *Nature*, 389(6648), 251–260.

[190] Lundgren, C., Bendahl, P. O., Borg, Å., Ehinger, A., Hegardt, C., Larsson, C., Loman, N., Malmberg, M., Olofsson, H., Saal, L. H., Sjöblom, T., Lindman, H., Klintman, M., Häkkinen, J., Vallon-Christersson, J., Fernö, M., Rydén, L., & Ekholm, M. (2019). Agreement between molecular subtyping and surrogate subtype classification: a contemporary population-based study of ER-positive/HER2-negative primary breast cancer. *Breast Cancer Research and Treatment*, 178(2), 459–467.

[191] Luo, C., Hajkova, P., & Ecker, J. R. (2018). Dynamic DNA methylation: In the right place at the right time. *Science*, 361(6409), 1336–1340.

[192] Lutsik, P., Slawski, M., Gasparoni, G., Vedeneev, N., Hein, M., & Walter, J. (2017). MeDeCom: Discovery and quantification of latent components of heterogeneous methylomes. *Genome Biology*, 18(1), 55.

[193] Magalhães, M., Rivals, I., Claustres, M., Varilh, J., Thomasset, M., Bergougnoux, A., Mely, L., Leroy, S., Corvol, H., Guillot, L., Murris, M., Beyne, E., Caimmi, D., Vachier, I., Chiron, R., & De Sario, A. (2017). DNA methylation at modifier genes of lung disease severity is altered in cystic fibrosis. *Clinical Epigenetics*, 9(1), 19.

[194] Magalhães, M., Tost, J., Pineau, F., Rivals, I., Busato, F., Alary, N., Mely, L., Leroy, S., Murris, M., Caimmi, D., Claustres, M., Chiron, R., & De Sario, A. (2018). Dynamic changes of DNA methylation and lung disease in cystic fibrosis: lessons from a monogenic disease. *Epigenomics*, 10(8), 1131–1145.

[195] Mall, M., Grubb, B. R., Harkema, J. R., O'Neal, W. K., & Boucher, R. C. (2004). Increased airway epithelial Na+ absorption produces cystic fibrosis-like lung disease in mice. *Nature Medicine*, 10(5), 487–493.

[196] Mall, M. A. (2009). Role of the amiloride-sensitive epithelial Na+ channel in the pathogenesis and as a therapeutic target for cystic fibrosis lung disease: Experimental Physiology - Symposium Report. *Experimental Physiology*, 94(2), 171–174.

[197] Mall, M. A., Harkema, J. R., Trojanek, J. B., Treis, D., Livraghi, A., Schubert, S., Zhou, Z., Kreda, S. M., Tilley, S. L., Hudson, E. J., O'Neal, W. K., & Boucher, R. C. (2008). Development of chronic bronchitis and emphysema in β-epithelial Na+ channel-overexpressing mice. *American Journal of Respiratory and Critical Care Medicine*, 177(7), 730–742.

[198] Mantovani, A. & Allavena, P. (2015). The interaction of anticancer therapies with tumor-associated macrophages. *Journal of Experimental Medicine*, 212(4), 435–445.

[199] Mantovani, A., Allavena, P., Sica, A., & Balkwill, F. (2008). Cancer-related inflammation. *Nature*, 454(7203), 436–444.

[200] Mantovani, A., Marchesi, F., Malesci, A., Laghi, L., & Allavena, P. (2017). Tumour-associated macrophages as treatment targets in oncology. *Nature Reviews Clinical Oncology*, 14(7), 399–416.

[201] Martinez, F. O. & Gordon, S. (2014). The M1 and M2 paradigm of macrophage activation: Time for reassessment. *F1000Prime Reports*, 6.

[202] Massó-Vallés, D. & Soucek, L. (2020). Blocking Myc to Treat Cancer: Reflecting on Two Decades of Omomyc. *Cells*, 9(4).

[203] Mayakonda, A. (2020). peakSeason.

[204] McAnulty, J. & Difeo, A. (2020). The molecular 'myc-anisms' behind myc-driven tumorigenesis and the relevant myc-directed therapeutics. *International Journal of Molecular Sciences*, 21(24), 1–28.

[205] Medina-Rivera, A., Defrance, M., Sand, O., Herrmann, C., Castro-Mondragon, J. A., Delerce, J., Jaeger, S., Blanchet, C., Van Helden, J., Vincens, P., Caron, C., Staines, D. M., Contreras-Moreira, B., Artufel, M., Charbonnier-Khamvongsa, L., Hernandez, C., Thieffry, D., Thomas-Chollier, M., & Van Helden, J. (2015). RSAT 2015: Regulatory sequence analysis tools. *Nucleic Acids Research*, 43(W1), W50–W56.

[206] Meissl, K., Macho-Maschler, S., Müller, M., & Strobl, B. (2017). The good and the bad faces of STAT1 in solid tumours. *Cytokine*, 89, 12–20.

[207] Minnoye, L., Marinov, G. K., Krausgruber, T., Pan, L., Marand, A. P., Secchia, S., Greenleaf, W. J., Furlong, E. E. M., Zhao, K., Schmitz, R. J., Bock, C., & Aerts, S. (2021). Chromatin accessibility profiling methods. *Nature Reviews Methods Primers*, 1(1), 1–24.

[208] Mirza, N. & Gabrilovich, D. (2007). Comment on "Cutting edge: induction of B7-H4 on APCs through IL-10: novel suppressive mode for regulatory T cells". *Journal of immunology (Baltimore, Md. : 1950)*, 178(8), 4705–6; author reply 4706.

[209] Misharin, A. V., Morales-Nebreda, L., Reyfman, P. A., Cuda, C. M., Walter, J. M., McQuattie-Pimentel, A. C., Chen, C. I., Anekalla, K. R., Joshi, N., Williams, K. J., Abdala-Valencia, H., Yacoub, T. J., Chi, M., Chiu, S., Gonzalez-Gonzalez, F. J., Gates, K., Lam, A. P., Nicholson, T. T., Homan, P. J., Soberanes, S., Dominguez, S., Morgan, V. K., Saber, R., Shaffer, A., Hinchcliff, M., Marshall, S. A., Bharat, A., Berdnikovs, S., Bhorade, S. M., Bartom, E. T., Morimoto, R. I., Balch, W. E., Sznajder, J. I., Chandel, N. S., Mutlu, G. M., Jain, M., Gottardi, C. J., Singer, B. D., Ridge, K. M., Bagheri, N., Shilatifard, A., Budinger, G. R., & Perlman, H. (2017). Monocyte-derived alveolar macrophages drive lung fibrosis and persist in the lung over the life span. *Journal of Experimental Medicine*, 214(8), 2387–2404.

[210] Mohandas, T., Sparkes, R. S., & Shapiro, L. J. (1981). Reactivation of an inactive human X chromosome: Evidence for X inactivation by DNA methylation. *Science*, 211(4480), 393–396.

[211] Montgomery, S. T., Dittrich, A. S., Garratt, L. W., Turkovic, L., Frey, D. L., Stick, S. M., Mall, M. A., Kicic, A., & AREST CF (2018). Interleukin-1 is associated with inflammation and structural lung disease in young children with cystic fibrosis. *Journal of Cystic Fibrosis*.

[212] Morrow, J. D., Cho, M. H., Hersh, C. P., Pinto-Plata, V., Celli, B., Marchetti, N., Criner, G., Bueno, R., Washko, G., Glass, K., Choi, A. M. K., Quackenbush, J., Silverman, E. K., & Demeo, D. L. (2016). DNA methylation profiling in human lung tissue identifies genes associated with COPD. *Epigenetics*, 11(10), 730–739.

[213] Mosser, D. M. & Edwards, J. P. (2008). Exploring the full spectrum of macrophage activation. *Nature Reviews Immunology*, 8(12), 958–969.

[214] Mould, K. J., Jackson, N. D., Henson, P. M., Seibold, M., & Janssen, W. J. (2019). Single cell RNA sequencing identifies unique inflammatory airspace macrophage subsets. *JCI insight*, 4(5).

[215] Murray, P. J., Allen, J. E., Biswas, S. K., Fisher, E. A., Gilroy, D. W., Goerdt, S., Gordon, S., Hamilton, J. A., Ivashkiv, L. B., Lawrence, T., Locati, M., Mantovani, A.,

Martinez, F. O., Mege, J. L., Mosser, D. M., Natoli, G., Saeij, J. P., Schultze, J. L., Shirey, K. A., Sica, A., Suttles, J., Udalova, I., VanGinderachter, J. A., Vogel, S. N., & Wynn, T. A. (2014). Macrophage Activation and Polarization: Nomenclature and Experimental Guidelines. *Immunity*, 41(1), 14–20.

[216] Nakagawa, R., Naka, T., Tsutsui, H., Fujimoto, M., Kimura, A., Abe, T., Seki, E., Sato, S., Takeuchi, O., Takeda, K., Akira, S., Yamanishi, K., Kawase, I., Nakanishi, K., & Kishimoto, T. (2002). SOCS-1 participates in negative regulation of LPS responses. *Immunity*, 17(5), 677–687.

[217] Newman, A. M., Liu, C. L., Green, M. R., Gentles, A. J., Feng, W., Xu, Y., Hoang, C. D., Diehn, M., & Alizadeh, A. A. (2015). Robust enumeration of cell subsets from tissue expression profiles. *Nature Methods*, 12(5), 453–457.

[218] Nicod, L. P. (2005). Lung defences: An overview. *European Respiratory Review*, 14(95), 45–50.

[219] Nicodeme, E., Jeffrey, K. L., Schaefer, U., Beinke, S., Dewell, S., Chung, C. W., Chandwani, R., Marazzi, I., Wilson, P., Coste, H., White, J., Kirilovsky, J., Rice, C. M., Lora, J. M., Prinjha, R. K., Lee, K., & Tarakhovsky, A. (2010). Suppression of inflammation by a synthetic histone mimic. *Nature*, 468(7327), 1119–1123.

[220] Nowicka, M., Krieg, C., Crowell, H. L., Weber, L. M., Hartmann, F. J., Guglietta, S., Becher, B., Levesque, M. P., & Robinson, M. D. (2019). CyTOF workflow: differential discovery in high-throughput high-dimensional cytometry datasets. *F1000Research*, 6, 748.

[221] Noy, R. & Pollard, J. W. (2014). Tumor-Associated Macrophages: From Mechanisms to Therapy. *Immunity*, 41(1), 49–61.

[222] Ojalvo, L. S., King, W., Cox, D., & Pollard, J. W. (2009). High-density gene expression analysis of tumor-associated macrophages from mouse mammary tumors. *American Journal of Pathology*, 174(3), 1048–1064.

[223] Okabe, Y. & Medzhitov, R. (2014). Tissue-specific signals control reversible program of localization and functional polarization of macrophages. *Cell*, 157(4), 832–844.

[224] Okano, M., Bell, D. W., Haber, D. A., & Li, E. (1999). DNA methyltransferases Dnmt3a and Dnmt3b are essential for de novo methylation and mammalian development. *Cell*, 99(3), 247–257.

[225] Orkin, S. H. & Zon, L. I. (2008). Hematopoiesis: An Evolving Paradigm for Stem Cell Biology. *Cell*, 132(4), 631–644.

[226] Ozsolak, F., Song, J. S., Liu, X. S., & Fisher, D. E. (2007). High-throughput mapping of the chromatin structure of human promoters. *Nature Biotechnology*, 25(2), 244–248.

[227] Pagiatakis, C., Musolino, E., Gornati, R., Bernardini, G., & Papait, R. (2019). Epigenetics of aging and disease: a brief overview. *Aging Clinical and Experimental Research*, 33(4), 737–745.

[228] Palis, J., Robertson, S., Kennedy, M., Wall, C., & Keller, G. (1999). Development of erythroid and myeloid progenitors in the yolk sac and embryo proper of the mouse. *Development*, 126(22), 5073–5084.

[229] Paolicelli, R. C., Bolasco, G., Pagani, F., Maggi, L., Scianni, M., Panzanelli, P., Giustetto, M., Ferreira, T. A., Guiducci, E., Dumas, L., Ragozzino, D., & Gross, C. T. (2011). Synaptic pruning by microglia is necessary for normal brain development. *Science*, 333(6048), 1456–1458.

[230] Park, Y. & Wu, H. (2016). Differential methylation analysis for BS-seq data under general experimental design. *Bioinformatics*, 32(10), 1446–1453.

[231] Paulus, P., Stanley, E. R., Schäfer, R., Abraham, D., & Aharinejad, S. (2006). Colony-stimulating factor-1 antibody reverses chemoresistance in human MCF-7 breast cancer xenografts. *Cancer Research*, 66(8), 4349–4356.

[232] Peat, J. R. & Smallwood, S. A. (2018). Low input whole-genome bisulfite sequencing using a post-bisulfite adapter tagging approach. In *Methods in Molecular Biology*, volume 1708 (pp. 161–169). Humana Press Inc.

[233] Pedroza-Gonzalez, A., Xu, K., Wu, T. C., Aspord, C., Tindle, S., Marches, F., Gallegos, M., Burton, E. C., Savino, D., Hori, T., Tanaka, Y., Zurawski, S., Zurawski, G., Bover, L., Liu, Y. J., Banchereau, J., & Palucka, A. K. (2011). Thymic stromal lymphopoietin fosters human breast tumor growth by promoting type 2 inflammation. *Journal of Experimental Medicine*, 208(3), 479–490.

[234] Pello, O. M., De Pizzol, M., Mirolo, M., Soucek, L., Zammataro, L., Amabile, A., Doni, A., Nebuloni, M., Swigart, L. B., Evan, G. I., Mantovani, A., & Locati, M. (2012). Role of c-MYC in alternative activation of human macrophages and tumor-associated macrophage biology. *Blood*, 119(2), 411–421.

[235] Perdiguero, E. G. & Geissmann, F. (2016). The development and maintenance of resident macrophages. *Nature Immunology*, 17(1), 2–8.

[236] Perou, C. M., Sørile, T., Eisen, M. B., Van De Rijn, M., Jeffrey, S. S., Ress, C. A., Pollack, J. R., Ross, D. T., Johnsen, H., Akslen, L. A., Fluge, Ø., Pergammenschlkov, A., Williams, C., Zhu, S. X., Lønning, P. E., Børresen-Dale, A. L., Brown, P. O., & Botstein, D. (2000). Molecular portraits of human breast tumours. *Nature*, 406(6797), 747–752.

[237] Pertea, M., Pertea, G. M., Antonescu, C. M., Chang, T. C., Mendell, J. T., & Salzberg, S. L. (2015). StringTie enables improved reconstruction of a transcriptome from RNA-seq reads. *Nature Biotechnology*, 33(3), 290–295.

[238] Pickup, M., Novitskiy, S., & Moses, H. L. (2013). The roles of TGFβ in the tumour microenvironment. *Nature Reviews Cancer*, 13(11), 788–799.

[239] Plank, M. W., Maltby, S., Tay, H. L., Stewart, J., Eyers, F., Hansbro, P. M., & Foster, P. S. (2015). MicroRNA expression is altered in an ovalbumin-induced asthma model and targeting miR-155 with antagomirs reveals cellular specificity. *PLoS ONE*, 10(12), 1–25.

[240] Platanitis, E. & Decker, T. (2018). Regulatory networks involving STATs, IRFs, and NFκB in inflammation. *Frontiers in Immunology*, 9(NOV).

[241] Poliska, S., Csanky, E., Szanto, A., Szatmari, I., Mesko, B., Szeles, L., Dezso, B., Scholtz, B., Podani, J., Kilty, I., Takacs, L., & Nagy, L. (2011). Chronic obstructive

pulmonary disease-specific gene expression signatures of alveolar macrophages as well as peripheral blood monocytes overlap and correlate with lung function. *Respiration*, 81(6), 499–510.

[242] Pollard, J. W. (2009). Trophic macrophages in development and disease. *Nature Reviews Immunology*, 9(4), 259–270.

[243] Pro, S. C., Imedio, A. D., Santoso, C. S., Gan, K. A., Sewell, J. A., Martinez, M., Sereda, R., Mehta, S., & Fuxman Bass, J. I. (2018). Global landscape of mouse and human cytokine transcriptional regulation. *Nucleic Acids Research*, 46(18), 9321–9337.

[244] Pyonteck, S. M., Akkari, L., Schuhmacher, A. J., Bowman, R. L., Sevenich, L., Quail, D. F., Olson, O. C., Quick, M. L., Huse, J. T., Teijeiro, V., Setty, M., Leslie, C. S., Oei, Y., Pedraza, A., Zhang, J., Brennan, C. W., Sutton, J. C., Holland, E. C., Daniel, D., & Joyce, J. A. (2013). CSF-1R inhibition alters macrophage polarization and blocks glioma progression. *Nature Medicine*, 19(10), 1264–1272.

[245] Qian, B. Z., Li, J., Zhang, H., Kitamura, T., Zhang, J., Campion, L. R., Kaiser, E. A., Snyder, L. A., & Pollard, J. W. (2011). CCL2 recruits inflammatory monocytes to facilitate breast-tumour metastasis. *Nature*, 475(7355), 222–225.

[246] Qian, B. Z. & Pollard, J. W. (2010). Macrophage Diversity Enhances Tumor Progression and Metastasis. *Cell*, 141(1), 39–51.

[247] Quaderi, S. A. & Hurst, J. R. (2018). The unmet global burden of COPD. *Global Health, Epidemiology and Genomics*, 3, 1–3.

[248] Raivo Kolde (2019). Pheatmap.

[249] Ramachandran, P., Pellicoro, A., Vernon, M. A., Boulter, L., Aucott, R. L., Ali, A., Hartland, S. N., Snowdon, V. K., Cappon, A., Gordon-Walker, T. T., Williams, M. J., Dunbar, D. R., Manning, J. R., Van Rooijen, N., Fallowfield, J. A., Forbes, S. J., & Iredale, J. P. (2012). Differential Ly-6C expression identifies the recruited macrophage phenotype, which orchestrates the regression of murine liver fibrosis. *Proceedings of the National Academy of Sciences of the United States of America*, 109(46), E3186–E3195.

[250] Ramsey, B. W., Davies, J., McElvaney, N. G., Tullis, E., Bell, S. C., Dřevínek, P., Griese, M., McKone, E. F., Wainwright, C. E., Konstan, M. W., Moss, R., Ratjen, F., Sermet-Gaudelus, I., Rowe, S. M., Dong, Q., Rodriguez, S., Yen, K., Ordoñez, C., & Elborn, J. S. (2011). A CFTR Potentiator in Patients with Cystic Fibrosis and the G551D Mutation. *New England Journal of Medicine*, 365(18), 1663–1672.

[251] Ratjen, F., Bell, S. C., Rowe, S. M., Goss, C. H., Quittner, A. L., & Bush, A. (2015). Cystic fibrosis. *Nature reviews. Disease primers*, 1(1), 15010.

[252] Reisinger, E., Genthner, L., Kerssemakers, J., Kensche, P., Borufka, S., Jugold, A., Kling, A., Prinz, M., Scholz, I., Zipprich, G., Eils, R., Lawerenz, C., & Eils, J. (2017). OTP: An automatized system for managing and processing NGS data. *Journal of Biotechnology*, 261, 53–62.

[253] Ritchie, M. E., Phipson, B., Wu, D., Hu, Y., Law, C. W., Shi, W., & Smyth, G. K. (2015). Limma powers differential expression analyses for RNA-sequencing and microarray studies. *Nucleic Acids Research*, 43(7), e47.

[254] Robertson, K. D. (2005). DNA methylation and human disease. *Nature Reviews Genetics*, 6(8), 597–610.

[255] Robinson, M. D., Mccarthy, D. J., & Smyth, G. K. (2010). edgeR: a Bioconductor package for differential expression analysis of digital gene expression data. *BIOINFORMATICS APPLICATIONS NOTE*, 26(1), 139–140.

[256] Rosas, M., Davies, L. C., Giles, P. J., Liao, C. T., Kharfan, B., Stone, T. C., O'Donnell, V. B., Fraser, D. J., Jones, S. A., & Taylor, P. R. (2014). The transcription factor Gata6 links tissue macrophage phenotype and proliferative renewal. *Science*, 344(6184), 645–648.

[257] Rose, M. C. & Voynow, J. A. (2006). Respiratory tract mucin genes and mucin glycoproteins in health and disease. *Physiological Reviews*, 86(1), 245–278.

[258] Ross-Innes, C. S., Stark, R., Teschendorff, A. E., Holmes, K. A., Ali, H. R., Dunning, M. J., Brown, G. D., Gojis, O., Ellis, I. O., Green, A. R., Ali, S., Chin, S. F., Palmieri, C.,

Caldas, C., & Carroll, J. S. (2012). Differential oestrogen receptor binding is associated with clinical outcome in breast cancer. *Nature*, 481(7381), 389–393.

[259] Roy, M. G., Livraghi-Butrico, A., Fletcher, A. A., McElwee, M. M., Evans, S. E., Boerner, R. M., Alexander, S. N., Bellinghausen, L. K., Song, A. S., Petrova, Y. M., Tuvim, M. J., Adachi, R., Romo, I., Bordt, A. S., Bowden, M. G., Sisson, J. H., Woodruff, P. G., Thornton, D. J., Rousseau, K., De La Garza, M. M., Moghaddam, S. J., Karmouty-quintana, H., Blackburn, M. R., Drouin, S. M., Davis, C. W., Terrell, K. A., Grubb, B. R., O'Neal, W. K., Flores, S. C., Cota-gomez, A., Lozupone, C. A., Donnelly, J. M., Watson, A. M., Hennessy, C. E., Keith, R. C., Yang, I. V., Barthel, L., Henson, P. M., Janssen, W. J., Schwartz, D. A., Boucher, R. C., Dickey, B. F., Evans, C. M., Garza, M. M. D., Moghaddam, S. J., Karmouty-quintana, H., Blackburn, M. R., Drouin, S. M., Davis, C. W., Terrell, K. A., Grubb, B. R., Neal, W. K. O., Flores, S. C., Cota-gomez, A., Lozupone, C. A., Donnelly, J. M., Watson, A. M., Hennessy, C. E., Keith, R. C., Yang, I. V., Barthel, L., Henson, P. M., Janssen, W. J., Schwartz, D. A., Boucher, R. C., Dickey, B. F., & Evans, C. M. (2014). Muc5b is required for airway defence. *Nature*, 505(7483), 412–416.

[Ryan] Ryan, D. MethylDackel.

[261] Saini, Y., Dang, H., Livraghi-Butrico, A., Kelly, E. J., Jones, L. C., O'Neal, W. K., Boucher, R. C., O'Neal, W. K., Boucher, R. C., O'Neal, W. K., & Boucher, R. C. (2014). Gene expression in whole lung and pulmonary macrophages reflects the dynamic pathology associated with airway surface dehydration. *BMC genomics*, 15(1), 726.

[262] Sallenave, J. M. (2014). Phagocytic and signaling innate immune receptors: Are they dysregulated in cystic fibrosis in the fight against Pseudomonas aeruginosa?

[263] Samokhvalov, I. M., Samokhvalova, N. I., & Nishikawa, S. I. (2007). Cell tracing shows the contribution of the yolk sac to adult haematopoiesis. *Nature*, 446(7139), 1056–1061.

[264] Sarode, P., Zheng, X., Giotopoulou, G. A., Weigert, A., Kuenne, C., Günther, S., Friedrich, A., Gattenlöhner, S., Stiewe, T., Brüne, B., Grimminger, F., Stathopoulos,

G. T., Pullamsetti, S. S., Seeger, W., & Savai, R. (2020). Reprogramming of tumor-associated macrophages by targeting β-catenin/FOSL2/ARID5A signaling: A potential treatment of lung cancer. *Science Advances*, 6(23), eaaz6105.

[265] Schafer, D. P., Lehrman, E. K., Kautzman, A. G., Koyama, R., Mardinly, A. R., Yamasaki, R., Ransohoff, R. M., Greenberg, M. E., Barres, B. A., & Stevens, B. (2012). Microglia Sculpt Postnatal Neural Circuits in an Activity and Complement-Dependent Manner. *Neuron*, 74(4), 691–705.

[266] Schmidt, E. P. & Tuder, R. M. (2010). Role of apoptosis in amplifying inflammatory responses in lung diseases. *Journal of Cell Death*, 2010(3), 41–53.

[267] Schones, D. E., Cui, K., Cuddapah, S., Roh, T. Y., Barski, A., Wang, Z., Wei, G., & Zhao, K. (2008). Dynamic Regulation of Nucleosome Positioning in the Human Genome. *Cell*, 132(5), 887–898.

[268] Schulz, C., Perdiguero, E. G., Chorro, L., Szabo-Rogers, H., Cagnard, N., Kierdorf, K., Prinz, M., Wu, B., Jacobsen, S. E. W., Pollard, J. W., Frampton, J., Liu, K. J., & Geissmann, F. (2012). A lineage of myeloid cells independent of myb and hematopoietic stem cells. *Science*, 335(6077), 86–90.

[269] Sebastian, A., Hum, N. R., Martin, K. A., Gilmore, S. F., Peran, I., Byers, S. W., Wheeler, E. K., Coleman, M. A., & Loots, G. G. (2020). Single-cell transcriptomic analysis of tumor- derived fibroblasts and normal tissue-resident fibroblasts reveals fibroblast heterogeneity in breast cancer. *Cancers*, 12(5), E1307.

[270] Senkus, E., Kyriakides, S., Ohno, S., Penault-Llorca, F., Poortmans, P., Rutgers, E., Zackrisson, S., & Cardoso, F. (2015). Primary breast cancer: ESMO Clinical Practice Guidelines for diagnosis, treatment and follow-up. *Annals of Oncology*, 26, v8–v30.

[271] Sethi, S. (2000). Infectious etiology of acute exacerbations of chronic bronchitis. *Chest*, 117(5 SUPPL. 2), 380S–385S.

[272] Sha, H., Zhang, D., Zhang, Y., Wen, Y., & Wang, Y. (2017). ATF3 promotes migration and M1/M2 polarization of macrophages by activating tenascin-C via Wnt/β-catenin pathway. *Molecular Medicine Reports*, 16(3), 3641–3647.

[273] Shan, M., Gentile, M., Yeiser, J. R., Walland, A. C., Bornstein, V. U., Chen, K., He, B., Cassis, L., Bigas, A., Cols, M., Comerma, L., Huang, B., Blander, J. M., Xiong, H., Mayer, L., Berin, C., Augenlicht, L. H., Velcich, A., & Cerutti, A. (2013). Mucus enhances gut homeostasis and oral tolerance by delivering immunoregulatory signals. *Science*, 342(6157), 447–453.

[274] Shechter, R., London, A., Varol, C., Raposo, C., Cusimano, M., Yovel, G., Rolls, A., Mack, M., Pluchino, S., Martino, G., Jung, S., & Schwartz, M. (2009). Infiltrating Blood-Derived Macrophages Are Vital Cells Playing an Anti-inflammatory Role in Recovery from Spinal Cord Injury in Mice. *PLoS Medicine*, 6(7), e1000113.

[275] Sheffield, N. & Furey, T. (2012). Identifying and Characterizing Regulatory Sequences in the Human Genome with Chromatin Accessibility Assays. *Genes*, 3(4), 651–670.

[276] Sheffield, N. C. & Bock, C. (2016). LOLA: Enrichment analysis for genomic region sets and regulatory elements in R and Bioconductor. *Bioinformatics*, 32(4), 587–589.

[277] Shiao, S. L., Ruffell, B., De Nardo, D. G., Faddegon, B. A., Park, C. C., & Coussens, L. M. (2015). TH2-polarized CD4+ T Cells and macrophages limit efficacy of radiotherapy. *Cancer Immunology Research*, 3(5), 518–525.

[278] Skene, P. J. & Henikoff, S. (2017). An efficient targeted nuclease strategy for high-resolution mapping of DNA binding sites. *eLife*, 6.

[279] Smith, Z. D. & Meissner, A. (2013). DNA methylation: Roles in mammalian development. *Nature Reviews Genetics*, 14(3), 204–220.

[280] Sood, A., Petersen, H., Blanchette, C. M., Meek, P., Picchi, M. A., Belinsky, S. A., & Tesfaigzi, Y. (2010). Wood smoke exposure and gene promoter methylation are associated

with increased risk for COPD in smokers. *American Journal of Respiratory and Critical Care Medicine*, 182(9), 1098–1104.

[281] Stadler, M. B., Murr, R., Burger, L., Ivanek, R., Lienert, F., Schöler, A., Wirbelauer, C., Oakeley, E. J., Gaidatzis, D., Tiwari, V. K., & Schübeler, D. (2011). DNA-binding factors shape the mouse methylome at distal regulatory regions. *Nature*, 480(7378), 490–495.

[282] Stark, R. & Brown, G. (2011). DiffBind : differential binding analysis of ChIP-Seq peak data.

[283] Steven, J. L. (1892). Metchnikoff on the Comparative Pathology of Inflammation. *Glasgow medical journal*, 38(3), 195–205.

[284] Stöger, J. L., Gijbels, M. J., van der Velden, S., Manca, M., van der Loos, C. M., Biessen, E. A., Daemen, M. J., Lutgens, E., & de Winther, M. P. (2012). Distribution of macrophage polarization markers in human atherosclerosis. *Atherosclerosis*, 225(2), 461–468.

[285] Stricker, S. H., Köferle, A., & Beck, S. (2016). From profiles to function in epigenomics. *Nature Reviews Genetics*, 18(1), 51–66.

[286] Stuart, T., Butler, A., Hoffman, P., Hafemeister, C., Papalexi, E., Mauck, W. M., Hao, Y., Stoeckius, M., Smibert, P., & Satija, R. (2019). Comprehensive Integration of Single-Cell Data. *Cell*, 177(7), 1888–1902.e21.

[287] Su, S., Liu, Q., Chen, J., Chen, J., Chen, F., He, C., Huang, D., Wu, W., Lin, L., Huang, W., Zhang, J., Cui, X., Zheng, F., Li, H., Yao, H., Su, F., & Song, E. (2014). A Positive feedback loop between mesenchymal-like cancer cells and macrophages is essential to breast cancer metastasis. *Cancer Cell*, 25(5), 605–620.

[288] Subramanian, A., Tamayo, P., Mootha, V. K., Mukherjee, S., Ebert, B. L., Gillette, M. A., Paulovich, A., Pomeroy, S. L., Golub, T. R., Lander, E. S., & Mesirov, J. P. (2005).

Gene set enrichment analysis: A knowledge-based approach for interpreting genome-wide expression profiles. *Proceedings of the National Academy of Sciences of the United States of America*, 102(43), 15545–15550.

[289] Sumitomo, R., Hirai, T., Fujita, M., Murakami, H., Otake, Y., & long Huang, C. (2019). PD-L1 expression on tumor-infiltrating immune cells is highly associated with M2 TAM and aggressive malignant potential in patients with resected non-small cell lung cancer. *Lung Cancer*, 136, 136–144.

[290] Sun, C., Mezzadra, R., & Schumacher, T. N. (2018). Regulation and Function of the PD-L1 Checkpoint. *Immunity*, 48(3), 434–452.

[291] Sundar, I. K. & Rahman, I. (2016). Gene expression profiling of epigenetic chromatin modification enzymes and histone marks by cigarette smoke: implications for COPD and lung cancer. *American Journal of Physiology - Lung Cellular and Molecular Physiology*, 311(6), L1245–L1258.

[292] Sung, H., Ferlay, J., Siegel, R. L., Laversanne, M., Soerjomataram, I., Jemal, A., & Bray, F. (2021). Global cancer statistics 2020: GLOBOCAN estimates of incidence and mortality worldwide for 36 cancers in 185 countries. *CA: A Cancer Journal for Clinicians*, 71(3), 209–249.

[293] Suzuki, T., Arumugam, P., Sakagami, T., Lachmann, N., Chalk, C., Sallese, A., Abe, S., Trapnell, C., Carey, B., Moritz, T., Malik, P., Lutzko, C., Wood, R. E., & Trapnell, B. C. (2014). Pulmonary macrophage transplantation therapy. *Nature*, 514(7523), 450–454.

[294] Tacke, F., Alvarez, D., Kaplan, T. J., Jakubzick, C., Spanbroek, R., Llodra, J., Garin, A., Liu, J., Mack, M., Van Rooijen, N., Lira, S. A., Habenicht, A. J., & Randolph, G. J. (2007). Monocyte subsets differentially employ CCR2, CCR5, and CX3CR1 to accumulate within atherosclerotic plaques. *Journal of Clinical Investigation*, 117(1), 185–194.

[295] Takahashi, K., Koga, K., Linge, H. M., Zhang, Y., Lin, X., Metz, C. N., Al-Abed, Y., Ojamaa, K., & Miller, E. J. (2009). Macrophage CD74 contributes to MIF-induced pulmonary inflammation. *Respiratory Research*, 10(1), 33.

[296] Talbert, P. B. & Henikoff, S. (2010). Histone variants ancient wrap artists of the epigenome. *Nature Reviews Molecular Cell Biology*, 11(4), 264–275.

[297] Tamoutounour, S., Guilliams, M., MontananaSanchis, F., Liu, H., Terhorst, D., Malosse, C., Pollet, E., Ardouin, L., Luche, H., Sanchez, C., Dalod, M., Malissen, B., & Henri, S. (2013). Origins and functional specialization of macrophages and of conventional and monocyte-derived dendritic cells in mouse skin. *Immunity*, 39(5), 925–938.

[298] Tan, S. Y. & Krasnow, M. A. (2016). Developmental origin of lung macrophage diversity. *Development (Cambridge)*, 143(8), 1318–1327.

[299] Tap, W. D., Wainberg, Z. A., Anthony, S. P., Ibrahim, P. N., Zhang, C., Healey, J. H., Chmielowski, B., Staddon, A. P., Cohn, A. L., Shapiro, G. I., Keedy, V. L., Singh, A. S., Puzanov, I., Kwak, E. L., Wagner, A. J., Von Hoff, D. D., Weiss, G. J., Ramanathan, R. K., Zhang, J., Habets, G., Zhang, Y., Burton, E. A., Visor, G., Sanftner, L., Severson, P., Nguyen, H., Kim, M. J., Marimuthu, A., Tsang, G., Shellooe, R., Gee, C., West, B. L., Hirth, P., Nolop, K., van de Rijn, M., Hsu, H. H., Peterfy, C., Lin, P. S., Tong-Starksen, S., & Bollag, G. (2015). Structure-Guided Blockade of CSF1R Kinase in Tenosynovial Giant-Cell Tumor. *New England Journal of Medicine*, 373(5), 428–437.

[300] Taylor, M. A., Yong-Hun, L. E., & Schiemann, W. P. (2011). Role of TGF-β and the tumor microenvironment during mammary tumorigenesis. *Gene Expression*, 15(3), 117–132.

[301] Team, R. D. C. (2020). A Language and Environment for Statistical Computing.

[302] Tessarz, P. & Kouzarides, T. (2014). Histone core modifications regulating nucleosome structure and dynamics. *Nature Reviews Molecular Cell Biology*, 15(11), 703–708.

[303] Therneau, T. M. (2021). survival: Survival Analysis.

[304] Tomasz Konopka (2020). umap: Uniform Manifold Approximation and Projection.

[305] Topalian, S. L., Drake, C. G., & Pardoll, D. M. (2015). Immune checkpoint blockade: A common denominator approach to cancer therapy. *Cancer Cell*, 27(4), 450–461.

[306] Trojanek, J. B., Cobos-Correa, A., Diemer, S., Kormann, M., Schubert, S. C., Zhou-Suckow, Z., Agrawal, R., Duerr, J., Wagner, C. J., Schatterny, J., Hirtz, S., Sommerburg, O., Hartl, D., Schultz, C., & Mall, M. A. (2014). Airway mucus obstruction triggers macrophage activation and matrix metalloproteinase 12-dependent emphysema. *American Journal of Respiratory Cell and Molecular Biology*, 51(5), 709–720.

[307] Tugal, D., Liao, X., & Jain, M. K. (2013). Transcriptional control of macrophage polarization. *Arteriosclerosis, thrombosis, and vascular biology*, 33(6), 1135–44.

[308] Tuit, S., Salvagno, C., Kapellos, T. S., Hau, C. S., Seep, L., Oestreich, M., Klee, K., de Visser, K. E., Ulas, T., & Schultze, J. L. (2019). Transcriptional Signature Derived from Murine Tumor-Associated Macrophages Correlates with Poor Outcome in Breast Cancer Patients. *Cell Reports*, 29(5), 1221–1235.e5.

[309] Tunney, M. M., Field, T. R., Moriarty, T. F., Patrick, S., Doering, G., Muhlebach, M. S., Wolfgang, M. C., Boucher, R., Gilpin, D. F., McDowell, A., & Elborn, J. S. (2008). Detection of anaerobic bacteria in high numbers in sputum from patients with cystic fibrosis. *American Journal of Respiratory and Critical Care Medicine*, 177(9), 995–1001.

[310] Tymoszuk, P., Evens, H., Marzola, V., Wachowicz, K., Wasmer, M. H., Datta, S., Müller-Holzner, E., Fiegl, H., Böck, G., van Rooijen, N., Theurl, I., & Doppler, W. (2014). In situ proliferation contributes to accumulation of tumor-associated macrophages in spontaneous mammary tumors. *European Journal of Immunology*, 44(8), 2247–2262.

[311] Ulrich, M., Worlitzsch, D., Viglio, S., Siegmann, N., Iadarola, P., Shute, J. K., Geiser, M., Pier, G. B., Friedel, G., Barr, M. L., Schuster, A., Meyer, K. C., Ratjen, F., Bjarnsholt, T., Gulbins, E., & Döring, G. (2010). Alveolar inflammation in cystic fibrosis. *Journal of Cystic Fibrosis*, 9(3), 217–227.

[312] Van Gassen, S., Callebaut, B., Van Helden, M. J., Lambrecht, B. N., Demeester, P., Dhaene, T., & Saeys, Y. (2015). FlowSOM: Using self-organizing maps for visualization and interpretation of cytometry data. *Cytometry Part A*, 87(7), 636–645.

[313] van Heeringen, S. J. & Veenstra, G. J. C. (2011). GimmeMotifs: a de novo motif prediction pipeline for ChIP-sequencing experiments. *Bioinformatics*, 27(2), 270–271.

[314] van Ravenswaay Claasen, H. H., Kluin, P. M., & Fleuren, G. J. (1992). Tumor infiltrating cells in human cancer. On the possible role of CD16+ macrophages in antitumor cytotoxicity. *Laboratory investigation; a journal of technical methods and pathology*, 67(2), 166–174.

[315] Viniol, C. & Vogelmeier, C. F. (2018). Exacerbations of COPD. *European Respiratory Review*, 27(147).

[316] Waddington, C. H. (1942). The Epigenotype. *International Journal of Epidemiology*, 41(1), 10–13.

[317] Wang, L., Rubinstein, R., Lines, J. L., Wasiuk, A., Ahonen, C., Guo, Y., Lu, L. F., Gondek, D., Wang, Y., Fava, R. A., Fiser, A., Almo, S., & Noelle, R. J. (2011). VISTA, a novel mouse Ig superfamily ligand that negatively regulates T cell responses. *Journal of Experimental Medicine*, 208(3), 577–592.

[318] Wang, M. & Lemos, B. (2019). Ribosomal DNA harbors an evolutionarily conserved clock of biological aging. *Genome Research*, (pp. 325–333).

[319] Wang, Q., Gu, L., Adey, A., Radlwimmer, B., Wang, W., Hovestadt, V., Bähr, M., Wolf, S., Shendure, J., Eils, R., Plass, C., & Weichenhan, D. (2013). Tagmentation-based whole-genome bisulfite sequencing. *Nature protocols*, 8(10), 2022–32.

[320] Wang, X., Park, J., Susztak, K., Zhang, N. R., & Li, M. (2019). Bulk tissue cell type deconvolution with multi-subject single-cell expression reference. *Nature Communications*, 10(1), 1–9.

[321] Wang, Z., Li, W., Guo, Q., Wang, Y., Ma, L., & Zhang, X. (2018). Insulin-Like Growth Factor-1 Signaling in Lung Development and Inflammatory Lung Diseases. *BioMed Research International*, 2018, 17–19.

[322] Wiener, D. & Schwartz, S. (2020). The epitranscriptome beyond m6A. *Nature Reviews Genetics*, 22(2), 119–131.

[323] Wilke, M., Buijs-Offerman, R. M., Aarbiou, J., Colledge, W. H., Sheppard, D. N., Touqui, L., Bot, A., Jorna, H., De Jonge, H. R., & Scholte, B. J. (2011). Mouse models of cystic fibrosis: Phenotypic analysis and research applications. *Journal of Cystic Fibrosis*, 10(SUPPL. 2).

[324] Wilkerson, M. D. & Hayes, D. N. (2010). ConsensusClusterPlus: A class discovery tool with confidence assessments and item tracking. *Bioinformatics*, 26(12), 1572–1573.

[325] Wills-Karp, M., Luyimbazi, J., Xu, X., Schofield, B., Neben, T. Y., Karp, C. L., & Donaldson, D. D. (1998). Interleukin-13: Central mediator of allergic asthma. *Science*, 282(5397), 2258–2261.

[326] Woolf, E., Xiao, C., Fainaru, O., Lotem, J., Rosen, D., Negreanu, V., Bernstein, Y., Goldenberg, D., Brenner, O., Berke, G., Levanon, D., & Groner, Y. (2003). Runx3 and Runx1 are required for CD8 T cell development during thymopoiesis. *Proceedings of the National Academy of Sciences of the United States of America*, 100(13), 7731–7736.

[327] Wu, C. T. & Morris, J. R. (2001). Genes, genetics, and epigenetics: A correspondence. *Science*, 293(5532), 1103–1105.

[328] Wu, D., Pan, P., Su, X., Zhang, L., Qin, Q., Tan, H., Huang, L., & Li, Y. (2016). Interferon Regulatory Factor-1 Mediates Alveolar Macrophage Pyroptosis during LPS-Induced Acute Lung Injury in Mice. *Shock*, 46(3), 329–338.

[329] Wynn, T. A. (2008). Cellular and molecular mechanisms of fibrosis. *Journal of Pathology*, 214(2), 199–210.

[330] Wynn, T. A., Chawla, A., & Pollard, J. W. (2013). Macrophage biology in development, homeostasis and disease. *Nature*, 496(7446), 445–455.

[331] Xue, J., Schmidt, S. V., Sander, J., Draffehn, A., Krebs, W., Quester, I., DeNardo, D., Gohel, T. D., Emde, M., Schmidleithner, L., Ganesan, H., Nino-Castro, A., Mallmann, M. R., Labzin, L., Theis, H., Kraut, M., Beyer, M., Latz, E., Freeman, T. C., Ulas, T., & Schultze, J. L. (2014). Transcriptome-Based Network Analysis Reveals a Spectrum Model of Human Macrophage Activation. *Immunity*, 40(2), 274–288.

[332] Yan, D., Kowal, J., Akkari, L., Schuhmacher, A. J., Huse, J. T., West, B. L., & Joyce, J. A. (2017). Inhibition of colony stimulating factor-1 receptor abrogates microenvironment-mediated therapeutic resistance in gliomas. *Oncogene*, 36(43), 6049–6058.

[333] Yates, A. D., Achuthan, P., Akanni, W., Allen, J., Allen, J., Alvarez-Jarreta, J., Amode, M. R., Armean, I. M., Azov, A. G., Bennett, R., Bhai, J., Billis, K., Boddu, S., Jos′, J., Carlos, J., Marugán, M. M., Cummins, C., Davidson, C., Dodiya, K., Fatima, R., Gall, A., Giron, C. G., Gil, L., Grego, T., Haggerty, L., Haskell, E., Hourlier, T., Izuogu, O. G., Janacek, S. H., Juettemann, T., Kay, M., Lavidas, I., Le, T., Lemos, D., Gonzalez Martinez, J., Maurel, T., Mcdowall, M., Mcmahon, A., Mohanan, S., Moore, B., Nuhn, M., Oheh, D. N., Parker, A., Parton, A., Patricio, M., Sakthivel, P., Imran, A., Salam, A., Schmitt, B. M., Schuilenburg, H., Sheppard, D., Sycheva, M., Szuba, M., Taylor, K., Thormann, A., Threadgold, G., Vullo, A., Walts, B., Winterbottom, A., Zadissa, A., Chakiachvili, M., Flint, B., Frankish, A., Hunt, S. E., Iisley, G., Kostadima, M., Langridge, N., Loveland, J. E., Martin, F. J., Morales, J., Mudge, J. M., Muffato, M., Perry, E., Ruffier, M., Trevanion, S. J., Cunningham, F., Howe, K. L., Zerbino, D. R., & Flicek, P. (2020). Ensembl 2020. *Nucleic Acids Research*, 48.

[334] Yin, Y., Morgunova, E., Jolma, A., Kaasinen, E., Sahu, B., Khund-Sayeed, S., Das, P. K., Kivioja, T., Dave, K., Zhong, F., Nitta, K. R., Taipale, M., Popov, A., Ginno, P. A., Domcke, S., Yan, J., Schübeler, D., Vinson, C., & Taipale, J. (2017). Impact of cytosine methylation on DNA binding specificities of human transcription factors. *Science*, 356(6337).

[335] Yona, S., Kim, K. W., Wolf, Y., Mildner, A., Varol, D., Breker, M., Strauss-Ayali, D., Viukov, S., Guilliams, M., Misharin, A., Hume, D. A., Perlman, H., Malissen, B., Zelzer,

E., & Jung, S. (2013). Fate Mapping Reveals Origins and Dynamics of Monocytes and Tissue Macrophages under Homeostasis. *Immunity*, 38(1), 79–91.

[336] Yong, W. S., Hsu, F. M., & Chen, P. Y. (2016). Profiling genome-wide DNA methylation. *Epigenetics and Chromatin*, 9(1), 1–16.

[337] Yoo, S., Takikawa, S., Geraghty, P., Argmann, C., Campbell, J., Lin, L., Huang, T., Tu, Z., Feronjy, R., Spira, A., Schadt, E. E., Powell, C. A., & Zhu, J. (2015). Integrative Analysis of DNA Methylation and Gene Expression Data Identifies EPAS1 as a Key Regulator of COPD. *PLoS Genetics*, 11(1).

[338] Yu, G., Wang, L. G., Han, Y., & He, Q. Y. (2012). ClusterProfiler: An R package for comparing biological themes among gene clusters. *OMICS A Journal of Integrative Biology*, 16(5), 284–287.

[339] Yu, G., Wang, L. G., & He, Q. Y. (2015). ChIP seeker: An R/Bioconductor package for ChIP peak annotation, comparison and visualization. *Bioinformatics*, 31(14), 2382–2383.

[340] Yu, X., Wang, Y., Deng, M., Li, Y., Ruhn, K. A., Zhang, C. C., & Hooper, L. V. (2014). The basic leucine zipper transcription factor NFIL3 directs the development of a common innate lymphoid cell precursor. *eLife*, 3.

[341] Yuan, A., Hsiao, Y. J., Chen, H. Y., Chen, H. W., Ho, C. C., Chen, Y. Y., Liu, Y. C., Hong, T. H., Yu, S. L., Chen, J. J., & Yang, P. C. (2015). Opposite Effects of M1 and M2 Macrophage Subtypes on Lung Cancer Progression. *Scientific Reports*, 5.

[342] Zaret, K. S. & Carroll, J. S. (2011). Pioneer transcription factors: Establishing competence for gene expression. *Genes and Development*, 25(21), 2227–2241.

[343] Zhao, Z. & Shilatifard, A. (2019). Epigenetic modifications of histones in cancer. *Genome Biology*, 20(1), 1–16.

[344] Zheng, T., Zhu, Z., Wang, Z., Homer, R. J., Ma, B., Riese, R. J., Chapman, H. A., Shapiro, S. D., & Elias, J. A. (2000). Inducible targeting of IL-13 to the adult lung causes

matrix metalloproteinase- and cathepsin-dependent emphysema. *Journal of Clinical Investigation*, 106(9), 1081–1093.

[345] Zhou, L., Dey, C. R., Wert, S. E., DuVall, M. D., Frizzell, R. A., & Whitsett, J. A. (1994). Correction of lethal intestinal defect in a mouse model of cystic fibrosis by human CFTR. *Science*, 266(5191), 1705–1708.

[346] Zhou, Y., Zhou, B., Pache, L., Chang, M., Khodabakhshi, A. H., Tanaseichuk, O., Benner, C., & Chanda, S. K. (2019). Metascape provides a biologist-oriented resource for the analysis of systems-level datasets. *Nature Communications*, 10(1).

[347] Zhou-Suckow, Z., Duerr, J., Hagner, M., & Mall, M. A. (2017). Airway mucus, inflammation and remodeling: emerging links in the pathogenesis of chronic lung diseases. *Cell and Tissue Research*, 367(3), 537–550.

[348] Zigmond, E., Varol, C., Farache, J., Elmaliah, E., Satpathy, A. T., Friedlander, G., Mack, M., Shpigel, N., Boneca, I. G., Murphy, K. M., Shakhar, G., Halpern, Z., & Jung, S. (2012). Ly6Chi Monocytes in the Inflamed Colon Give Rise to Proinflammatory Effector Cells and Migratory Antigen-Presenting Cells. *Immunity*, 37(6), 1076–1090.

[349] Ziller, M. J., Gu, H., Müller, F., Donaghey, J., Tsai, L. T., Kohlbacher, O., De Jager, P. L., Rosen, E. D., Bennett, D. A., Bernstein, B. E., Gnirke, A., & Meissner, A. (2013). Charting a dynamic DNA methylation landscape of the human genome. *Nature*, 500(7463), 477–481.

Manuscripts, poster presentations and conference talks

Manuscripts

Manuscripts addressed in the present thesis

Epigenetic reprogramming of airway macrophages drives polarization and inflammation in muco-obstructive lung disease. Joschka Hey*, Michelle Paulsen*, Reka Toth, Dieter Weichenhan, Simone Butz, Reinhard Liebers, Pavlo Lutsik, Christoph Plass†, and Marcus A. Mall†
Under revision at Nature Communications

Cancer-specific DNA methylation landscape of tumor-associated macrophages and monocytes in breast cancer. Joschka Hey, Coral Halperin, Mark Hartmann, Maximilian Schönung, Dieter Weichenhan, Daniel Lipka, Ruth Scherz-Shouval, and Christoph Plass
Manuscript in preparation

Additional manuscripts from the Ph.D.

Diverse routes of Club cell evolution in lung adenocarcinoma. Yuanyuan Chenz*, Reka Toth*, Sara Chocarro, Dieter Weichenhan, Joschka Hey, Pavlo Lutsik, Stefan Sawall,

*Equal contribution
†Equal contribution

Georgios Stathopoulos, Christoph Plass, and Rocio Sotillo
bioRxiv. 06/2021. DOI: 10.1101/2021.06.10.447936

Epigenetic blueprint identifies poor outcome and hypomethylating agent-responsive T-ALL subgroup. Aurore Touzart*, Anand Mayakonda*, Charlotte Smith, Joschka Hey, Reka Toth, Agata Cieslak, Guillaume P. Andrieu, Christine Tran Quang, Mehdi Latiri, Jacques Ghysdael, Salvatore Spicuglia, Hervé Dombret, Norbert Ifrah, Elizabeth Macintyre, Pavlo Lutsik, Nicolas Boissel, Christoph Plass†, and Vahid Asnafi†
Science Translational Medicine. 05/2021. DOI: 10.1126/scitranslmed.abc4834. PMID: 34039737

Methrix: an R/bioconductor package for systematic aggregation and analysis of bisulfite sequencing data. Anand Mayakonda, Maximilian Schönung, Joschka Hey, Rajbir N. Batra, Clarissa Feuerstein-Akgoz, Kristin Köhler, Daniel Lipka, Rocio Sotillo, Christoph Plass, Pavlo Lutsik, and Reka Toth
Bioinformatics. 12/2020. DOI: 10.1093/bioinformatics/btaa1048. PMID: 33346800

Globally altered epigenetic landscape and delayed osteogenic differentiation in H3.3-G34W-mutant giant cell tumor of bone. Pavlo Lutsik*, Annika Baude*, Daniela Mancarella*, Simin Özv*, Alexander Kühn, Reka Toth, Joschka Hey, Umut H. Toprak, Jinyeong Lim, Viet Ha Nguyen, Chao Jiang, Anand Mayakonda, Mark Hartmann, Felix Rosemann, Kersten Breuer, Dominik Vonficht, Florian Grünschläger, Suman Lee, Maren Kirstin Schuhmacher, Denis Kusevic, Anna Jauch, Dieter Weichenhan, Jozef Zustin, Matthias Schlesner, Simon Haas, Joo Hyun Park, Yoon Jung Park, Udo Oppermann, Albert Jeltsch, Florian Haller, Jörg Fellenberg, Anders M. Lindroth†, and Christoph Plass†
Nature Communications. 10/2020. DOI: a10.1038/s41467-020-18955-y. PMID: 33110075

AmpliconDesign – an interactive web server for the design of high-throughput targeted DNA methylation assays. Maximilian Schönung, Jana Hess, Pascal Bawidamann,

*Equal contribution
†Equal contribution

Sina Stäble, Joschka Hey, Jens Langstein, Yassen Assenov, Dieter Weichenhan, Pavlo Lutsik, and Daniel B. Lipka
Epigenetics. 10/2020. DOI: 10.1080/15592294.2020.1834921. PMID: 33100132

ID3 promotes homologous recombination via non-transcriptional and transcriptional mechanisms and its loss confers sensitivity to PARP inhibition. Ali Bakr, Joschka Hey, Gianluca Sigismondo, Ashish Goyal, Chun-Shan Liu, Ramya Lakshmana Iyer, Max Trauernicht, Kersten Breuer, Pavlo Lutsik, Jeroen Krijgsveld, Dieter Weichenhan, Christoph Plass, Odilia Popanda, and Peter Schmezer
Under revision at Nucleic Acids Research

The age of the bone marrow microenvironment influences B-cell acute lymphoblastic leukemia progression via CXCR5- CXCL13. Costanza Zanetti, Rahul Kumar, Joscha Ender, Parimala S. Godavarthy, Mark Hartmann, Joschka Hey, Kersten Breuer, Eva S. Weissenberger, Valentina R. Minciacchi, Christina Karantanou, Zhaohui Gu, Kathryn G. Roberts, Markus Metzler, Wendy Stock, Charles G. Mullighan, Clara D. Bloomfield, Natalie Filmann, Antony Cousins, Christina Halsey, Christoph Plass, Daniel B. Lipka, and Daniela S. Krause
Under revision at Blood

Poster presentations

Epigenetic reprogramming of airway macrophages drives polarization and inflammation in muco-obstructive lung disease. Joschka Hey, Michelle Paulsen, Reka Toth, Dieter Weichenhan, Simone Butz, Reinhard Liebers, Pavlo Lutsik, Marcus A. Mall, and Christoph Plass
Ph.D. Poster Presentation. 11/2020, Heidelberg, Germany

Alveolar macrophages from muco- obstructive mice show a dysregulated epigenome. Joschka Hey, Michelle Paulsen, Simone Butz, Malte Paulsen, Reka Toth, Pavlo Lutsik, Marcus A. Mall, and Christoph Plass
Annual meeting of the German Center for Lung Research. 01/2020, Lübeck-Travemünde, Germany (best poster award)

Alveolar macrophages from muco-obstructive mice show a dysregulated epigenome. Joschka Hey, Michelle Paulsen, Simone Butz, Malte Paulsen, Reka Toth, Pavlo Lutsik, Marcus A. Mall, and Christoph Plass
Stress and Inflammation in Tumor Progression and Metastasis. 05/2019, Rehovot, Israel

Alveolar macrophages from muco-obstructive mice show a dysregulated epigenome. Joschka Hey, Michelle Paulsen, Simone Butz, Malte Paulsen, Reka Toth, Pavlo Lutsik, Marcus A. Mall, and Christoph Plass
Annual meeting of the German Center for Lung Research. 01/2019, Mannheim, Germany (best poster award)

Conference talks

The epigenetic landscape of cancer-associated fibroblasts. Joschka Hey and Coral Halperin.
DKFZ-MOST 44th Joint Scientific Program Committee Meeting. 05/2021, online

Epigenetic reprogramming of airway macrophages drives polarization and inflammation in muco-obstructive lung disease. Joschka Hey
TLRC young scientist meeting. 12/2020, online

Alveolar macrophages from muco- obstructive mice show a dysregulated epigenome. Joschka Hey
Annual meeting of the German Center for Lung Research. 01/2020, Lübeck-Travemünde, Germany

Alveolar macrophages from muco-obstructive mice show a dysregulated epigenome. Joschka Hey
Annual Retreat of the International Graduate Programme "Molecular Biology and Medicine of the Lung". 06/2019, Giessen, Germany.

Alveolar macrophages from muco-obstructive mice show a dysregulated epigenome. Joschka Hey
Annual meeting of the German Center for Lung Research. 01/2019, Mannheim, Germany

An Epigenetic Approach to the Cell of Origin of COPD. Joschka Hey
TLRC young scientist meeting. 11/2017, Heidelberg, Germany

Oh, I get by with a little help from my friends
Mm, I get high with a little help from my friends
Mm, gonna try with a little help from my friends

The Beatles

Acknowledgments

The work presented in the present thesis was only possible with the support of many individuals. In particular, I want to address my words to:

- **Christoph Plass**, for the opportunity to pursue my doctoral thesis in your lab and the chance to learn new scientific skills. The freedom you granted me to engage in various research projects and follow my curiosity has allowed me to acquire the expertise I needed to complete my Ph.D. and become the researcher I am now. Whenever possible, you supported my work with collaborations, resources, and time. I also highly appreciate your personal support and sympathy, especially during the last year of my Ph.D.
- **Marcus Mall**, for the successful collaboration. Despite your busy schedule, you always found time for our project and supported us with valuable input and advice.
- **Ruth Scherz-Shouval**, for the excellent collaboration on several projects and the supervision during my time in Israel. Although I could only spend a short time in your lab, it helped me broaden my scientific and personal horizon.
- **Odilia Popanda**, for being both my first examiner and a member of my thesis advice committee. Your input and feedback have greatly improved this thesis.
- **Michelle Paulsen**, for your devotion to the muco-obstructive lung disease project and for doing most of the experimental work presented in the first half of this thesis. With your help, I understood many aspects of the illness a lot faster and could quickly progress in my Ph.D. I think we became a great team over the last four years.
- **Mark Hartmann**, for the preparation of PBAT libraries, proofreading my dissertation, and most important, for the countless chats and discussions regarding all my projects and life. I

enjoyed working with you on the JMML project and valued the drinks and jokes after work even more. Keep up your great attitude!

- **Coral Halperin**, for the collaboration on the TAM project and doing all the mouse and further experimental work presented in the second half of this thesis. Thank you for the warm welcome and great time in Israel.
- **Pavlo Lutsik**, **Reka Toth**, and **Anand Mayakonda**, for the introduction into bioinformatics and the unconditional support in computational analysis of any kind. Without you, I wouldn't have been able to learn how to process and analyze next-generation sequencing data that fast. Most importantly, thank you for your friendship, personal support, and many waves of laughter we had together.
- **Maria Llamazares Prada**, for proofreading my dissertation and many interesting collaborations on chronic lung diseases. You always show genuine interest in your own and other's people research. Please keep that attitude and continue to contribute to such a great atmosphere in the lab.
- **Dieter Weichenhan** and **Marion Bähr**, for technical advice and support in the lab. Especially the preparation of tWGBS libraries would not have been possible without you.
- **Simone Butz** and **Jolanthe Schatterny**, for technical support over the years, especially in the last months of revisions. Without your help, I would not have been able to perform the requested experiments.
- **Maxmilian Schönung**, for supporting PBAT library preparations and other fruitful collaborations. I think your enthusiasm and scientific aims are inspiring.
- **Reinhard Liebers**, for initiating the muco-obstructive lung disease project and helping me to transition into my Ph.D. smoothly.
- The **Flow Cytometry Core Facility**, in particular, **Malte Paulsen** and **Diana Ordonez**, for their outstanding technical support during numerous FACS appointments. I always enjoyed my time at EMBL.
- The **Genomics and Proteomics Core Facility**, **Gene Core Facility**, and **Omics IT and Data Management Core Facility,** for sequencing my libraries, storing all the data, as well as technical support when I was lost in wrong fragment sizes or data uploads.

- The **German-Israeli Helmholtz International Research School in Cancer Biology**, for funding my Ph.D. position and the opportunity to travel to the Weizmann Institute of Science in Israel.

In addition, I am very grateful to all current and former members of the division Cancer Epigenomics and other colleagues at DKFZ. You were always a great company and supported me with discussions, practical assistance, and advice. Especially I want to acknowledge:

- **Clarissa Gerhäuser**, for her input during division seminars and helpful advice throughout my Ph.D. I enjoyed our countless conversations before going home.
- **Daniel Lipka** and **Peter Schmezer**, for including me in your research projects and for supporting a prosperous scientific environment in the division of Cancer Epigenomics.
- **Ashish Goyal**, for the great work on the TINAT project and our friendship. Thank you for being such a relaxed scientist. I think this attitude would help me a lot sometimes.
- **Oliver Mücke**, for being such a fun person in the lab and after work. Your cheerful and easy-going character was very supportive throughout my Ph.D.
- **Alexander Kühn**, **Daniela Mancarella**, **Clarissa Feuerstein**, **Sina Stäble**, and **Jens Langstein**, for treading the path of Ph.D. with me. Without your support and exchange, I couldn't envision my time at DKFZ.
- **Agustin Rodriguez**, **Magdalena Szczygiel**, and **Dimitri Lindijer**, for the fantastic times on the way and at DZL meetings. I am grateful for the conversations we had and the friends we became.
- All additional members of the **Cancer Epigenomics** division, which were not explicitly mentioned here. You provided a great scientific atmosphere and were a vital part of my life in the last four years.

Furthermore, I want to emphasize the unnoticed heroes of the internet, who provided and contributed to the fantastic open-source landscape in science that enables our daily work:

- **Stack Overflow**, for providing an amazing forum for most of my bioinformatic questions.

- **CRAN**, **Bioconductor**, and **Conda**, for the great tools and packages that enabled me to perform most of my work.

A special acknowledgment is addressed to all the people outside of work. You have empowered and supported me to pursue my Ph.D. in various ways. In particular, I want to express my gratitude to:

- **Ahmad**, for the beautiful friendship we have developed since you started your M.Sc. in our division.
- **Can**, **Christian**, **Luca**, **Joe**, and **Stefan** for the constant companionship over the last years.
- **Simon** and **Julian**, for the fantastic time we spent at countless events and deep conversations we had.
- **Linda**, **Agnes**, **Toni**, and **Dominik**, for your company throughout the lockdown and the friendship we developed.
- **Paul** and **Johannes**, for always being a fantastic support when we needed a place to retire in Berlin. Thank you for your friendship!
- **Tom**, **David**, and **Erez**, for a warm welcome and a great time in Israel.
- **Armin**, **Georg**, **Janina**, **Johnny**, and **Mathis**, for our friendship. I am glad that we were able to share many moments over the last years.
- **Anita**, for being my best friend and love of my life. Thank you for always being there in difficult times, when all hope seems lost.
- My Parents, **Christoph** and **Uli**, for the unconditional love and the possibility to achieve everything I ever wanted in life.